

Fluid Migration into Porous Biomaterials under High Hydrostatic Pressure

By

Hamed Vatankhah

Department of Food Science and Agricultural Chemistry
Macdonald Campus, McGill University
Montreal, Canada

March 2018

A thesis submitted to McGill University in partial fulfillment of the requirements for the degree of Doctor of Philosophy

© **Hamed Vatankhah**

Suggested short title:

High Pressure Impregnation Modeling

ABSTRACT

In this study, the fluid migration into porous biomaterials such as fruits and vegetable tissues was fully characterized. In a major part of this study, various computational procedures were introduced to model such transport phenomena.

First, the fluid migration trend was evaluated into the fresh-cut apple as the selected porous medium. The mass transfer was monitored at 100 to 600 MPa pressure levels and 0 to 30 min pressurization time. The mass transfer during pressure holding time fitted Fick's second law. Using inverse methods of parameter estimation algorithms, the calculated diffusivity values ranged between 4.38×10^{-9} to $2.19 \times 10^{-8} \text{ m}^2\text{s}^{-1}$.

The effect of pressurization come-up time at different pressurization rates was found to be a key factor affecting the final mass transfer. In this regard, an inverse linear relationship was seen between the come-up time and the final mass intake. Considering both pressure come-up and holding time, a comprehensive model was proposed to evaluate the mass intake as a function of pressurization rate, come-up time, final pressure level, and pressure holding time. Also, simplified linear models were introduced for certain industrial applications- such as freezing, blanching for thermal processing, and nutritional fortifications- regarding the final mass intake at constant pressure levels and different holding times.

A novel algorithm was developed to couple the identified Fickian mass transfer to Darcy's equation for unsaturated porous media. The coupling led to an approximation of transient flow-induced pressure gradient profile within the tissue. The numerical simulation was also conducted assuming various scenarios regarding the effective permeability of the tissue. A variable permeability function was also introduced using the Kozeny-Carman model to consider the pressure-induced inhomogeneity within the texture of the porous biomaterials. Along with the numerical solutions, analytical solutions to Darcy's law were used to approximate the permeability range as a function of the approximated flow front function.

The studied phenomenon was introduced as “high pressure impregnation (HPI)” in case of intentional addition of selected solutions into the porous media. In this regard, novel concepts were introduced to demonstrate the potential capabilities of HPI in the food industry. First, it was tried to study HPI as a means of impregnation of hydrocolloid solutions into porous media. In order to find a pressure resistant impregnant, physical stability of selected hydrocolloid solutions was evaluated. A novel methodology was proposed regarding the assessment of the effect of pressure on the thermoviscoelasticity of hydrocolloid fluids. The results showed a high pressure resistance of chitosan solutions. Thus, different levels of chitosan solutions were used as an impregnant phase to evaluate the effect of final mass intake as a function of chitosan concentration. The mass intake vs. chitosan concentration showed a quadratic relationship. In addition, the effect of impregnation of mentioned viscose fluids, as novel pre-treatment to frozen products, was studied. Impregnation of chitosan solution before freezing showed considerable reduction in drip loss and higher textural quality.

HPI was also introduced as a novel method of impregnation of W/O emulsions in various fruits. At first, the effect of pressure on emulsion stability parameters such as particle size, viscosity, and pH was studied. A pseudo-second order kinetics model was used to evaluate the time transient impregnation yield at 100 MPa. Moreover, the effect of various levels of oil/emulsifier combinations showed an inverse relationship between the oil percentage and final mass intake. Light microscopy and Fourier transform infrared spectroscopy was used to validate the migration of droplets into the tissue.

Microstructural analysis and subsequent image analysis techniques were used to demonstrate the flow migration within the tissue. Impregnation of dyes was introduced and conducted as a strong method of evaluation of microscopic flow paths. The obtained images were also used to identify endurance of porous structure of the medium during pressurization. In addition, impregnating food colors helped a visual understanding and verification of the numerical simulation of Fick’s law for fluid transfer within the tissue. The watershed algorithm was used to identify the flow paths inside the porous media. It was seen that flow paths were perpendicular to the surface at the outer layer of the geometry. Scanning Electron microscopy (SEM) was also conducted to evaluate the

textural changes after HPI. The results showed that the incompressibility of the impregnant helped the tissue to maintain its cellular arrangement. However, certain changes in the path directions and cell wall shrinkages occurred.

RÉSUMÉ

Dans cette étude, la migration des fluides dans les biomatériaux poreux tels que les fruits et les tissus végétaux a été caractérisée. Dans une grande partie de cette étude, diverses procédures de calcul ont été introduites pour modéliser ces phénomènes de transport.

Tout d'abord, la tendance à la migration des fluides a été entièrement évaluée dans la pomme fraîche comme milieu poreux sélectionné. Le transfert de masse a été surveillé à un niveau de pression de 100 à 600 MPa et de 0 à 30 min de temps de compression. Le transfert de masse, durant le temps de maintien de la pression, correspondait à la deuxième loi de Fick. En utilisant des méthodes inverses d'algorithmes d'estimation de paramètres, les valeurs de diffusivité calculées variaient de $4,38 \times 10^{-9}$ à $2,19 \times 10^{-8} \text{ m}^2\text{s}^{-1}$.

L'effet du temps de mise en place de la pression à différents taux a été considéré comme un facteur clé affectant le transfert de masse final. À cet égard, une relation linéaire inverse a été observée entre le temps de mise en place et l'apport massique final. Compte tenu de la pression et du temps de maintien de la pression, un modèle complet a été proposé pour évaluer l'apport de masse en fonction du taux de compression, du temps de mise en place, du niveau de pression finale et du temps de maintien de la pression. En outre, des modèles linéaires simplifiés ont été introduits pour certaines applications industrielles -telles que la congélation, le blanchiment comme traitement thermique, et l'enrichissement des aliments- concernant l'apport massique final à des niveaux de pression constants et à différents temps de maintien.

Un nouvel algorithme a été développé pour fusionner le transfert de masse Fickien identifié à l'équation de Darcy pour les milieux poreux non-saturés. Cette fusion a conduit à une approximation du profil de gradient de pression induit par l'écoulement transitoire dans le tissu. La simulation numérique a également été réalisée en supposant divers scénarios évaluant la perméabilité du tissu. Une fonction de perméabilité variable a également été introduite en utilisant le modèle de Kozney-Carman qui considère l'inhomogénéité induite par la pression dans la texture des biomatériaux poreux. Parallèlement aux solutions

numériques, des solutions analytiques à la loi de Darcy ont été utilisées pour estimer l'étendue de perméabilité indépendamment de l'estimation du front d'écoulement.

Le phénomène étudié a été introduit comme "imprégnation à haute pression" en cas d'addition intentionnelle de solutions sélectionnées dans les milieux poreux. À cet égard, de nouveaux concepts ont été introduits pour démontrer les capacités potentielles de l'IHP dans l'industrie alimentaire. Tout d'abord, a été étudiée l'IHP comme moyen d'imprégnation des solutions hydrocolloïdes dans les milieux poreux. Afin de trouver un imprégnant résistant à la pression, la stabilité physique des solutions hydrocolloïdes sélectionnées a été évaluée. Une nouvelle méthodologie a été proposée concernant l'évaluation de l'effet de la pression sur la thermoviscoélasticité des fluides hydrocolloïdes. Les résultats ont montré une résistance à la pression élevée des solutions de chitosane. Ainsi, différents niveaux de solutions de chitosane ont été utilisés comme phase imprégnante pour évaluer l'effet de l'absorption de masse finale en fonction de la concentration de chitosane. L'apport massique par rapport à la concentration en chitosane a montré une relation quadratique. L'imprégnation de ces fluides visqueux a été étudiée concernant un nouveau traitement préalable des produits surgelés. L'analyse de la texture et la perte d'égouttage d'échantillons congelés ont montré une amélioration de la texture lors de l'imprégnation de pommes fraîches avec un taux de chitosane de 0,5%.

L'IHP a également été introduit comme une nouvelle méthode d'imprégnation des émulsions eau/huile dans divers fruits. Au début, on a étudié l'effet de la pression sur les paramètres de stabilité de l'émulsion tels que la taille des particules, la viscosité et le pH. Un modèle de cinétique de pseudo-second ordre a été utilisé pour évaluer le rendement temporaire d'imprégnation transitoire à 100 MPa. En outre, l'effet de divers niveaux de combinaisons huile / émulsifiant a montré une relation inverse entre le pourcentage d'huile et l'apport massique final. La microscopie classique et la spectroscopie infrarouge à transformée de Fourier ont été utilisées pour valider la migration des gouttelettes dans le tissu.

L'analyse microstructurale et les techniques d'analyse d'image ont été utilisées pour démontrer la migration du flux dans le tissu. L'imprégnation des colorants a été introduite et réalisée comme une forte méthode d'évaluation des voies d'écoulement microscopiques.

Les images obtenues ont également été utilisées pour identifier l'endurance de la structure poreuse du milieu pendant la mise sous pression. En outre, l'imprégnation des couleurs alimentaires a permis une compréhension et une vérification visuelles de la simulation numérique de la loi de Fick pour le transfert de fluide dans le tissu. L'algorithme des lignes de partages des eaux a été utilisé pour identifier les chemins d'écoulement à l'intérieur du milieu poreux. On a vu que le chemin d'écoulement était perpendiculaire à la surface sur la couche extérieure de la forme. La microscopie électronique à balayage (SEM) a également été menée pour évaluer les changements de texture après HPI. Les résultats ont montré que l'incompétence de l'imprégnation a aidé le tissu à maintenir son arrangement cellulaire. Cependant, certains changements de direction et les rétrécissements de la paroi cellulaire ont été démontrés. Les observations ont également été utilisées pour obtenir les paramètres du modèle de porosité variable.

STATEMENT FROM THE THESIS OFFICE

According to the regulation of the Faculty of Graduate Studies and Research of McGill University, Guidelines for Thesis Preparation include:

Candidates have the option of including, as part of the thesis, the text of one or more papers submitted, or to be submitted for publication, or the clearly-duplicated text of one or more published papers. These texts must conform to the “Guidelines for Thesis Preparation” and must be bound together as an integral part of the thesis.

The thesis must be more than a collection of manuscripts. All components must be integrated into a cohesive unit with a logical progression from one chapter to the next. In order to ensure that the thesis has continuity, connecting texts that provide logical bridges between the different papers are mandatory.

The thesis must conform to all other requirements of the “Guideline for Thesis Preparation” in addition to the manuscripts.

As manuscripts for publication are frequently very concise documents, where appropriate additional material must be provided in sufficient detail to allow a clear and precise judgement to be made of the importance and originality of the research reports in the thesis.

In general, when co-authored papers are included in a thesis, the candidate must have made a substantial contribution to all papers included in the thesis. In addition, the candidate is required to make an explicit statement in the thesis as to who contributed to such work and to what extent. This statement should appear in a single section entitled “Contribution of Authors” as a preface of the thesis.

When previously published copyright material is presented in a thesis, the candidate must obtain, if necessary, signed waivers from the co-authors and publishers and submit these to the Thesis Office with the final deposition.

CONTRIBUTIONS OF AUTHORS

Several parts of this research have been presented at international conferences and submitted for publication in journals. Some authors have been involved in manuscripts. Their contributions are as follows:

Hamed Vatankhah is the PhD candidate who planned and conducted experiments, gathered and analyzed data, developed the models, wrote the computer codes, and wrote all manuscripts under the supervision of Professor Ramaswamy.

Dr. H.S. Ramaswamy is the thesis supervisor, under whose guidance the research was planned and conducted. In addition, submission of all the manuscripts was carried out by him after his careful correction, edition, and reviewing.

Dr. Ali Taherian offered technical advice and instructions regarding the rheological measurements, providing hydrocolloid gums and contribution in reviewing two manuscripts.

Dr. Abdolhamid Akbarzadeh provided scientific assistance regarding model developments, arranged access to scanning electron microscopy facilities, and reviewed the manuscripts submitted from chapter.6.

LIST OF PUBLICATIONS AND PRESENTATIONS

Peer-Reviewed Publications:

Vatankhah, H., Akbarzadeh, A. H., Ramaswamy, H. S. (2018). A Hybrid Fickian-Darcian Flow Model for High Pressure Impregnation of Fluids into Porous Biomaterials, *Biosystems Engineering*, 166, 200-209.

Vatankhah, H., Taherian, A. R., Ramaswamy, H. S. (2018). High-Pressure Induced Thermo-Viscoelasticity and Dynamic Rheology of Gum Arabic and Chitosan Aqueous Dispersions Research paper LWT - Food Science and Technology, *LWT-Food Science and Technology*, 89, 291-298.

Vatankhah, H., Ramaswamy, H. S. (2018). High Pressure Impregnation (HPI) of Apple Cubes: Effect of Pressure Variables and Carrier Medium, *Food Research International*. (under review).

Vatankhah, H., Ramaswamy, H. S. (2018). High Pressure Impregnation of Emulsions into Selected Fruit Tissues: Mass Transfer Dynamics and Emulsion Stability. (*Prepared for submission*).

Vatankhah, H., Ramaswamy, H. S. (2018) Challenges in High pressure impregnation of functional compounds: A review. (*Prepared for submission*).

Vatankhah, H., Ramaswamy, H. S., (2017). Dynamics of fluid migration into porous solid matrix during high pressure treatment. *Food and Bioproducts Processing*, 103, 122-130.

Other Relevant Works Published During PhD Studies:

Hussain, R., Singh, A., **Vatankhah, H.**, & Ramaswamy, H. S. (2017). Effects of locust bean gum on the structural and rheological properties of resistant corn starch. *Journal of Food Science and Technology*, 54(3), 650-658.

Hussain, R., **Vatankhah, H.**, Singh, A., & Ramaswamy, H. S. (2016). Effect of high-pressure treatment on the structural and rheological properties of resistant corn starch/locust bean gum mixtures. *Carbohydrate Polymers*, 150, 299-307.

Conference Presentations:

Vatankhah, H., Taherian, A. R., Ramaswamy, H. S. Evaluation and modeling of thermoviscoelasticity of high hydrostatic pressure-induced semi-concentrated aqueous gum Arabic and chitosan solutions. Northeast Agricultural and Biological Engineering Conference (NABEC), July 2016, Orono, ME, USA.

Vatankhah, H., Ramaswamy, H. S. Effect of Pressurization Rate on Fluid Transfer into Porous Media during High Pressure Processing. Northeast Agricultural and Biological Engineering Conference (NABEC), July 2017, Groton, CT, USA.

Vatankhah, H., Ramaswamy, H. S., Mass transfer modeling during high pressure impregnation, Canadian Institute of Food Science and Technology (CIFST), May 2018, Niagara-on-the-Lake, ON, Canada.

Vatankhah, H., Ramaswamy, H. S., Hybrid modeling of High pressure impregnation into porous biomaterials, CSBE/SCGAB Technical conference, July 2018, Guelph, ON, Canada.

Dedicated to

My lovely parents Kamidreza and Soheila;

my brother, Milad; and my sister, Atefeh

ACKNOWLEDGEMENTS

I would like to express, my deepest gratitude to my supervisor to Dr. Ramaswamy because of his limitless supports, valuable guidance, and his encouragement during my program. He taught me how to be passionate about what I am doing, and he believed in me from the early days of my studies. I will never forget all his kindness, and I will always feel proud of being his student. Besides the scientific career, I ought to take my hat off to him because of all unbelievable life lessons he taught me.

I would like to thank Dr. V. Yaylayan, the Department Chair, for his support. Also, I truly appreciate my research and defense committee members, Dr. Valerie Orsat, and Dr. Ashraf Ismail, Dr. Stephane Bayen, and Dr. Ian Strachan for their constant helps and meticulous comments.

I would extend my appreciation to Dr. Ali Taherian for freely sharing his scientific and spiritual support from the first day of the beginning of my studies at McGill University. He put his best efforts to teach me how to overcome any toughness during my life.

My thanks are also extended to Dr. Hamid Akbarzadeh for his scientific advice and true motivations. He welcomed me in his research group and did not hesitate to help me at any time needed.

I would thank Mr. Ebrahim Noroozi and Dr. Reza Zareifard for their useful comments and support. I also would like to thank all the helpfulness and supports by our department secretaries Ms. Leslie Ann LaDuke and Ms. Patricia Singleton.

My friends were one of the most valuable assets I gained during my studies. I would like to extend my regards to my colleagues in food processing group: Dr. Raza Hossein, Ms. Dalia John, Mrs. Bhakti Shinde, Dr. Yamei Ren, Mr. Prasant Prusty, Dr. Neda Maftoonazad, Dr. Anubhav Singh, Dr. Anika Singh, Dr. Derek Wray, Dr. Ajaypal Singh, Dr. Cristina Guimarães, Ms. Mengting Xu, Mr. Mulugeta Taemir, Mr. Siddhesh Salunke,

Mr. Prabhjot Singh, Mr. Saurabh Ner, Ms. Jia You, Dr. Meiyang Yang, Dr. Rodrigo Cavalcanti, Mrs. Fatemah Alsalman, Ms. Hanieh Golpira, Ms. Chunfang Wang and Mrs. Kshitija Pawar. I am so thankful to Mr. Reza Sarhangpour and Mrs. Amal Mohamed for their technical supports during experiments. Thank you all for your support and beautiful days we spent together.

I also wish to convey my profound gratitude to Mr. Salim El-Hage, Mrs. Katia Aoun, and Ms. Sabine El-Hage for their incredible support during all these hard days. They were always passionate about my progression and helped unbelievably during all years of my student life at McGill university.

This thesis is dedicated to my beautiful, lovely parents, Hamidreza and Soheila. Words cannot express my gratitude and appreciation to you. I know I can never make it up to you. During all these years thinking about your happiness after my graduation was the most influential and touching picture in my mind. I wish my graduation would bring a smile on your face. That's all I need. You mean everything to me.

TABLE OF CONTENTS

ABSTRACT.....	II
RÉSUMÉ	V
STATEMENT FROM THE THESIS OFFICE.....	VIII
CONTRIBUTIONS OF AUTHORS.....	IX
LIST OF PUBLICATIONS AND PRESENTATIONS.....	X
ACKNOWLEDGEMENTS	XIII
TABLE OF CONTENTS	XV
NOMENCLATURE.....	XXIII
LIST OF FIGURES.....	XXV
LIST OF TABLES	XXIX
CHAPTER 1: INTRODUCTION	1
1.1 Objectives.....	1
1.1.1 Overall objectives	3
1.1.2 Specific objectives	3

CHAPTER 2: LITERATURE REVIEW 5

2.1 Historical Overview 5

2.2 Principles of Processing 5

2.3 High pressure processing of fruits and vegetable products 10

2.4 Fruit/ plant tissues as Porous media 17

2.5 Apple as a porous medium 17

2.6 Mass transfer into porous media 19

 2.6.1 Mass Transfer modeling 20

 2.6.2 Fickian Mass transfer 25

 2.6.3 Diffusivity 25

 2.6.4 Hydrodynamic mechanism of flow through a pore 26

 2.6.4.1 Representative Elementary Volume (REV) 29

 2.6.4.2 Saturation model 30

 2.6.4.3 Darcy’s equation 30

 2.6.4.4 Unsaturated Darcian Flow 31

 2.6.4.5 Permeability 32

2.7 Microstructural studies of mass transfer 32

Preface to chapter 3 34

**CHAPTER 3: STUDYING BEHAVIOUR AND DYNAMICS OF FLUID
MIGRATION INTO POROUS MATRIX DURING HIGH PRESSURE
TREATMENT 35**

3.1 Abstract 35

3.2	Introduction	35
3.3	Theory/Calculations	38
3.4	Problem definition using Fick’s second law	38
3.5	Experimental Validation	41
3.5.1	Sample Preparation	41
3.5.2	High pressure processing	41
3.5.2.1	Impregnation of fresh and blanched texture	42
3.6	Results and Discussion.....	44
3.6.1	Estimation of X_{eq}	44
3.7	Estimation of Mass Diffusivity	46
3.7.1	Linear Model.....	51
3.7.2	Impregnation of fresh and blanched texture	53
3.8	Conclusions	55
	Preface to Chapter 4.....	56

CHAPTER 4: MODELING AND CHARACTERIZATION OF THE EFFECT OF PRESSURIZATION RATE, COME-UP TIME AND HOLDING TIME ON PRESSURE DRIVEN-FLUID TRANSFER INTO POROUS MEDIA 57

4.1	Abstract	57
4.2	Introduction	57
4.3	Material and Methods	59

4.3.1	Sample Preparation	59
4.3.2	High pressure processing	59
4.3.3	Calculation of total mass intake ratio.....	61
4.3.4	Modeling and mass diffusivity estimation using Levenberg-Marquardt algorithm.....	61
4.4	Results and discussion.....	62
4.4.1	Effect of pressurization rate on AA impregnation.....	62
4.4.2	Mass transfer during holding time	65
4.4.3	Modeling of HPI during the pressure come-up time	66
4.4.4	Modeling HPI during pressure holding.....	67
4.4.5	A coupled model for the entire process	68
4.5	Conclusion.....	69
	Preface to Chapter 5.....	71
 CHAPTER 5: MICROSTRUCTURAL EVALUATION OF HIGH PRESSURE IMPREGNATION OF BIOMATERIALS		72
5.1	Abstract	72
5.2	Introduction	72
5.3	Material and methods	73
5.3.1	Light microscopy	73
5.3.2	Scanning electron microscopy (SEM)	74
5.3.3	Image processing	74
5.3.4	Numerical simulation.....	74

5.4	Results and Discussion.....	75
5.4.1	SEM analysis of the samples	75
5.4.2	Observation of the flow paths in light microscopy and SEM.....	76
5.4.3	Numerical simulation and image processing	77
5.5	Conclusion.....	80
	Preface to Chapter 6.....	81
	CHAPTER 6: HYBRID FICKIAN-DARCIAN FLOW MODEL FOR HIGH PRESSURE IMPREGNATION OF FLUIDS INTO POROUS BIOMATERIALS.....	82
6.1	Abstract	82
6.2	Introduction	82
6.3	Theory/calculation.....	85
6.3.1	Moisture Diffusion.....	85
6.3.2	Representative Volume Element (RVE).....	86
6.3.3	Saturation model:	86
6.3.4	Unsaturated Darcian Flow	86
6.3.5	Numerical Simulation	87
6.3.6	Analytical Darcian model and lumped permeability estimation.....	89
6.4	Experimental Verification.....	91
6.4.1	Model Application	91
6.4.2	Image Analysis.....	91

6.5	Results and Discussions	92
6.6	Conclusions	102
	Preface to chapter 7	103
 CHAPTER 7: PHASE STABILITY AND MASS TRANSFER		
EFFICIENCY OF IMPREGNATION OF VISCOS FLUIDS INTO FRUIT		
TISSUE..... 105		
7.1	Abstract	105
7.2	Introduction	106
7.3	Materials and Methods.....	109
7.3.1	Sample preparation	109
7.3.2	High pressure processing (HPP).....	109
7.3.3	Rheological measurements	110
7.3.3.1	Dynamic oscillation tests.....	110
7.3.3.2	Flow rheology tests.....	110
7.3.3.3	Applicability of Cox–Merz rule between steady shear and oscillation data....	110
7.3.3.4	Temperature sweep tests.....	111
7.3.4	Impregnation of the selected solution into the apple tissue	111
7.3.5	Freezing.....	112
7.3.6	Texture profile analysis (TPA)	112
7.3.7	Drip loss measurement after freezing	112
7.4	Results and discussion.....	112
7.4.1	Flow tests	112
7.4.2	Dynamic oscillation tests	115

7.4.3	Cox-Merz model	117
7.4.4	Thermo-viscoelasticity	118
7.4.4.1	Temperature sweep tests	118
7.4.4.2	Modeling	120
7.4.4.3	Compatibility analysis	122
7.4.5	HPI of Chitosan	125
7.4.6	Proposed model for HPI of non-Newtonian fluids	125
7.4.7	Texture analysis	126
7.4.8	Drip loss	127
7.5	Conclusion	128
	Preface to Chapter 8	129

CHAPTER 8: HIGH PRESSURE IMPREGNATION OF EMULSIONS INTO SELECTED FRUIT TISSUES: MASS TRANSFER DYNAMICS AND EMULSION STABILITY 130

8.1	Abstract	130
8.2	Introduction	130
8.3	Materials and methods	133
8.3.1	Emulsion Preparation	133
8.3.2	Emulsion stability factors after HPP	133
8.3.3	Flow rheology tests	134
8.3.4	Particle size distribution	134
8.3.5	pH measurement	134
8.3.6	HPI of emulsions into fruit tissue	135

8.3.6.1	Sample preparation for HPI.....	135
8.3.7	HPI operation	135
8.3.8	Emulsion intake calculation.....	135
8.3.9	Light microscopy	135
8.3.10	Spectroscopic Verification of HPI of Emulsions.....	136
8.4	Results and discussions	136
8.4.1	Emulsion stability	136
8.4.2	Mass Intake data	141
8.4.3	Mass intake modeling	143
8.4.4	Effect of emulsifier level	144
8.4.5	Microstructure studies.....	147
8.4.6	Spectrophotometric evaluation of HPI.....	151
8.5	Conclusion.....	152
 CHAPTER 9: GENERAL CONCLUSIONS, CONTRIBUTION TO THE KNOWLEDGE AND RECOMMENDATIONS		153
9.1	General conclusions	153
9.2	Contribution to knowledge.....	155
9.3	Recommendations for future research	156
 REFERENCES.....		157

NOMENCLATURE

η'	viscose components of dynamic
η''	elastic components of dynamic
G'	loss modulus
$\dot{\gamma}$	oscillatory shear rate (Hz)
Δ	gradient
α	elasticity (Pa)
ε	Porosity
J	sensitivity coefficient
K	intrinsic permeability (m ²)
L	length (m)
n	flow behavior index
q	volumetric fluid flow (m ³ /s)
Z	z-axis
β	constant
δ	constant
η	viscosity (Pa.s)
Λ	damping parameter
ξ	constant
σ	shear stress (Pa)
τ	Shear stress (Pa)
Ω	diagonal
F	fractal coefficient
Γ	Constant
\mathcal{K}	consistency coefficient
Π	constant
A	area (m ²)
C	specific heat (J/kg. °K)
CH	compression heat (°C/100MPa)
D	diffusion coefficient (m ² s ⁻¹)
G''	elastic modulus
I	integral
M	mass intake (kg kg ⁻¹)
MR	total moisture ratio
P	pressure (MPa)
R	apparent compression ratio
S	saturation
T	temperature (°K)
V	volume (m ³)

W	displacement (m)
X	mass intake (kg kg ⁻¹)
Y	pore diameter (m)
d	diameter (m)
f	flow front
i	number of iterations
k	Permeability (m ²)
m	flow front speed (m/s)
r	Actual compression ratio
$\tan\delta$	loss tangent
z	pore length (m)
β	thermal expansivity (K ⁻¹)
μ	viscosity (Pa.s)
ρ	density (kg/m ³)
t	Time (s)
φ	shift factor
ω	shear rate (1/s)
subscripts	
F	fluid
H	enthalpy (kJ)
Tot	total
atm	atmosphere
b	bulk
c	capillary
$comp$	compression
$decomp$	decompression
eff	effective
eq	equilibrium
i	initial
int	intrinsic
mat	matrix
p	pressure
pl	plate
rel	relative
w	water
x	x-axis
Superscript	
*	complex

LIST OF FIGURES

Fig. 2.1. Pressure-Temperature history during high pressure processing (Gupta and Balasubramaniam, 2012).....	7
Fig. 2.2. High pressure by direct (top) and indirect (bottom) compression generation of the pressure-transmitting medium (Mertens 1995).....	8
Fig. 2.3. Some of commercially available high pressurized products.....	11
Fig. 2.4. SEM micrograph of intercellular porous media (Fito, 1994).....	19
Fig. 2.5. Typical values of water vapor diffusivity in foods (Guillard et al., 2013).....	26
Fig. 2.6. The Hydrodynamic mechanism in an ideal pore (Fito, 1994).....	28
Fig. 2.7. Values of X_v from Eq. (2.9) for different P_r and R values (Fito, 1994).....	29
Fig. 3.1. High pressure apparatus used for the experimental observation.....	43
Fig. 3.2. The initial mass intake ratio at the beginning of pressure holding time.....	46
Fig. 3.3. Mass transfer model fitted to experimental mass intake data as a function of holding time. (a) 200 MPa, (b) 300 MPa, (c) 400 MPa, and (d) 500 MPa pressure level of holding time.....	49
Fig. 3.4. Application of developed linear model for mass intake-holding time data for (a) 100 MPa and (b) 600 MPa pressurizing condition.....	52
Fig. 3.5. Mass intake data of blanched and unblanched apple cubes at 300MPa for 30 min of holding time.....	54
Fig. 4.1. The experimented P-t profiles using 100, 150, 200, 300 MPa/min pressurization rate.....	60
Fig. 4.2. The Mass intake -Pressurization time of model system containing 1% aqueous ascorbic acid solution and 1.728 mm ³ apple cubes at (a) 100 MPa/min, (b) 150 MPa/min (c) 200 MPa/min and (d) 300 MPa/min. Error bars represent standard deviation.....	63

Fig. 4.3. Mass intake during HPP of 1% aqueous ascorbic acid solution in 1.728 mm³ apple cubes while reaching 300MPa and 600MPa at 100, 150, 200, and 300 MPa/min pressurization rate. Error bars represent standard deviation.....64

Fig. 4.4. Semi-logarithmic plot of Crank’s formula for HPP at (a) 100MPa, (b) 300 MPa, and (c) 600 MPa during holding time up to 30 min. X(t), X₀, and X_{eq} indicate the mass intake (kg/kg) of the model system after t seconds of pressure holding, initial mass intake (kg/kg), and predicted equilibrium mass intake (kg/kg), respectively.....66

Fig. 5.1. SEM images of (a) untreated (b) impregnated for 15 min at 300MPa.....75

Fig. 5.2. Light microscopy illustration of apple tissue impregnated for 15 min at 300MPa. The samples are treated and fixed using toluidine blue and ethanol right after the impregnation. Yellow arrows indicate the void intercellular space (pores).....76

Fig. 5.3. SEM images of (a) untreated (b) impregnated for 15 min at 300MPa.....77

Fig. 5.4. Illustration of mass transfer using image processing and numerical simulation for samples held for 5min (a) and 15 min (b) under 200 MPa. Indices 1, 2, and 3 indicate the RGB scale photos of samples, contour of grayscale of the samples, and contour of samples, contour of grayscale of the samples, and contour of infused mass, respectively.....78

Fig. 5.5. The light microscopy of apple tissues impregnated with toluidine blue (0.1% w/w): (a) a color image of the 100 μm thickness slice (a) the modeled flow paths (in green) within the tissue suing a watershed algorithm. The image is coupled with the binary structure of the color image.....79

Fig. 6.1. Process diagram of the calculation procedure for the simulation of Fickian-Darcian model.....90

Fig. 6.2. Evolution of relative blueness as a representation for the diffusion of fluid into the apple as a porous biological tissue under high pressure. The uptake of samples was measured at (a) 0 min, (b) 2 min, (c) 5 min, (d) 10 min (e) 15min of pressure holding time. The original images (RGB scale) of the samples are embedded in the figure.....93

Fig. 6.3. SEM images of cuts of untreated (left) and impregnated samples for 15 min at 100 MPa (right) The arrows represent pressure-driven flow currents during HPP in a corner of the apple cubes (The whole cube is not shown).....95

Fig. 6.4. Contour of pressure drop in the middle plane of samples at different pressure holding times: 5, 10, 12, and 15 (min) at 100 MPa processing pressure.....97

Fig. 6.5. Pressure profile at the center of the apple cubes during the HPI under 100 MPa pressure level considering: (A) presents the intrinsic permeability function and (B) presents the corrected relative permeability function.....98

Fig. 6.6. Calculated pressure profile on the half thickness line ($y= 0.5\text{mm}$) of the apple model systems for a range of diffusivity values during HPP at 100-500 MPa. Letters: A, B, C represent Diffusivity = 10^{-7} , 10^{-8} , and $10^{-9} \text{ m}^2 \text{ S}^{-1}$, respectively.....99

Fig. 6.7. lumped permeability estimation based on experimental data: (a) The experimental measurement (●) and linear regression of infusing fluid front as a function of time; (b) the log-log illustration of lumped permeability estimation in a range of pressure drop between 100 to 10000 Pa according to the analytical solution of Darcian flow.....101

Fig. 7.1. Storage modulus as a function of the frequency at CH-I (a), CH-II (b), GA-I (c), GA-II (d), and GA-III (e) after pressurization at 200-600 MPa for 30 min.....116

Fig. 7.2. Storage moduli during temperature sweep tests after pressure treatment of (a) GA-I, (b) GA-II, (c) GA-III, (d) CH-I, and (e) CH-II at 200, 400, and 600 MPa for 30 min....120

Fig. 7.3. The gradient of phase shift ($\Delta\phi$) vs. temperature semi-log graphs of Viscoelastic compatibility of samples after HP treatment at 200, 400, 600 MPa. Letters indicate as following: (a) GA-I, (b) GA-II, (c) GA-III, (d) CH-I, and (e) CH-II.....124

Fig. 7.4. The mass intake data (kg/kg) for impregnation of 0 % (water), 0.5%, 1%, 2%, 4% aqueous solution of chitosan into apple tissue after pressurization for 20 min at 100MPa.....125

Fig. 7.5. The hardness of the apple cubes impregnated with 0% to 4% CH (green) immediately after HPI and (blue) after freezing and thawing of the HPI apple cubes. The HPI conditions: 20min at 100MPa.....127

Fig. 7.6. The drip loss (%) after freezing (-18 °C, 10h) and thawing (23 °C, 2h) apple cubes impregnated (20min at 100MPa) with 0% to 4% CH.....128

Fig. 8.1. Effect of HPP (100 MPa for 20 min) on apparent viscosity of different emulsions.....137

Fig. 8.2. Effect of high pressure (100 MPa, 20 min) on particle size distribution. The blue and red graphs are related to pressurized and unpressurized samples. The letters belong to (a) emulsion I, (b) emulsion II, (c) emulsion III, (d) emulsion IV.....140

Fig. 8.3. Mass intake data of impregnation of emulsion I into apple (a), pear (b), asian pear (c), melon (d), and strawberry (e). The HPI was done in different holding times including 0, 2, 5, 10, 15, and 20 min at 100 MPa.....143

Fig. 8.4. Effect different of levels of oil/emulsifier(s), water, and pure oil after HPI (100MPa, 20min) on mass intake percentage into selected fruits.....146

Fig. 8.5. The microstructural demonstration of cellular tissue of impregnation of emulsion I into selected fruits for 20 min at 100 MPa. The images belong to strawberry (a,b), pear (c,d), melon (e,f), asian pear (g,h), and apple (i,j). the right and left side images are taken at 80X and 40X magnification.....150

Fig. 8.6. FTIR spectra of selected fruits after impregnation of emulsion IV into for 20 min at 100 MPa.....152

LIST OF TABLES

Table 2.1. Some of mass transfer models used in food engineering (Guillard et al., 2013).....	23
Table 3.1. The parameters related to Peleg’s equation Θ_1 and Θ_2 , measured initial mass intake (X_0), and estimated equilibrium mass intake (X_{eq}) parameters.....	45
Table 3.2. The estimated effective diffusivity values using classic and trust region method.....	47
Table 3.3. The calculated parameters regarding the linear model of mass intake during HPI at selected pressure levels.	53
Table 4.1. Estimated model parameters during HPP at different pressurization rates. φ is the estimated apparent porosity, and k represents the rate constant.....	67
Table 4.2. The estimated effective diffusivity values during holding time at high pressure operation levels of 100, 300, and 600 MPa using Levenberg-Marquardt optimization algorithm.....	68
Table 7.1. Power law model parameters of ascending (n_1 , K_1) and descending (n_2 , K_2) shear sweeps of 6% GA, 15% GA 20% GA, 2% CH and 4% CH after pressurization at 200, 400, and 600 MPa for 30 min (mean \pm standard deviation, $n = 2$).....	114
Table 7.2. The shift function parameters regarding the Cox-Merz rule for GA-I, GA-II, GA-III, CH-I, and CH-II after pressurization at 200, 400, and 600 MPa for 30 min.....	118
Table 7.3. Exponential model parameters of temperature sweeps tests (22-70-22 °C) loss modulus during cooling periods (letters A, B, C, D are related to Eq. 7.5 and letters a1, b1, c1, a2, b2, and c2 are calculated according to Eq. 7.6.....	121
Table 8.1. Effect of high pressure on pH and particle mean diameter of selected emulsions.....	138

Table 8.2. Estimated HPI mass transfer parameters based on a pseudo-second order model (Eq. 8.2) of impregnation of Emulsion I into selected fruits during 0 to 20 min pressure holding at 100 MPa.....144

CHAPTER 1

INTRODUCTION

The growing demand for obtaining extended shelf-life foods with desirable sensory characteristics has been the reason for the development of many nascent ‘non-thermal treatments for foods such as irradiation, light pulse treatment, usage of natural bio-preservatives, and high pressure processing (HPP)’ (Aymerich et al., 2000). In this category of processing techniques, the processing is carried out at relatively lower temperatures which leads to quality maintenance and prevent thermal denaturation and degradation of various components of foods.

High pressure processing is a way to have minimally processed foods in which the nutritional quality and fresh-likeness are retained as well as achieving the microbial and chemical safety (Zhu et al., 2003). The primary goal regarding HPP has been implementing a process to result in a certain level of microbial destruction. HPP, as one of the best food processing innovations of the last 50 years, is deemed as a “natural” preservative or ‘clean label technology’ for processed foods since no chemical or heat treatment is involved. Although, the cost of equipment and novelty of technology are the major problems for its commercialization (Yordanov, and Angelova 2010).

In industrial processing, the food is usually pressurized at 300-700 MPa for 3-5 min at either room or refrigerated temperature (Mertens 1995). During HPP, microbial destruction mostly happens in vegetative microorganisms (Balasubramaniam et al., 2008) which is due to the structural changes at the cell membrane or inactivation of enzyme systems responsible for controlling metabolic actions (Knorr et al., 2006).

Many food categories such as vegetables, meats, fruit juices, purees, fish and seafood, and dairy products, have been commercially processed by HPP by different companies. Consequently, HPP has been studied and reviewed in various areas of technological, microbial, (bio)chemical, energy consumption and environmental issues. (Borda et al., 2013).

In other words, most of the research in this field has been dedicated to biological responses of the bacterial load under high pressure. Such studies have mostly helped to understand the reasons behind microbial destructions. Also, kinetics of destruction of microbial spores have been extensively studied (Hygreeva & Pandey 2016; Su et al., 2014; Ramaswamy & Shao 2010). Furthermore, a part of research in HPP has been focused on the effect of high pressure on the chemical structure of food components. Specifically, the susceptibility of proteins to high pressure would lead to enzymatic inactivation and denaturation of other proteins (Terefe et al., 2014). The third category of the research has also been dedicated to the effect of high pressure on the physical properties of food materials. Specifically, texture evaluations have been done to study the textural changes in the solid food products (Sila et al., 2008; Zhu et al., 2004). In addition, rheological evaluations have also been conducted to characterize the effect of high pressure on a wide range of hydrocolloid solutions (Hussain et al., 2016). However, the physical studies have gone less further to study multiphase food systems, mainly including both solid and fluid phases.

A wide range of our food comprises of plant-based biomaterials. In most plant products including fruits and vegetables, the parenchyma tissue contains intercellular spaces mostly filled with vapor and air. In such tissues, there is an anisotropic distribution of cells and pores (Reeve, 1953, Boukouvalas et al., 2006, Ting et al., 2013). Due to their specific porous structure, certain processing limitations and considerations exist. In fact, this void space can be a suitable medium to allow fluids enter the tissue. This phenomenon is triggered by a pressure difference between the confined medium and the confining fluid. As stated, high pressure processing could provide a considerable pressure over a food system. Thus, having multiphase systems involving a porous biomaterial and liquid phase would lead to fluid flow into the porous structure. This issue might significantly affect the final pressure treated product. In addition, one can take advantage of using the fluid as a carrier of certain products and intentionally conduct the mentioned fluid transport operation on the porous biomaterials. In the past several years, high pressure infusion of acids, antioxidants, firming agents has been investigated as a pre-treatment to other food processing techniques such as thermal processing (Rastogi, Nguyen, & Balasubramaniam, 2008; Rastogi, Nguyen, Jiang, & Balasubramaniam, 2010; Tola, & Ramaswamy, 2013).

However, the above-mentioned research works mainly cover the practical outcome of the technique and do not cover the physical aspect of the transport phenomenon.

Studying such phenomena is difficult due to the lack of access to the sample –and even the chamber medium- during the processing due to the ultrahigh pressures involved in the chamber. In addition, the common sensors to measure the pressure and concentration are also not suitable to be used in HPP due to the fact they cannot be sealed within an intact biomaterial tissue. As a result, the limited measurable parameters would only allow to use the physical models and develop computational ways to describe and characterize the phenomenon. This type of studying flow inside porous tissues is different from similar practices in hydrology, mechanics and oil engineering. Because studying a biomaterial is more complex due to a dissimilar scale and physio-chemical response of the porous matrix. Further, characterization of this technique would definitely help to optimize the process as an efficient way of introduction of fluids to porous biomaterials as well and to take advantage of the functional properties of the fluid phase.

1.1 Objectives

Thus, the above-mentioned pressure-driven flow under high pressure could be an important transport phenomenon while high pressure processing of fruits and vegetables when soaked in liquids. A deep literature search indicates that there are no specific studies to physically describe and characterize such flows into biomaterials under high hydrostatic pressures. This type of research includes enough knowledge of porous media, mass transfer, and mutual interaction of porous media and confined porous biomaterials. Thus, in this study, we tried to define our overall and specific objectives as:

1.1.1 Overall objectives

Characterization of pressure-driven mass transfer during high pressure processing of food systems containing porous media confined in a fluid phase.

1.1.2 Specific objectives

1- Studying dynamics of fluid migration into porous media under steady high pressure conditions and describing the important mass transfer variables and parameters involved in high pressure impregnation.

2- Modeling and characterization of the effect of pressurization rate, come-up time and holding time on pressure driven-fluid transfer into porous media.

3- Evaluation of Hybrid Fickian-Darcian flow model for high pressure impregnation of fluids into porous biomaterials.

4- Microstructural evaluation of high pressure impregnation of biomaterials.

5- Utilization of high pressure impregnation in food processing.

CHAPTER 2

LITERATURE REVIEW

2.1 Historical Overview

Although HPP has been used for most of the food categories, it was first used for microbial destruction of milk in the USA. The process lasted 10 minutes and a 5-6 microbial logarithmic destruction was reported (Hite 1899). The first notable attempt to commercialize the HPP was carried out in a Japanese fruit jam industry in the 1990s. About 160 HPP based industries had been known by the end of 2010. The units could be installed with 0.5-2.5 million US \$ which is dependent on the function and level of automation (Mújica-Paz et al., 2011).

2.2 Principles of Processing

High pressure processing has many advantages over other processing techniques. Among these advantages, two of them are very general and attractive; first, HPP is a non-mass/time-dependent 'process with short treatment time. Second, it is also not dependent on equipment and geometrical characteristics of foods. The mentioned distinctive features of HPP has also enabled industries to feel free and secure of performing changes as a result of new marketing demands or equipment renewal in their industrial units (Pérez Lamela & Torres 2008a, b).

An HPP system includes several important parts such as the processing vessel and its closure(s), pressure-generation system, temperature monitoring device and material handling system. The most important part of HPP is the vessel in which all the food processing is done. Thus, having the well designed and dimensionally stable vessel could be critical. Especially, in case the system fails, the vessel should be such safe that the failure would happen first with a leak rather than a fracture (Mertens 1995). During HPP, the pressure is transmitted by a fluid in a uniform and instant way. Glycol solutions, silicone oil, sodium benzoate solutions, ethanol solutions, inert gases, castor oil or even plain water, are the common pressure-transmitting fluids (Borda et al., 2013).

The HPP can be done in the form of a) batch processing, suitable for pre-packed foods, b) semi-continuous processing, having an alternative compression and decompression on more than one vessel, or c) continuous, done in long stainless-steel coil pipes (Mertens 1995). In this form, the fluid enters the vessel by a hydraulic pump and, consequently, the processed product releases by an outlet valve in a continuous way. However, the continuous HPP is not available in a readily commercial system. (Gupta & Balasubramaniam, 2012).

The behavior of under pressure foods could be assessed according to three basic principles:

a) Le Chatelier's principle: implying on the enhancement of any reaction, conformational change, and phase transition with a decrease in volume (Cheftel 1995, Farkas & Dallas 2000).

b) The principle of microscopic ordering: indicating an increase in degrees of ordering of molecules of a given substance as a function of the increase in pressure and as a result, antagonistic forces of pressure and temperature on chemical reactions and molecular structures (Balny & Masson 1993).

c) Isostatic principle: expressing the uniform compression of food products in all directions.

As a result, the pressurization would act independently of the size and shape of the foods (Cheftel 1995, Farkas & Dallas 2000).

To process, pre-packaged foods are loaded into the vessel filled with the pressure transmitting fluid. It is recommended to use water as the medium which is more compatible with foods (Earnshaw 1996). Afterwards, the pump will increase the pressure of the chamber. When the vessels reach the desired pressure, the holding time starts, and no more energy is used. The last step is the decompression which is done by releasing the pressurized media. (Farkas & Dallas 2000). The final stage of the process is unloading the vessel and storing the processed food in a recommended way (Yordanov & Angelova 2010). Figure 2.1 shows the typical change in pressure and temperature conditions of an HPP.

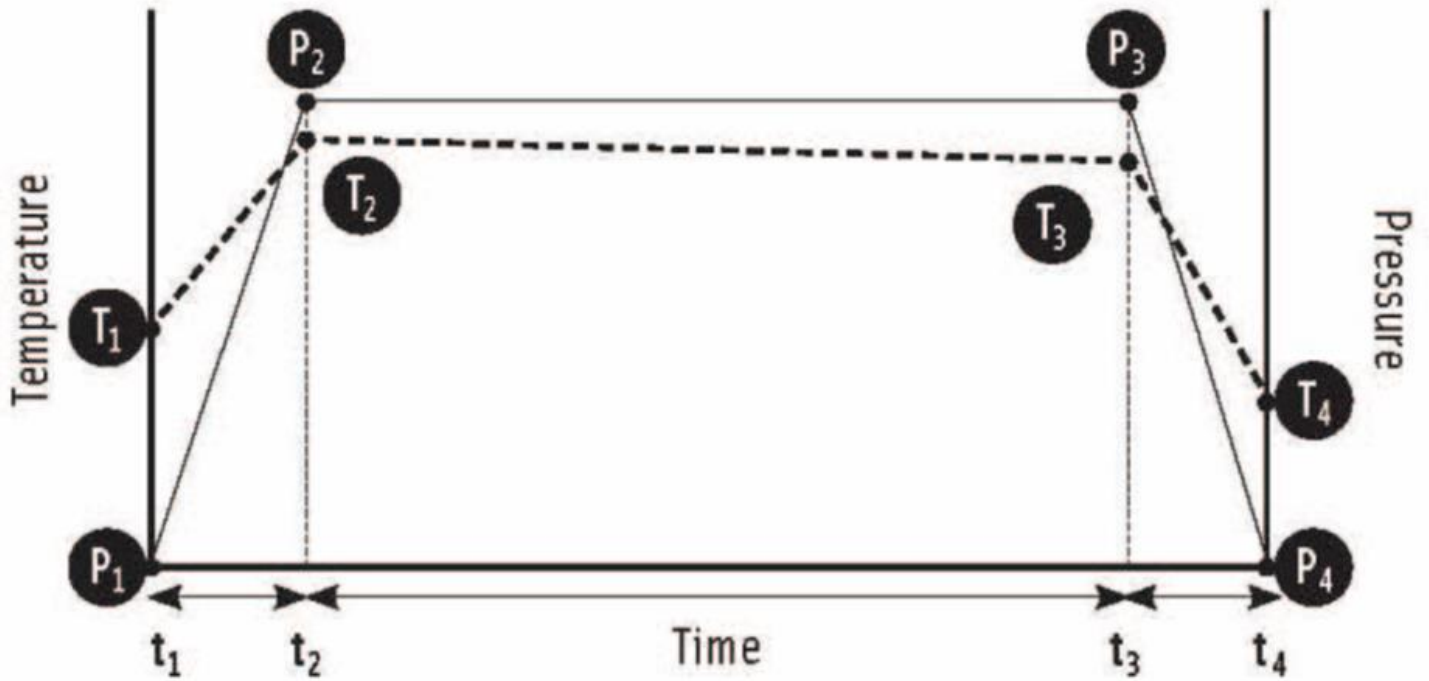


Fig. 2.1. Pressure-Temperature history during high pressure processing (Gupta & Balasubramaniam, 2012).

The high pressure, imposed on the vessel, could be brought into being in three ways: Direct compression: it is a fast compression method in which pressurization is done by a low-pressure pump in a piston (Figure 2-2).

Indirect compression: in this method, a pressure fluid is pumped by a high-pressure intensifier from a reservoir to a closed vessel (Fig. 2.2).

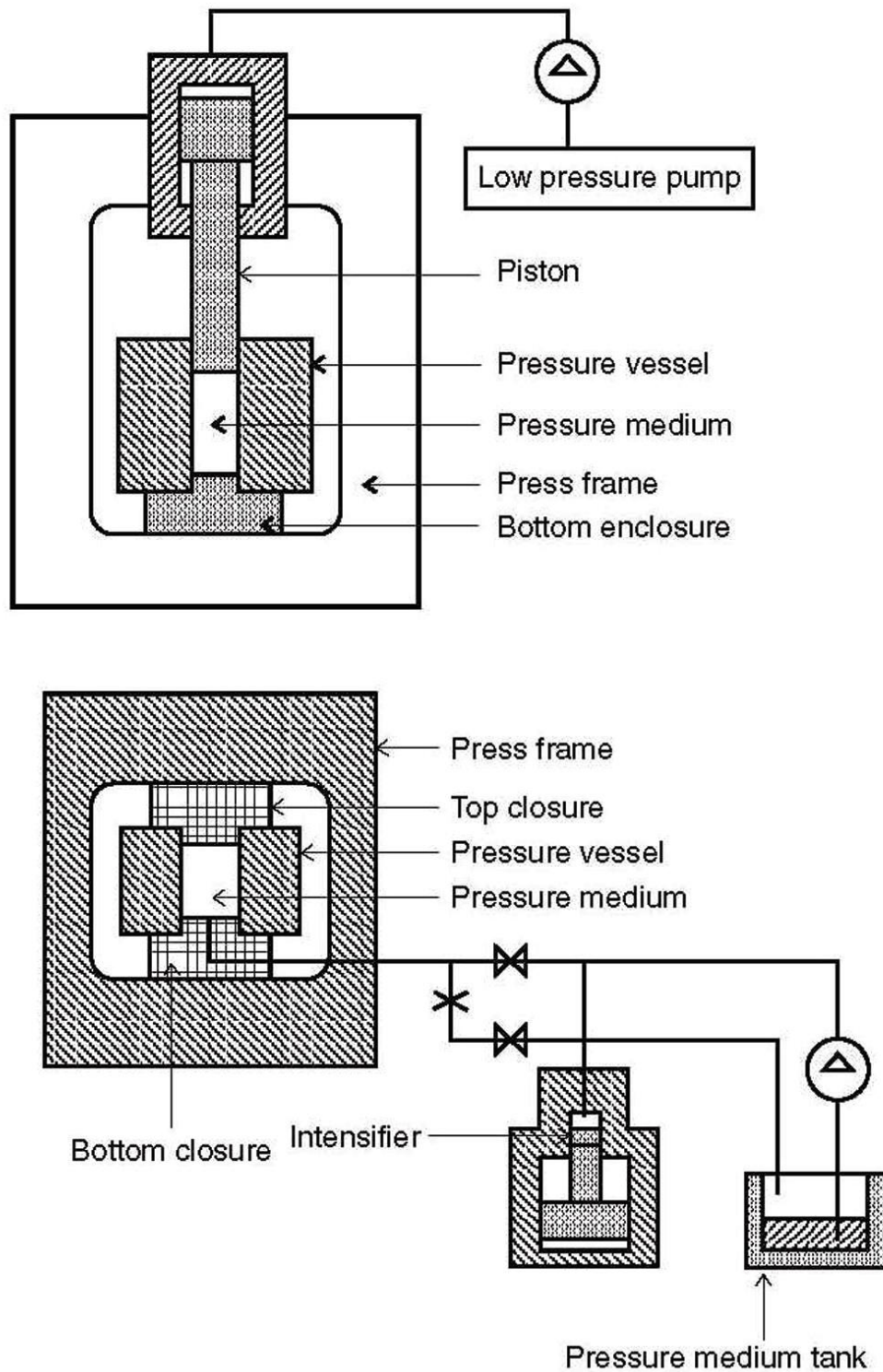


Fig. 2.2. High pressure by direct (top) and indirect (bottom) compression generation of the pressure-transmitting medium (Mertens 1995).

Heating of the pressure medium: this technique is based on the thermal expansion of the fluids which leads to the generation of pressure. This method could also be used to maintain higher pressures in combination with temperature. However, a precise temperature monitoring is needed for the internal pressure-transmitting medium (Barbosa-Canovas et al., 1997). The undesirable effects of adiabatic heat could be minimized by decreasing the temperature of food before processing and using a pre-cooled pressure-transmitting medium (Mújica-Paz et al., 2011).

The results of a heat transfer simulation of an HPP unit showed that transient temperature profiles exist during processing (Zhu et al., 2007). Though in the processing of solid materials the temperature inhomogeneity is mostly seen in the vessel walls while the central part of solid geometry is not affected by temperature fluctuations (Chen et al., 2007).

During recent years researchers have studied thermodynamic characteristics of the system by some particular types of high pressure processors. Typically, certain features such as phase transition, freezing and thawing and lipid crystallization are among relevant domains of studies in food processing (Knorr 1999). These phenomena are usually studied by differential scanning calorimetry (DSC). Nevertheless, the thermodynamic condition in such equipment is based on the atmospheric isobaric condition (Zhu et al., 2006; Ousegui et al., 2006; Zhu et al., 2004).

Several engineering aspects are important in high pressure processing equipment design. Also, two important degrees of freedom known as temperature and the pressure are the main parameters which should be monitored and carefully studied. Besides the pressure level, there is a certain amount of adiabatic temperature rise in the system. The heat of compression follows Eq. (2.1):

$$\frac{dT}{dP} = \frac{T_i \times \beta_p}{Cp_p \times \rho_p} \quad (2.1)$$

where T_i , β_p , Cp_p , ρ_p represent initial temperature (K), thermal expansivity (K^{-1}) at pressure p , specific heat (J/kg. °K) and density (kg/m^3), respectively.

Obtaining the compression heat, researchers have proposed an empirical expression to estimate the temperature of the food products under high pressure (Nguyen 2007), (Eq. 2.2).

$$T_i = T_p - [CH \times (P_p - P_{atm}) + \Delta T_H] \quad (2.2)$$

where T_i , T_p , CH , P_p , P_{atm} , and ΔT_H represent initial temperature (°C), target process temperature (°C), compression heat (°C/100MPa), target pressure level (MPa), atmospheric pressure level (=0.1MPa), and the heat gain during pressure holding time, respectively.

On the other hand, these days, the HPP is assisted with high temperature. The primary aim for such processing conditions is to intensify the microbial destruction. In other words, the high pressure processing at high temperatures could reach a certain level of commercial sterilization.

As a result, there have been several efforts to measure the temperature and the pressure level while processing. To measure the temperature, K-type thermocouples are reported to be functional up to 700MPa and 100°C with less than 2°C deviations (Bundy 1961).

2.3 High pressure processing of fruits and vegetable products

Many high pressurized fruit/vegetable products are available in the market. These products could be categorized in pasteurized purees, fruit juices, jams, ready to eat meals, etc. The primary purpose of using high pressure processing is the cold pasteurization regarding undesirable microorganisms and enzymes. However, based on the selected pressure level, the effect of high pressure could be different on each component. For instance, the normal pressurization at room temperature could be operated at 400 to 600 MPa to decrease the microbial load. This procedure would be useful to keep fruit juices, smoothies, vegetable mixes for 4-6 weeks at 4 °C. Figure 2.3 shows some of the typical plant-based HPP products in the market.



Fig. 2.3. Some of commercially available high pressurized products.

Considering the high importance of quality maintenance of the products as well as their safety, several articles have introduced and optimized the effect of HPP on plant products.

The main key element which distinguishes the use of high pressure processing as an efficient way of processing is that after the processing the natural flavor and nutritional compounds of the product will be preserved as well. Thus, as an essential key to success in fruit/vegetable processing, the product could be as close as possible to a fresh-like product. Also, HPP could be a more attractive processing technique due to its environmentally friendly character and least requirement of water (Knorr et al., 2011). Due to the considerable success of high pressure treated products regarding retention of nutrients, and improvement of the appearance of the process product, the technique was distinguished as one of the best innovations in the field of food processing in last 50 years (Dunne 2005).

Fruit and vegetable samples processed by HPP showed little effects on quality and safety of food products. The changes in texture experienced by HP-processed fruits and vegetables are related to the variations in the cell permeability. The degree of cell disruption by the movement of water, enzymes, and metabolites from inside to outside depends on the pressure applied to the type of plant cell. The cells of the plant are degraded, and void spaces appear because they are no longer filled with gas. Therefore, a cavity is formed due to the occurrence of HP processing which may lead to either tissue softening or texture firmness (Zhang et al., 2011). Under such processing, the action of pectin found in processed vegetables and fruit juices can break down by the action of pectin methylesterase (PME) and polygalacturonase (PG), (Duvetter et al., 2009). PME catalyzes the de-esterification of pectin to acidic pectin with a weaker degree of esterification and methanol (Terefe et al., 2014). Involved in fruits ripening, PME can extend cell wall during cell growth. On the other hand, PG catalyzes the cleavage of the glycosidic bonds between the two galacturonic acid residues in pectin resulting in pectin depolymerization. By increasing the activity of PME and decreasing the effect of PG resulting in texture and viscosity modification (Balasubramaniam et al., 2016). The modification brought to the texture and thickness is another advantage of nonthermal processing over thermally processed fruits and vegetables. Endogenous PME is favored under HPP increasing carboxylated pectin that enhances the cross-link with divalent ions like calcium to form rigid structures. Tissue softening due to thermal processing is counteracted by an HP-pre-treatments allowing PME-mediated pectin changes (Sila et al., 2008). Also, texture can be

reinforced for processed fruits and vegetables by using HPP combined with pre-treatments such as exogenous pectinases infusion and soaking in calcium chloride solutions (Duvetter et al., 2005).

High-pressure processing can be alternative to conventional freezing technique. It is known as high-pressure shift freezing (Sulaiman & Silva, 2013) This method consists of inducing instant uniform ice nucleation instantaneously throughout the food product. Small ice crystals cause this uniformity after pressure release (0-200MPa) at a temperature close to the freezing point for an extended period (Urrutia et al., 2007). This method is advantageous over conventional techniques of freezing because it can maintain cell functions, enhance texture, and lower drip losses of fruits and vegetables. Furthermore, at low pressures, the phospholipids in the cell membranes crystallize leading to increased permeability of the membrane. Thus, extracting components becomes possible under such conditions.

Besides, commercialized high-pressure treatments are alternative to blanching. It can be used as a pre-treatment for other processing. High pressure can be utilized for product modification, for instance, combining HPP with divalent ions such as calcium can be used to enhance the texture of vegetables during pasteurization and sterilization. Concerning pasteurization and sterilization of vegetables and fruits, several effects can be observed resulting from the impact of high pressure on the texture (De Roeck et al., 2009).

Firstly, products under high-pressure treatments can withstand compression to a vast extent. As a result, food products that contain a large quantity of air can decompress during the treatment resulting in modification of the texture. For instance, strawberries often possess cavities, and under this treatment, the strawberries modify to puree-like products (Cioni 2006). However, not all fruits and vegetables behave similarly because of the presence of air. For instance, grapes or berries are mostly composed of water (Balasubramaniam et al., 2016). Therefore, they stay intact during HPP at room temperatures. However, mushrooms turn brown because of enzymatic activities due to the air compression. Then, sensorial changes occur when plant cells undergo compression with HPP at room temperature. For example, potato, carrot, and red radish tissues lose

turgor, and a softer texture is observed. The loss of turgor is due to the disruption of cellular membranes. They lose their crunchiness with an increase of permeability after treatment (Luscher et al., 2005). Third, gelatinization of starches occurs at a pressure generally above 500 MPa resulting in texture modification of fruits and vegetables that contain a significant amount of carbohydrate (Nasehi & Javaheri, 2012).

The consideration of chemical reactions in fruits and vegetables is crucial since it has an impact on their quality attributes. Non-enzymatic reactions are related to oxidative reactions that shorten the shelf-life of plants derived products. On the other hand, enzymes are essential biocatalysts in the metabolism and physiology of plants. However, most of them are detrimental to post-harvest storage of fruits and vegetables due to extensive changes in quality attributes. Color, flavor, texture, and nutritional value are profoundly affected. For instance, the enzymatic reaction is responsible for pectin degradation, and network build-up modifying the surface.

The color is one of the primary physical attributes that has a greater role than any other parameter in consumer perceptions and the decision of purchase. Color is critical to inform us about several factors. A color change characterizes ripeness. The maturity of a product can be due to degradation for instance. The main groups of pigments related to color in fruits and vegetables are carotenes and carotenoids, anthocyanins, chlorophylls, and phenolic compounds (Terefe et al., 2014).

Enzymatic reactions do not only influence the color of commodities they change the flavor and the taste as well. This is when sensory panels come into play to judge sensorial attributes and analyze the taste of fruits and vegetables. In general, small flavor molecules are not much affected by such known thermal treatment; however, HPP is a good process to use when you want to preserve fruits and vegetables freshness for a longer period on the shelves of the grocery stores. It can maintain brightness, sweetness, flavor, and crunchiness of texture and odor, of carrots, and raw onions, respectively (Barrett et al., 2010). However rancid flavors can arise from pressure treatments like in tomato or onions as described by several studies. Generally, the activity of oxidative enzymes such polyphenol oxidase (PPO), lipoxygenase (LOX), pectin methylesterase (PME), peroxidase (POD),

chlorophyllase has been always under investigation (Terefe et al., 2014). PPO can affect sliced apples exposed to air to turn brown. PPO is relatively stable in some commodities like of apple and grape. PPO is sensitive to pressure. In other fruits like plum or pear, PPO resists the pressure inactivation more than other enzymes, such as peroxidase (Garcia & Barrett, 2002). Enzyme inactivation is more likely to occur during high pressure treatments as compared to low-pressure treatments. However, most of the time the inactivation of the pressure ranges is dependent on some conditions. These conditions consist of the enzyme type, pH, temperature and the type of medium (Cano & De Ancos, 2005). Moreover, color change could occur once high pressure is combined with high temperature. This change, for instance, can occur in green beans turning to an intense green during the pressure-assisted thermal sterilization treatment. The intensity of the color is due to the leakage of chlorophyll pigments out of the disrupted cell membrane and remain in the intercellular space Chlorophyll is the green pigment of the plant's leaves and stems and chlorophyll pigments degrade under constant temperature and increased pressure. The reciprocal effect is real as well, once the pressure is constant and temperature increases, the pigments degrade. However, at ambient temperature color change is not affected (Oey et al., 2008).

In the case of green beans, the enzymes can induce adverse changes in color and flavor. LOX has synergistic effects between weaker temperatures and higher pressures. LOX can trigger off-flavor in green peas, green beans, and corn. despite the mentioned the texture and color changes, high pressurized green beans can be stored over 1-month and still be retained (Krebbbers et al., 2002). Another example where color changes are affected by pressure processing is when the anthocyanin pigments are affected by the presence of glucosidases (Oey et al., 2008). Anthocyanins are water-soluble flavonoid pigments responsible for the red to the blue color of fruits and vegetables, and they are maintained under HPP treatments at ambient temperatures.

Strawberries and blackberry purées had shown to well preserve the color of the treated samples under HPP as compared to thermal processing. The color and nutritional values are preserved with such processing. Therefore, processing strawberries and blackberries by HPP could be an efficient way to maintain these food products quality (Patras et al., 2009).

The brightness is affected under pressurization more than under thermal applications. The green color of guava demonstrated a Browning processing due to PPO activity (Palou et al., 2000). Furthermore, when HPP is combined with another preservation technique, it can enhance the inactivation of spoilage bacteria and control enzymatic activity by accelerating the rate of inactivation which is another spectrum to analyze for further studies (Rodriguez et al., 2005).

High-pressure processing of fruits and vegetables has been shown to cause some changes in the bioavailability of bioactive compounds. The stability of bioactive compounds such as fat-soluble vitamins known as A, D, E and K are studied in foods (Albahrani & Greaves, 2016). It is shown that those vitamins are fat-soluble. A, D, E and K vitamins are less affected by the HPP as compared to water-soluble vitamins. A number of studies prove that under pressure processing, fat-soluble vitamins amount increases in selected products. The increase in the amount of those vitamins is due to the extraction done by high-pressure processing. During processing, vitamin A (retinol) amount decreases at elevated temperatures. For instance, the degradation of retinol under high-temperature processing leads to the formation of kitol compounds triggered by reaction mechanism known as Diels-Alder (Mahadevan & Karwe, 2016). This reaction occurs under elevated pressures as well. Some studies show to be able to retain retinol more under high-pressure treatments at room temperature than at higher temperatures. These studies apply to vitamin E as well. However, other shows to maintain more retinol under high-pressure treatments at higher temperatures for extended periods. For instance, freshly squeezed orange juice containing vitamin A precursors are treated by high-pressure treatment and then stored for ten days. It is found that the amount of vitamin A increased after HP-treatments. Before storage, the increase of both carotenoids and provitamin A occurred due to extraction. This extraction is due to the high-pressure treatments (De Ancos et al., 2002). As they explain in their findings, it is due to the ability of extraction from the food matrix after HPP. Hence, fat-soluble vitamins are less sensitive to the combination of elevated temperatures with high-pressure treatments as compared to water-soluble vitamins (Balasubramaniam et al., 2016).

On the other hand, carotenoids pigments are yellow-orange and are mostly found in fruits and vegetables. Under high-pressure treatments, trans-lycopene transforms to its cis form

causing the increase in lycopene bioavailability in the human body due to the isomerization (Honest et al., 2011). Among fruit-and vegetable-based products, carotenoid is the most stable pigment within food matrices under HPP (Oey et al., 2008). The pressure in contact with tomato juice on the other can increase lycopene content in tomato juice by extraction as well explaining the growth of red color in HP-processed tomato as compared to untreated tomato juice (Oey et al., 2008).

Furthermore, the levels of carotenoids in fruits and vegetables depends on the cultivar (Kaushik et al., 2014). For instance, Rojo Brillante cultivar yields fewer carotenoids than in Sharon variety in the case of persimmon puree (de Ancos et al., 2000). The increased amounts generated by extraction of HPP from food matrices have a direct impact on the antioxidant activities. Carotenoids, under HPP at moderate temperatures produce less free radical contrarily to untreated juices containing carotenoid pigments. Thus, applying HPP is beneficial and contributes to antiradical activities (Patras et al., 2009). In studies, antioxidant capacities of tomato and carrot puree are much higher after HPP than untreated samples. Moreover, the rate loss of the antioxidant capacity is lower in treated samples than in untreated ones. The little antioxidant capacities may be related to the risk of chronic diseases by reducing oxidative stress and inflammatory biomarkers in untreated samples (Pham-Huy et al., 2008).

2.4 Fruit/ plant tissues as Porous media

In fact, porosity is a physical characteristic of certain kinds of tissues which have confined a volume of a gas phase. This character is also separated into two concepts of general and effective porosity. The first one indicates the ratio of the total amount of gas to the total volume while the second one, which is a more applicational term, means the amount of gas phase which is in access to flow the fluids within them. The latter parameter is always a lower number than the overall porosity (Civan, 2011). Figure 2.4 shows a pore in apple as a fruit tissue which is a result of the existence of intercellular space.

2.5 Apple as a porous medium

Apple has always been an important fruit for plant science studies. It's the second leading produced and consumed food in the North America. The Native Canadian apple, McIntosh

has a noticeable potency of formulation due to its crispy and white flesh as well as its pleasant aroma. The physical properties of this variety, in terms of porosity, has been measured and the pore size and total porosity have been reported about 72 μ m and 0.63 respectively (Bazhal et al., 2003).

Apple has been processed in different fields of industries such as drying, freezing, canning, and juice while about 40% of the produced apple is consumed as fresh-cut. There are certain criteria about the desirability of apple including texture, firmness, color, and flavor. Also, mentioning about the most common problems with fresh-cut foods, there are two general characteristics of deterioration of apple. First is the internal browning of the tissue which is due to oxidation of polyphenols by polyphenol oxidase enzymes and consequently the production of brown pigments (Martinez & Whitaker, 1995). The second problem would be softening of the tissue as a result of moisture loss of the cells. It is noteworthy to mention that from a processing point of view, infusion of solutions with particular functional properties into the fruit texture can play a very important role in solving these two problems. About the first issue, impregnation is a cause of deaerating of the texture which means the oxygen content of intercellular phase will be exhausted. Also adding some anti-browning agents like ascorbic acid solution is the next pro about this technology. Solving the second problem by impregnation is just by impregnation of either isotonic or hypotonic solution which lead the cells at least not to lose water. Also, like the previous part, adding some specific chemicals will also make additional characters. In this case, calcium chloride will be useful as a firming agent.

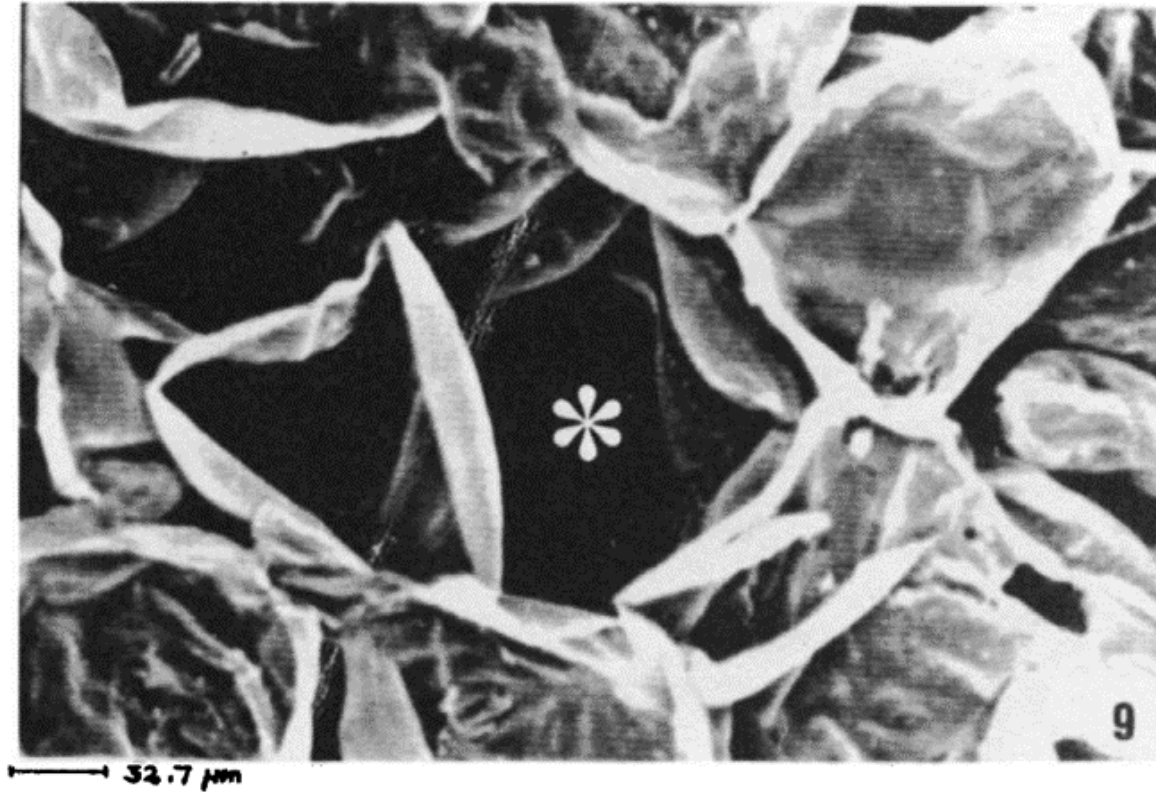


Fig. 2.4. SEM micrograph of intercellular porous media (Fito, 1994).

2.6 Mass transfer into porous media

The science of fluid transport into porous media is a computationally complex phenomenon which requires sufficient knowledge about the topology of each pore within the porous media, flow paths, and mutual interaction of fluid and matrix solid phase (Civan, 2011). Numerical simulation of flow in porous media requires the complete understanding of nature of flow patterns, the fluid properties, and multi-physical properties of a solid phase that the porous architecture is made of (Sahimi 2011). As a result, there have been several approaches introduced to study this transport phenomenon (Chhabra et al., 2001). Among these methods, the most important ones could be mentioned as (1) Bundle capillary tube method which emphasizes on the consideration of the porous media as tortuous flow paths. In this case, the wall friction effect is a significant resistant force for the fluid flow (Kozeny, 1927; Carman, 1937); (2) Pack of solid grains, in which the drag forces of a simplified pack of defined shapes of grains are the primary element of simulation calculations (Chhabra et al., 2001); (3): Averaging microscopic field equations, in which flow and

momentum continuity equations based on the conservation of mass equations are solved, and the mass transport is averaged over a representative volume element. In fact, in this category of modeling, different mass transfer equations such as Fick's first and second law, Navier-Stokes equations and Darcy's equation for saturated and unsaturated flows have been used. Also, in Non-Fickian behaviours of flow, diffusion equations analogous with non-Fourier heat conduction were introduced as means of mass transfer modeling (Akbarzadeh & Chen 2014, 2013, 2012; Berkowitz et al., 2008); (4) Dimensional empirical correlation method that is based on the empirically obtained mathematical relationships between certain physical conditions and the rate of mass transfer in the within the matrix and (5) Hybrid method which is based on utilising a mixed approach of the previously 4 mentioned modeling and calculation viewpoints.

2.6.1 Mass Transfer modeling

Mass transfer modeling is an important aspect of the qualitative and quantitative evaluation of food processing. There are numerous food processing operations involving a mass transfer. These mass transfer phenomena are in some cases intentional. For instance, as a common process, drying is the deliberate removal of water from the high moisture content foods. Also, diffusion of salt within a food matrix, loss of volatile compounds from food matrix, rehydration of dried products, etc. (Singh & Heldman 2014).

There should be a clarification that the term "mass transfer" does not mean the transfer of a certain mass from point A to point B. In fact, in Engineering and modeling aspects, the exact meaning of such phenomenon is the continuous "migration" of a certain property with a certain mass toward a point. This transfer is mostly based on the gradient of concentration of the property as a function of time. Though, different external forces can expedite the rate of mass transfer. To sum up, the term "driving force" is used to describe the dominant force which leads to a mass transfer into a matrix. The natural diffusion processes are mostly due to the chemical potential of property or osmotic pressure change in a domain (Singh & Heldman 2014). Table 2.1 presents some developed methods for mass transfer in porous media.

Table 2.1. Some of mass transfer models used in food engineering (Guillard et al., 2013).

Model	Reference	Driving force	Postulated mechanisms	Mass transport equation
Theoretical models	Fick	∇X_L	Liquid diffusion	$\frac{\partial X}{\partial t} = \frac{\partial}{\partial x} (D_{eff} \frac{\partial X}{\partial x})$
	Okozuno & Doi (2008)		Liquid diffusion + stress-driven diffusion term	
	Colon & Aviles (1993)	∇P	Liquid capillarity	$\frac{1}{A} \frac{\partial X}{\partial t} = -K_H \nabla P$
	Philip & De Vries (1957)	$\nabla X_V, \nabla P, \nabla T$	Liquid capillarity + vapour diffusion	$\frac{\partial X}{\partial t} = \nabla \cdot (D_m \nabla X) + \nabla \cdot (K_{Tm} \nabla T) + \frac{\partial K_H}{\partial Z}$
	Berger & Pei (1973)	$\nabla X_V, \nabla X_L$	Liquid capillarity + Liquid diffusion + vapour diffusion	$D_L \rho_L \frac{\partial^2 X}{\partial x^2} + D_V \left[(\varepsilon - X) \left(\frac{\partial^2 \rho w}{\partial x^2} \right) - \left(\frac{\partial X}{\partial x} \right) \left(\frac{\partial \rho w}{\partial x} \right) \right] = (\rho_L - \rho_w) \left(\frac{\partial X}{\partial t} \right) + (\varepsilon - X) \left(\frac{\partial \rho w}{\partial t} \right)$
	Whitaker (1980)	$\nabla X_L, \vec{g}, \nabla X_V, \nabla P$	Bulk flow	$\left(\frac{\partial \langle \Psi_V \langle \rho \rangle_V}{\partial t} \right) + \nabla \cdot (\langle \rho_1 \rangle_V \langle v \rangle_V) + \frac{1}{V} \int \rho_1 (v_1 - w) \vec{n}_{VL} dA = \nabla \cdot (\langle \rho_V \rangle_V \cdot D_{eff\ v} \cdot \nabla \left(\frac{\langle \rho_l \rangle_V}{\langle \rho_V \rangle_V} \right))$

	Kerkhof (1994)	∇X_{avg}	Bulk flow	$F_s X_{in} - F_{sout} X_{out} = \frac{d(M_p X_{avg})}{dt} + G F_{sfines} X_{wfines} + V(Y_{out} - T_{in})$
Model	Thovaldsson & Janestod (1999)	$\nabla X_V, \nabla X_L$	Liquid diffusion + Vapour diffusion	$\frac{\partial X_v}{\partial t} = \frac{\partial}{\partial x} \left(D_v \frac{\partial X_v}{\partial x} \right)$ <p style="text-align: center;">and</p> $\frac{\partial X_L}{\partial t} = \frac{\partial}{\partial x} \left(D_L \frac{\partial X_L}{\partial x} \right)$
Semi-theoretical	Henderson & Pabis (1961)	[–]	Bulk flow	$MR = a \exp(-kt)$
	Henderson (1974)	[–]	Bulk flow	$MR = a \exp(-k_1 t) + b \exp(-k_2 t)$
	Bruce (1985)	[–]	Bulk flow	$MR = \exp(-kt)$
Phenomenological	Luikov (1966, 1975)	$\nabla X, \nabla P, \nabla T$	Vapour diffusion, bulk flow, liquid	$\vec{J}_i \sum L_{ik} \vec{X}_i$
Stephan-Maxwell	Gekas (1992)	∇X_i	Bulk flow	$\frac{\Delta x_i}{\bar{x}_i} = \sum_j \bar{x}_j \frac{\bar{u}_j - \bar{u}_i}{k_{ij}}$
Empirical models	Thompson et al. (1968)	[–]	[–]	$t = a \ln(MR) + b(\ln(MR))^2$

Wang &
Singh
(1978)

$$MR = 1 + at + bt^2$$

Nomenclature			
$\langle \rangle$	Average value	\vec{J}_i	Heat and mass diffusion flux (Luikov's theory)
α	The volume fraction of air in the pores	\vec{X}_i	Thermodynamics forces giving rise to \vec{J}_i (Luikov's theory)
ε	Void fraction of the solid	A	Exposed area
ρ	Density	$D_{eff\ v}$	Gas phase effective diffusivity
v	Individual mass velocity (Whitaker theory)	D_{eff}	Effective diffusivity (Fick's law)
Ψ	Volume fraction of the phase	D_L	Liquid conductivity
∇	Gradient	D_m	Overall isotherm moisture diffusivity
a	Constant	D_V	Vapor diffusion coefficient
b	Constant	F_s	Solid feed
k_1	Constant	G	Dry air stream
k_2	Constant	K_H	Unsaturated hydraulic conductivity
k_{ij}	Mass transfer coefficient	K_{Tm}	Overall thermal moisture diffusivity
l	Evaporating species (Whitaker theory)	L_{ik}	Luikov phenomenological coefficient
\vec{n}	Unit normal vector	M_p	Dry solid holdup in the dryer
t	Time	MR	Moisture ratio $(X-X_e/X_0-X_e)$ with X_0 and X_e as initial and equilibrium moisture content, respectively
u	Velocity	P	Pressure
x	Spatial dimension	T	Temperature
\bar{x}_i	Arithmetic mean mole fraction of component i	V	Dimensionless heat parameter
S	Solid phase	X	Moisture content in kg of water/kg of dry solids
Fines	Particles carried by air	Y	Air moisture content
γ	Gas phase	Z	Coordinate where mass transfer occurs
w	Vapor phase		

2.6.2 Fickian Mass transfer

This approach defines the diffusivity as a proportionality ratio of mass flux to the differentiation of gradient of the concentration changes due to the position:

$$\frac{\partial X}{\partial t} = D \cdot \nabla^2 X \quad (2.3)$$

where D could be defined as the transfer rate. In fact, considering the existence of Fickian mass transfer, all the rate of the problem would be based on the mass transfer rate which is also called diffusivity value.

2.6.3 Diffusivity

Mass transfer is one of the first research fields which should be studied in every new concept of food processing. Generally, mass transfer is about considering the migration of a particular phase like water or oil in a medium. There has been extensive research about the rate of mass transfer in certain food processing techniques such as drying, baking, freezing, storage and impregnation (Fig. 2.5). The general strategy is an assessment of mass loss or mass intake of the samples and fits them to the theoretical models which describe the convective and diffusional motion of liquids in a certain medium. The outcome of a mass transfer study is a determination of diffusivity value as both qualitative and quantitative value. By having the exact term of diffusivity, the process seems to be highly controllable.

Thus, diffusivity is defined as the ability of a medium to diffuse a certain fluid in its texture. Although there is no standard method of diffusivity estimation, many scientists have proposed valuable approaches toward a precise estimate of the parameter (Guillard et al., 2013).

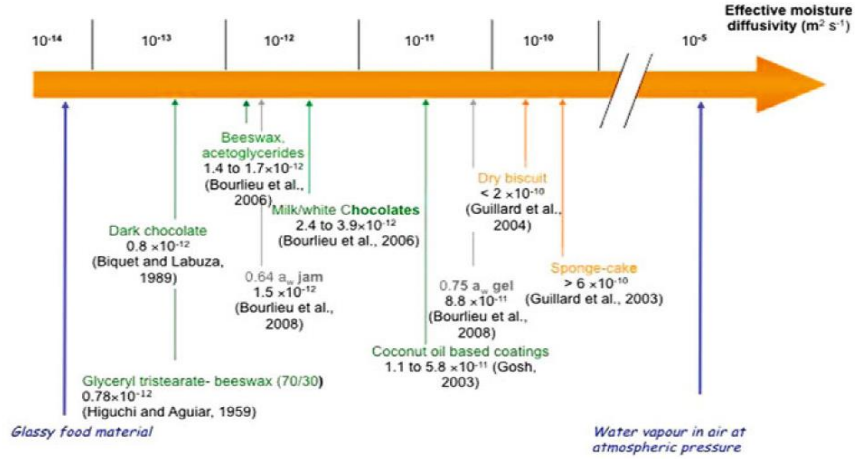


Fig. 2.5. Typical values of water vapor diffusivity in foods (Guillard et al., 2013).

2.6.4 Hydrodynamic mechanism of flow through a pore

The hydrodynamic mechanism is a microscale method of infusion of the fluid inside a pore which is based on the pressure difference of the gas inside the pore and the fluid phase. In fact, the total mass intake would be the volume of the fluid which is in an equilibrium state with the remaining gaseous phase. By extending the fluid intake of one pore to the entire portion of the porous part, the final mass transferred in a product could be studied (Fito, 1994).

where the capillary pressure is defined using Young-Laplace:

$$p_c = \frac{8\sigma}{Y^2} \quad (2.4)$$

Assuming isothermal condition:

$$-\Delta p = p_{eq} - \frac{p_{i0}}{1-x_v} \quad (2.5)$$

Penetration of fluid into an ideal pore (Fito, 1994):

$$-\Delta p + \frac{32\mu z^2}{Y^2} x_v \frac{dx_v}{dt} = 0 \quad (2.6)$$

where p , μ , Y , z , x_v are pressure (Pa), viscosity (Pa.s), pore diameter (m), pore length (m) and the volume portion of pores occupied by the fluid.

Reaching an equilibrium condition:

$$\frac{dx_v}{dt} = 0 \quad (2.7)$$

Thus:

$$x_v = \frac{(p_{eq} - p_{i0})}{p_{eq}} \quad (2.8)$$

Reaching $P_1 = P_2$, P_c will be the only driving force:

$$x_v = \frac{p_c}{(p_c + p_2)} \quad (2.9)$$

where, the P_{i0} =initial gas pressure of the pore at $t=0$, P_1 =Gas pressure inside the pore, P_{eq} =Equilibrium gas pressure at $t=t_{eq}$, P_2 =System Pressure, and P_c =Capillary pressure (Fig. 2.6).

Defining Actual compression ratio:

$$r = \frac{P_2}{P_1} + \frac{P_c}{P_1} \quad (2.10)$$

And:

$$x_v = 1 - \frac{1}{r} \quad P_r = \frac{P_c}{P_1} \quad r = R + P_r \quad (2.11)$$

where R is the apparent compression ratio, and since the $R \gg P_r$, $r=R$ (Fig. 2.6).

Extending the solution to an overall volume of the food, the volume fraction of the liquid will be:

$$x = \varepsilon_{eff} x_v \quad (2.12)$$

where ε_{eff} is the effective porosity.

As can be seen in Fig. 2.7, the effect of capillary pressure inside a pore is only effective in the case where the pressure gradient of the system between the fluid and the gaseous phase

is small. In the case of high pressure processing, this ratio would vary from 10 to 60 depending on the used pressure level. Thus, the capillary pressure could be neglected as the least effective parameter.

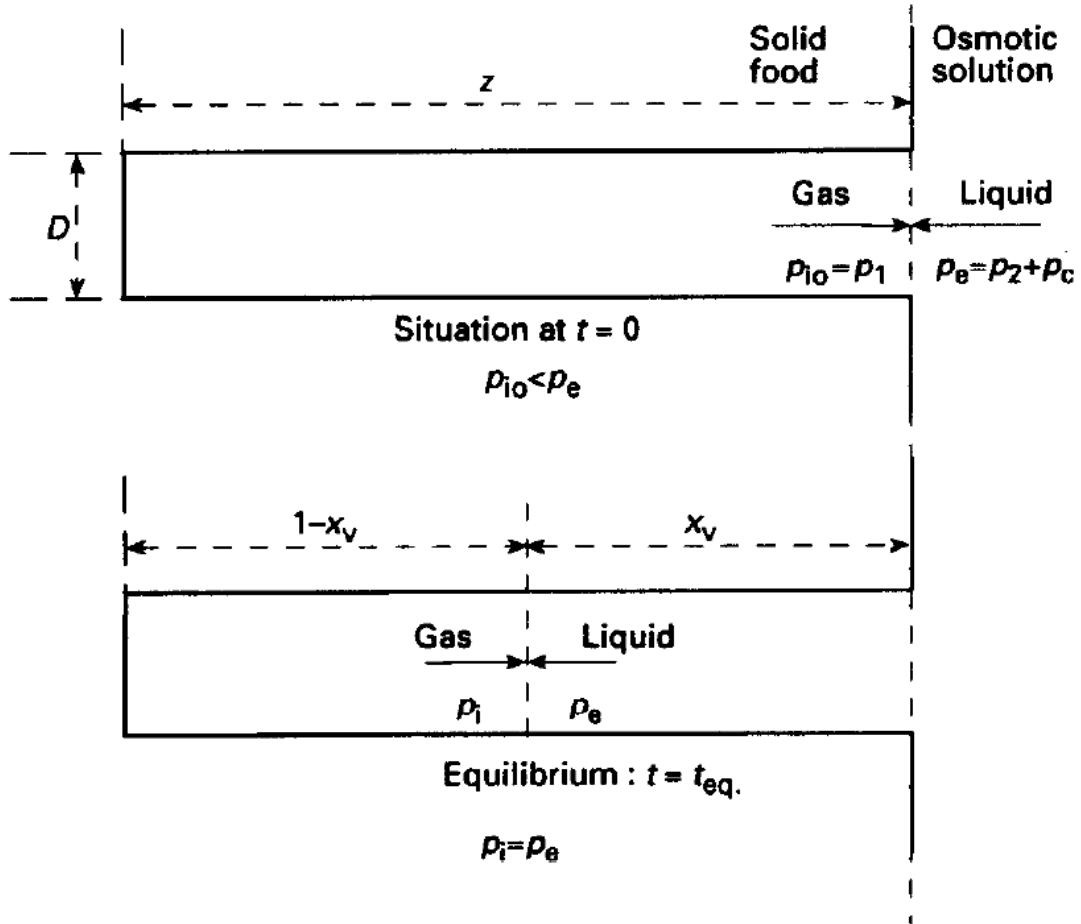


Fig. 2.6. The Hydrodynamic mechanism in an ideal pore (Fito, 1994).

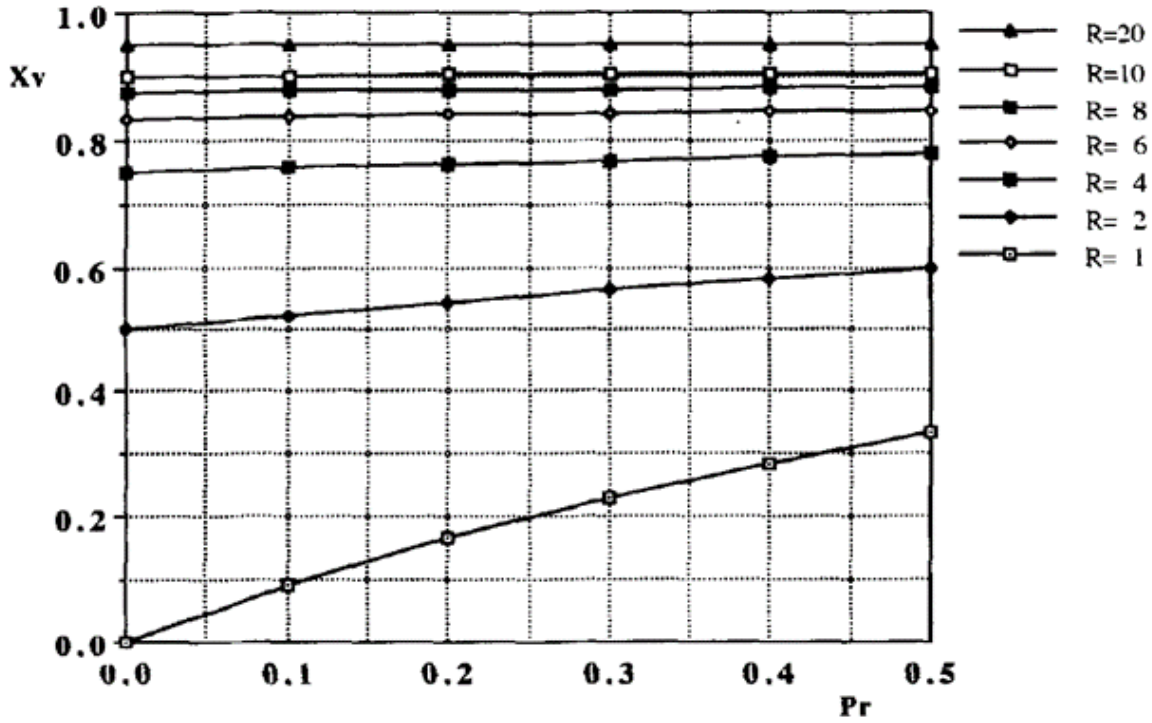


Fig. 2.7. Values of X_v from Eq. (2.9) for different P_r and R values (Fito, 1994).

2.6.4.1 Representative Elementary Volume (REV)

A porous medium consisting a solid part, known as solid matrix, and void space, called the pore space, has the capability of being a filled with different fluids. The porosity mostly defined as ε is calculated using Eq. (2.12).

$$\varepsilon = \frac{V_{void}}{V_{total}} \quad (2.12)$$

where V_{void} and V_{total} represent the volume of the porous phase and the total volume of the porous material, respectively. In this study, the porous material is defined as a REV which all the calculations would be done in such domain (Bear, 1979).

2.6.4.2 Saturation model

The behavior can be explained by introducing the notion of saturation parameter represented as “S”. $0 \leq S \leq 1$. In fact, saturation can be defined as the ratio between the fluid present in a volume and the total available volume. For an REV, the Saturation parameter for any liquid phase would be defined as Eq. (2.13), (Bréard et al., 2003):

$$S = \frac{V_F}{V_{total}} \quad (2.13)$$

where S , V_F and V_{total} total represent saturation, the volume of fluid and the total volume of pore space, respectively.

2.6.4.3 Darcy's equation

Darcy's equation is a widely used concept for studying the current of flow in a porous phase. The equation determines the volumetric fluid flow as a function of the pressure difference, fluid viscosity, and length of flow permeability index of the porous tissue. However, the equation has been used while assuming the porous phase as a perfectly elastic material with fine pores. In practice, the porous media can deform under pressure and also the shape and size of the porous medium is not homogeneous. Thus, there have been several modifications about making the Darcy's approach more applicational and precise in the scientific studies (Siena et al., 2015).

In this regard, there have been modifications about the introduction of fractal patterns of porous media as well as utilization of elasticity terms in Darcy's equation (Civan, 2010).

The permeability (m/s) like diffusivity (m^2/s) could be both a qualitative and quantitative parameter of the mass transfer rate in impregnation at different levels of processing.

While integrating Darcy's equation of flow through porous media will calculate permeability of the tissue at decompression state possible (Civan, 2010).

$$\frac{A}{A_b} = \Gamma_f^{d/3} \quad (2.14)$$

A and A_b represent surface area of two-dimensional porous network and bulk media, respectively.

In Eq. (2.15):

$$P_b = [\alpha + (1 - \alpha)\Gamma_f^{d/3}]P \quad (2.15)$$

$$q_x = -\frac{K_x}{\mu} \left[\frac{(P_{comp} - P_{atm})}{\Delta x} \right] \quad (2.16)$$

$$\int_{t_{atm}}^{t_{comp}} q \, dt = -\frac{K_x}{\mu} \int_{P_{atm}}^{P_{comp}} \left[\frac{[\alpha + (1 - \alpha)\Gamma_f^{d/3}]P - P_{atm}}{L/2} - \tau_w A_w \right] dP \quad (2.17)$$

$$V \Big|_{t_{decomp}}^{t_{comp}} = -\frac{2K_x P}{\mu L} \left[\frac{[\alpha + (1 - \alpha)\Gamma_f^{d/3}]P}{2} - (P_{atm} + \tau_w A_w) \right] \frac{P_{comp}}{P_{atm}} \quad (2.18)$$

where P , q , K , L , μ , τ , ε , and α are Pressure (bar), volumetric fluid flow (m^3/s), Permeability, length (m), viscosity (Pa s), Shear stress (Pa), fractal coefficient and elasticity.

2.6.4.4 Unsaturated Darcian Flow

In unsaturated flows, the pore rearrangements could be neglected comparing the change in the amount of saturation in the phase. As a result, the flow through a non-deformable porous medium could be defined as the combination of the continuity equation and the temporal saturation function for unsaturated flows. Thus, Eq. (2.19) indicates dependence of volumetric flow rate, q (m^3s^{-1}) in the derivative of saturation:

$$\nabla \cdot q = -\varepsilon \frac{\partial S}{\partial t} \quad (2.19)$$

A flow driven by the gradient of pressure is described as a generalized Darcian flow combined with Darcy's equation (Feng 2000), (Eq. 2.20):

$$\nabla \cdot \left(\frac{K(s)}{\mu} \nabla p \right) = \varepsilon \frac{\partial S}{\partial t} \quad (2.20)$$

where $K(s)$, p and μ are Permeability of the porous medium, pressure (Pa) and Dynamic viscosity (Pa.s).

2.6.4.5 Permeability

The permeability is considered as a function of saturation. The intrinsic permeability is a characteristic of the porous medium when a permanent flow in a saturated medium is present. The relative permeability is defined as the effective permeability at different stages of saturation of the porous medium, and it could be a comprehensive representation of resistance to flow in a porous medium at different levels of saturation. Thus, the total K could be defined in Eq. (2.21), (Muskat et al., 1937; Whitaker 1986):

$$K(S) = k_{rel} K_{int} \quad (2.21)$$

where K_{int} and k_{rel} indicate intrinsic and relative permeability, respectively.

2.7 Microstructural studies of mass transfer

Image processing methods are generally fast and accurate ways of studying different textural changes in the food materials. This field of study mainly includes various techniques of providing either two- or three-dimensional images of the tissue and then using the image analysis methods to assess a specific target. To study the apple texture, one of the most accurate ways is making the microtomes according to a method of fixation, and dehydration of the product (Xanthakis et al., 2014).

Considering the range of pore sizes, images by a resolution of 100 μ m would help us giving much data about the pore size and shape of the texture before and after high pressure processing. Several algorithms have been proposed as commercial or academic packages to obtain scientific information out of images. The principle is based on the conversion of a color image to HSV color scale, which is a representative of three main parameters of a color including hue, saturation, and value. The range of each scale is 0-360, 0-100 and 0-100 respectively. The next function of the algorithm would convert the HSV to a grayscale ranging 0-250. Finally, the grayscale could be converted to Binary scale in the form of 1

for white and 0 from black. Thus, by defining appropriate filtration of color, it is possible to have the porous phase as a black and solid phase as white scale. The final pic could give worthy information about changes in the shape and size of the porous media as a function of pressure variation. Moreover, estimation of the area of porous phase would give a two-dimensional porosity parameter (Marion 2013).

Preface to chapter 3

According to the literature review, despite significant efforts done on the characterization of non-thermal destruction of microorganisms and enzymes, there are lots of more features of such promising technology. In this regard, it is attempted to study the fluid migration within the biomaterials to present more novel aspects of utilization of high pressure processing in the applied sciences. In this chapter, basics of fluid migration during the holding time are discussed, it is attempted to theorize the transport phenomenon based on the familiar concepts which are used in food and drug industries. After explaining the nature of the phenomenon and the parameters involved, the computational procedure is applied, and a Fickian model is verified regarding the dynamics of migration of a standard solution into the apple texture as a representative of porous biomaterials.

Parts of this chapter have been published as an original research article as follows:

Vatankhah, H., Ramaswamy, H. S., (2017). Dynamics of fluid migration into porous solid matrix during high pressure treatment. *Food and Bioproducts Processing*, 103, 122-130.

CHAPTER 3

STUDYING BEHAVIOUR AND DYNAMICS OF FLUID MIGRATION INTO POROUS MATRIX DURING HIGH PRESSURE TREATMENT

3.1 Abstract

A mathematical approach was used to describe the mechanism of pressure-driven flow during the holding period of high pressure processing (HPP). A lumped method was used for the estimation of mass transfer parameters using an analogy to Fick's second law. In addition, a least squares optimization algorithm was introduced as inverse parameter estimators to obtain the associated mass diffusivity coefficients. The approach was verified using a model system involving liquid diffusion (1% w/w ascorbic acid solution) into a porous solid matrix (apple cubes) under HPP conditions (100 - 600 MPa) with different holding times (0 - 30 min). The associated fluid diffusivity values ranged between 4.38×10^{-9} to $2.19 \times 10^{-8} \text{ m}^2\text{s}^{-1}$. Finally, a simple linear model was fitted to the experimental data at 100 and 600 MPa which could be used to estimate the total porosity of the solid matrix. Thus, finite element numerical solutions combined with simple Fickian approach could be used to model the unsaturated liquid flow into a porous solid matrix. The study also showed that the fluid in-flow decreased in blanched apples subjected to similar HPP confirming the need for a porous structure for the efficient liquid flow.

3.2 Introduction

High pressure processing (HPP) is considered a technologically innovative way to process food materials. Numerous publications point out the success of industrial HPP for destroying microorganisms and inactivating the enzymes while minimally affecting the flavor and textural characteristics of various foods (Barba et al., 2015; Gill & Ramaswamy, 2008; Hiremath & Ramaswamy, 2012; Knorr et al., 2006; Ramaswamy & Shao, 2010; Serment-Moreno et al., 2015).

Moreover, several modifications in functional and physical properties of proteins and carbohydrates have been achieved using HPP (Ahmed et al., 2014; Alvarez et al., 2008; De Maria et al., 2015, Hussain et al., 2016). Several of these characteristics are deemed highly positive attributes of HPP over conventional processing techniques. Sila et al. (2004) proposed HP infusion of calcium chloride solutions to improve the hardness of carrots as a pre-treatment for thermal processing. There also have been some studies on the infusion of texture improver compounds in carrots (Rastogi et al., 2010; Rastogi et al., 2008). George et al. (2016) evaluated some physicochemical characteristics of apples when using HPP for infusing selected anthocyanins.

During HPP, the porous matrix of plant/animal tissues can be affected by the pressure induced flow of fluids around and into the matrix. A considerable amount of fluid transfer into the solid matrix could result in this regard. This fluid transport could have two important implications: (1) to intentionally impregnate the tissue with active agents in a multi-phase food system which could consist of a porous medium confined in fluids such as water, syrups or anti-browning agents etc., or (2) it could simply happen, as an unavoidable consequence of HPP, in any food system containing both phases.

The first situation, introduced as high pressure impregnation (HPI), is a forced transport phenomenon based on the ability of HPP to achieve forced flow of agents under the influence of pressure resulting in a rapid, controllable and homogeneous mass transfer.

Generally, impregnation techniques are used as efficient ways to rapidly introduce liquids &/or solid components into fruits and vegetables to accomplish specific functions such as anti-browning, nutrient enhancement, etc. High controllability, rapidity, and simplicity are the main technologically attractive characteristics of such methods (Petersen, 2014). The success of such processing techniques mainly depends on the characteristics of impregnating agent and its capability of having certain functions in further processing stages. Thus, using different types of sugars, acids, colorants, chemical, functional ingredients, minerals, and vitamins could help food processing units to improve products' quality attributes (color, flavor, texture) as well as achieve nutritional fortifications. It is noteworthy to mention that so far, vacuum impregnation (VI) has been known as the most

common impregnation method done based on exchange of gas or liquid in the intercellular space of the fruit tissue by an external liquid (Betoret et al., 2012; Castagnini et al., 2015; Schulze et al., 2012).

According to the hydrodynamic mechanism, impregnation of the pores is reached by capillary action as well as pressure gradient between solid matrix and external liquid phase. However, because of the extremely high pressure gradient, mass transfer due to capillary action can be negligible (Fito et al., 1996) under HPP.

Because of the extremely high pressure involved in HPP, heavy gauge stainless steel vessels with very effective safety seals are used to maintain safe processing conditions. Unlike other commercial equipment that operates at pressures of a few atmospheres, HPP employs pressure in the range 4000 to 7000 atm and therefore in-line monitoring of mass transfer mechanisms under HPP seems to be technically unachievable, especially in terms of using the common gravimetric techniques, and therefore are estimated only before and after the HP process. This issue makes the use of mass transfer modeling as well as subsequent experimental validations. Developing such a model needs to adopt a logical and practical approach, and consider possible assumptions and approximations based on the nature of such problems. There is a lack of specific studies on fluid transfer processes in the field of HPP.

Therefore, this study was focused on developing an empirical model for the estimation of mass transfer parameters during HP impregnation of a liquid into a solid matrix. To validate the approach, a model system of apple -as a solid matrix- and ascorbic acid (1% W/W) solution -as the fluid phase- was chosen. Having a high porosity and a homogeneous porous structure, apple is undoubtedly one of the best solid food matrices that can be employed as a model porous plant food matrix. Moreover, apple is reported to have highly similar textural characteristics regarding porosity value and pore shape among other fruits (Salvatori et al., 1998). Further, a comparison of mass transfer between blanched and unblanched samples was made to demonstrate the necessity for the prior existence of unsaturated porous medium for the efficient HP infusion process.

3.3 Theory/Calculations

3.4 Problem definition using Fick's second law

Choosing a correct approach for studying mass transfer phenomena could give useful clues and comprehensive insight into newly designed mass transport processing technique. At first glance, it is obvious that a positive mass transport phenomenon towards the porous matrix is being done during first two stages of the high pressure processing (pressure come up and holding times). Thus, to scrutinize the effectiveness of holding time on the total mass transfer - as is common with most pressure and heat processing techniques - the diffusivity parameter would be the best representative of the mass transport rate. In the case of HPP, assuming that the temperature and pressure level are homogenous at all points of the system, the Fick's second law could be used to model the mass transfer regarding time transient dimensionless mass intake during the hold time.

Moreover, according to isostatic principle, due to uniform and quasi-instantaneous transmittance of pressure throughout the whole sample, the mass flux can be assumed to be equal on all 6 surfaces of a cube (Eq. 3.1). As a result, considering the assumptions in Da Silva et al. (2009), the problem could be solved as a mass transfer in three infinite slabs of $2L$ thickness using the analytical solution of Fick's second law (Crank, 1975; Ramaswamy et al., 1982), (Eq. 3.5).

$$MR_{Tot} = \frac{\bar{X}(t) - X_{eq}}{X_0 - X_{eq}} = MR_{pl}^3 \quad (3.1)$$

Using initial condition:

$$X = X_0, \quad 0 < z < L, t = 0 \quad (3.2)$$

And boundary condition:

$$\frac{\partial X}{\partial z} = 0, \quad z = 0, t > 0 \quad (3.3)$$

$$X = X_e, \quad z = L, t > 0 \quad (3.4)$$

$$MR_{pl} = \frac{8}{\pi^2} \sum_{n=0}^{\infty} \frac{1}{(2n+1)^2} \exp \left[-(2n+1)^2 \pi^2 D \frac{t}{4L^2} \right] \quad (3.5)$$

where MR_{Tot} is total moisture ratio, MR_{pl} is moisture ratio at on each plate, X is the mass intake (kg kg^{-1}), D is the diffusion coefficient ($\text{m}^2 \text{s}^{-1}$), and z and t are the position at each direction of the Cartesian system(m) and time (s), respectively.

It is possible to describe an analogy between mass transfer under pressure and Fick's second law. As a result, to solve such problems, the initial mass intake (X_0) and mass intake at the equilibrium state (X_{eq}) have to be adequately defined.

Regarding the unique processing conditions of the described problem, an appropriate definition of two parameters including initial (X_0) and equilibrium mass intake (X_{eq}) is vital for having a successful mass transfer modeling. As described before, the time domain of solution starts when the process pressure is attached to the pressure vessel, i.e., from the end of pressure come-up time. High pressure processing involves a gradual build-up of pressure (1-3 min in laboratory size equipment and much longer in commercial equipment) to the operating levels. This is termed as the pressure come-up time, and during this time the transient kinetics are difficult to evaluate since both pressure and time change simultaneously. However, once the processing pressure conditions are achieved, the system is held at this pressure for an additional time (pressure holding time) when only time will be the variable at a constant pressure. Thus, the moment of reaching the maximum pressure is termed as the zero time for the transport phenomenon in a steady pressure condition.

On the other hand, considering the porous biological medium on a mesoscopic scale, the pores are the primary domain of transfer since the processing time is too short, and the confining fluid is considerably dilute to have a considerable osmotically boosted mass transfer along the cell walls. Moreover, at the start of pressure holding time, some of the pores would have been already filled with the liquid (during the pressure come-up time).

Hence, X_0 , which represents an important parameter in mass transfer modeling, was estimated as the mass intake at the end of the come-up time. In other words, this approach includes the trapped moisture content of intercellular phase at the beginning of hold time

in X_0 computation. Due to technical limitations of carrying out HPP for extended processing times (especially at higher pressure levels), measurement of X_{eq} becomes a more serious challenge.

In addition, the process is not verified to have a perfect equilibrium condition since there could be possible forced diffusion phenomena due to the automatic pressure optimization of the equipment to maintain the desired level of pressure and also the existence of a fast decompression. As a result, this parameter was found by extrapolation techniques based on reaching an asymptotical equilibrium of Peleg's equation as described in Eq. (3.6) and Eq. (3.7), (Peleg, 1988).

$$\bar{X}(t) = X_0 \pm \frac{t}{\theta_1 + \theta_2 t} \quad (3.6)$$

$$X_{eq} = \lim_{t \rightarrow \infty} \left(X_0 \pm \frac{t}{\theta_1 + \theta_2 t} \right) = X_0 \pm \frac{1}{\theta_2} \quad (3.7)$$

where \bar{X} is the product's average mass intake along the length of the diffusion path (kg per kg initial weight of sample).

2.2. Inverse Methods

The Trust-Region-Reflective Least Squares algorithm of optimization (TRRLS) is a useful tool for parameter estimation according to a target function and the measured data. This method is also useful for some of the ill-conditioned problems because of possession of second order convergence for the iterations.

To sum up briefly, using the constrained condition of the above-mentioned algorithm, the problem would be solved according to the computation of a local minimizer of a smooth nonlinear function which is subjected to predefined bounds for the variables. The standard trust-region method possesses a sub-problem of a quadratic function representing a spherical or ellipsoidal shape local model to the target function defined by interpolation of data at an iterative system. The extensive procedure following MATLAB notation could be found in part: Algorithm-2 in Coleman and Li (1996).

3.5 Experimental Validation

3.5.1 Sample Preparation

Fresh McIntosh apples were obtained from the Horticultural Research Farm on the Macdonald Campus of McGill University, Ste. Anne de Bellevue, Canada. Visually fresh apples of similar shape, size and approximately same date of harvesting were obtained. The apples were washed, peeled and cut into 1.2 x 1.2 x 1.2 cm cubes. Two cubes were weighed with a precision of ± 0.0001 g (APX-200 Digital Weighing Balance, Denver Instruments, USA) and immersed into 25 mL of 1% (w/w) aqueous ascorbic acid solution (Sigma Aldrich, USA) in double distilled water (conductance: 18 V, Milli-Q, Millipore, Bedford, USA) and kept in low-density 2 oz. Polyethylene bags (Whirl Pak (R), Nasco, Fort Atkinson, WI, USA). The bags were heat sealed and immediately transferred to the HPP unit.

3.5.2 High pressure processing

High pressure treatments were given in a laboratory isostatic HP apparatus consisting of a cylindrical pressure chamber of 5 L volume (ACIP 6500/5/12VB-ACB Pressure Systems, Nantes, France). The pressure-time (P-t) program was applied using a computer connected to a data logger (SA-32, AOIP, Nantes, France). The scheme of the HPP apparatus is shown in Fig. (3.1).

The medium used in the system for pressure transmission was water. The P-t program designed included the following sequence: i) A compression (come-up) stage involving pressurization of the chamber to the desired pressure level (100-600 MPa) at 300 MPa/min compression rate ii) a predefined holding time (0-30 min) at the target pressure iii) a rapid decompression (<15 s) until the atmospheric pressure is reached.

The tests were conducted at 6 different pressure levels: 100, 200, 300, 400, 500 and 600 MPa and 7 different holding times: 0, 5, 10, 15, 20, 25, 30 min. The samples were introduced into the high pressure vessel at 15-18 °C, so the temperature of the medium and sample was around 25°C during the treatment.

During the processing, it was expected that there would be an increase of about 3°C/100MPa due to the adiabatic heating. However, because the vessel was jacketed and held at room temperature, an approximate average temperature around the room temperature conditions (~25°C) was achieved by taking the sample and liquid lower temperatures according to the targeted pressure level (Khurana & Karwe, 2009; Zhu et al., 2004).

Small variations in adiabatic temperature rise in the system were neglected due to the weak effect on the structural characteristics of the porous medium, such as tortuosity and total permeability, regarding low volumetric thermal expansion coefficient of the plant tissues and assumption of elastic compression of the medium.

Concerning the Darcian approach, the effect of temperature on permeability has been found to be inconsistent and contradicting because of showing increasing, decreasing or no trend on flow in porous media (Gobran et al., 1987), and neglected in this study. Basically, considering the applied approach for the results of this investigation, it was decided to conduct the experiments at room temperature conditions and the tests was performed in two repetitions at each P-t point. After the processing, apple cubes were taken out and weighed after 10 s rinsing.

3.5.2.1 Impregnation of fresh and blanched texture

Some blanched apple cubes were prepared after immersion of tissue in boiling water for 30 s to obtain a more practical and industrial viewpoint. Afterwards, the cubes were HP treated using the same procedure to see the possible effect of blanching on mass transfer. The obtained data were compared with unblanched apples of the same batch of apples. The high pressure level and holding time were 300 MPa and 30 min, respectively. The mass intake was monitored every 10 min.

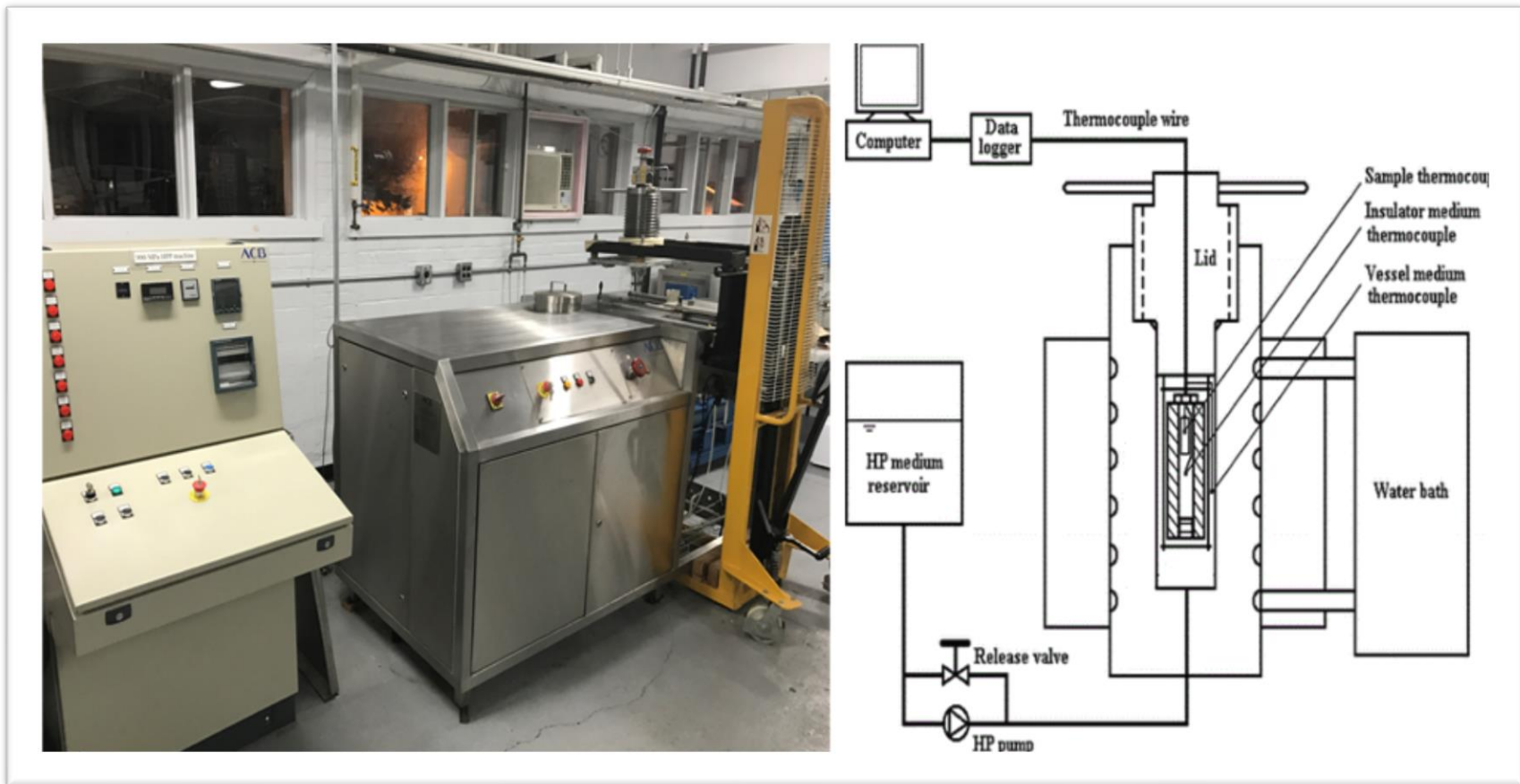


FIG. 3.1. HIGH PRESSURE APPARATUS USED FOR THE EXPERIMENTAL OBSERVATION.

3.6 Results and Discussion

3.6.1 Estimation of X_{eq}

The X_0 data were chosen as the net amount of mass intake at the end of the comp-up time. According to Table 3.1, the initial intake at 100 MPa was the lowest value which is logical. For other pressure levels, the values were in the range of 0.21 to 0.26. Due to the use of high levels of pressure, obtained data were quite close and did not show any distinct trend at HP levels of 200 to 600 MPa.

To elaborate, the X_0 could be as a function of two opposing parameters: the compression effect and the decompression effect. Looking at the data, it could be hypothesised that at pressure ≤ 300 MPa, the compression effect is dominant and more effective; thus, the mass flow inside the pores could show an increasing trend as a function of pressure; while at higher pressure levels, there is a destructive outflux effect due to rapid decompression from high to atmospheric level of pressure. According to the hydrodynamic mechanism of flow inside a pore, Fito (1994) stated while having a pressure difference between the liquid outside and the gas inside a pore, there would be a gas outflow (same as the step of reaching a vacuum pressure in a VI system) or a liquid inflow (same as the last step of the VI in which the pressure is raised to atmospheric pressure).

Thus, while rapid decompression at higher levels of pressure, the gaseous phase trapped in the pores would make a more intense liquid outflow impeller force due to expansion from a higher pressure to the atmospheric pressure. Thus, the net mass intake gain would be moderated negating some of the positive effects of the HPI.

Table 3.1. The parameters related to Peleg’s equation Θ_1 and Θ_2 , measured initial mass intake (X_0), and estimated equilibrium mass intake (X_{eq}) parameters.

Pressure (MPa)	Θ_1	Θ_2	R^2	RMSE	X_0	X_{eq}
100	2494	4.49	0.90	0.016	0.17	0.58
200	612.1	10.08	0.96	0.001	0.21	0.31
300	14600	6.75	0.93	0.005	0.26	0.41
400	1418	16.11	0.96	0.001	0.22	0.28
500	4869	6.46	0.97	0.005	0.22	0.37
600	13300	1.93	0.76	0.027	0.23	0.75

Figure 3.2 shows the above-mentioned loss in the mass intake for HP treatment at ≥ 400 MPa relative to lower pressures. Moreover, at higher levels of pressure, due to high compression rate at the beginning, the trapped gaseous phase in the porous phase will be slow to get out of the tissue. In addition, the high pressure level of the outer boundaries will make the gas outflow much more difficult. While at the lower pressure levels of processing, both lower compression rate and lower liquid phase pressure make the outflow of gas easier.

As a result, higher volume of gas inside the pores and greater possibility of outflow, affect the calculations leading to obtaining a higher X_{eq} .

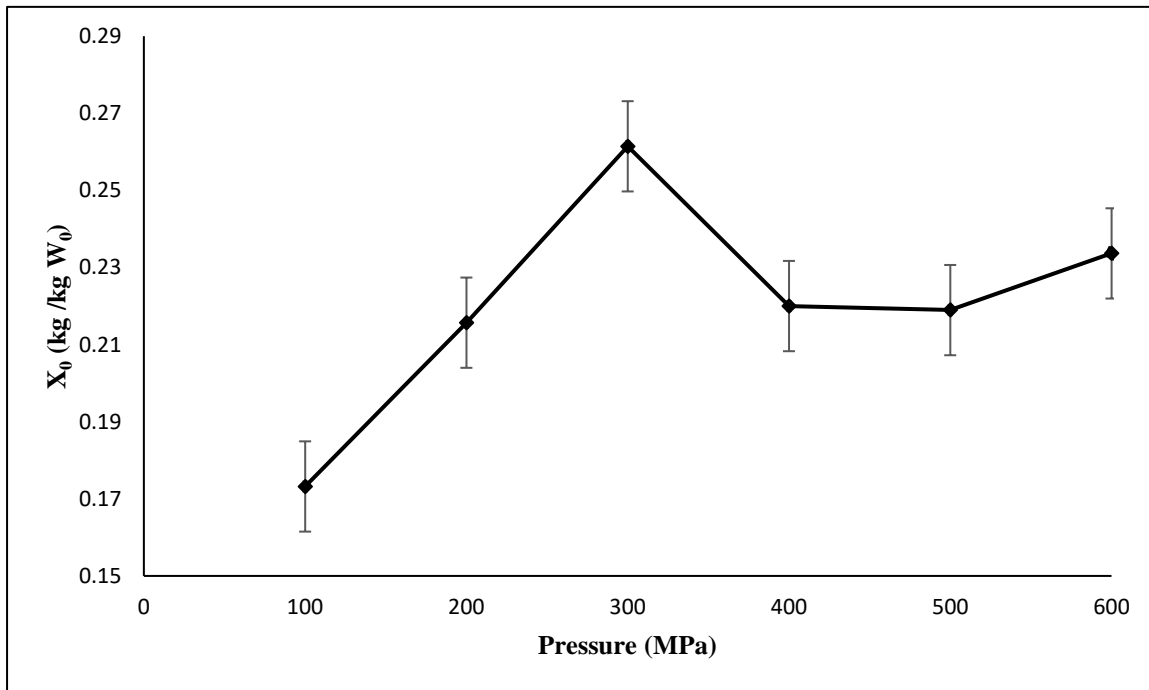


Fig. 3.2. The initial mass intake ratio at the beginning of pressure holding time.

At 200, 400 and 500 MPa, the Fick's analogy found to be suitable (Fig. 3.3). There was a possibility for all groups to be modeled using mentioned approach. However, the main factor which prohibited other groups to fit the model was the concept of the extrapolation for estimation of X_{eq} .

3.7 Estimation of Mass Diffusivity

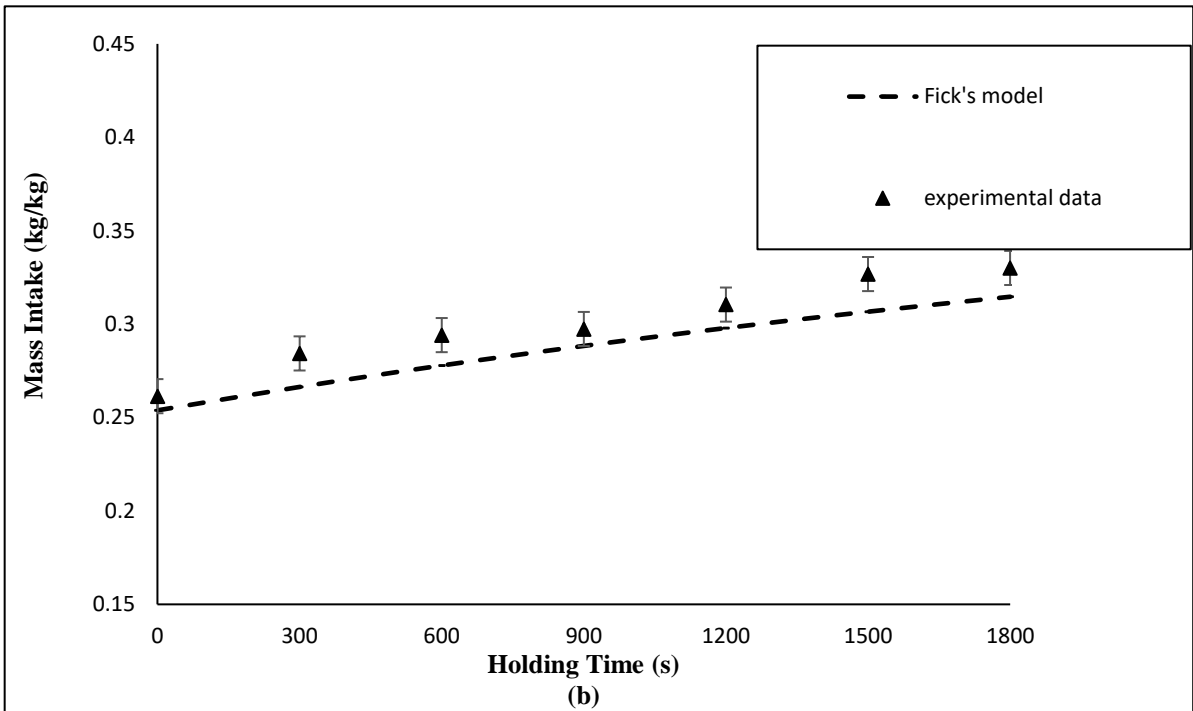
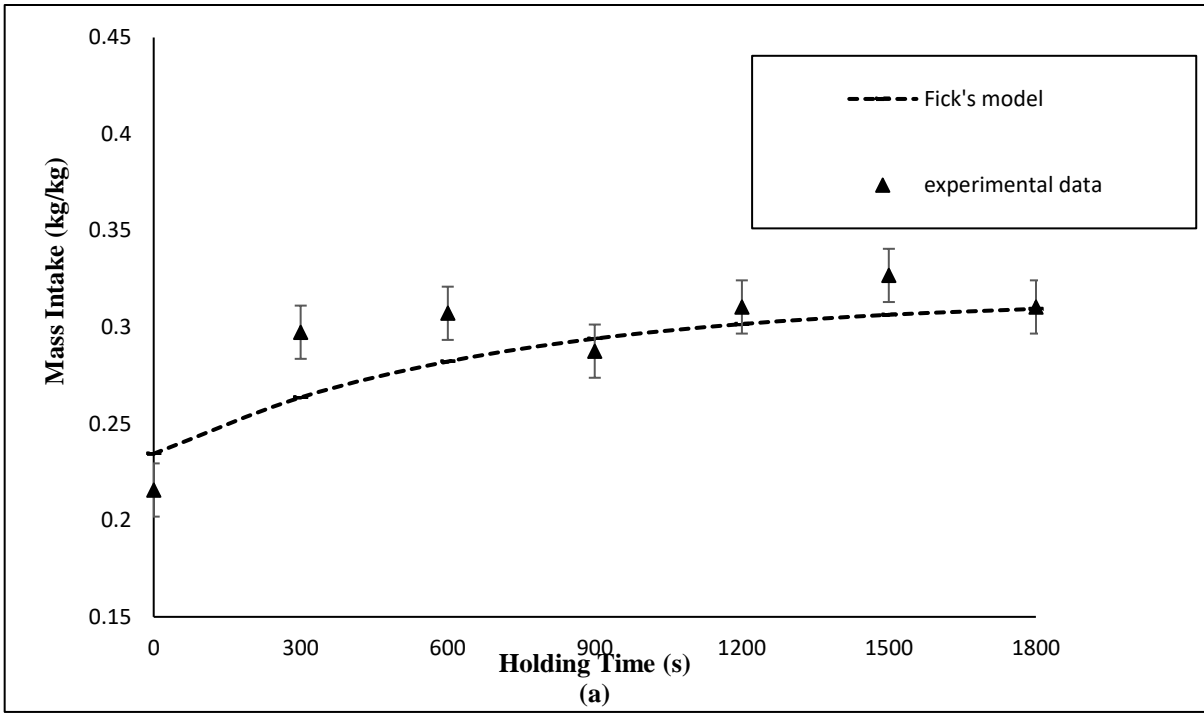
The described mass transfer model consists a two-stage approach. The first is a supposition of X_0 and X_{eq} as the initial mass intake after pressure come-up time and extrapolation of data by Peleg's approach respectively and the second would be choosing the Crank's analytical solution for modeling mass transfer data and estimation of diffusivity value.

Table 3.2. The estimated effective diffusivity values using classic and trust region method.

Pressure	D_{eff} (Classic Method)	R^2	RMSE	D_{eff} Trust Region	R^2	RMSE
100	4.38E-09 ^{gf}	0.91	0.039	3.58E-09 ^k	0.93	0.068
200	2.19E-08 ^{hc}	0.74	0.019	5.27E-08 ^b	0.89	0.063
300	4.4E-09 ^{gcf}	0.89	0.018	3.45E-09 ^c	0.93	0.024
400	2.19E-08 ^{ke}	0.88	0.014	4.18E-08 ^d	0.88	0.042
500	7.30E-09 ^{hc}	0.68	0.016	7.69E-09 ^e	0.86	0.053
600	-	-	-	1.00E-11 ^f	0.89	0.064

According to Table 3.2, same as initial X_0 values, the diffusivity values at lower pressures such as 200 and 400 MPa were slightly higher than diffusivity at 600 MPa. The diffusivity values ranged $\approx 10^{-9}$ to $10^{-8} \text{ m}^2\text{s}^{-1}$. The paired t-test statistical results showed no important trends in alteration of diffusivity as a function of pressure level.

The range of diffusivity values could introduce useful information about the nature of mass transfer in the porous media; the range of data fall in the same range of liquid water diffusion which is about $10^{-9} \text{ m}^2\text{s}^{-1}$. In contrast, this parameter for diffusion of water vapor is $10^{-5} \text{ m}^2\text{s}^{-1}$. Since the mass transfer is occurred in a porous medium, having the diffusivity in the range of water diffusion in liquid form could be an indication that a high portion of porous phase had been filled with the fluid before the holding time.



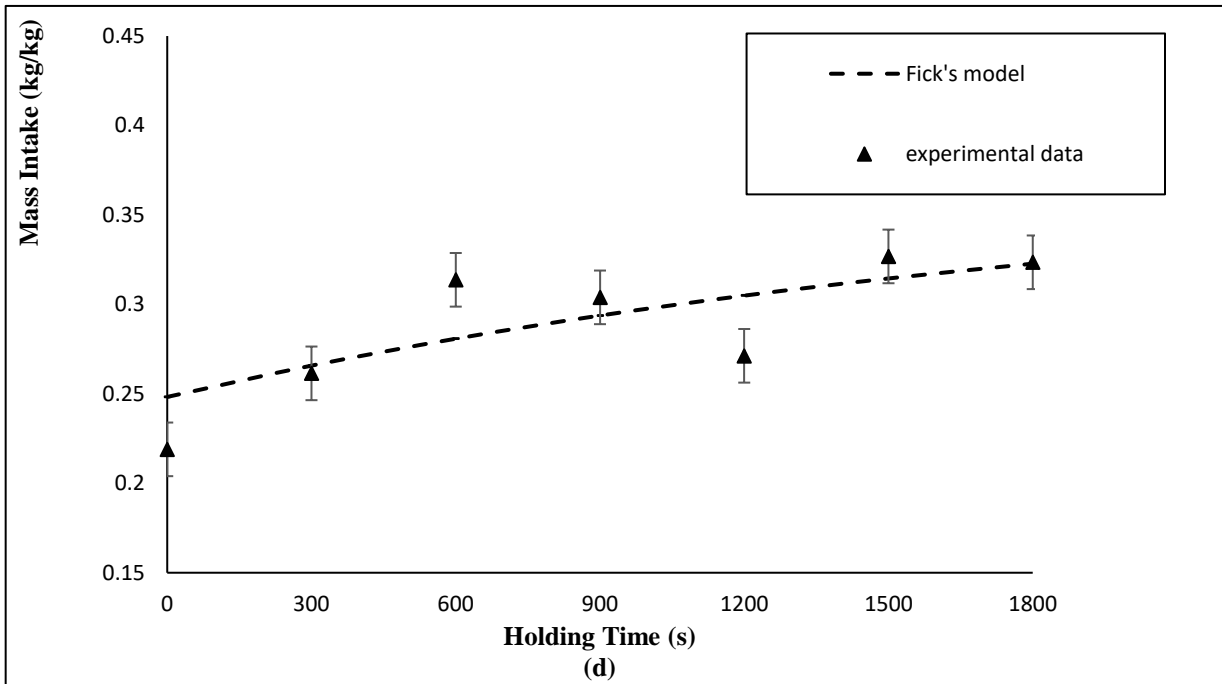
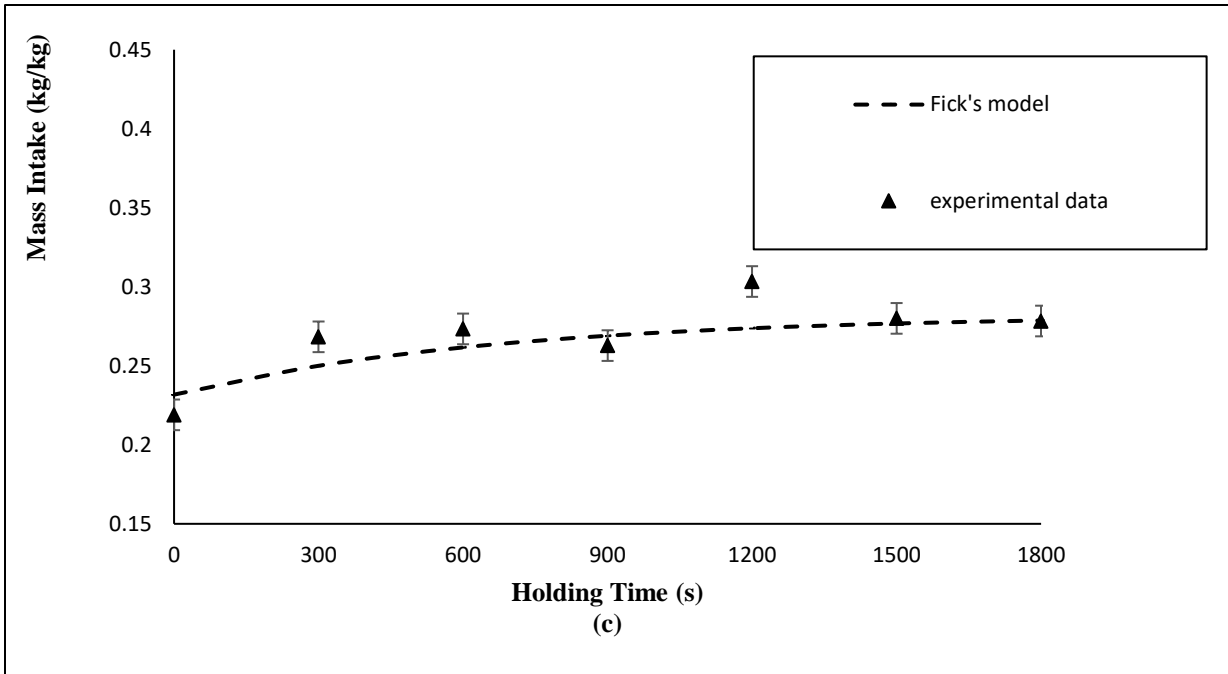


Fig. 3.3. Mass transfer model fitted to experimental mass intake data as a function of holding time. (a) 200 MPa, (b) 300 MPa, (c) 400 MPa, and (d) 500 MPa pressure level of holding time.

Except at 100 MPa processing, which had a highly unsaturated phase (empty pores) at the beginning of the holding time, 25-45% of the mass was transported at other pressure levels after 30 min of processing relative to the come-up time which further suggests the domination of diffusion in liquid form. The research on diffusivity in sponge cake done by Guillard et al. (2003) indicated that near saturation, water transport took place predominantly in the liquid phase within the swollen matrix.

Peleg's equation fitness parameters showed low linear correlation at 600 MPa, and computed data of diffusivity also demonstrated a very weak mass transfer at this pressure level. The low diffusivity values confirm a dominance of a weak natural diffusion inward the texture.

The diffusivity values obtained by optimization method are presented in Table 3.2. The slight difference of the optimized values versus the computed ones is due to the limitations of approximations used to describe characteristics of the process. It should be noted that gravitational measurements of mass transfer of small cubes after pressurization at ultra-high levels of hydrostatic pressure would indeed involve an inevitable margin of error.

Moreover, the flow through porous plant tissues have been reported to be influenced by pressure gradient, time of processing, viscosity, temperature and osmotic pressure of the external solution, product/solution ratio as well as the texture characteristics including porosity, firmness, cellular arrangement, intercellular space accessibility, surface/volume ratio and etc. (Bilbao-Sáinz et al., 2005; Fito et al., 2001; Gras et al., 2002; Guamis et al., 1997; Mendoza et al., 2010; Petersen, 2014; Schulze et al., 2012; Tylewicz et al., 2012).

The fluid migration could be affected by several factors during the processing; however, the most important concept would be considering the effect of different stages of HPP on such phenomenon. During such pressure-driven flows, it is more obvious that the come-up and the holding time represent as important “positive” factors of impregnation. Meanwhile, during pressurizing, the texture undergoes mechanical changes in terms of change in pore shapes and sizes, which could possibly make significant differences in the rate of mass transfer.

In reality, the Fick's approach in diffusion phenomena neglects the structural changes which occurred during the mass transport such as definite changes in porosity (including changes in pore shapes and pore sizes) as well as shrinkage. In addition, the high pressure has been reported effective in variations of the final volume of the plant tissue.

However, the change in volume is more likely to be considerable in case the gas inside the pores escape out without any substitution with another phase, which is observed in common HPP of fruits and vegetables. This will also inevitably occur during the blanching step which is commonly used prior to thermal processing – the purpose being enzyme inactivation and expulsion of tissue gases which would result simultaneously in tissue collapse.

3.7.1 Linear Model

The estimated low diffusivity values as well as low processing time- as two main reasons for obtaining gentle curvature of a mass transfer graph- would give a chance to develop other more applicable models. The effective porosity, as the reachable portion of porous phase, is directly proportional to pore interconnectivity characteristics of pores (Petrich et al., 2006).

During flow in porous media confined in a fluid phase under high pressure levels, the maximum volume of the pores occupied by the fluid could be deemed as the effective porosity. Moreover, considering Leaky-Tube model of flow through porous media, the idle spaces of gaseous phase during the flow are defined as different forms of pores such as dead-end, naturally isolated and induced isolated pores which are not taken into account as the effective porosity (Civan, 2011).

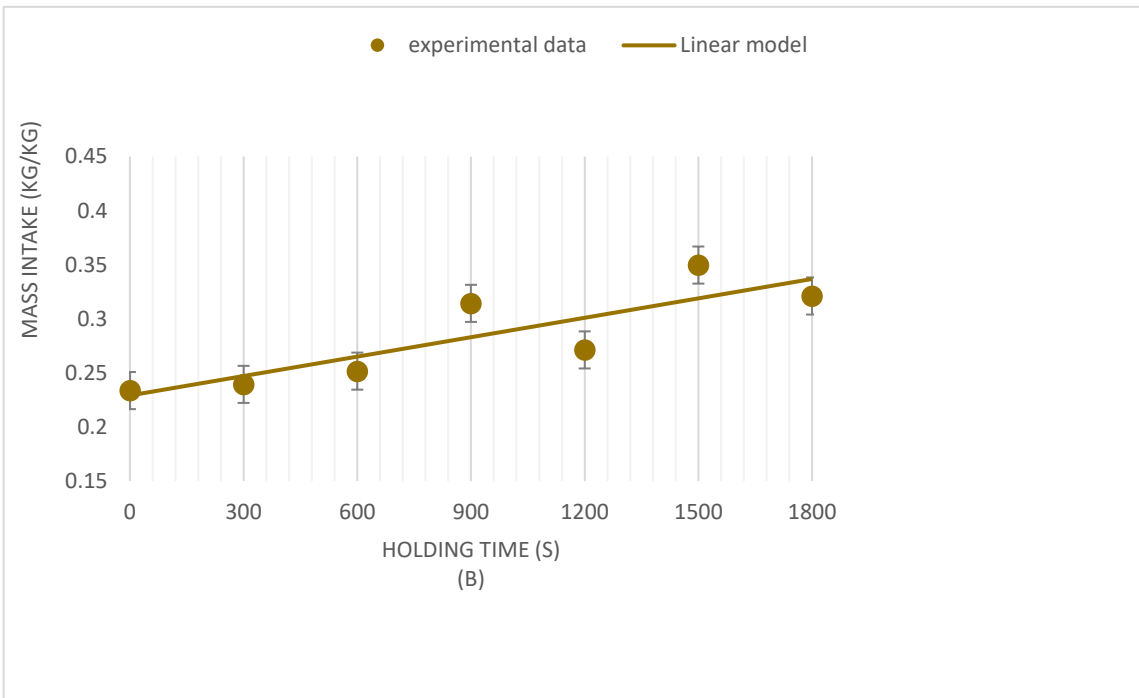
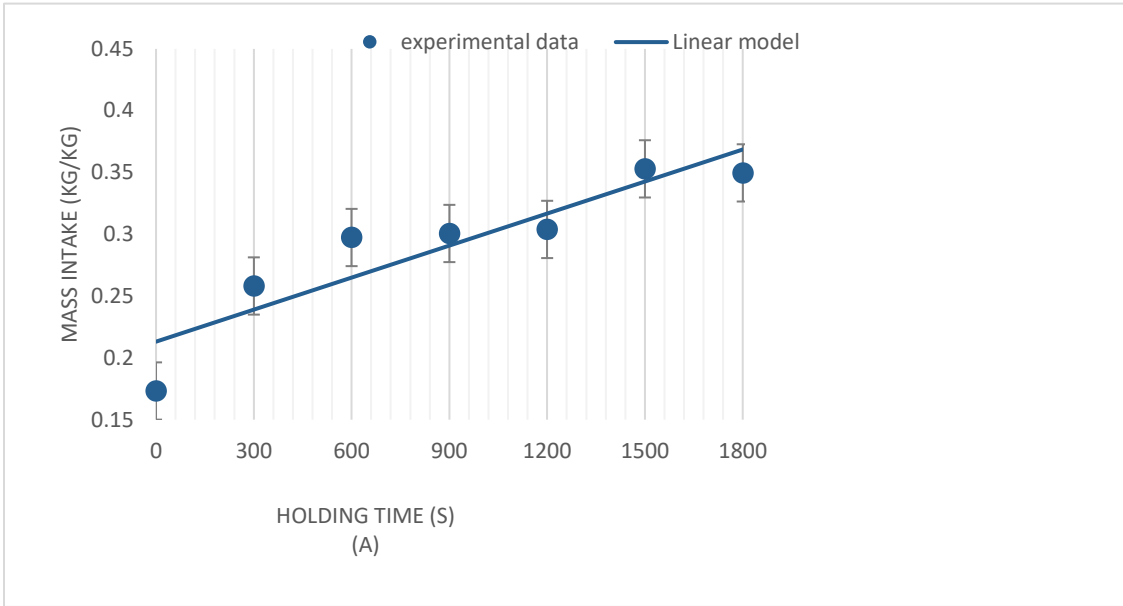


Fig. 3.4. Application of developed linear model for mass intake-holding time data for (a) 100 MPa and (b) 600 MPa pressurizing condition.

Table 3.3 shows the computed model parameters at the highest and the lowest levels of the studied range of pressure. Comparing the mass transfer parameters in the 100 MPa and 600 MPa, it is worth mentioning that the mass transfer at 300 MPa does obey both Fickian and linear models with acceptable fitness parameters ($\epsilon=0.26$, $D'_p = 3.65 \times 10^{-5}$, $R^2=0.96$).

The regression intercept of 100 MPa (= 0.2131) following the overall trend of mass transfer, indicate that although pressure come-up to 100 MPa is not sufficient to achieve a high yield of impregnation close to $\epsilon = 0.22$, there is compensation in mass transfer rate due to high amount of unsaturated texture at first 5 min of holding process. Moreover, as described before, due to other non-Fickian in- and outflows, at 600 MPa the linear model was more logical to be used (Simpson et al., 2015).

Table 3.3. The calculated parameters regarding the linear model of mass intake during HPI at selected pressure levels.

Pressure Level (MPa)	ϵ	D'_p	R2	RMSE
100	0.21	8.63E-5	0.83	0.027
600	0.22	5.98E-5	0.81	0.023

The estimated total porosity at 600 MPa- as a representative of total available space for embodying the fluid- decreased which could indicate destructive mechanical effects of higher pressure levels on the porous medium structure (Table 3.3).

3.7.2 Impregnation of fresh and blanched texture

In terms of food processing applications, the experiments with blanched vs. unblanched tissues present valuable viewpoints (Fig. 3.5). The mass transfer in both cases showed an asymptotical trend while the mass transfer in unblanched samples was higher and showing parallel trends. As can be seen in Fig. 3.5, a 10% mass intake gap between blanched and unblanched samples represent the difference between collapsed and fresh pores. This difference in value shows the efficiency of the porous network to transfer the fluid into open pore spaces. Thus, in practice, using unblanched porous biomaterials provide better

fluid transfer and hence better infusion of solids present in the fluid. In acidic conditions common to fruits, the employed HPP conditions may contribute to inactivating the enzymes because of the synergic effect of high pressure inactivation and acidification of the product. The main purpose of blanching treatment is enzyme inactivation which becomes redundant in HPP/HPI.

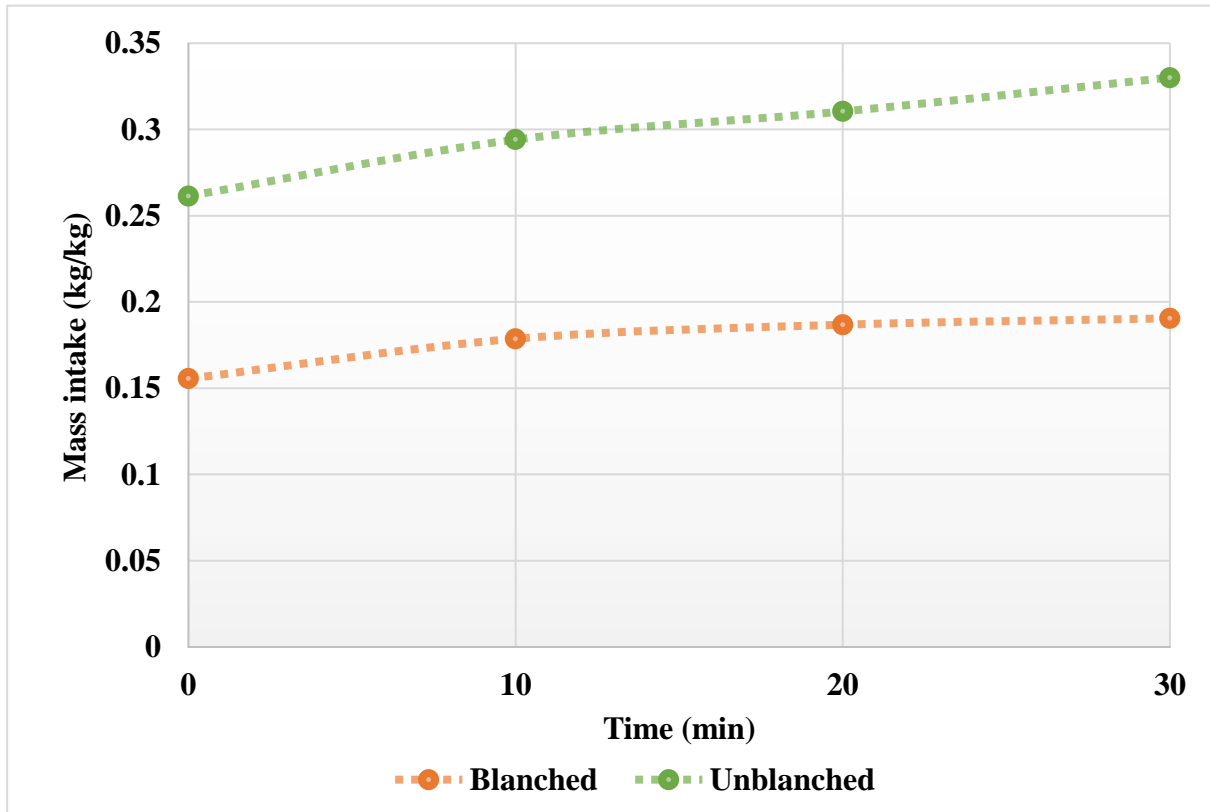


Fig. 3.5. Mass intake data of blached and unblached apple cubes at 300MPa for 30 min of holding time.

3.8 Conclusions

Analogies to Fick's second law as well as zero-order kinetic models could be used to study the dynamics of a forced diffusion process during HPP. This kind of transfer of fluids under high pressure could be an indication of significant non-homogeneity of pressure domain in food systems involving porous media. Thus, further studying of pressure gradients in the matrix could reveal probable critical points in HPP of porous matrix contained food systems. On the other hand, the mass intake data showed that the method could sufficiently perform for intentional impregnation of fluids in a short operation time. Although this could be only achieved by designing an efficient come-up and a short holding time condition

Preface to Chapter 4

In chapter 3, the basics of modeling the fluid flow under high pressure were discussed. Fick's second law was an appropriate model to describe the flow during high pressure processing holding time. During the holding time, the existence of a constant pressure was assumed to force the fluids into the porous media. This, helped the model to be valid due to decreasing on the degree of freedom in the problem condition. On the other hand, the high pressure operation is a collection of three main stages. During the first stage, the pressure is built up by the force of the pump which leads to the injection of more water in a constant volume. After reaching the desired level of the pressure, the holding time starts, and at the end of the pressurization, the decompression takes place.

Just like thermal processing, several parameters would affect the processing condition. In non-thermal HPP, the general parameters could be the pressure level, the time. A combination of pressure level at the time would be the concept of pressurization rate.

In chapter 4, the effect of pressurization rate on the mass intake efficiency of a model system including a standard solution and a plant tissue was studied. The relationship between pressurization rate, and mass intake is investigated. In general, compression rate, compression time, and final pressurization level are three main variables during come-up time. Thus, the obtained results, in companion with the holding-time results- could be useful to obtain a better understanding of the whole HPP process.

Parts of this chapter have been adapted for presentations and publications as follows:

Vatankhah, H., Ramaswamy, H. S. Effect of Pressurization Rate on Fluid Transfer into Porous Media during High Pressure Processing. Northeast Agricultural and Biological Engineering Conference (NABEC), July 2017, Groton, CT, USA.

Vatankhah, H., Ramaswamy, H. S. (2018). High Pressure Impregnation (HPI) of Apple Cubes: Effect of Pressure Variables and Carrier Medium, *Food Research International*. (submitted).

CHAPTER 4

MODELING AND CHARACTERIZATION OF THE EFFECT OF PRESSURIZATION RATE, COME-UP TIME AND HOLDING TIME ON PRESSURE DRIVEN-FLUID TRANSFER INTO POROUS MEDIA

4.1 Abstract

High pressure impregnation (HPI) is a novel technique to infuse desired fluids into porous biomaterials. In this study, the effect of 24 different pressure–time combination treatments were studied: come-up time (0 to 6 min), pressurization rate [100, 150, 200, 300 (MPa/min)] and pressure holding times (0 – 30 min) at 100, 300 & 600 MPa. Experiments were carried out based on HPI of ascorbic acid (AA) as a low viscosity aqueous (1%) Newtonian fluid. AA infusion reached 215 to 250 mg/kg when reaching operating pressure of 200 MPa irrespective to pressurization rate or come-up time. As a function of holding time (0 to 30 minutes) at different pressure levels (100MPa, 300MPa, 600MPa) the calculated D_{eff} values were 2.67×10^{-9} , 2.35×10^{-9} , and 1.47×10^{-13} (m^2s^{-1}), respectively. The data indicated an inverse correlation between the pressure level and D_{eff} . A model for the entire process was developed based on the combination of a first-order kinetics during the come-up time and a linear diffusion process during pressure holding time.

4.2 Introduction

High pressure processing (HPP) is a non-thermal preservation technique (Knorr et al., 2006; Medina-Meza et al., 2014; Norton, & Sun, 2008; Singh & Ramaswamy, 2015; Wang et al., 2015) and has been recognized for the destruction of vegetative microorganisms and known as a cold pasteurization technique (Bignon, 1996; Tola & Ramaswamy, 2014; Ahmed et al., 2014). HPP has also been reported as a promising technique to achieve an

acceptable microbial and enzymatic destruction while having a minimally affected texture (Balasubramaniam et al., 2008; Singh & Ramaswamy, 2014).

While subjecting foods to HPP, different physical, biological, and chemical phenomena are likely to occur (Ahmed et al., 2014; Alvarez et al., 2008; De Maria et al., 2015; Hussain et al., 2017; Hussain et al., 2016). Another phenomenon that happens is mass transfer when the food system contains a liquid and a porous medium in contact with each other (George et al., 2016; Sila et al., 2004). These porous matrices could be formed from any fruit or vegetable tissue. Such mass transfer techniques could occur naturally, due to the formulation features, or intentionally as a planned infusion/impregnation of fluids into such parenchymatic tissues. The latter technique is also known as high pressure impregnation (HPI) (Vatankhah et al., 2018a; Vatankhah & Ramaswamy, 2017). The impregnation techniques have been both industrially and traditionally used for different purposes based on the functionality of solutes. The traditional way of impregnation has been mostly conducted under atmospheric pressure or, recently, under vacuum pressure (Petersen, 2014).

HPI is a type of application of high pressure processing. During HPP, after loading the chamber, there is a pressure build-up stage (come-up time or pressurization or compression time) during which the pressure is gradually elevated to the operating pressure level. Then follows a holding time, the main pressure treatment application stage of processing for preservation purposes, and, finally, the rapid depressurization period through which the HP process is terminated. Pressurization rates during the come-up time, the operating process pressure level and the holding times, and the depressurization to a lesser degree are main HPP parameters considered important in the operation design (Farkas & Hoover, 2000). The important advantage about HPP is the roughly uniform distribution of pressure and temperature throughout the geometry of food matrices (Torres & Velazquez, 2005). This uniform distribution of thermodynamic parameters allows for the study of mass transfer based on the pressurizing rate and pressure holding time. This type of study could be achieved by conducting the HPI as a function of different processing conditions including different pressurization rates, pressure level, and pressure treatment (holding) times.

HPI can be conducted using a wide range of fluids with different physical behavior and functionalities. Since the process of impregnation is directly related to the fluid flow phenomena, the physical behavior of fluid phase could play an important role in the intensity of mass transfer within the tissue (Vatankhah & Ramaswamy, 2017). These physical behaviors include viscosity, and rheological properties (Newtonian/non-Newtonian), density, and pressure resistance of the mentioned variables.

This research was done based on HPI of ascorbic acid which is a recognized anti-oxidant and well recognized vitamin. The objective was to evaluate the HPI performance as a function of different pressurization rates, come-up times, holding time, and final operating pressure level.

4.3 Material and Methods

4.3.1 Sample Preparation

Fresh McIntosh apples were collected from the horticultural research farm on the Macdonald Campus of McGill University, Ste. Anne de Bellevue, Canada. The apples were selected after visual inspection to ensure similarity in shape and size and same date of harvesting. Apple cubes of size 1.2 cm × 1.2 cm × 1.2 cm were prepared after washing and peeling. For each test, two cubes were weighed (APX-200 Digital weighing Balance, Denver Instruments) and kept in low-density 2 oz. polyethylene bags (Whirl Pak(R), Nasco, Fort Atkinson, WI, USA) containing 25 ml of desired solutions. The bags were immediately heat sealed and transferred to the HPP chamber for treatment. Also, aqueous solution of 1% (w/w) ascorbic acid (AA), (Sigma Aldrich, USA) was prepared as a simple dilute Newtonian fluid.

4.3.2 High pressure processing

High pressure impregnation (HPI) treatment was carried out using an isostatic high pressure unit with a cylindrical pressure chamber of 5 L volume (ACIP 6500/5/12VB-ACB Pressure systems, Nantes, France). A computer controller and a data logger (SA-32, AOIP, Nantes, France) was used for recording the pressure, time, and temperature. Water was used as the pressure transmission medium in the system. The samples were introduced into

high pressure vessel at 15-18 (°C), so the temperature of the medium and sample were around 25 °C during the treatment (Zhu et al., 2004). Jemai and Vorobiev (2002) stated that the critical temperature which makes mechanical changes in the plant cells is approximately 50 to 55 (°C) and the conditions used in this study were well below this temperature.

With ascorbic acid solution, HPI treatments included various pressure-time combinations of pressure level, pressurization (compression, or come-up) time, and holding time. First, the pressure-time (P-t) profiles were designed to achieve selected target pressures (100, 200, 300, 400, 500 and 600 MPa) at different pressurization rates (100, 150, 200, 300 MPa/min) (Fig. 4.1). The pressure holding-times were then varied between 0 and 30 min at 100 MPa, 300 MPa, and 600 MPa test runs.

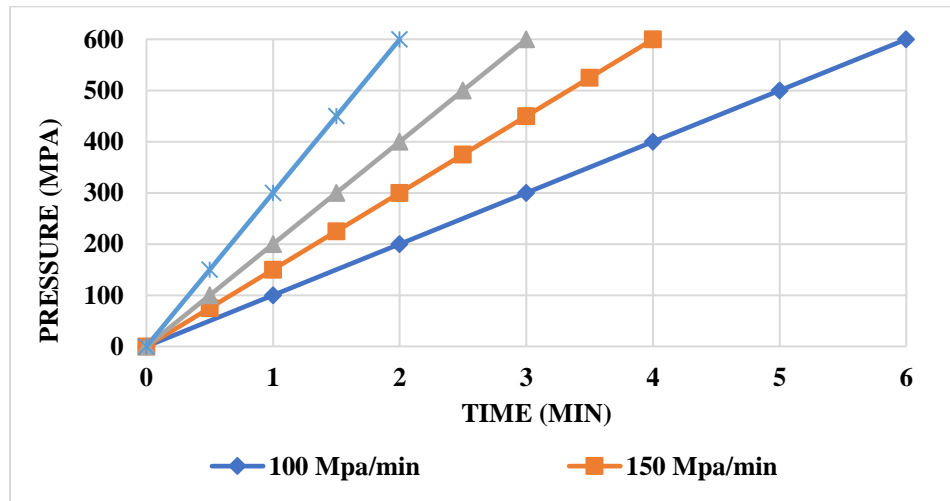


Fig. 4.1. The experimented P-t profiles using 100, 150, 200, 300 MPa/min pressurization rate

Following the pressure treatment for the required holding time, the pressure in the vessel was released rapidly (< 3 s). After the treatment is completed, the bags were opened, and the liquid drained out for 10 s to remove the free excess liquid adhering to the surface, blotted using a wet towel and then weighed.

4.3.3 Calculation of total mass intake ratio

At each P-t processing condition, the AA intake would be proportional to the mass intake of the dilute solution (fluid) intake since solid separation is unlikely through the loosely structured porous solid (apple cube). The impregnation yield of AA (mg/kg apple) was measured as a function of time using Eq. 4.1 as the concentration fraction of the fluid intake.

$$W_t = (M_t^\circ - M_0^\circ)/(1000 \times M_t^\circ) \quad (4.1)$$

where, W_t , M_t° , and M_0° represent total mass change at time t, the mass of cubes at time t of pressurizing at a constant pressurization rate and the initial mass of cubes, respectively.

4.3.4 Modeling and mass diffusivity estimation using Levenberg-Marquardt algorithm

According to isostatic principle, due to uniform and quasi-instantaneous transmittance of pressure throughout the whole sample, the ascorbic acid mass flux can be assumed to be the same on all 6 surfaces of the cube (Eq. 4.2). As a result, considering the assumptions in Da Silva et al. (2009), the problem can be solved as a mass transfer phenomena in three infinite slabs of 2L thickness using the analytical solution of Fick's second law (Crank, 1975; Ramaswamy et al., 1982), (Eq. 3).

$$W_T^H = \omega \frac{\bar{X}(t) - X_e}{X_0 - X_e} = W_p^3 \quad (4.2)$$

$$W_p = \frac{8\omega}{\pi^2} \sum_{n=0}^{\infty} \frac{1}{(2n+1)^2} \exp \left[-(2n+1)^2 \pi^2 D \frac{t}{4L^2} \right] \quad (4.3)$$

where, W_T^H is the total mass content during holding time, W_p is the mass at each plate, X is the transient mass intake (kg kg^{-1}), D is the mass diffusion coefficient ($\text{m}^2 \text{s}^{-1}$), and z and t are the position at each direction of Cartesian system(m) and time (s), respectively.

The X_0 was assumed as the initial concentration fraction at the start of the impregnation process (not the initial concentration) characterized by the pressurization followed by an immediate depressurization (no pressure holding time). The measured X_0 and mass intakes at all holding times were used to estimate equilibrium mass fraction X_e based on reaching

an asymptotical equilibrium of Peleg's equation (Peleg, 1988). The boundary conditions and model assumptions are stated in Vatankhah and Ramaswamy (2017).

As the final step, the mass diffusivity values were estimated using inverse methods of parameter estimation optimization (Eq. 4.4) which has been successfully used as a tool for inverse estimation of diffusivity parameters considering the Crank formula as a target function (Da Silva et al., 2009):

$$\beta^{k+1} = \beta^k + \left[(J^k)^T J^k + \lambda^k \Omega_m^k \right]^{-1} (J^k)^T (Y - X(\beta^k)) \quad (4.4)$$

Where, k , λ , and Ω_m are the number of iterations, damping parameter, and a diagonal matrix, respectively.

J is the sensitivity coefficient matrix defined as described in Eq. 4.5:

$$J(\beta) = \frac{\partial X^T(\beta)}{\partial \beta} \quad (4.5)$$

And the matrix term $\lambda^k \Omega_m^k$ is for damping the oscillations and instabilities due to the pour problem conditions.

The iterative method (similar to the *Gauss* iterative method) starts with an initial guess (β_0), and each step vectors gets modified until the precondition is achieved (Eq. 4.6):

$$\frac{|\beta_i^{(k+1)} - \beta_i^k|}{|\beta_i^k| - \xi} < \delta \quad \text{For } i=1, 2, 3 \dots \quad (4.6)$$

where ξ and δ are defined according to the parameter range expectations.

4.4 Results and discussion

4.4.1 Effect of pressurization rate on AA impregnation

Figure 4.2 shows the AA intake vs. pressurization time graphs at different pressurization rates. The mass intake of AA at pressurization rates higher than 100 MPa/min were between 220 and 240 (mg/kg). In all cases, the overall trend showed a decrease in the AA intake as a function of pressure level (Fig. 4.2). The least relative decrease in AA mass intake was associated with 100 MPa/min pressurization rate (Fig. 4.2a).

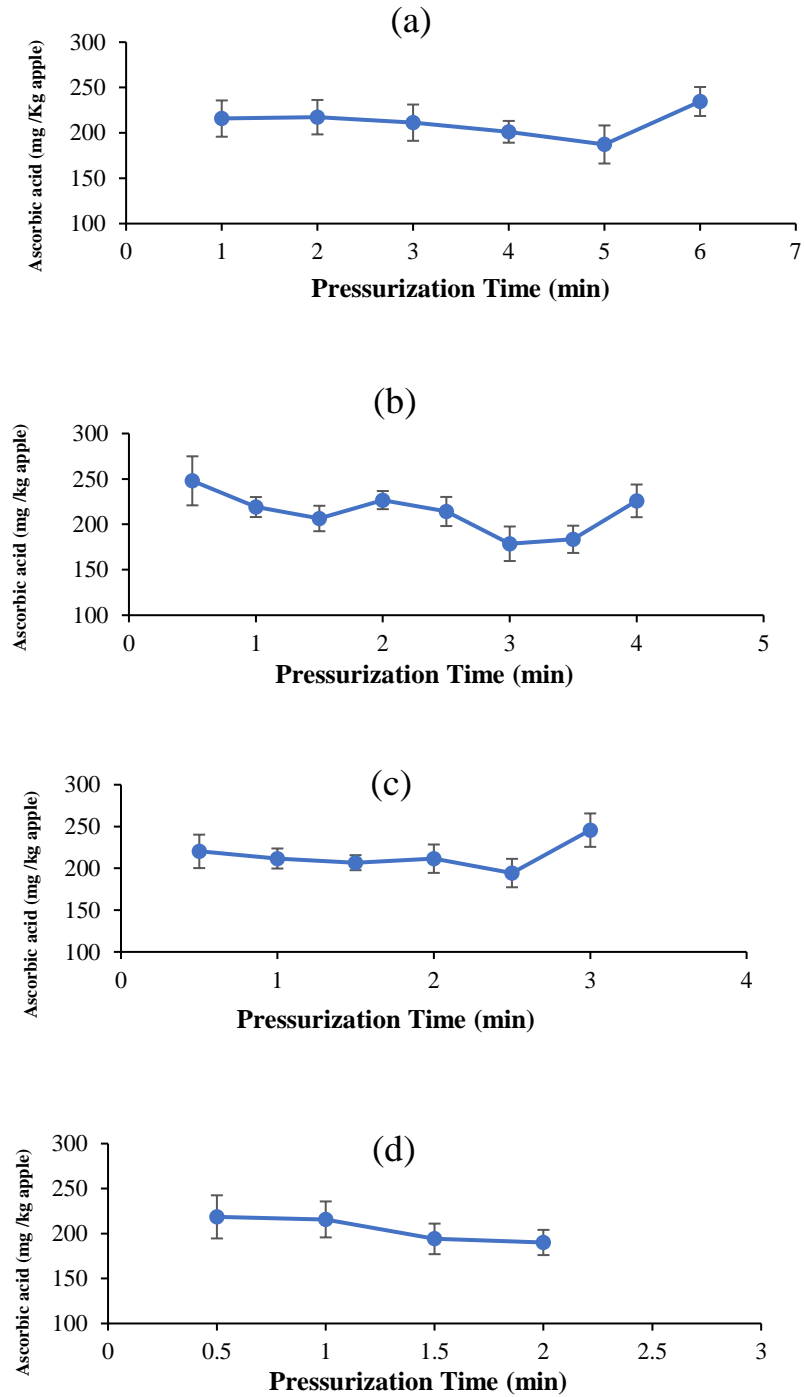


Fig. 4.2. The AA intake versus Pressurization Time of model system containing 1% aqueous ascorbic acid solution and 1.728 mm³ apple cubes at (a) 100 MPa/min, (b) 150 MPa/min (c) 200 MPa/min and (d) 300 MPa/min. Error bars represent standard deviation.

According to Fig. 4.2, at ≤ 200 MPa/min, there was an increase in the AA mass intake in the samples while reaching the highest at pressure level 600MPa. Thus, the effect of instant pressurization on texture, especially on porous shape and characteristics of apple, was less prominent at these pressurization rates. This increase in the final AA mass intake also indicated that at ≤ 200 MPa/min, the tissue did not reach a full saturation at the initial stages of pressurization. However, at all pressurization rates ≤ 200 MPa/min, the final AA intake when reaching 600 MPa was less than 40 mg/kg but higher than that of pressurization for 1 min. Thus, considering energy saving and production efficiency, it is more logical to focus on primary stages of pressurization.

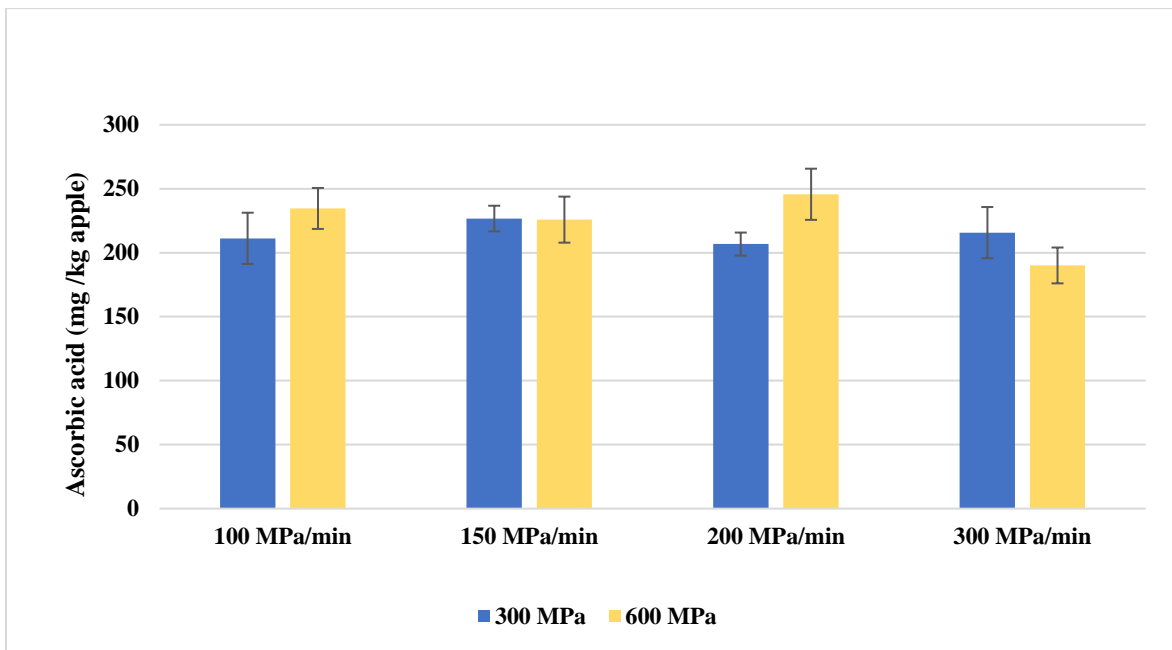
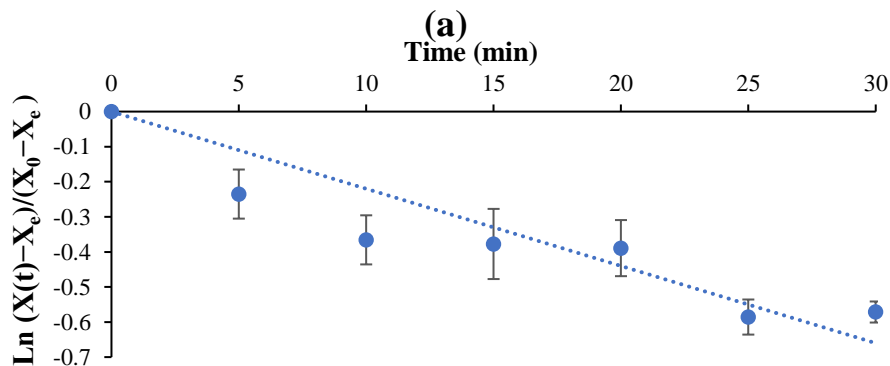


Fig. 4.3. HPI of 1% aqueous ascorbic acid solution in 1.728 mm³ apple cubes while reaching 300MPa and 600MPa at 100, 150, 200, and 300 MPa/min pressurization rates. Error bars represent standard deviation.

To illustrate this optimal situation, the AA impregnation yields were compared after reaching 300 MPa and 600 MPa at different compression rates (Fig. 4.3). The mass intake data ranged from 190 to 245 (mg/kg apple) regardless of the final pressure level and pressurization rate. However, the plots confirm lack of any specific trend.

4.4.2 Mass transfer during holding time

The semi-log graphs AA mass intake versus holding time are shown in Fig. 4.4. The experimental data showed that the final AA intake decreased at higher pressure level. After 30 min of HPI, the AA intake was 350, 330, and 320 (mg /kg apple) at 100, 300, and 600 (MPa). The slope of the linearized mass intake is also an indicator of effectiveness of HPI. As can be seen, at 600 MPa, the slope was the lowest which showed that there is a considerably lower mass intake rate. Thus, it should be mentioned that the AA intake did not simply show a direct effect to increasing high pressure. This behavior was also in agreement with the come-up time results which showed that providing more pressure would not necessarily increase the intake. As a result, HPI rate is a function of interaction of fluid and solid phases and the effect of high pressure in the porous medium. In this regard, it could be concluded that processing at higher pressure levels lead in two situations; first, the intercellular spaces develop new pressure-induced gaseous pores while there is a lack sufficient time for exhaustion of trapped gas. Second, the textural effect of compression on the fruit tissue at extremely high pressure levels would affect the total holding capacity of the cubes.



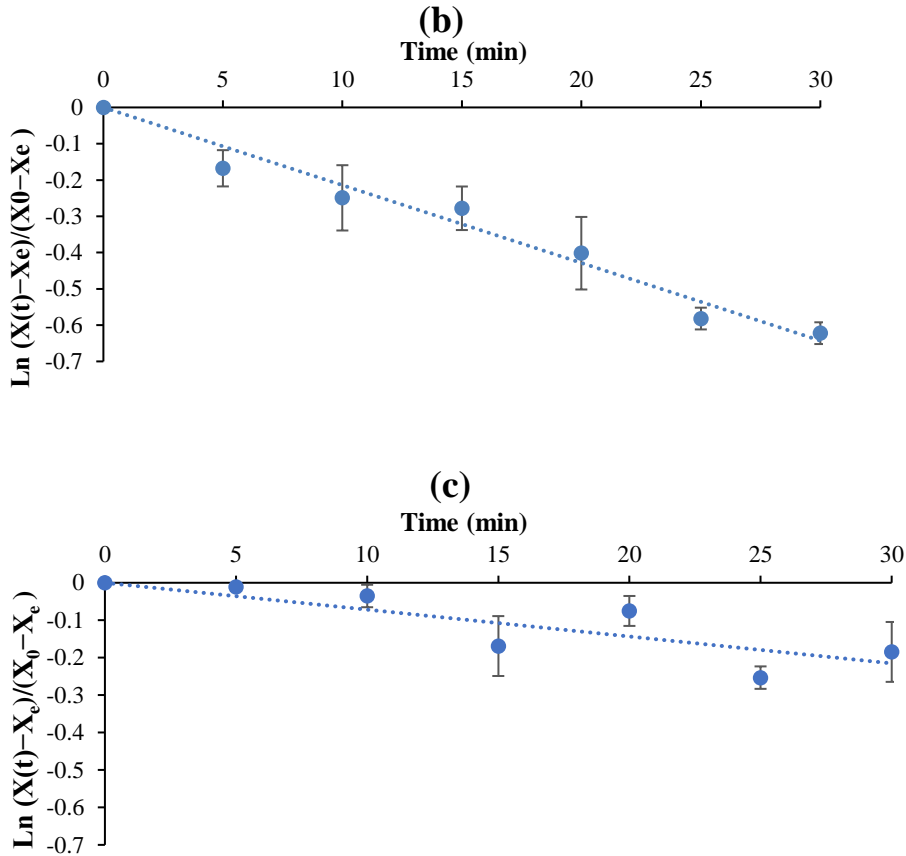


Fig. 4.4. Semi-logarithmic plot of Crank's formula for HPP at (a) 100MPa, (b) 300 MPa, and (c) 600 MPa during holding time up to 30 min. $X(t)$, X_0 , and X_{eq} indicate the mass intake (kg/kg) of the model system after t seconds of pressure holding, initial mass intake (kg/kg), and predicted equilibrium mass intake(kg/kg), respectively

4.4.3 Modeling of HPI during the pressure come-up time

Under HPI, the mass intake as an independent variable showed no consistent trend with pressure level, while an exponential trend was observed as a function of the duration of pressurization (come up time). Thus, a first-order kinetic model with respect to an apparent porosity value as the maximum reachable intake was used to fit the uptake data versus the pressure come up time (Eq. 4.7). The model parameters at each pressurization rate are presented in Table 4.1.

$$W = \omega\varphi e^{-kt} \quad (4.7)$$

where W , ω , φ , k , t represent the mass intake (mg AA/kg apple), AA mass fraction (mg/kg) in the impregnation solution, apparent porosity, rate constant, and compression time (min), respectively.

Table 4.1 Estimated model parameters during HPP at different pressurization rates. φ is the estimated apparent porosity, and k represents the rate constant.

Pressurization Rate (MPa/min)	φ (-)	k ($\times 10^2$) (min^{-1})	R^2	RMSE
100 ^a (up to 500MPa)	0.23	3.6	0.85	0.02
150 ^a (up to 500MPa)	0.25	9.1	0.78	0.02
200 ^a (up to 500MPa)	0.23	5.0	0.75	0.04
300 ^a (up to 600MPa)	0.23	10.5	0.90	0.01

The experimental results showed that according to Eq. (4.7), the constant rate ranges 5×10^{-2} to 10.5×10^{-2} (min^{-1}) The lowest and the highest k belonged to 100 MPa/min and 300 MPa/min indicating a less efficient mass transfer at highest compression rate (Table 4.1).

4.4.4 Modeling HPI during pressure holding

According to the estimated diffusivity values presented in Table 4.2, the mass transfer was more efficient at lower pressures. The experimental data at 600 MPa displayed more variability. In this case, a numerical restriction condition was defined to calculate the diffusivity in the range of $10^{-13} \text{ m}^2 \text{ s}^{-1}$ to $10^{-9} \text{ m}^2 \text{ s}^{-1}$. The diffusivity values at 100 MPa and 300 MPa fell between the typical range of diffusivity of liquid water ($10^{-9} \text{ m}^2 \text{ s}^{-1}$) and diffusivity of water vapor ($10^{-5} \text{ m}^2 \text{ s}^{-1}$). The obtained values were closer to diffusion of liquid water since the pores were essentially filled with a liquid during pressure come-up time. Guillard et al. (2003) found that water transport takes place predominantly in the liquid phase within the swollen matrix while reaching saturation in the porous media. To use the obtained diffusivities as an indicator of product yield a few studies on mass transfer

modeling of vacuum impregnation of apple used the Fickian formula. In this regard, Allali et al. (2010) found the diffusivity of sugar and citric solution with 83% moisture content to be about $7.7 \times 10^{-10} \text{ m}^2\text{s}^{-1}$. This indicates the higher impregnation force involved while using high pressure.

Table 4.2 The estimated effective diffusivity values during holding time at high pressure operation levels of 100, 300, and 600 MPa using Levenberg-Marquardt optimization algorithm

Pressure Level (MPa)	D_{eff} (m² s⁻¹)	R²	RMSE
100	2.67E-09 ^a	0.94	0.04
300	2.35E-09 ^c	0.94	0.06
600	1.47E-13 ^f	0.87	0.08

4.4.5 A coupled model for the entire process

Mass transfer behavior is the first step in the characterization of physical property of HPI processing technique. Evaluation of mass transfer kinetics gives useful insight with respect to the process yield. Moreover, modeling the mass intake data reveals the physical nature and main governing factors of transport phenomena. There have been numerous mass transfer models developed based on experimental and theoretical works resulting in some satisfactory practical and simplification approaches. For instance, the semi-theoretical or empirical models, which are mostly derived from simplifying the general series solution of Fick's second law, have the capability simplifying the calculations although they are valid only within the predefined conditions of the processing (Guillard et al., 2013).

A comprehensive model could be proposed after obtaining the mass transfer models during come-up and holding time. The general model included the first-order kinetics response of the mass transfer during to the compression stage. In addition, the Fickian mass transfer behavior of the holding time was reflected in the model. Thus, assuming an accumulative

trend during both come-up and holding time, Eq. 4.3 and Eq. 4.7 could be coupled as shown in Eq. 4.8

$$M_t|_{t>t_{come-up}} = \omega(\varphi e^{-kt_{come-up}} + \frac{512}{\pi^6} e^{\frac{-3\pi^2 D}{4L^2}(t-t_{come-up})}) \quad (4.8)$$

It is worth noting that, studying and implementation of a mass transfer during an intentional impregnation under HP could likely be important in the case of consideration of infusion of certain fluids as a pre-treatment for other techniques. Mainly, in case of coupling with thermal processing, it could be a unique multi-objectives pre-treatment since pressurization could be effective in inactivation of undesirable enzymes and vegetative pathogenic and spoilage microorganisms. However, HP microbial spore destruction under moderate temperatures is ineffective as compared to a heating process. A second and more important contribution of HPI is the degasification of the tissue structure and substitution of void phases by anti-browning agents like ascorbic acid which could help to maintain the product quality. Last, but not least, in high acidic conditions common to fruits, the employed HPI conditions selected could inactivate the oxidative enzymes (polyphenol oxidase) as well as pathogenic bacteria representing commercial sterilization because spores remain inactive under such conditions. The main purpose of blanching is enzyme inactivation and driving the dissolved gasses out, and HPI can accomplish both the tasks without the normal shrinkage associated with conventional blanching. With an acid incorporated in the porous tissue, acidification of low acid foods can be simultaneously accomplished leading to acidified low acid food commercial sterilization using high pressure. Buckow et al. (2009) reported that more than 90% inactivation of PPO was achieved after a 5-min treatment at 600 MPa. Further, FDA guidelines stipulate that an HP treatment of one minute at 550 MPa is likely to achieve safe pasteurization in acidic and acidified low acid products. In other words, the process guarantees a pasteurisation of acidified products and could compensate the lack of sterilisation abilities of high pressure at lower temperatures.

4.5 Conclusion

Transport of fluids into porous media under pressure is deemed as a complex phenomenon with numerous mechanical and thermodynamic parameters. Knowing the mechanical properties of the medium and its behavior under pressure, the rheological changes of the

fluid phase under pressure and effect of each stage of processing on the total mass transfer needs more investigations. This study presented highly applicable models which can present an estimation of total mass intake as a function of compression time. In addition, the comprehensive model could be a perfect example in terms of obtaining a conclusion out of results obtained from segmentation of each processing step. However, further investigations using Hybrid Micro-, Meso- and Macroscopic scale models, could reveal more information in terms of homogeneity and continuity of flow paths inside the porous media. In terms of processing applications, more attempt should be done to evaluate numerous capabilities of this process. In fact, the process can become popular due to its ability to physically modify the texture &/or chemically enrich the texture while reaching a level of pasteurization and enzymatic inactivation.

Preface to Chapter 5

In chapters 3 and 4, mass transfer models considering the effect of pressure level, holding time, and the combination of time and pressure – known as pressurization rate- were proposed to evaluate the dynamics of high pressure impregnation. The experimental data, as well as the proposed models, give a macroscopic knowledge regarding the accumulated mass within the tissue.

In chapter 5, it was attempted to see the HPI process from a different angle. In this regard, the microstructural studies were conducted using different ways of microscopy. The effect of HPI on the porous matrix was observed using different microscopy methods. In addition, novel methodologies were introduced to achieve a better qualitative demonstration of flow in porous media. Moreover, numerical simulations were carried out and the results were verified with captured and processed images of impregnated samples.

Parts of this chapter have been adapted for presentations and publications as follows:

Vatankhah, H., Ramaswamy, H. S., (2017). Dynamics of fluid migration into porous solid matrix during high pressure treatment. *Food and Bioproducts Processing*, 103, 122-130.

Vatankhah, H., Akbarzadeh, A. H., Ramaswamy, H. S. (2018). A Hybrid Fickian-Darcian Flow Model for High Pressure Impregnation of Fluids into Porous Biomaterials, *Biosystems Engineering*, 166, 200-209.

Vatankhah, H., Ramaswamy, H. S. (2018). High Pressure Impregnation (HPI) of Apple Cubes: Effect of Pressure Variables and Carrier Medium, *Food Research International*. (submitted).

CHAPTER 5

MICROSTRUCTURAL EVALUATION OF HIGH PRESSURE IMPREGNATION OF BIOMATERIALS

5.1 Abstract

In this study, several visualization techniques were used to monitor the high pressure impregnation(HPI) process. Scanning electron microscopy images showed endurance of porous network after HPI. Partial rearrangement of flow paths was observed after HPI at 300MPa for 15min. In addition, impregnation of apple with toluidine blue (0.1% W/W) was introduced as a microstructural method to trace the flow paths within the tissue. Watershed algorithm was used to simulate the flow paths of the light microscopy images. The results indicated perpendicular flow paths at the boundaries. The simulation results were in agreement with SEM images. In addition, blue color infused apple cubes were prepared, and using the image processing techniques, progression of impregnated tissue was illustrated. The latter experimental illustrations were used as an equivalent to numerical simulation of a diffusion model in a geometrical domain with same size.

5.2 Introduction

High-pressure processing (HPP) is a promising technology in the field of non-thermal applications. It is a preservation technique due to its ability to deactivate microbial growth in food products. It consists of subjecting all the sides of a food product to uniform isostatic pressures.

In high-pressure processing, the pressure applied onto food material can range from approximately 40 to 1000 MPa with or without combined heat. This pressure is compressing throughout the food materials uniformly and instantaneously. The compression is for a brief period using mostly water as a pressure-transmitting medium. The pressure resulting from the mentioned external force causes a compression of the food material and enhances the shelf-life and quality attributes of food.

In addition to quantitative facets of modeling of HPI outcomes, a qualitative image analysis approach was used to describe the nature of fluid flow dynamics under high pressure into a plant tissue. Numerical solutions were correlated with image analysis obtained from color impregnated apple tissues.

In this regard, two types of microscopy were used to observe the effect of the impregnation phenomenon into the porous media. The light microscopy, as the classic method of microscopic observations, was used. However, such observations needed certain preparation techniques which are known as the alcohol drying method of microtome preparation. Also, a new technique was used in order to trace the flow paths within the tissue. As described below, this method was based on using permanent dyeing agents which could be traceable after changing the cell wall color. The Scanning electron microscopy was also used to clarify the micro-scale effects of impregnation under high pressure on the cell wall and intercellular space.

In addition to mentioned methods, two different computational methods were used to simulate the mass transfer. These models were developed based on the images taken from the samples which were impregnated with dyes. First, numerical simulations using Fick's second based on the diffusivity values in Chapter. 2 were conducted. The second model was a qualitative model using a Watershed algorithm which could give useful insight regarding the modeled flow paths.

5.3 Material and methods

5.3.1 Light microscopy

To trace the flow paths during the impregnation, an aqueous 0.1%W/W toluidine blue (Sigma Aldrich, USA) was used as the fluid. HP treatment was carried out at mid-pressure level of holding time (300 MPa) for 15 min after 1 min come-up time. After the HP treatment, the samples were cut into 100 μm slices using Leica RM-2125 microtomes (Leica Microsystems, Concord, ON).

The slices were fixed using a series of aqueous 30%, 70%, and 100% ethanol solutions (v/v), (Adam et al., 2005). The microstructure observations were made using a light

microscope (Wild M3C, Leica Microsystems, Germany) fitted with a CCD RGB camera (MACC-C71, Sony, Japan). Images were gathered using an image analysis software (Visilog 5.4, Noesis, France).

5.3.2 *Scanning electron microscopy (SEM)*

The fresh and impregnated samples were freeze-dried, and the dried samples were mounted on aluminum stubs with conductive adhesive in a scanning electron microscopy (SEM), (TM3000, Hitachi, USA). The imaging was done at an accelerating voltage of 5 kV, from a working distance of 6 mm. The images were obtained at a range of 5x to 1500x magnification to observe the possible structural changes of the tissue after impregnation.

5.3.3 *Image processing*

To demonstrate the mass transfer behavior under pressure, 1 mL of food grade blue color (Club House, ON, Canada) was added to 50 ml of the test fluid, and high-quality RGB images were captured from the samples. The “B” matrix of the image, which represents the blueness of the image, was normalized to the values of the X_0 and X_{eq} and the contours of the images were obtained.

5.3.4 *Numerical simulation*

Mass transfer was numerically modeled using finite element methods; the calculated diffusivity parameters were used to obtain the transient mass transfer. The initial boundary conditions were set based on section 3.7. The X_{eq} and X_0 values were measured to be 0.31 and 0.21 (kg/kg), respectively. The calculations were done based on a 2D domain of the same size of the cubes. The meshing was performed using a triangular element of 1 mm sides. Typical results are shown for 200 MPa processing after 5 and 15 min of processing. The codes for simulation were written using MATLAB.

5.4 Results and Discussion

5.4.1 SEM analysis of the samples

The SEM image of the untreated sample showed a well-organized cell and pore distribution in fresh-cut apple (Fig. 5.1a). After pressurization and mass intake, the images showed clear rearrangements in porous shapes and their connectivity. In addition, cellular collapses are evident in Fig. 5.1b. One of the important points would be endurance of porous structures which are convincing evidence regarding the validity of the proposed method of mass transfer modeling. Although, in comparison with the homogenous distribution of small pores and well-organized cell-to-cell contacts, larger size and fewer numbers of pores in treated samples indicate structural rearrangements in terms of the development of two phases consisting collapsed cells and large fluid streamlines.

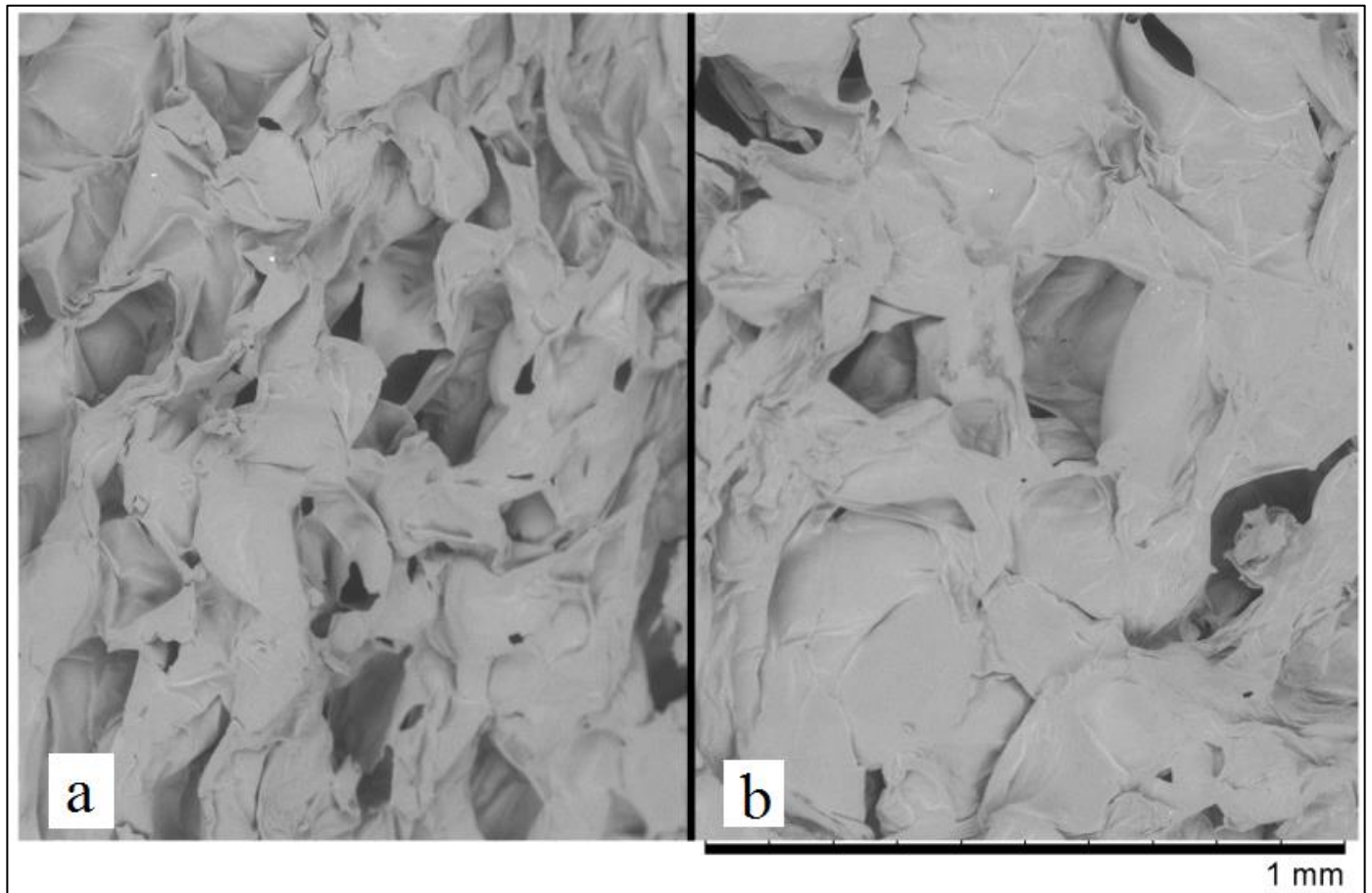


Fig. 5.1. SEM images of (a) untreated (b) impregnated for 15 min at 300MPa.

5.4.2 Observation of the flow paths in light microscopy and SEM

The light microscopy (Fig. 5.2) of the samples treated in the same condition showed a similar 2D porous network in agreement with the SEM data as well (Fig. 5.3). Comparing the images, it was evident that the porosity in the untreated apple consists randomly distributed paths which make the homogenous intercellular void space (yellow arrows shown in Fig. 5.3a). However, after HPI, due to forced currents toward the center, a cellular rearrangement takes place and as a result, the flow paths appear in a parallel and homogeneously aligned regarding the flow direction (yellow arrows shown in Fig. 5.3b).

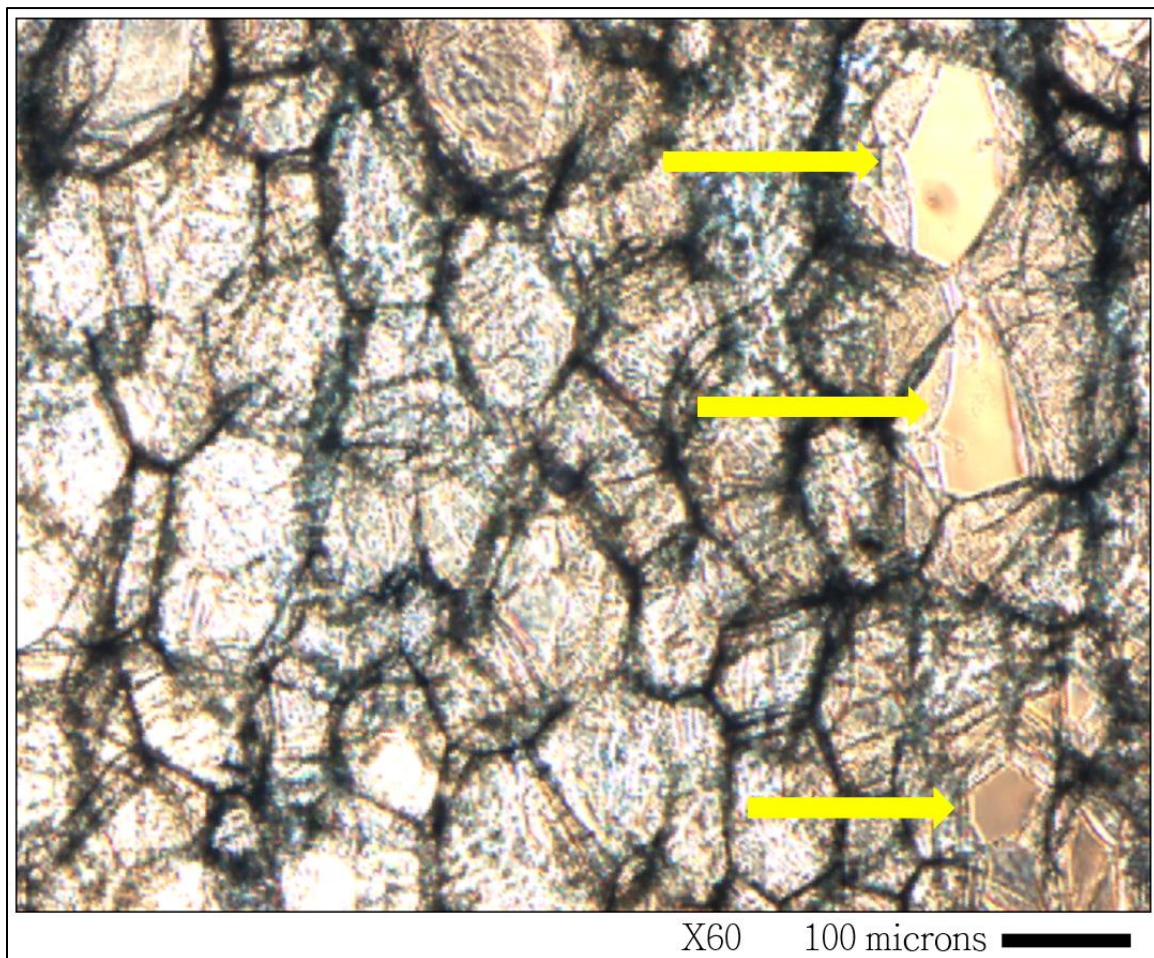


Fig. 5.2. Light microscopy illustration of apple tissue impregnated for 15 min at 300MPa. The samples are treated and fixed using toluidine blue and ethanol right after the impregnation. Yellow arrows indicate the void intercellular space (pores).

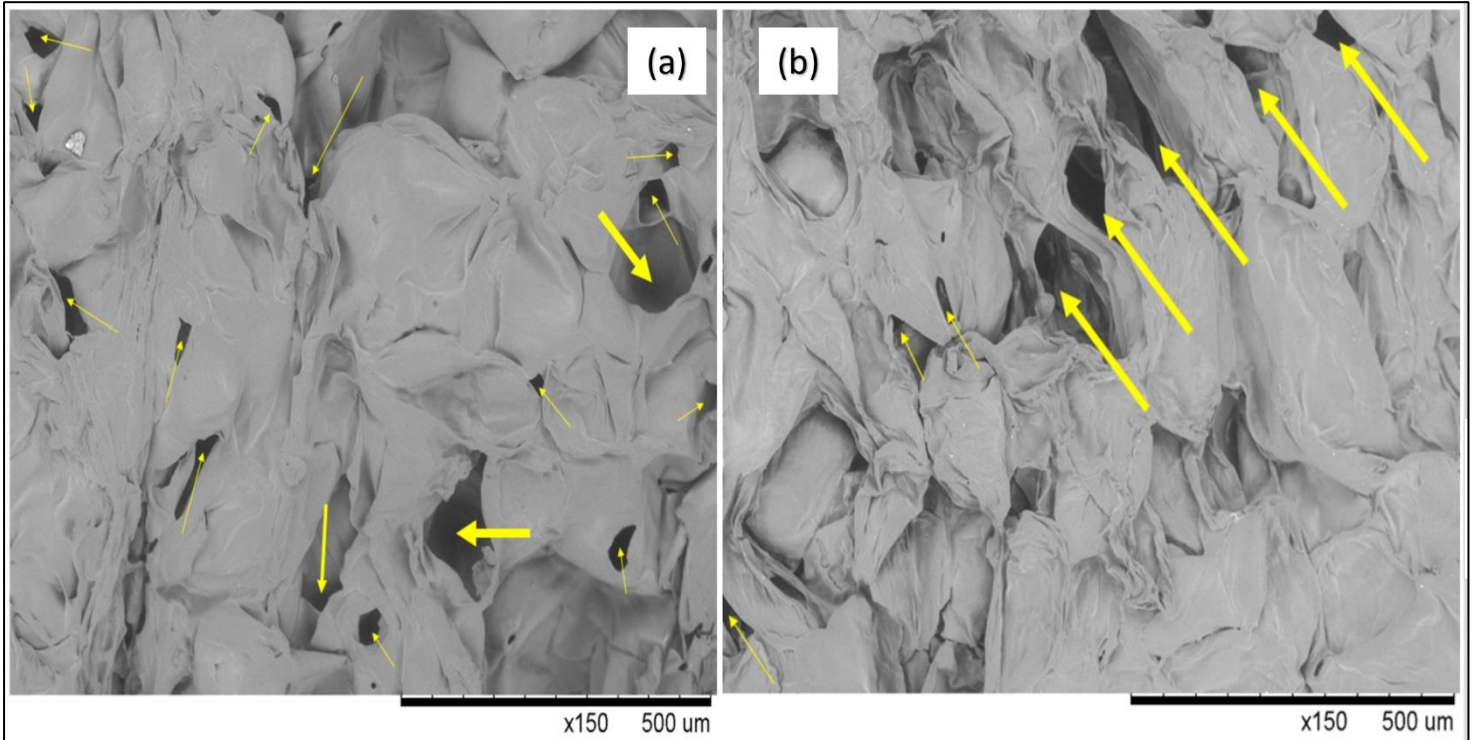


Fig. 5.3. SEM images of (a) untreated (b) impregnated for 15 min at 300MPa.

This fact was also in agreement with watershed modeling of the light microscopy images which are described below (Fig. 5.5). Moreover, considerable cell wall shrinkages were seen after high pressure processing, although the cells' connectivity parts seemed not to be considerably affected.

5.4.3 Numerical simulation and image processing

Figure 5.4 shows the processed image at 200 MPa after 5 and 15 min of pressure holding. The blue color component of the picture was normalized in the same range of the mass intake data. The image, as well as the contour of simulation, could give an insight of what happens after HP treatment. In fact, the X_{eq} could be an indication of the fully saturated porous medium. The a_2 and b_2 images of the contour of the blueness of the samples are verifications of the gradual migration of the fluid towards the center of the geometry. As can be seen, the liquid phase is transferred toward the geometrical center of the samples.

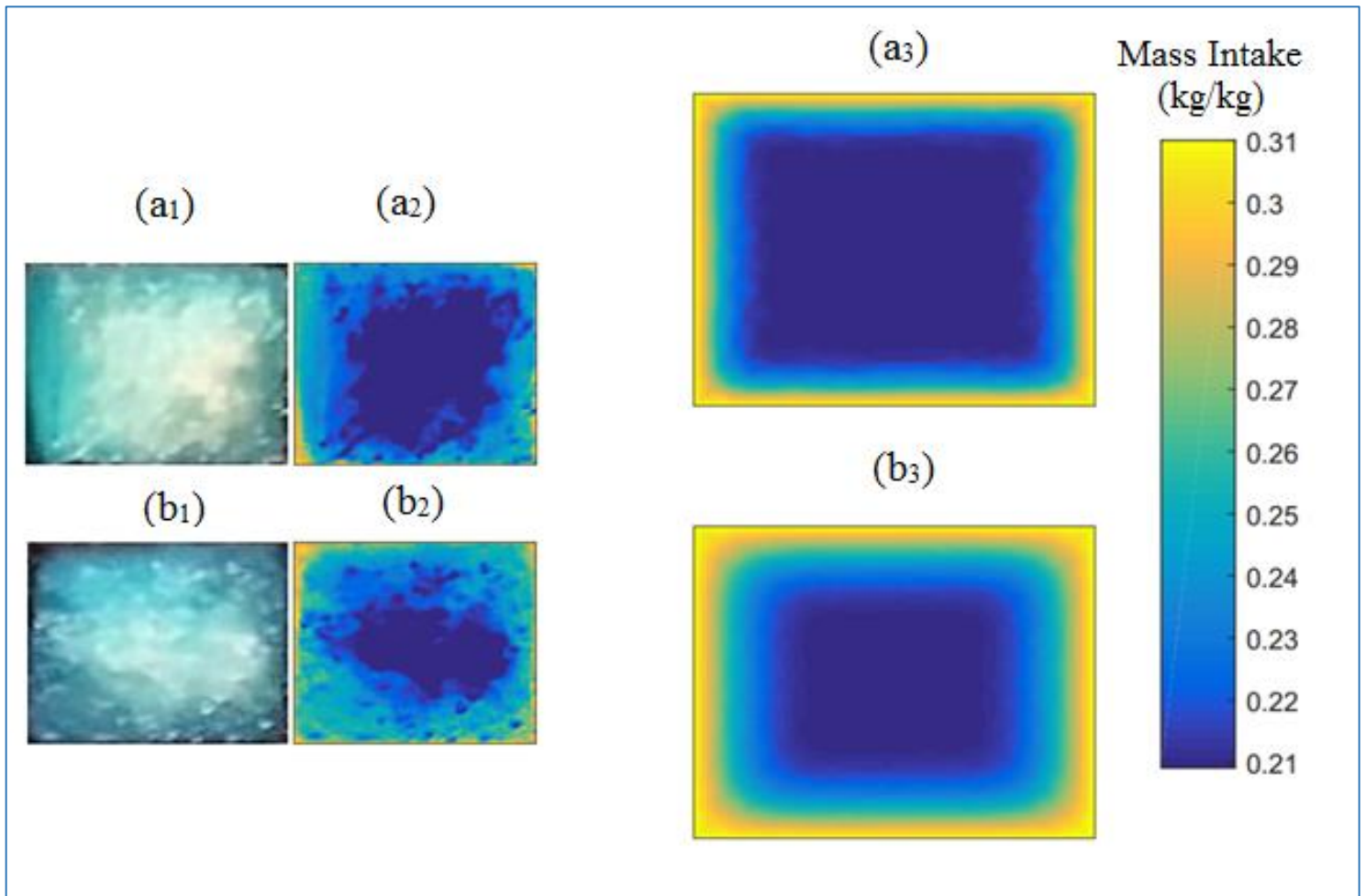


Fig. 5.4. Illustration of mass transfer using image processing and numerical simulation for samples held for 5min (a) and 15 min (b) under 200 MPa. Indices 1, 2, and 3 indicate the RGB scale photos of samples, contour of grayscale of the samples, and contour of infused mass, respectively.

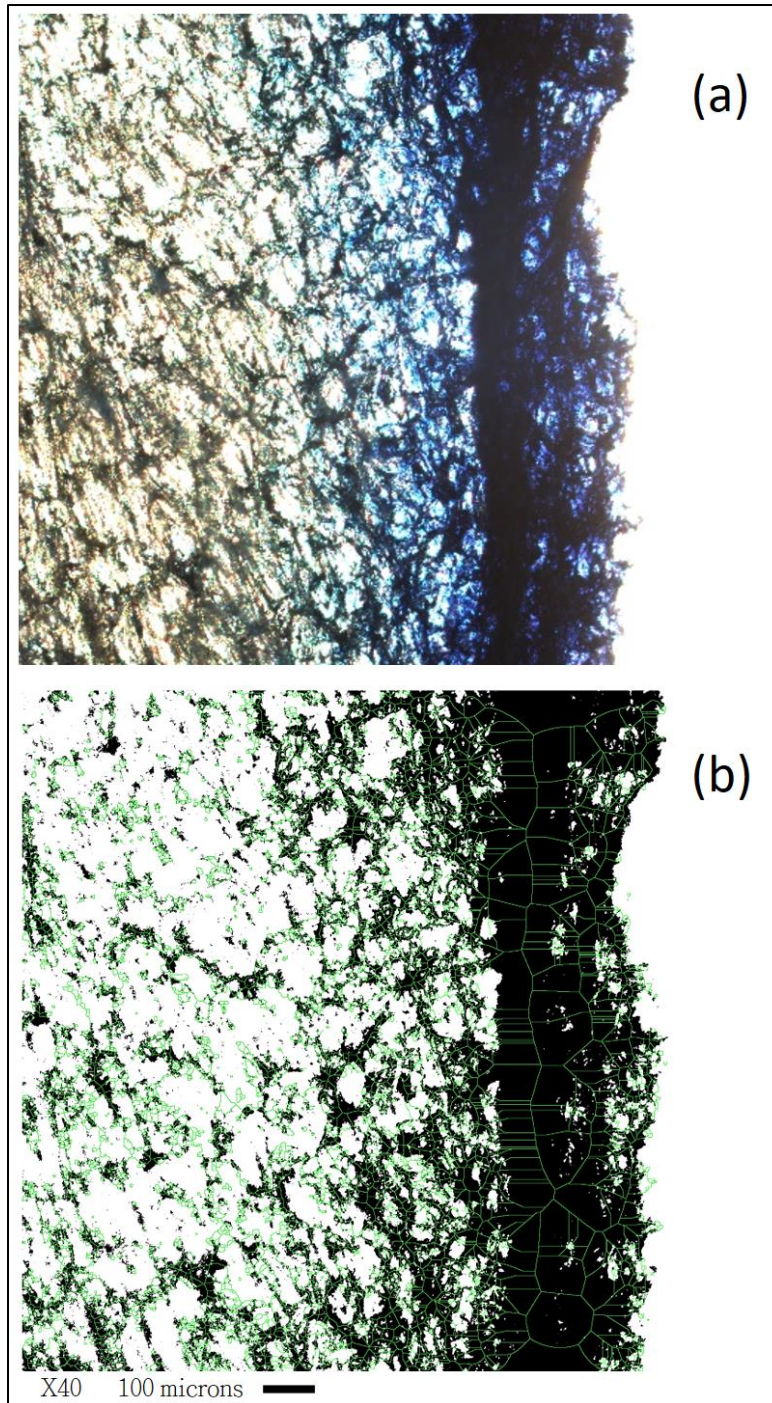


Fig. 5.5. The light microscopy of apple tissues impregnated with toluidine blue (0.1% w/w): (a) a color image of the 100 μm thickness slice (a) the modeled flow paths (in green) within the tissue using a watershed algorithm. The image is coupled with the binary structure of the color image.

Impregnation of the samples using permanent staining agents was an efficient strategy to trace the flow paths within the tissue. A cross-section of the microtome was chosen to be shown in Fig. 5.5. As can be seen, a continuous flow took place towards the geometrical center which verified the asymptotic progression of the inward flow. The high concentration of toluidine indicated a full saturation at the peripheral zones.

In addition, cellular collapses were observed in this area; although, both SEM and light microscopy verified endurance of the internal porous structure after impregnation. For further illustration of the development of the flow-path network, image processing algorithms were used. Using MATLAB, the image was converted to the grayscale. Using this scale, the abrupt changes due to the existence of the blue dye was traceable. Afterwards, a watershed algorithm was used to characterize the mentioned changes. As can be seen in Fig. 5.5b, a series of perpendicular streamlines is observable at the peripheral parts. In contrast, a more branched network was seen at the zones which are farther from the boundaries. This was obviously by the fact that due to the tortuosity of the porous network and existence of a mechanical resistance the flow progression was lower within the inner zones.

5.5 Conclusion

In general, microscopic methods show the high capability of demonstration of the fluid-texture interactions. In other words, the micrographs showed the changes in the cellular tissue including the cell was shrinkage, the flow path rearrangements and the flow pattern within the tissue. The microstructure studies gave us a chance that besides our macro-scale view toward the flow within the bulk geometry, we could precisely trace the complexities of the flow paths inside any porous medium.

Further investigations using Hybrid Micro-, Meso- and Macroscopic scale models, could reveal more information in terms of homogeneity and continuity of flow paths inside the porous media.

Preface to Chapter 6

In previous chapters, the Fick's second law was examined as a model for mass transfer studies. In fact, the main variable in analytical solution for Fick's second law was the moisture ratio. Considering the gradual mass transfer as a function of time and constant pressure level, the moisture ratio was in fact, a transient saturation model in the porous media. As discussed in chapter 2, the Darcian concept is the main means for researchers to model any fluid flow in the porous media.

Thus, in chapter 6, it was attempted to present a Darcian approach toward the mass transfer objective. The following chapter describes an innovative methodology to couple two of most important concepts in mass transfer modeling. The conducted research also shows a theoretical understanding of what we called as the "pressure-driven flow".

Parts of this chapter have been adapted for presentations and publications as follows:

Vatankhah, H., Akbarzadeh, A. H., Ramaswamy, H. S. (2018). A Hybrid Fickian-Darcian Flow Model for High Pressure Impregnation of Fluids into Porous Biomaterials, *Biosystems Engineering*, 166, 200-209.

CHAPTER 6

HYBRID FICKIAN-DARCIAN FLOW MODEL FOR HIGH PRESSURE IMPREGNATION OF FLUIDS INTO POROUS BIOMATERIALS

6.1 Abstract

Pressure-driven fluid flow is an inevitable consequence occurring during the high pressure processing of porous biological materials confined in a fluid phase. A hybrid numerical model was adopted to simulate the mass flow of fluids into an enclosed biological porous matrix under constant high hydrostatic pressure treatments. The numerical model was based on the finite element simulation of time-dependent Fickian mass transfer represented as saturation rate of fluid flow in the unsaturated media. The Kozney-Carman model was used for correction of relative permeability because of the pressure-induced textural changes. As a case study, the proposed methodology was applied to simulate the high pressure impregnation of apple cubes by ascorbic acid solution (1% by mass). The proposed model demonstrated the existence of a 4 MPa low-pressure zone in the geometrical center of the computational domain associated with the operating pressure level which provides sufficient driving force for liquid migration. The numerical results were corroborated through implementing gravimetric and image processing experiments. Finally, a linear flow front rate of 0.03 cm s^{-1} was estimated along the porous medium, and the analytical solutions to the Darcian model were used to determine the lumped permeability as a function of pressure difference at the impregnation flow front.

6.2 Introduction

High pressure processing (HPP) is a promising and recent industry adopted method for food preservation, quality retention, and the improvement of functional properties. HPP is of practical interest in the processing of biomaterials, biological materials, and pharmaceuticals (Daryaei et al., 2016; Su et al., 2014; Tola & Ramaswamy, 2014). A regular high pressure processing unit is made of a steel vessel filled with a pressure

transmitting fluid (commonly water) and a pumping system to cause a positive pressure in the vessel, a process that leads to a direct hydrostatic pressurisation (Mertens, 1995).

HPP of biomaterials involve a variety of porous media (e.g., fruit and vegetable tissues) in direct contact with a fluid phase. For example, most plant materials comprise a parenchyma tissue in which the intercellular spaces are mostly filled with water/vapor and air. In these heterogeneous natural tissues, there will be a non-uniform distribution of air and water in various cells and pores (Reeve, 1953; Boukouvalas et al., 2006; Ting et al., 2013).

Under HPP conditions, pressure-driven flows lead to a mass transfer and mass intake within the porous solid matrix. The abovementioned pores are likely to be filled with the pressure driven fluid unless they are already collapsed as a result of the pressure build-up. It is not yet clear what the dominant factor for the fluid transport is. The science of fluid transport into porous media is a computationally complex which requires knowledge about the morphology of each pore within the porous biomaterials, flow paths within the porous material, and mutual interaction of fluid and matrix solid phase (Civan, 2011). Numerical simulation of flow in porous materials also requires the understanding of nature of flow patterns, the fluid properties, and multiphysical properties of the solid phase that the porous material is made of (Sahimi, 2011). As a result, several approaches have been introduced to study the mass transport phenomenon (Chhabra et al., 2001). Among these, a number of generalised methods have been recognized. As a result, several approaches have been introduced to study the mass transport phenomenon (Chhabra et al., 2001). Among these, a number of generalized methods have been recognized such as:

- *Bundle capillary tube* method which emphasizes on the consideration of the porous media as tortuous flow paths. In this case, the wall friction effect is an important resistant force for the fluid flow (Kozeny, 1927; Carman, 1937).
- *Pack of solid grains*, in which the drag forces of a simplified pack of defined shapes of grains are the main element of simulation calculations (Chhabra et al., 2001).
- *Averaging microscopic field equations*, in which flow and momentum continuity equations based on the conservation of mass equations are solved, and the mass transport is averaged over a representative volume element. For numerical modeling, different mass transfer equations including Fick' first and second laws,

Navier-Stokes equations, and Darcy's equation for saturated &/or unsaturated flows have been used as the governing equations of mass transport. In addition, non-Fickian behavior of moisture diffusion, analogous to non-Fourier heat conduction, could be introduced as a means of accurate modeling of transient mass transfer modeling (Akbarzadeh & Chen, 2014; 2013;2012) specifically in porous materials (Akbarzadeh and Pasini, 2014).

- *Dimensional correlations* based on the empirically obtained mathematical relationships between certain physical conditions and the rate of mass transfer within the matrix and (5) Hybrid method which is based on utilizing a mixed approach of the different modeling and calculation procedures.

The majority of research on fluid flow in the porous media are found in some areas of hydrology, petroleum engineering, and porous biomedical devices (Vafai, 2015). Also, there have been numerous studies to simulate the mass transfer through biological materials in different conditions such as storage and drying process (Folch, 2016; Kowalski, 2015). Yet, there is a considerable lack of interdisciplinary knowledge on the fluid flow transport through a porous solid medium. A widely-recognized processing technique known as “impregnation” involves the addition of desirable solids/fluids into selected porous media. In this regard, High pressure impregnation (HPI) focuses on impregnation using HPP.

In the literature, there is a lack of macroscopic study of such transfer phenomena in porous media which emanates from the lack of possibility of usage of in-line pressure sensors to monitor the development of hydrostatic pressure within the porous materials during the high pressure processing. This present article is a novel macro-scale approach in presenting methodologies of coupling a hybrid Fickian-Darcian model to investigate the mass transfer and pressure level development within a confined geometry. To limit the complexities, the model development focuses on mass transport phenomena based on a small number of measurable variables and the use of lumped estimation of mass transport coefficients, collaborating the computational procedures with data collected using an experimental model system and microstructural studies.

6.3 Theory/calculation

6.3.1 Moisture Diffusion

In this approach, the mass transfer diffusivity was calculated based on the concept of the definition of a dimensionless mass transfer parameter which has been extensively used in different processing techniques such as drying and rehydration (Barbosa-Cánovas et al., 2005). As the first stage of the mass transfer modeling, Fick's second law was used to model the asymptotical mass intake during the pressure-induced infusion. Equation (6.1) indicates the total moisture ratio as the multiplication of the flow in three directions in the Cartesian system. The mass transfer was assumed to take place in a geometry as a combination of three infinite slabs of $2L$ thickness (Da Silva et al., 2009). Considering a constant diffusivity parameter during each pressurization and neglecting the shrinkage occurred by the impregnation of a non-compressible fluid, Eq. 2 was used as an analytical solution for the Fick's second law (Crank, 1975; Ramaswamy et al., 1982):

$$MR_{tot} = \frac{\bar{X}(t) - X_e}{X_0 - X_e} = MR_{pl}^3 \quad (6.1)$$

$$MR_{pl} = \frac{8}{\pi^2} \sum_{n=0}^{\infty} \frac{1}{(2n+1)^2} \exp \left[-(2n+1)^2 \pi^2 D \frac{t}{4L^2} \right] \quad (6.2)$$

where, MR_T is total moisture ratio, MR_p is moisture ratio on each plate, X is the mass intake (kg kg^{-1}), D is the diffusion coefficient ($\text{m}^2 \text{s}^{-1}$), and z and t are position at each direction of Cartesian system (m) and time (s), respectively.

To couple the Fickian and Darcian mass transfer equations in unsaturated porous media, it could be assumed that in a mesoscopic scope, the saturation (S) starts increasing from an initial to a final moisture uptake. These parameters are known as X_{init} and X_e in the solution Fick's law, respectively. To make the definition of boundary conditions easier, the saturation can be presented in a dimensionless form:

$$\begin{cases} X_{init} \rightarrow X_e \\ S = 0 \rightarrow S = 1 \end{cases}$$

$$\frac{\partial S}{\partial t} = 3D \cdot \frac{\partial^2 S}{\partial x_{init}^2} \quad (6.3)$$

Equation 3 represents a combination of Darcy's and continuity equation with respect to a pressure-driven flow in an unsaturated porous medium in which the term ds/dt is defined as the source term for unsaturated flows.

6.3.2 Representative Volume Element (RVE)

A porous medium consisting a solid part, known as solid matrix, and void space, called a pore space, has the capability of being infilled with different fluids. The porosity, mostly represented by φ , is calculated using Eq. (6.4):

$$\varphi = \frac{V_{void}}{V_{tot}} \quad (6.4)$$

where V_{void} and V_{total} represent the volume of the porous phase and the total volume of the porous material, respectively. In this study, the porous material is defined as a RVE which all the calculations would be done in such domain (Bear, 1979).

6.3.3 Saturation model:

The saturation concept is commonly explained by introducing the notion of saturation parameter represented by 'S', where $0 \leq S \leq 1$. In fact, saturation can be defined as the ratio of the volume of the filled pores to the total volume of the pores. The Saturation parameter for any fluid phase in the RVE would be defined by Eq. (6.5), (Bréard, et la., 2003):

$$S = \frac{V_F}{V_{tot}} \quad (6.5)$$

Where S , V_F and V_{total} total represent saturation, the volume of fluid and the total volume of pore space, respectively.

6.3.4 Unsaturated Darcian Flow

In unsaturated flows, the pore rearrangements could be neglected to compare the change in the amount of saturation in the phase. As a result, the flow through a non-deformable porous medium could be defined as the combination of the continuity equation and the temporal saturation function for unsaturated flows. As a result, Eq. (6.6) Indicates the relation between the flux q (m s^{-1}) and the derivative of saturation:

$$\vec{\nabla} \cdot \vec{q} = -\varphi \frac{\partial S}{\partial t} \quad (6.6)$$

A flow driven by the gradient of pressure is described as a generalised Darcian flow (Feng, 2000) combined with Darcy's Equation (Eq. 6.7):

$$\vec{\nabla} \cdot \left(\frac{K(s)}{\mu} \vec{\nabla} p \right) = \varphi \frac{\partial S}{\partial t} \quad (6.7)$$

where $K(s)$, p and μ are permeability of the porous medium, pressure (Pa) and dynamic viscosity (Pa s).

The permeability is considered as a function of saturation. The intrinsic permeability is a characteristic of the porous medium when a permanent flow in a saturated medium is present. The relative permeability is defined as the effective permeability in various stages of saturation of the porous medium, and it can be a comprehensive representation of resistance to flow in the porous medium at different levels of saturation. Considering both abovementioned permeability parameters, the saturation-dependent permeability could be obtained from Eq. (6.8), (Muskat et al., 1937; Whitaker, 1986):

$$K(S) = K_{rel} K_{int} \quad (6.8)$$

where K_{int} and K_{rel} indicate intrinsic and relative permeability, respectively.

6.3.5 Numerical Simulation

A hybrid method was used to calculate mass transfer and pressure distribution during the high pressure processing of porous biomaterials. The algorithms were implemented by writing MATLAB codes. The Fick's second law of diffusion was solved in a 2D geometry considering Dirichlet boundary conditions of $S = 1$ indicating flow transport from the saturated part to the RVE. The procedure was modeled for a total process time of 15 minutes and with 5 second time intervals for temporal calculations.

For the Darcian model, the physical parameters of the sample were used according to the ones reported by Feng et. al. (2004). They measured the K_{int} using the common method of measurement of pressure difference while passing water through a cylinder in which the porous material is confined. The measured pressure difference as well as the known value

of flow rate in the cylinder could be used to calculate the K_{int} . The reported value was $K_{int} = 8.89 \times 10^{-13}$ for an apple tissue with $\varphi = 0.33$.

A cubic function between the permeability and saturation parameter was used to calculate the permeability of parenchyma tissue Eq. (9). This function has been proposed in in several publications (Feng et al., 2004; Tsuruta et al., 2015).

$$K(S) = K_{int} \cdot \begin{bmatrix} S_i^3 \\ S_{i+1}^3 \\ \vdots \\ S_n^3 \end{bmatrix} \quad (6.9)$$

The above cubic relationship has also been tested for the flow of gas and fluid in apple tissues by Feng et al. (2004) and Feng, Tang, Cavalieri, and Plumb (2001). Thus, the relative permeability could be defined as:

when $S = 0$; $k_{rel} = 0$; $K = 0$

when $S = 1$; $k_{rel} = 1$; $K = K_{int}$

The total porosity was assumed as the available void space at the beginning of the holding time when the come-up time terminates. Therefore, the previously reported $\varphi = 0.33$ was corrected to be 0.17 which was measured based on the deduction of the volume of the infused liquid during the short come-up time. The viscosity was assumed to be equal to water viscosity that is about 8.9×10^{-4} Pa s.

The boundary conditions for Darcy's equation were assumed to be as Dirichlet and equal to 100 MPa. The first derivative of saturation value at each time step and each element was calculated using a first-order approximation of Taylor series as the Eulerian procedure for the finite difference method (FDM), (Eq. 6.10):

$$\frac{\partial S}{\partial t} = \frac{S_i^{n+1} - S_i^n}{\Delta t} \quad (6.10)$$

The derivatives are then put into a matrix indicating discretised domain of solution to use in calculations of Darcian flow (Eq. 6.9). To obtain the pressure field, Eq. (6.7) was solved as a linear system and finally the pressure data were obtained in a transient form. The

abovementioned procedure could be seen in the form of a process diagram as shown in Fig. 6.1.

6.3.6 Analytical Darcian model and lumped permeability estimation

Analytical models of pressure gradient as a function of saturation patterns were used to derive the permeability trend during impregnation. The permeability could be calculated using the analytical model of Darcian flow presented by Bréard et al. (2003) in Eq. 6.11:

$$2(n+1)\frac{I_p}{\mu\phi}K = \begin{cases} (n-1)W_f^2 \left[2\left(\frac{W_f}{W_0}\right)^{n-1} - (n+1) \right] + W_0^2 & \text{for } n = 0 \text{ or } 2 \\ W_f^2 \left[2\ln\frac{W_f}{W_0} - 1 \right] + W_0^3 & \text{for } n = 1 \end{cases} \quad (6.11)$$

where $n = 0, 1, 2$ correspond to Cartesian, polar and spherical coordinates, respectively. W_f and W_0 represent the position of the fluid at the front of impregnation and boundaries of the geometry, respectively. As can be found in Eq. 6.11, I_p represents the integral of the pressure difference while impregnation (Eq. 6.12):

$$I_p = \int_0^t [P_0(t) - P_f(t)] dt \quad (6.12)$$

Considering the Cartesian system for the model, Eq.6.11 could be rearranged in the form of a unidirectional flow (Eq. 6.13).

$$W_f^2 = \frac{2K}{\mu\phi} \int_0^t [P_0(t) - P_f(t)] dt \quad (6.13)$$

where P_0 and P_f represent pressure at the boundary and the flow front.

Using the methodology presented in section 6.4.2, a linear flow front function could be obtained in the form of $W_f = f(t)$. As can be seen in the results section, these types of functions represent the flow front displacement as a function of time. As a result, the slope (Γ) the function could be obtained from the progression of the fluid flow. Finally, considering the constant pressure at the boundaries, K could be obtained as a function of pressure difference in the flow front (Eq. 6.14), Bréard et al. (2003):

$$K = \frac{\mu\phi}{2[P_0 - P_f]} \Gamma$$

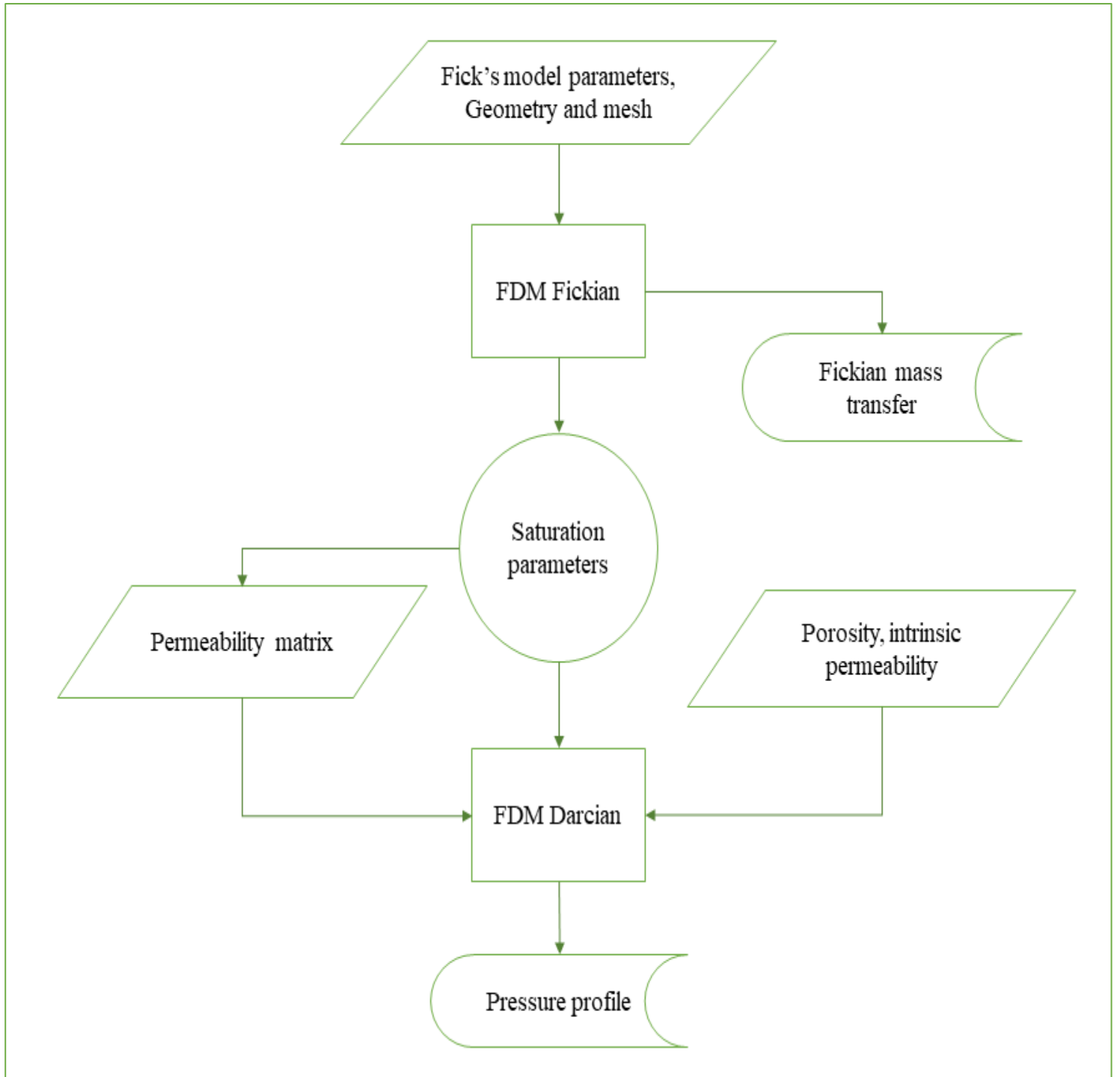


Fig. 6.1. Process diagram of the calculation procedure for the simulation of Fickian-Darcian model.

6.4 Experimental Verification

6.4.1 Model Application

The application of presented computational approach was demonstrated using fresh-cut apple cubes soaked into an aqueous ascorbic acid and food grade color solution. Fresh McIntosh apples were cut into 1.2 cm³ cubes after washing and peeling. It was tried to select the fruits which were in the same level of maturity and similar dimensions. The apples were harvested from Macdonald Campus Horticultural Research Farm located at McGill University, Ste. Anne de Bellevue, Canada. 1 g ascorbic acid was solved into 99 g double distilled water (conductance: 18 V, Milli-Q, Millipore, Bedford, USA) as the fluid phase. Also, for ease of further image analysis, 1 mL commercial food grade blue color was solved into each 100g of the final solution. Finally, two apple cubes were weighed (APX-200 Digital weighing Balance, Denver Instruments) and added to low-density 2 oz. Polyethylene bags (Whirl Pak(R), Nasco, Fort Atkinson, WI, USA) containing 25 ml of the solution. An HPP equipment (ACIP 6500/5/12VB-ACB Pressure Systems, Nantes, France) was used to pressurize the sample immediately after heat sealing the bags. The HPP operation was designed to reach 100 MPa (final pressure level) hydrostatic pressure at 300 MPa min⁻¹ pressurization rate. The pressure holding time was assumed as the moment when the machine reached the final pressure level. The processing was conducted in duplicate at 0, 2, 5, 15, 20, 25, and 30 min holding time followed by a rapid decompression.

The temperature of the HPP vessel increased from an initial temperature of 22-23°C to 25°C as a result of an approximately temperature increase of 3°C/100MPa as a consequence of the adiabatic heating. Nevertheless, the processing temperature was stable because the cylinder was jacketed (Khurana & Karwe, 2009; Zhu et al., 2004). To evaluate the gained mass during the HPP, the processed cubes were gravimetrically weighed after they were rinsed for 10 sec.

6.4.2 Image Analysis

Color (RGB scale) images were taken in same light intensity from half sliced samples after 2, 5, 10, and 15 minutes of pressure holding at 100 MPa. The sum of all elements of Blue

matrix of the pictures was calculated. The increase of blueness was calculated according to dividing the mentioned value by the maximum Blueness defined as a sum of the maximum value of same pixel count. The analysis was performed in Matlab ®. The images were also used to get the impregnation flow front function. In this regard, the images were converted to the LAB scale. It was assumed that the flow is developing in a rectangular front form towards the centre. Thus, the binary images of the images at a threshold of $L^*=90$ were prepared. This limit was chosen regarding a comparison with a fully saturated tissue. Finally, the area of the unimpregnated central part was assumed as an area of a rectangle. This way, the length of the flow front was considered at the mentioned time steps (Eq. 6.15).

$$\%W_f = \frac{1-\sqrt{A}}{2} \times 100 \quad (6.15)$$

where the A is the area of the unimpregnated central part.

Also, fresh and impregnated samples (for 15 min at 100 MPa) were used to obtain the scanning electron microscopy (SEM) images. The images were captured at 25X to 80X. The imaging condition was 5kV accelerating voltage and 6 mm working distance using (TM3000, Hitachi, USA) and all samples were freeze-dried prior to imaging.

6.5 Results and Discussions

To utilize the Fick's law, the calculated mass diffusivity during the HP treatment was $9 \times 10^{-7} \text{ m}^2\text{s}^{-1}$ ($R^2=0.92$). The estimated value is in the same range as the one reported by George et al. (2016) which is $2.63 \times 10^{-9} \text{ m}^2\text{s}^{-1}$ to $19.20 \times 10^{-9} \text{ m}^2\text{s}^{-1}$; although the difference between them could be as a result of the higher viscosity of commercial sucrose (10% to 50%) and kokum syrup which they used. The mass transfer value also falls between diffusion of vapor and diffusion of pure water although being close to the value for diffusivity of water; it shows a stronger and more continuous diffusion (Guillard et al., 2003). Using Eq. (6.15), Fickian trend in impregnation yield of the blue dye was evident. This was also in agreement with the mass intake data where the moisture content tended to an equilibrium moisture content as a function of time (Fig. 6.2).

Due to specific conditions of hydrostatic pressure which are embodying whole geometry and imposing equal pressure on all the sides, the mass transfer is deemed to be conducted in the form of equal fluxes in all directions. In practice, the transfer is likely to take place in the form of substitution of gaseous phase with the liquid.

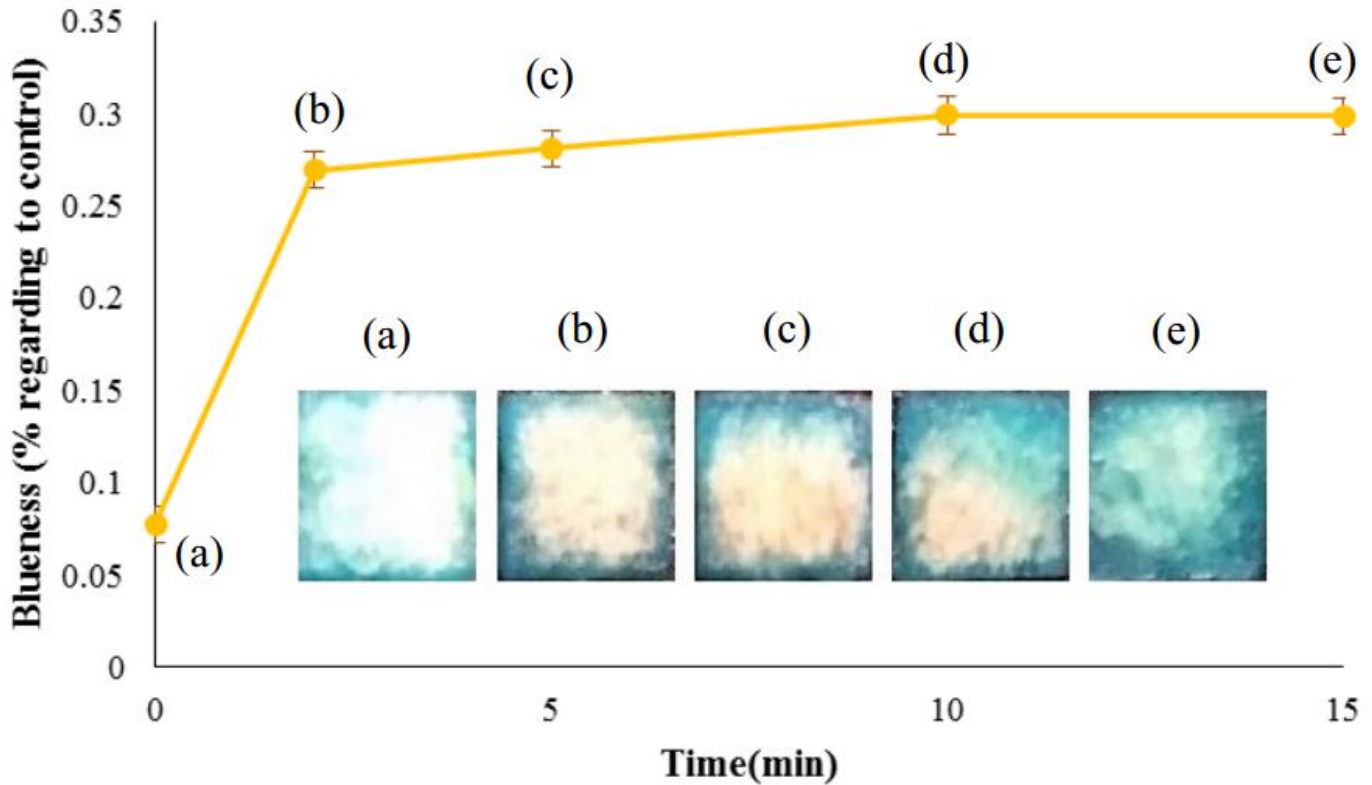


Fig. 6.2. Evolution of relative blueness as a representation for the diffusion of fluid into the apple as a porous biological tissue under high pressure. The uptake of samples was measured at (a) 0 min, (b) 2 min, (c) 5 min, (d) 10 min (e) 15min of pressure holding time. The original images (RGB scale) of the samples are embedded in the figure.

There are two parameters affecting the mass transfer in such cases. In other words, the mass transfer parameter - diffusivity in Fickian or permeability on Darcian approach - would be affected by two elements; first, the physical structure of the sample, which means the characteristic of porosity like pore size, tortuosity and pore connectivity and the second parameter which would be a barrier and negative element in the mass transfer, is the time needed to exchange the confined gaseous phase with the liquid. In fact, there is a resistance to mass transfer because of the confined mass gas phase, and there is time needed for

removal of gases while solving in the liquid phase or escape of the gaseous phase due to microstructural dissymmetric nature of the porous media.

There were slight fluctuations in the mass transfer phenomena at different holding times, and that could be a result of biological variations between the different apple cube samples. Each treatment time is a separate experiment and variations can, therefore, be expected, although it was attempted to use the same batch and same degree of ripened apples.

The flow through porous plant tissues has also been recognised to be strongly affected by several parameters such as pressure gradient, time of processing, viscosity of the fluid phase, temperature and osmotic pressure of the external solution, product/solution ratio as well as the texture characteristics including porosity, firmness, cellular arrangement, intercellular space accessibility, surface/volume ratio and etc. (Bilbao-Sáinz et al., 2005; Fito et al., 2001; Gras et al., 2002; Guamis et al., 1997; Mendoza et al., 2010; Petersen, 2014; Schulze et al., 2012; Tylewicz et al., 2012). However, in considering the mentioned parameters in porous media, especially under high pressure, would need micro-scale modeling (pointwise) which consequently leads to volume averaging of the data. This method has certain disadvantages, such as cumbersome repetitions of calculations as well as inexact data concerning the real world (Civan, 2002; Gray, 2000).

The obtained permeability values by Eq. 6.8 were regarding a fully homogeneous cellular pattern. However, the SEM images showed a continuous permanent deformation as a result of processing at high pressure (Fig. 6.3).

In this regard, a cubic- function showed the change in the porosity in each direction. The obtained equation in x-direction was $\varphi = 0.004x^3 - 0.0453x^2 + 0.1466x + 0.0228$ ($R^2=0.94$). The corrections in the permeability of the tissue was considered by assuming a 4-layer tissue with relative permeabilities in a series configuration as an indication of gradual pressure induced deformation within the porous medium (Eq. 6.16).

$$(k_{rel})_{corrected} = \sum_{i=1}^n (d \cdot k_{rel}^{\varphi})_i \quad (6.16)$$

A normalized Kozeny-Carman formula was used to obtain the $(k_{rel})_{corrected}$. According to this formula, the structural non-homogeneities could be calculated according to the final porosity at each layer (MacMinn et al., 2016).

$$k_{rel}^{\varphi_i} = k_{rel} \frac{(1-\varphi_0)^2}{\varphi_0^3} \frac{\varphi_i^3}{(1-\varphi_i)^2} \quad (6.17)$$

Combining Eq. (6.16) and Eq. (6.17) it could be possible to make the corrections regarding the permeability values.

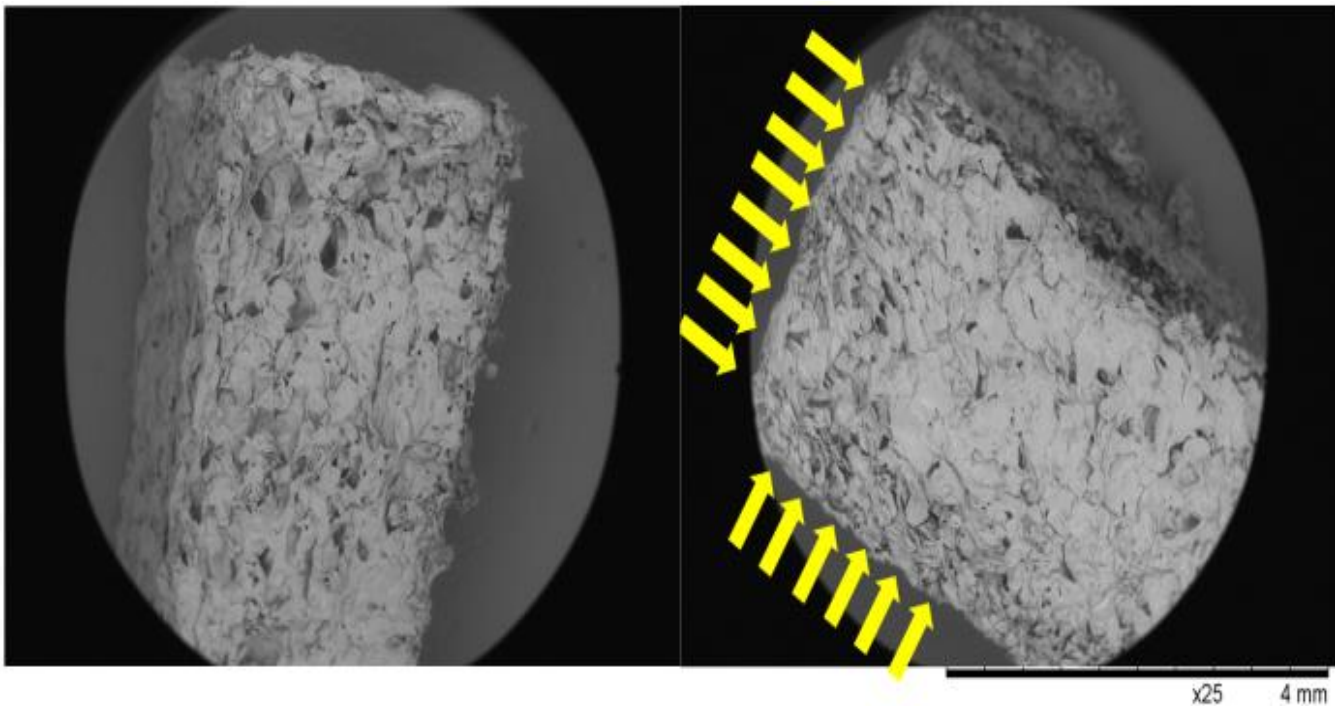


Fig. 6.3. SEM images of cuts of untreated (left) and impregnated samples for 15 min at 100 MPa (right) The arrows represent pressure-driven flow currents during HPP in a corner of the apple cubes (The whole cube is not shown).

Regarding the Darcian model, experimental validation was done according to the intrinsic value of permeability of apple tissue. The numerical calculations were tested for stability using van Neumann stability analysis criteria which are based on error decay into Fourier series (Crank & Nicolson, 1947). The pressure profile is shown at different time steps of processing (Fig. 6.4). The result showed a pressure drop toward the center of the porous medium. It was observed that the pressure difference was within a 10 MPa range during 5

to 15 min of processing. It could be seen that at 15 min, there is a -4 MPa low-pressure zone in the inner part of the geometry with respect to the boundaries.

The simulation data showed a rapid increase of pressure in the entire domain in a few minutes. The instant rise in the pressure level was also followed by a gradual pressure elevation at a lower pressurization rate. This trend was in agreement with the Fickian mass transfer behavior. Figure 6.5 shows the pressure profile due to a transient mass transfer diffusion condition at the geometrical center of the samples. As could be seen, after 3 min, the pressure level at the geometrical center of the sample increases by 80% of the operating pressure level.

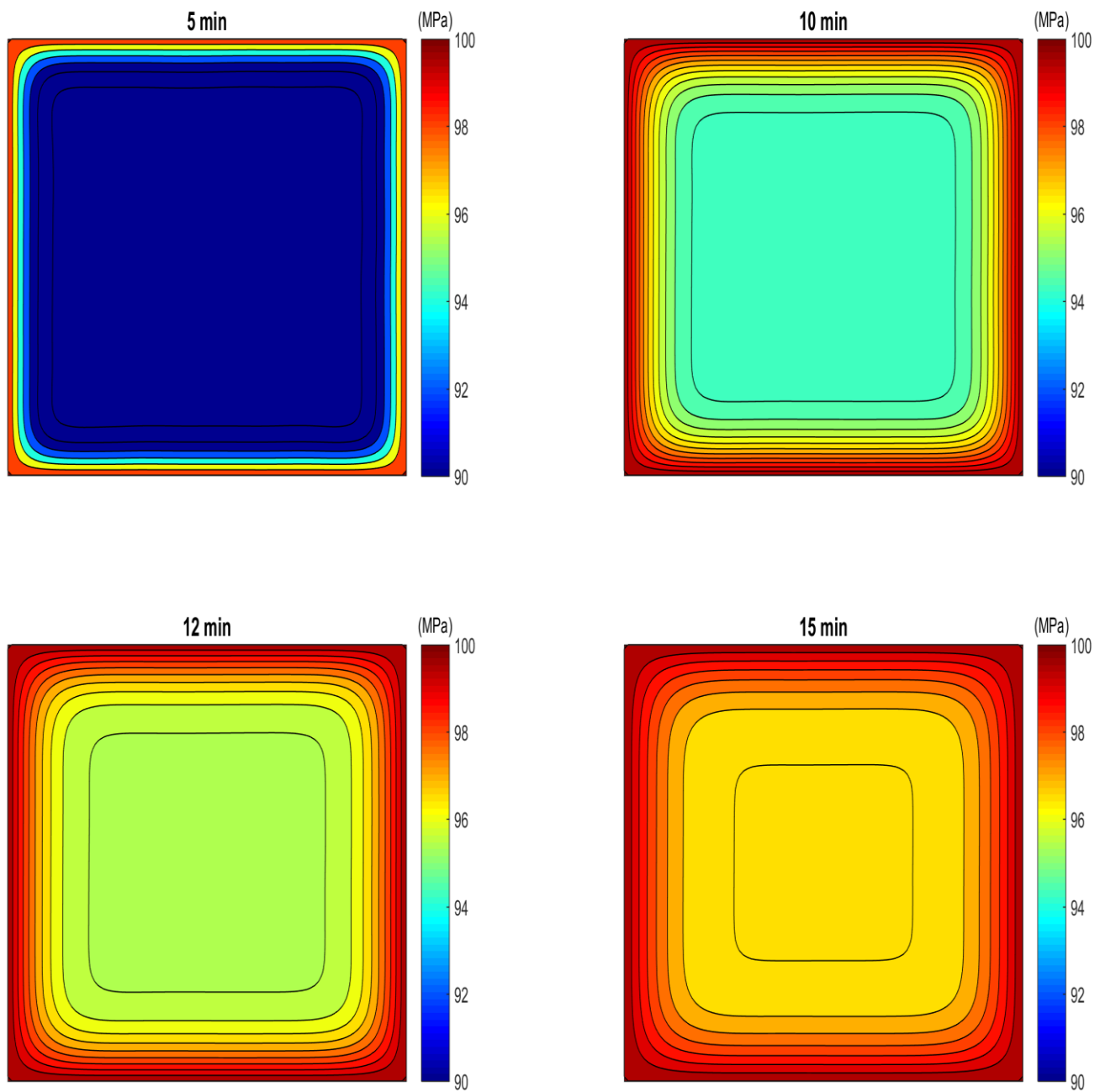


Fig. 6.4. Contour of pressure in the middle plane of samples at different pressure holding times: 5, 10, 12, and 15 (min) at 100 MPa processing pressure.

As per Pascal's law, it is generally perceived that the pressure transmission is instantaneous and uniform throughout the body. However, it is evident that there could be lower pressure points as compared to the system pressure in the porous materials because of the presence of compressible gaseous phase in the pores. The level of pressure difference could be small, but can still play a significant role in the fluid transfer process.

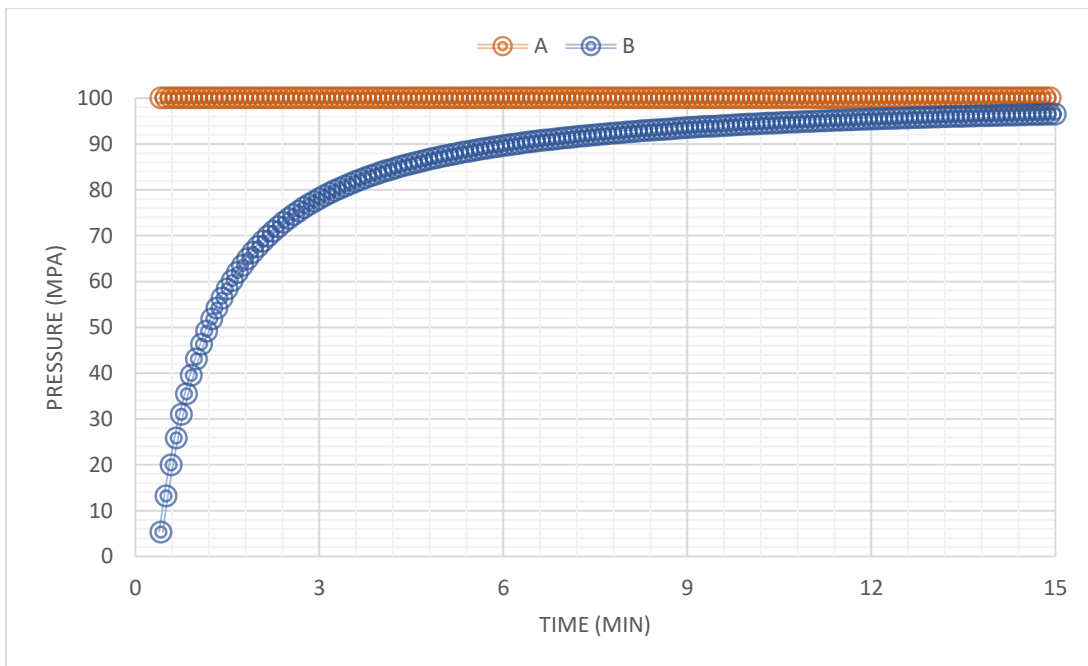


Fig. 6.5. Pressure profile at the center of the apple cubes during the HPI under 100 MPa pressure level considering: (A) presents the intrinsic permeability function and (B) presents the corrected relative permeability function.

Also, in Fig. 6.5, a comparison of the effect of neglecting the relative permeability in the Darcian modeling on the obtained pressure profile at the geometrical center is illustrated. According to Eq. 6.8, theoretically, the highest permeability in a porous media occurs when it has its intrinsic value of permeability which it attains in a saturated medium. In case of HPI, the numerical simulation while using only the intrinsic permeability showed almost

the same final pressure level in the geometrical center. This would be because of the dominance of effect of high pressure rather than the assumed resistance while considering different permeability values.

According to the previous studies done by the authors, the diffusivity of apple under high pressure (100 to 500 MPa) ranged between $\approx 10^{-7}$ to 10^{-9} ($\text{m}^2 \text{s}^{-1}$), (Vatankhah & Ramaswamy, 2017). An illustration of accordance of pressure drop during high pressure processing is shown in Fig. 6.6 As can be seen, the lower diffusivities obtained indicate the existence of higher pressure difference between the center and the boundaries of the samples.

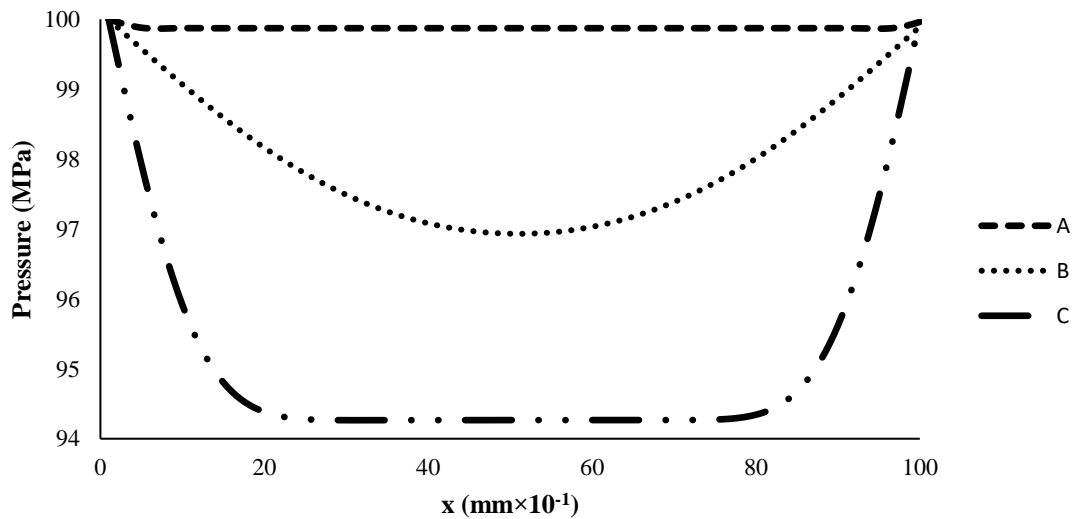
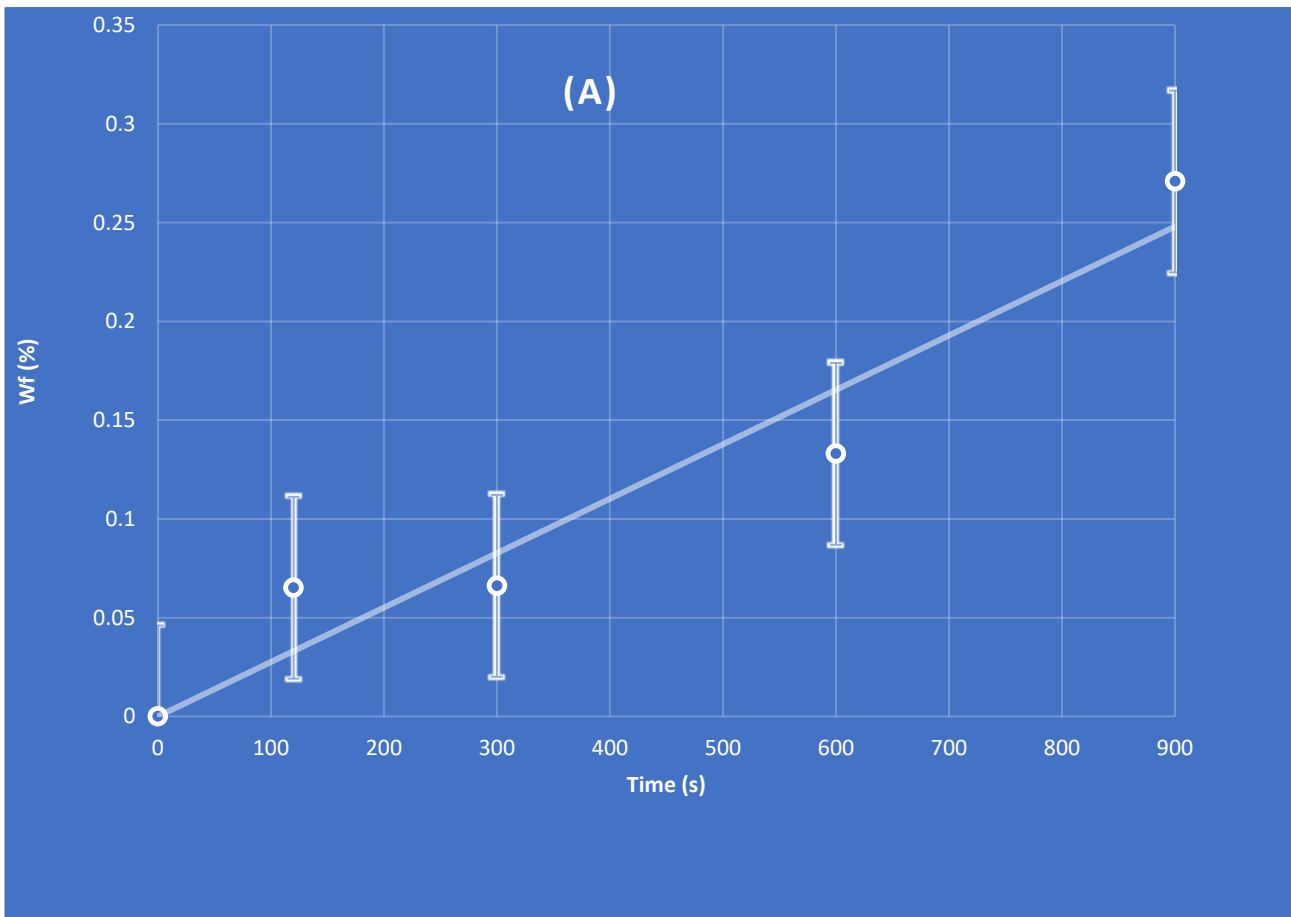


Fig. 6.6. Calculated pressure profile on the half thickness line ($y= 0.5\text{mm}$) of the apple model systems for a range of diffusivity values during HPP at 100-500 MPa. Letters: A, B, C represent Diffusivity = 10^{-7} , 10^{-8} , and 10^{-9} $\text{m}^2 \text{S}^{-1}$, respectively.

As can be seen, the nature of the coupling has some special considerations; in this method, the pressure profile is obtained from a transient mass diffusion solution. On the other hand, the classical Darcy's equation is not a transient equation, while the linking parameter which facilitates the time dependency of the problem would be the definition of a time-dependent saturation function as described in Darcy's equation for unsaturated flows (Eq. 6.7). In other words, time dependency of saturation is the main factor in achieving a transient Darcian flow. It is perceptible that in such lumped parameter estimation of diffusivities, taking the integral of the saturation profile gives the same dimensionless mass parameter versus time trend.



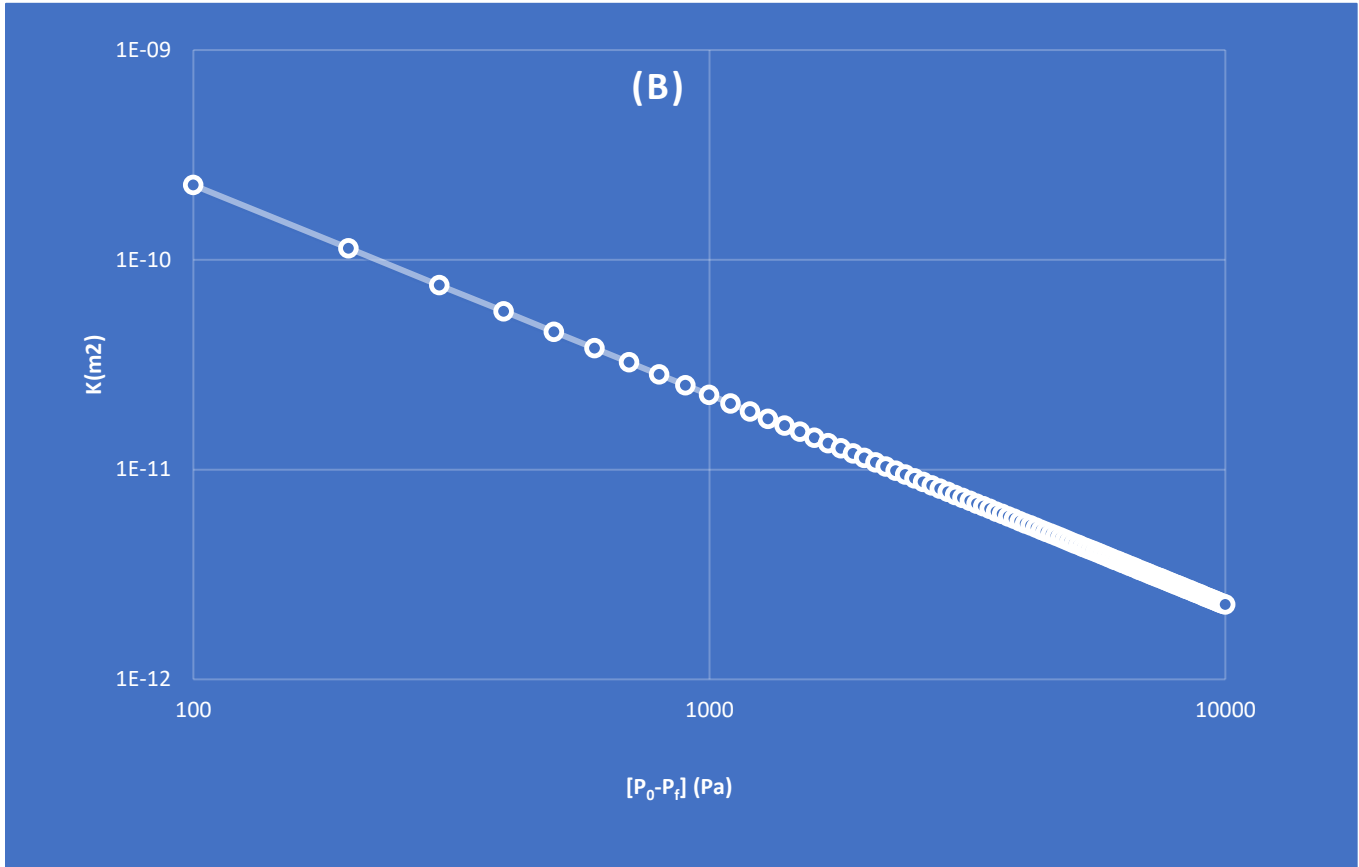


Fig. 6.7. Lumped permeability estimation based on experimental data: (a) the experimental measurement (●) and linear regression of infusing fluid front as a function of time; (b) the log-log illustration of lumped permeability estimation in a range of pressure drop between 100 to 10000 Pa according to the analytical solution of Darcian flow.

Along with numerical simulations, the analytical model for Darcian flow presented in section 6.3.6 could give valuable data and a logical range for the estimation of permeability during the high pressure impregnation. As described in section 6.4.2, the images shown in Fig. 6.2 were analyzed, and the flow front showed a linear trend as a function of processing time. The W_f data are presented in Fig. 6.7a. The regression equation was $Y = 0.0003X$ ($R^2=0.93$). The slope of 0.0003 indicated the linear velocity of the flow front in m s^{-1} , with respect to the model assumption. According to Fig. 6.7a, the permeability evolved in a log-linear form as a function of the pressure gradient in the front border of the flow. It is also worth mentioning that the estimated permeability range is a result of integration of an

unsaturated domain- with approximate assumption of a front domain- followed by a fully saturated flow in the outer parts of the tissue.

6.6 Conclusions

The mathematical and experimental modeling of the liquid mass transport within porous biological biomaterials has been discussed in this paper. The introduced mathematical algorithm based on the coupling of fundamental mass transport models helps to identify the existence of pressure profile variations implicitly. The proposed methodology can be a useful simulation tool for the HPP applications, in which the monitoring of physical properties such as pressure is technically cumbersome. The numerical results showed that the Fick's diffusion method is an appropriate approach to infer the transient pressure profile during the flow transport in porous biomaterials. In addition, the suggested computational procedure facilitates researchers to assess the mass transfer through heterogeneous materials with micropores.

Preface to chapter 7

One of the most important aspects of the reliable implementation of impregnation techniques is the stability of the fluid phase. The common way of studying the fluid stability is to identify the changes in its rheological behavior. The general types of the rheological tests include the dynamic flow tests and the oscillation stress experiments. After high pressure processing, it is likely to see chemical alterations within the fluid phase. The temperature sweep tests also show the molecular state in a purer state. In other words, using high temperature during the rheological tests, the weaker bonds can be dissociated, and the pure chemical alterations can be interpreted.

In this regard, we introduced a novel procedure to ensure the fluid phase stability. Reaching a stable fluid phase, one can implement trustable mass transfer calculations. At the first stage of this objective, we evaluated two commonly used hydrocolloid gums known as chitosan and gum Arabic. After high pressurization of selected concentrations of these gums, various rheological tests are done to ensure the stability of the solutions. Then, it was tried to choose the more stable solution for impregnation purposes. The kinetics of the impregnation into apple tissue is evaluated and discussed in detail. The obtained results showed the possibility of using HPI of viscos fluids as a texture improver for freezing process applications.

Parts of this chapter have been adapted for presentations and publications as follows:

Vatankhah, H., Taherian, A. R., Ramaswamy, H. S. (2018). High-Pressure Induced Thermo-Viscoelasticity and Dynamic Rheology of Gum Arabic and Chitosan Aqueous Dispersions Research paper LWT - Food Science and Technology, *LWT-Food Science and Technology*, 89, 291-298.

Vatankhah, H., Ramaswamy, H. S. (2018). High Pressure Impregnation (HPI) of Apple Cubes: Effect of Pressure Variables and Carrier Medium, *Food Research International*. (under review).

Vatankhah, H., Taherian, A. R., Ramaswamy, H. S. Evaluation and modeling of thermoviscoelasticity of high hydrostatic pressure-induced semi-concentrated aqueous gum Arabic and chitosan solutions. Northeast Agricultural and Biological Engineering Conference (NABEC), July 2016, Orono, ME, USA.

CHAPTER 7

PHASE STABILITY AND MASS TRANSFER EFFICIENCY OF IMPREGNATION OF VISCOUS FLUIDS INTO FRUIT TISSUE

7.1 Abstract

The high pressure impregnation of viscous fluids was performed to study the changes in the mass intake as a result of the viscosity level of the fluid phase. To select a stable and pressure resistant fluid phase, the effect of high pressure treatment (200MPa, 400MPa, 600MPa) on rheological properties of aqueous dispersions of gum Arabic (6 g/100g, 15 g/100g, and 20 g/100g) and chitosan (2 g/100g, 4 g/100g) was studied. Dynamic properties were assessed using an angular frequency range of 1-25 rad/s. Flow properties were measured by applying a programmed shear rate of 0.1-100 s⁻¹ for 10 min (upward) and 100-0.1s⁻¹ for the next 10 min (downward). A power-law shift function was used to describe the deviations from the Cox-Merz theory in all samples. Thermo-viscoelasticity was evaluated using a programmed heat/hold/cool cycle (22°C/70°C/20°C). Two term-exponential and a Gaussian model well fitted the thermo-viscoelastic behavior of both gums. The thermal compatibility, regarding a logarithmic phase shift of loss tangent ratios, was also studied. Results showed higher incompatibilities at lower temperatures, while the shift phases tended to zero at higher temperatures. Overall, HP treatment intensified the existence of a stronger and temperature sensitive hydrocolloid network for 4 g/100g chitosan and 20 g/100g GA. The highest incompatibility was seen in 20 g/100g gum Arabic which was a 1-1.5 order of magnitude. Finally, impregnation of 0.5 g/100g, 1 g/100g, 2 g/100g, and 4 g/100g chitosan (CH) into apple cubes, as a pressure-resistant high viscosity non-Newtonian carrier fluid, showed a quadratic trend for CH uptake at 100MPa. Moreover, HPI pre-treatment with CH prior to freezing demonstrated significant reduction in texture breakdown and drip loss in frozen-thawed apple cubes.

7.2 Introduction

Food and pharmaceutical products are complex systems containing different fractions of major constituents such as moisture, carbohydrates, proteins, fats, and several minor components like vitamins and minerals. During various stages of processing, the components transform &/or relocate either individually &/or through interaction with other components and ultimately influence the physical, functional, nutritional and sensory characteristics of the final product. In this regard, major structural alterations of macromolecules such as proteins, carbohydrates, and fatty acids have been recognized during thermal processing techniques. Recently, attention has been focused on non-thermal methods of food processing techniques to minimize these changes (Hussain et al., 2017; Ramaswamy et al., 2015). High pressure processing (HPP) has been widely explored and has demonstrated a high potential for several food processing applications in recent years. The effect of HPP on different components of the food matrix is variable and need detailed studies to exploit their full potential (Hussain et al., 2016; Knorr et al., 2006).

Among several aspects of physical and chemical properties, rheological/flow behavior of liquid food systems are critical due to their direct effect on processing conditions such as processing efficiency, design, and evaluation of the process equipment as well as consumer acceptance and physical stability of the finished product. Our recent studies (Hussain et al., 2017, 2016) focused on the interaction of locust bean gum, and resistant starch revealed an enhancement of rheological properties such as apparent viscosity as well as storage and viscous moduli. Several previous studies have highlighted the effects of HPP on rheological, thermal and morphological properties of important macromolecules associated with different food matrices (Hussain et al., 2016; Ramaswamy et al., 2015). The current study is directed in a similar fashion but to further explore the pressure-induced rheological changes on selected aqueous hydrocolloid gum dispersions at relatively much high concentration levels as used in specific applications such as film formation, food thickening for gel production, drug delivery vehicle, cosmetology, artificial skin, etc. (Muzzarelli et al., 2007; Patel & Goyal, 2015).

Chitosan (CH), an important derivative of crustacean chitins containing partially deacetylated N-acetyl glucosamine (Wang, 2015), is one of the most abundant

polysaccharides and is recognized as a promising nontoxic biocompatible and bioactive compound. Regarding the molecular structure, CH has amino groups at C-2. Moreover, there are primary and secondary hydroxyl groups located at C-3 and C-6, respectively (Chen et al., 2008). CH is known as an improving agent of other weak, and brittle polymers like gelatin and this functional character of CH reveals the importance of its inter- and intra-molecular interactions (Lin et al., 2012). Moreover, low diffusion characters of CH have attracted many researchers and industry in areas such as surgical dressings, drug encapsulation, tissue engineering, 3D printing, water filtration, wastewater treatment, cosmetics and fruit coating (Rayner et al., 2016). Furthermore, being the only naturally cationic polysaccharide, CH has shown a high capability to bind to anionic surfaces. It is a copolymer of a random composition of two monosaccharides, N-acetyl-b-d-(1, 4)-glucosamine and b-d-(1,4)-glucosamine generally in a 1:4 ratios in commercial materials. CH is commonly derived by deacetylation of chitin in aqueous sodium hydroxide solution. The complete deacetylation yields up to 98 % product. The commercially available CH has a molecular weight between 3800 to 20,000 Da (Thomas et al., 2005).

Another high demand hydrocolloid gum which is widely accepted as a stabilizing agent in soft drinks formulae is gum Arabic (GA), (Lopez-Torrez et al., 2015). It is a natural exudate of Acacia tree which consists about 2 % (w/w) proteinaceous weight fraction. Basically, this gum made of three groups of components including arabinogalactans (AG), arabinogalactan proteins (AGP), and glycoproteins (GP). The effect of HPP at remarkably high concentrations of GA dispersions was studied by Panteloglou et al. (2010) who reported that significant changes in both viscous (G'') and elastic (G') moduli occurred in 40 g/100g GA dispersions after treatment at 800 MPa for 10 min. However, usage of such high concentrations in food processing is not common, and further studies are therefore required at lower concentrations.

Considering the need for robust research on introduction of pressure resistant thickening agents, as well as assessment of their rheological behaviors, the objective of this study was to assess the effect of industrially relevant HPP treatments on selected of GA and CH dispersions which are more in line with their applications, in mid-range concentrations, in food, drug, biomedical, and biomaterials industries. In this article, a novel methodology

for evaluating thermo-viscoelasticity was established for elucidating the changes in rheology after HPP. Also, a comprehensive set of systematic steady flow and dynamic shear rheology experiment were carried out and compared to obtain an applied view of possible rheological behavior alterations. The results were used to select the more pressure resistant hydrocolloid gum for HPI purposes.

In addition, Vatankhah et al. (2018b) found that aqueous chitosan (CH) solutions are pressure resistant at mid-level concentrations. Obviously, this type of pressure resistance for non-Newtonian viscous fluids could be important with respect to process stability and uniformity of HPI operations. However, there are no studies on mass transfer or applications of HPI of viscous fluids.

Also, some studies have introduced transfer of certain functional ingredients into plant tissues using high pressure to improve the quality of the product. For instance, Sila et al. (2004) proposed infusion of calcium chloride to improve the texture hardness of carrots as a pre-treatment for thermal processing. There also have been other studies on the infusion of texture improvement compounds in carrots (Rastogi et al., 2008; Rastogi et al., 2010; Tola, & Ramaswamy, 2013). George et al. (2016) studied some physical characteristics of infusion of anthocyanin into apple textures. Such studies were mostly conducted in a process and product development approach while no attempts were made to provide a quantitatively dynamic and physically model describe the transfer into the samples. Furthermore, it is seen that the significant part of the research has been done on the infusion of low-viscosity Newtonian fluids such as selected juices, or anthocyanin, and calcium solutions. Thus, there is a need for studying the yield of HPI of non-Newtonian solutions.

While in previous objectives HPI of ascorbic acid represented a simple low viscosity medium, in the current objective, HPI of chitosan, as a hydrocolloid dispersion, provides more a more complex non-Newtonian high viscosity medium. In addition, the mass intake kinetics and technological applications of such processing techniques as a pre-treatment to conventional freezing operations is also discussed.

7.3 Materials and Methods

7.3.1 Sample preparation

Food grade purified and instant gum Arabic (GA) (Nexira, France) powder was added to double distilled water (conductance: 18 V, Milli-Q, Millipore, Bedford, USA) to make 6 g/100g (GA-I), 15 g/100g (GA-II), and 20 g/100g (GA-III) dispersions. Aqueous CH dispersions of 2 g/100g (CH-I) and 4 g/100g (CH-II) were made by adding CH powder (Nex-xus, Montreal, Canada) to 0.2 mol equi/L aqueous solution of hydrochloric acid (Fisher Scientific, Fair Lawn, New Jersey, USA). All aqueous dispersions were prepared at room temperature (22 °C) and kept for 24 h to obtain full hydration of hydrocolloids. Sodium azide (0.02 g/100g) aqueous solution was used as an antimicrobial agent to prevent spoilage during the hydration process. As the last step of preparation, the dispersions were centrifuged at $5000 \times g$ for 30 min, and the supernatant was used for further experiments.

7.3.2 High pressure processing (HPP)

HP treatment was given in an isostatic pressure unit with a cylindrical pressure chamber of 5 L volume (ACIP 6500/5/12VB-ACB Pressure Systems, Nantes, France) using water as the pressure transfer medium. A 30-mL aliquot of each sample was filled and sealed in polyethylene bags (Whirl Pak, Nasco, Fort Atkinson, WI, USA). The samples were HP-treated individually for 30 min at 200, 400 and 600 MPa. The HP treatment operation included three stages: compression (pressure build-up), pressure hold and decompression (pressure release). Pressure build-up time was approximately 1, 2 and 3 min, respectively with a pressurization rate of 200 MPa/min. The treatments were terminated after a rapid decompression (~5 s) to atmospheric pressure level.

The samples were introduced into the high pressure vessel at 15-18 °C so that temperatures of the medium and sample were around 25 °C after the pressure treatment. During the pressurization, it is expected that there will be an increase in sample temperature of about 3 °C / 100 MPa due to the adiabatic heating. Because the vessel was jacketed and held at room temperature, an approximate average process temperature around the room temperature conditions was achieved by taking the sample and liquid at selected

predetermined lower temperatures according to the targeted pressure level (Ramaswamy et al., 2010).

7.3.3 Rheological measurements

The rheology measurements were made out using a cone/plate AR2000 Rheometer (TA Instruments, New Castle, DE, U.S.A.) equipped with 60 mm, 1.59° solvent trap cone and attached computer and run by the software supplied by the company (Rheology Advantage Data Analysis Program, TA Instrument). A 2-min equilibrium phase was designed for all the rheological tests. All measurements were done in duplicate.

7.3.3.1 Dynamic oscillation tests

The viscoelastic properties of samples were measured in the same rheometer in the angular frequency range of 1-25 (rad/s). An oscillation stress of 1Pa (obtained from the linear region of stress sweep 0.1-100 Pa) was used to conduct the experiments at the constant temperature of 22°C.

7.3.3.2 Flow rheology tests

The flow tests were carried out using the same TA instrument based on application of an upward-downward one cycle shear ramping in which the shear rate was increased linearly from 0.1 s⁻¹ to 100 s⁻¹ in 7 min and then decreased from 100 down to 0.1 s⁻¹ in the next 7 min for a total cycle time of 14 min.

7.3.3.3 Applicability of Cox–Merz rule between steady shear and oscillation data

The Cox-Merz rule was used to investigate the relationship between the flow and oscillation results (Cox & Merz, 1959). The rule states that the steady shear viscosity (η) and magnitude of the complex viscosity (η^*) have a linear superimposition at the same magnitude of steady shear rate (ω) and oscillatory shear rate ($\dot{\gamma}$), (Eq. 7.1).

$$|\eta^*|(\omega) = \eta(\dot{\gamma}) \Big|_{\omega=\dot{\gamma}} \quad (7.1)$$

The magnitude of complex viscosity was obtained using Eq. (7.2):

$$|\eta^*| = \sqrt{(\eta')^2 + (\eta'')^2} \quad (7.2)$$

where η' and η'' were viscose and elastic components of dynamic viscosity (Pa.s).

7.3.3.4 Temperature sweep tests

The temperature sweep tests were performed to study the change in viscoelastic properties of test samples as a function of temperature. The complete sweep cycle included a heating stage to increase the temperature at a linear rate from room temperature (22 °C) to 70 °C in 10 min followed by a hold at this temperature for 10 min and finally a cooling stage from 70 °C to 22 °C in the next 10 min. So, each programming step lasted 10 min with a linear increase, steady hold, and a linear decrease. The viscoelastic measurements were measured at a steady oscillation shear stress 1 Pa. Test samples were thermally equilibrated before each step. The evolution of storage and loss moduli were modeled as a function of temperature using MATLAB®.

7.3.4 Impregnation of the selected solution into the apple tissue

Selected concentration of aqueous CH dispersions (0.5%, 1%, 2% and 4%) were prepared by adding CH powder (Nex-xus, Montreal, Canada) to 0.2 mol equi/L aqueous solution of hydrochloric acid (Fisher Scientific, Fair Lawn, New Jersey, USA). All dispersions were kept for 24 h to facilitate full hydration of hydrocolloids. All preparations were made at room temperature (22 °C) and the water used was of double distilled grade (conductance: 18 V, Milli-Q, Millipore, Bedford, USA).

HPI tests were done at selected concentrations of chitosan solutions mainly for two purposes. One was to test the influence of high vs low viscosity fluid on HPI. The second one was to test the benefit of using chitosan for quality improvement in freezing preservation. In this case, the effect of CH impregnation into apple cubes was studied at a treatment pressure of 100 MPa and holding time of 20 min. The pressurization time (come-up time) was 0.5 min and the process was terminated by an instant depressurization.

The solutions and apple cubes were packed and sealed in the nylon pouches and the experiments were done according to section 3.5.2 and the mass intake data were evaluated based on the procedure presented in section 4.3.1.

7.3.5 Freezing

For testing the influence of chitosan on textural quality of frozen apple cubes, both CH-impregnated and untreated control samples were room frozen in a conventional air freezer (-18°C) overnight (10 h). The samples were thawed next day at room temperature (23°C) for 2 h and evaluated for textural quality and drip loss.

7.3.6 Texture profile analysis (TPA)

The texture analysis was carried out using a TA-XT Plus Texture Analyzer (Texture Technologies Corporation, Scarsdale, N.Y., U.S.A./Stable Micro Systems, Godalming, Surrey, U.K.). The machine was equipped with a 25-mm diameter flat head cylindrical compression probe. To obtain the TPA, a two-cycle compression test was used. The hardness was calculated based on the first compression peak. For each experiment, an apple cube was placed under the probe. The pre- and post-test speeds were 1mm/s and 5 mm/s, respectively. The TPA was done before freezing and after thawing in duplicate.

7.3.7 Drip loss measurement after freezing

The drip loss after thawing of CH impregnated samples was determined according to the difference in weight of the frozen and thawed samples. The drip loss was reported in the form of percentage regarding the initial weight (%).

7.4 Results and discussion

7.4.1 Flow tests

Table 7.1 shows the flow behavior index and consistency coefficient values for HP treated aqueous GA and CH dispersions, respectively. Power law model was used to describe the viscosity and shear rate relationship (Eq. 7.3).

$$\sigma = K \dot{\gamma}^n \quad (7.3)$$

where, σ , K , n and $\dot{\gamma}$ are the shear stress (Pa), consistency coefficient, flow behavior index and shear rate (1/s), respectively.

Using the shear ascending-shear descending cycles (upward and downward flow curves), the shear descending viscosity values at higher concentration and pressure levels including

GA-III at 600 MPa, were equal to or higher than in shear ascending. This contrasts with the control which showed a similarity in both shear sweeps, although the range of incompatibility was negligible.

The flow behavior index for GA dispersions in the higher concentration range (GA-II and GA-III) showed almost Newtonian behavior ($n \approx 1$), (Table 7.1) both in the shear ascending and descending tests. Only GA-I dispersions showed the non-Newtonian character in the shear ascending tests. The up-curves are characteristic of the virgin previously un-sheared product and tend to display more non-Newtonian character while the down curve data represent more shear-equilibrated values that have better applications in fluid handling. The n and K values agreed with Li et al. (2011), and Sanchez et al. (2002).

The flow behavior index values for GA-II and GA-III increased after HP treatment. This rheological change towards a plateau viscosity region (Newtonian behavior) might be due to a slight increase in weak bonds such as hydrogen bonds which mostly exist between aggregates that form a developed uniform network (Table 7.1). The HP treatment was not effective in changing n values for CH-I and CH-II, but these were characteristically more pseudoplastic than GA even at much higher concentration levels. This resistance was related to the homogeneous and monophasic chemical structure of CH. Unlike GA-II and GA-III, GA-I showed a different trend of flow behavior; the n and K values showed a shear thinning behavior and the shear ascending and descending didn't show superimpositions. Li et al. (2009) found that the viscosity in the shear ascending and descending curves of GA-I showed the least resemblance among GA dispersions of 1 to 30 g/100g.

Table 7.1. Power law model parameters of ascending (n_1 , K_1) and descending (n_2 , K_2) shear sweeps of 6%GA, 15%GA 20%GA, 2% CH and 4% CH after pressurization at 200, 400, and 600 MPa for 30 min (mean \pm standard deviation, $n = 2$).

Sample details	Flow Behavior	Consistency	Flow Behavior	Consistency
	Index (n_1)	Index (K_1)	Index (n_2)	Index (K_2)
GA-I/Control	0.85 \pm 0.03	8.52E-3 \pm 0.000	0.99 \pm 0.01	3.55 E-4 \pm 0.000
GA-I/200MPa	0.85 \pm 0.04	8.65 E-3 \pm 0.000	0.99 \pm 0.00	3.62 E-4 \pm 0.000
GA-I/400MPa	0.83 \pm 0.03	9.23 E-3 \pm 0.000	0.98 \pm 0.01	3.47 E-4 \pm 0.000
GA-I/600MPa	0.81 \pm 0.04	1.03 E-2 \pm 0.003	1.0 \pm 0.00	5.21 E-4 \pm 0.001
GA-II/Control	0.94 \pm 0.04	1.94 E-2 \pm 0.005	1.0 \pm 0.00	1.38 E-2 \pm 0.003
GAI/200MPa	0.96 \pm 0.01	1.72 E-2 \pm 0.003	0.99 \pm 0.01	1.41 E-2 \pm 0.004
GAI/400MPa	0.99 \pm 0.01	1.62 E-2 \pm 0.001	1.0 \pm 0.00	1.31 E-2 \pm 0.003
GAI/600MPa	0.97 \pm 0.01	1.64 E-2 \pm 0.003	1.0 \pm 0.00	1.36 E-2 \pm 0.002
GAII/Control	0.92 \pm 0.02	4.82 E-2 \pm 0.002	0.99 \pm 0.01	3.35 E-2 \pm 0.004
GAII/200MPa	0.99 \pm 0.01	3.21 E-2 \pm 0.019	0.99 \pm 0.00	3.18 E-2 \pm 0.008
GAII/400MPa	0.99 \pm 0.01	3.22 E-2 \pm 0.020	0.99 \pm 0.01	3.43 E-2 \pm 0.018
GAII/600MPa	0.99 \pm 0.00	3.36 E-2 \pm 0.019	0.99 \pm 0.00	3.44 E-2 \pm 0.012
CH-I/Control	0.78 \pm 0.03	4.72 E-2 \pm 0.004	0.78 \pm 0.02	4.02 E-2 \pm 0.020
CH-I/200 MPa	0.78 \pm 0.01	4.64 E-2 \pm 0.012	0.78 \pm 0.06	4.07 E-2 \pm 0.010
CH-I/400 MPa	0.79 \pm 0.01	4.62 E-2 \pm 0.013	0.78 \pm 0.01	4.03 E-2 \pm 0.051
CH-I/600 MPa	0.78 \pm 0.02	4.73 E-2 \pm 0.011	0.78 \pm 0.03	4.02 E-2 \pm 0.024
CH-II/Control	0.77 \pm 0.03	8.96 E-1 \pm 0.019	0.77 \pm 0.02	9.01 E-1 \pm 0.084
CH-II/200MPa	0.77 \pm 0.01	9.03 E-1 \pm 0.083	0.77 \pm 0.01	9.14 E-1 \pm 0.039
CH-II/400MPa	0.77 \pm 0.01	8.63 E-1 \pm 0.032	0.77 \pm 0.02	8.77 E-1 \pm 0.021
CH-II/600MPa	0.77 \pm 0.02	8.56 E-1 \pm 0.048	0.77 \pm 0.01	8.52 E-1 \pm 0.012

When a shear rate is applied on aqueous hydrocolloid dispersions, a disentanglement takes place between the polymer molecules. The disentanglement is obviously proportional to the level of shear rate. As a result, at lower shear rates, it is expected that a high viscosity is maintained because of a development of entanglements due to the Brownian motion of the macromolecules. At higher shear rates, the Brownian-driven re-entanglements cannot keep up with the shear-driven disentanglements and consequently the viscosity drops. This drop continues to a level that any increase in shear rate would be roughly ineffective to

change the viscosity. Approximately the time needed to form new such entanglements is on the order of the reciprocal of apparent shear rate.

A more specific way to study the hydrocolloid's behavior while neglecting the Brownian-driven re-entanglements could be done by providing an amount of energy for the destruction of the weak entanglements before specific rheological measurements. In this regard, the down-curve rheology data or the thermo-viscoelastic tests, such as part 3.4, would reveal a better rheological demonstration (Williams & Phillips, 2009).

7.4.2 Dynamic oscillation tests

In both GA and CH, the loss modulus values were higher than the storage modulus values. No crossover was observed in the CH and GA except at GA-I samples which were previously reported by others for its different behavior (Li et al., 2009). It seemed that at the mentioned concentration levels, the pressure could not noticeably change the viscoelastic pattern. This indicates that the aqueous hydrocolloid systems showed a liquid-like behavior in the angular frequency range of 1-25 (rad/s).

According to Fig. 7.1 at CH-I and CH-II, the storage modulus appeared to merge to their control samples at higher frequencies. This might be due to the destruction of pressure-induced weaker bonds at lower frequencies. The same trend was observed at GA-I, GA-II, and GA-III, except at GA-III processed at 600 MPa. This agreed with the research done by Panteloglou et al. (2010). Several works have demonstrated that HPP has the least effect on the covalent bonds which are assumed as the primary chemical bonds and this resistance to rupture is because of negligible compressibility of these bonds (Galazka & Ledward, 1995). In other words, the secondary and tertiary bonds are most likely to be affected by HPP. Thus, considering the key role of such bonds in the development of the secondary and the tertiary configurations, macromolecules are assumed as the most susceptible chemical components to the HPP (Heremans, 1995).

In general, proteins contain a high number of hydrogen, oxygen and nitrogen atoms which impart as the main factor of development of weak intermolecular interactions such as hydrogen bond. Thus, the proteinaceous part of the GA could be responsible for the rheological changes since this gum has a proteinaceous part that is involved in the highest

molecular weight fraction of GA (<10% (w/w)) despite its less proportional content (>2% (w/w)), (Randall et al., 1988).

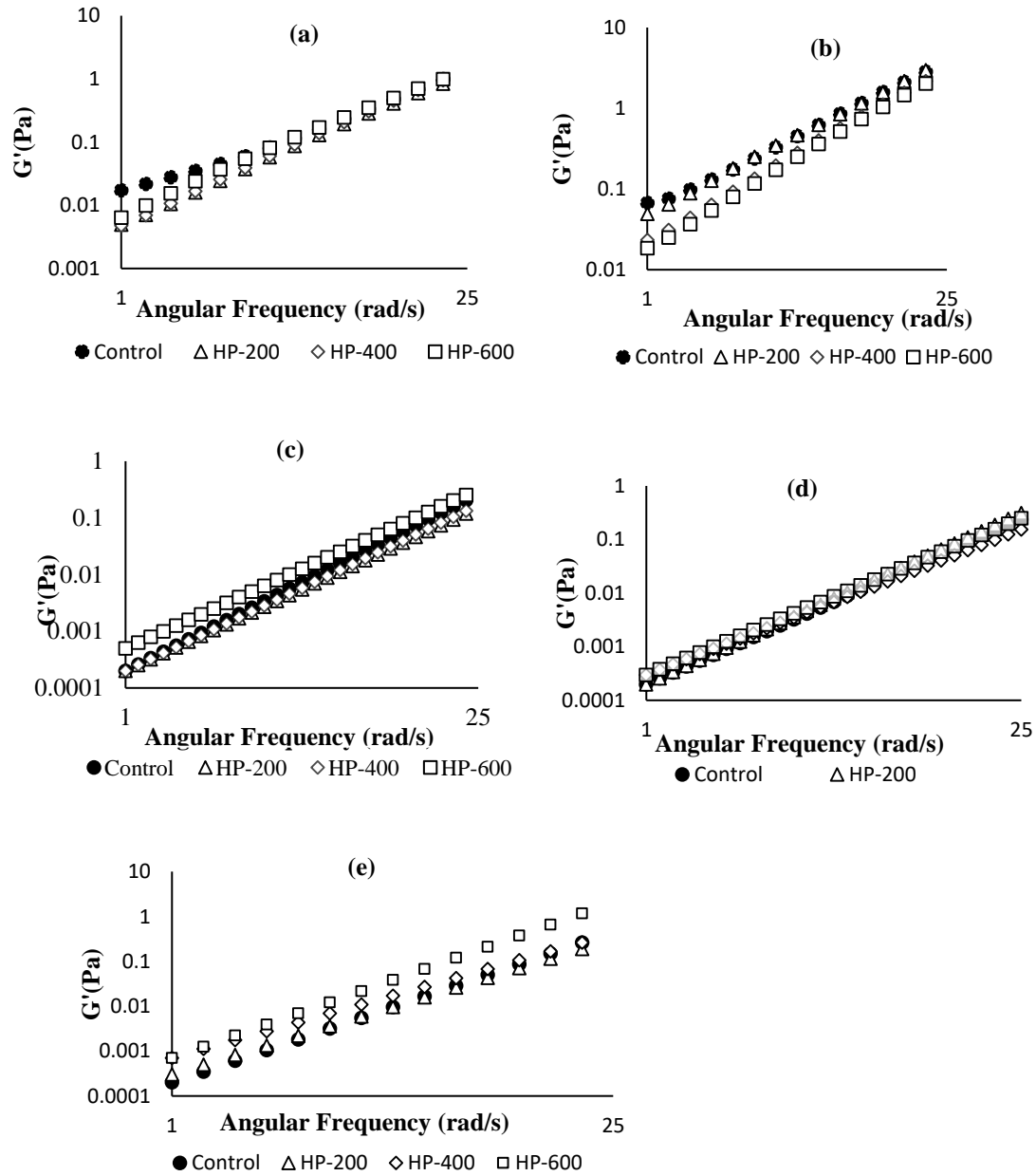


Fig. 7.1. Storage modulus as a function of the frequency at CH-I (a), CH-II (b), GA-I (c), GA-II (d), and GA-III (e) after pressurization at 200-600 MPa for 30 min.

7.4.3 Cox-Merz model

The steady shear flow data and oscillatory shear data were used in the range of 1-25 rad/s. For all samples, the $\eta(\dot{\gamma})$ and $|\eta^*|(\omega)$ did not show linear superimposition. Regarding the empirical nature of the rule, some researchers have added modifications &/or correction coefficients. Ahmed and Ramaswamy (2006) proposed a constant shift factor in the steady shear values. However, in the current research, a systematic non-linear deviation was observed between the $|\eta^*|$ and η at a similar shear rate and frequency values. The deviation was presented in a form of a power law shift function regarding the fitness of $\frac{\eta}{|\eta^*|}$ versus the frequency range of 1 to 25 rad/s (Eq. 7.4). The equation constant (Π) and power exponent (α) for each sample are presented in Table 7.2.

$$\frac{\eta}{|\eta^*|} = \Pi \omega^\alpha \quad (7.4)$$

According to Table 7.2, the data, the Π values were higher in control samples (except in GA-I). The α values, as a representative of the curvature of the deviation trend, could be an indication of stronger decay in the molecular network.

Table 7.2. The shift function parameters regarding the Cox-Merz rule for GA-I, GA-II, GA-III, CH-I, and CH-II after pressurization at 200, 400, and 600 MPa for 30 min.

Sample details	Π	α	R^2
GA-I/Control	0.48	-0.40	0.99
GA-I/200 MPa	0.51	-0.33	0.98
GA-I/400 MPa	0.55	-0.35	0.98
GA-I/600 MPa	0.61	-0.51	0.96
GA-II/Control	0.18	-0.11	0.97
GA-II/200 MPa	0.16	-0.10	0.97
GA-II/400 MPa	0.10	-0.16	0.96
GA-II/600 MPa	0.13	-0.11	0.95

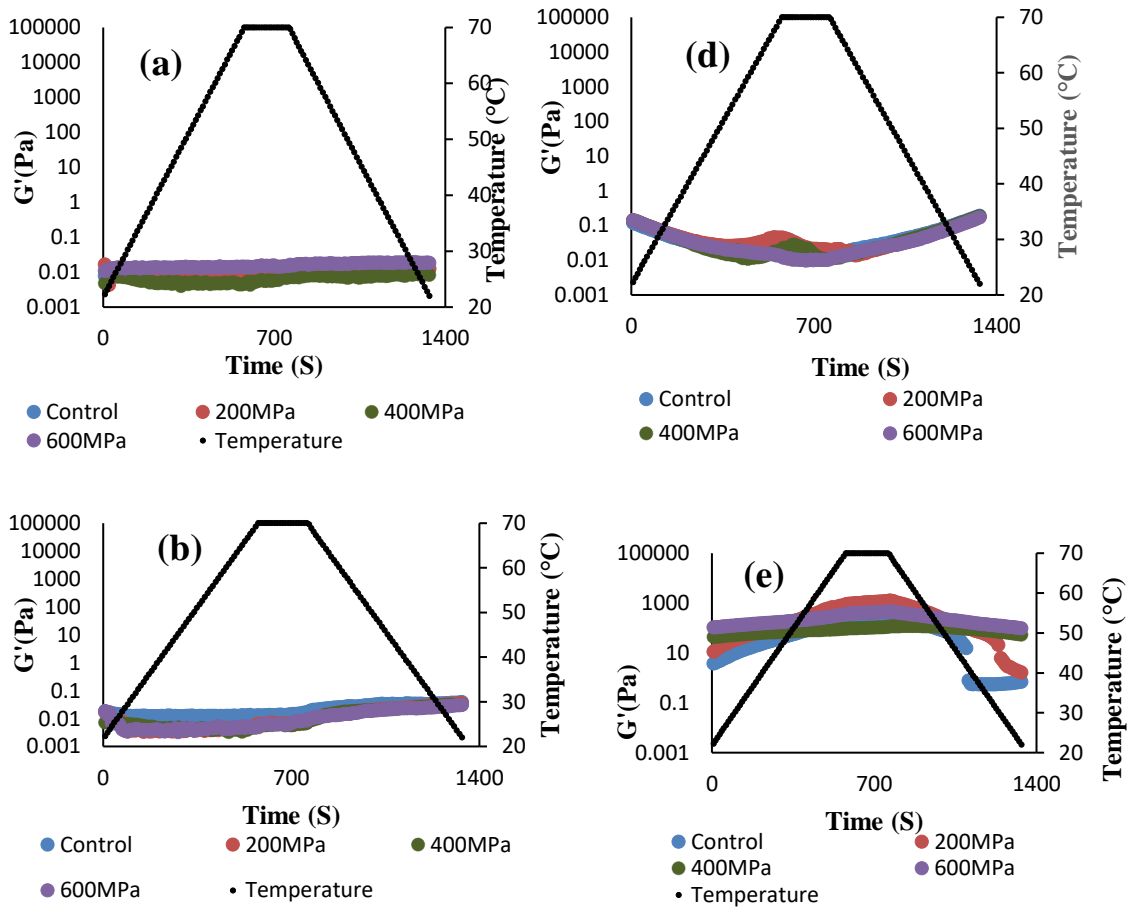
GA-III/Control	0.22	-0.06	0.93
GA-III/200 MPa	0.15	-0.03	0.85
GA-III/400 MPa	0.15	-0.04	0.87
GA-III/600 MPa	0.15	-0.03	0.90
CH-I/Control	0.02	-0.19	0.99
CH-I/200 MPa	0.02	-0.20	0.99
CH-I/400 MPa	0.01	-0.19	0.99
CH-I/600 MPa	0.02	-0.19	0.99
CH-II/Control	0.21	-0.16	0.99
CH-II/200 MPa	0.27	-0.18	0.99
CH-II/400 MPa	0.10	-0.15	0.99
CH-II/600 MPa	0.20	-0.15	0.99

7.4.4 Thermo-viscoelasticity

7.4.4.1 Temperature sweep tests

The possible structural changes in the overall pattern of viscoelastic modulus would present more information on the intensity of pressure-induced rheological changes. Figure 7.2 shows the change in the elastic modulus as a function of temperature. The elastic modulus showed a similar trend with GA-I and GA-II. The G' decreased during the heating, and there was a recovery during the cooling period. Heating dissociates the molecules due to an increase in kinetic energy and results in moderate changes; on the other hand, a cooling stage, after the thermal treatment, allows the molecules to rearrange and realign to their most desired and stable thermodynamic state thereby causing a greater influence on the resulting rheological changes. The GA-III control samples showed a considerable increase in G' during the heating period, and the similar slight increase was observed during the cooling section. Although, the similar trend was not seen after HP treatment of GA-III. At this concentration level, there was a considerable drop of almost 3 log reductions after HP treatment at 200, 400 and 600 MPa of GA-III samples. This could be an indication of the

effect of HP treatment in terms of lowering the ability of proteinous phase to maintain its quaternary characteristics after HP treatment. To clarify, the HP treatment can change the secondary and the tertiary structures of proteins by making irreversible or sometimes reversible unfolding. Furthermore, the change in the quaternary structure of proteins is due to the alterations in hydrophobic interactions (Wu et al., 2009). It has also been reported that HP processing above 200 MPa can affect the tertiary and the quaternary structure of proteins by changing hydrophobic and ionic interactions (Hendrickx et al., 1998).



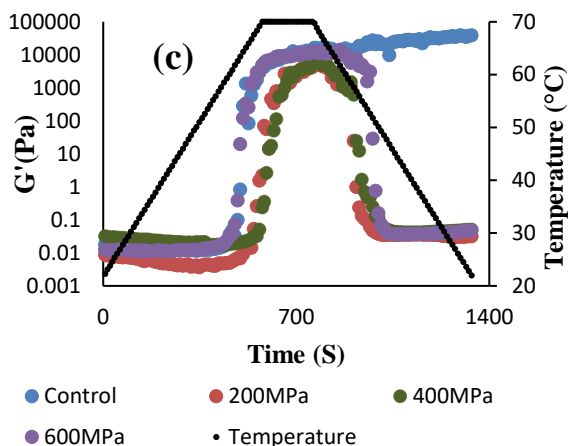


Fig. 7.2. The gradient of phase shift ($\Delta\phi$) vs. temperature semi-log graphs of Viscoelastic compatibility of samples after HP treatment at 200, 400, 600 MPa. Letters indicate as following: (a) GA-I, (b) GA-II, (c) GA-III, (d) CH-I, and (e) CH-II.

The loss moduli of all GA-I samples were higher than the storage modulus. Nevertheless, after HP treatment at 600 MPa, two crossover points including $G' > G''$ (during heating) and $G'' > G'$ (during cooling) were observed at 65.9 °C and 48.5 °C, respectively. The HP treatment was ineffective in the development of such behavior at GA-II concentration, and all samples showed $G'' > G'$ pattern which indicates a higher liquid-likeness. Only one crossover ($G' > G''$) was observed at GA-III controlled samples at 65 °C. In addition to the one $G' > G''$ crossover, HP treatment of GA-III led to observation of two crossovers. The second crossover took place once the loss modulus became higher than the elastic modulus during the cooling period. These temperature (°C) values ($T_{G' > G''}$, $T_{G'' > G'}$) were (68.4, 51.8), (70, 47.52), (70, 56.8), (68.4, 51.8) for 200, 400 and 600 (MPa) treated samples, respectively. Regarding the CH samples, at CH-I control $G' > G''$ at 27.7 °C and HP treated CH-I samples showed $G'' > G'$ during both heating and cooling period. At CH-II, the $G' > G''$ and $G'' > G'$ points were observed at 47.7 °C (during heating) and 52.6 °C (during cooling). HP treatment led to permanent $G' > G''$ in all CH-II samples.

7.4.4.2 Modeling

Generally, two kinds of viscoelastic behavior as a function of temperature was observed. The first one was the “smooth curve” of G' or G'' (T). It was recognizable during all the

heating stages for all samples. In this regard, a two-term exponential model, widely used for interpretation of variation of biophysical phenomena as a function of temperature, seemed to be appropriate (Eq. 7.5). However, at GA-III, due to the abrupt changes (Fig. 7.2c), the storage modulus could be modeled by a two-term Gaussian function (Eq. 7.6).

Eq. 7.5: Exponential model of viscoelasticity as a function of Temperature ($^{\circ}\text{C}$)

$$G', G''(T) = Ae^{BT} + Ce^{DT} \quad (7.5)$$

Eq. 7.6: Gaussian model of viscoelasticity as a function of Temperature ($^{\circ}\text{C}$)

$$G', G''(T) = a_1 e^{-\left(\frac{(T-b_1)}{c_1}\right)^2} + a_2 e^{-\left(\frac{(T-b_2)}{c_2}\right)^2} \quad (7.6)$$

The calculated model parameters for loss modulus are shown in Table 7.3. The model parameters showed that the storage modulus had fewer changes in terms of thermo-viscoelastic model parameters which was also in agreement with isothermal oscillatory tests; results depicted in Fig. 7.1.

Table 7.3. Exponential model parameters of temperature sweeps tests (22-70-22 $^{\circ}\text{C}$) loss modulus during cooling periods (letters A, B, C, D are related to Eq. 7.5 and letters a1, b1, c1, a2, b2, and c2 are calculated according to Eq. (7.6).

loss Modulus (G'')	A	B	C	D	R^2	RMSE		
CH-I/600 MPa	5.40	-5.31 E-2	2.19 E-1	-2.08 E-3	0.99	1.63 E-3		
CH-II/600 MPa	5.65	-5.03 E-2	1.16 E-1	6.97 E-3	0.99	2.12 E-3		
GA-I/600 MPa	4.63E-2	-2.24E-2	8.39E-5	5.49E-2	0.99	4.53E-4		
GA-II/600 MPa	7.82	-3.37E-1	2.33E-1	-2.02E-2	0.99	5.78E-4		
	a1	b1	c1	a2	b2	c2	R^2	RMSE
GA-III/600 MPa	3.47 E+3	7.05 E+1	7.95	1.98 E+3	6.13E+1	4.62	0.99	5.88 E+1

7.4.4.3 Compatibility analysis

During the temperature ramp, two kinds of changes could be seen. First, the changes due to the difference between the loss tangent ($\tan\delta$) between heating and cooling (Eq. 7.7).

$$\tan\delta = \frac{G''}{G'} \quad (7.7)$$

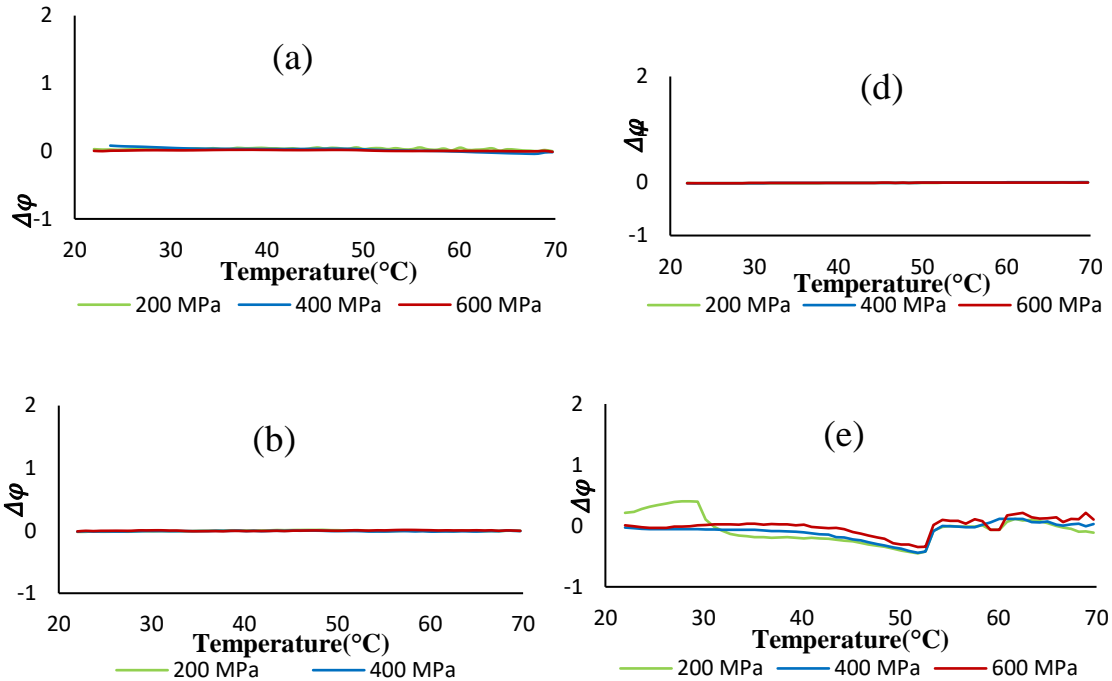
Second, the differences in heating/cooling curves as a function of pressure. Due to the dependence of each factor to the other, any comparison should be made while considering both factors. In this respect, a shift factor regarding the difference of the treated samples with the control samples was calculated (Eq. 7.8). To obtain the shift factor change between heating and cooling cycles, Eq. (7.9) was used for the pressure treated samples.

$$\varphi = \log \left[\frac{\tan\delta_2}{\tan\delta_1} \right] \quad (7.8)$$

$$[\Delta\varphi]_T = \varphi_{cooling}^T - \varphi_{heating}^T \quad (7.9)$$

where φ is the shift factor. The phase shift data represents the heating vs. cooling “compatibility” of viscoelastic behavior of the samples. The obtained graphs indicate the gradient of the shift phase between each treated sample and the control samples. In the case of no changes in the thermo-viscoelastic behavior of the samples, the graph would be zero line at the temperature ranges. While, as can be seen, the non-zero values reflect the phase change because of high pressure, during the thermal ramp. The data could be acceptable demonstrations of the chemical and physical changes of the samples after pressurization. The changes cover both permanent and temporary alterations on the molecules and network structure of the dispersions. As shown in Fig. 7.3, the $\Delta\varphi$ trends for all samples show that the shift phases tend to merge at higher temperatures. This would indicate the higher incompatibility at the lower temperatures. The incompatibilities at lower temperatures indicate pressure induced permanent changes. It should be motioned that such changes remained after a full temperature cycle ending at the start point. The descending trend at higher temperature is due to the higher molecular kinetic energy and disappearance of the intermolecular bonds. The $\Delta\varphi$ value for all GA-I and GA-II were in a close range to each other, while at GA-III, the incompatibility was considerably higher than lower concentrations. The incompatibility patterns were almost the same at all pressure levels,

however, there were no specific trends regarding the pressure level. At GA-III and 25 °C, compared to the lower concentrations, the $\Delta\phi$ value was about 1 order of magnitude higher. The CH dispersions showed different patterns at different concentration. Like the GA samples, the high $\Delta\phi$ values were considerably evident at higher concentrations. However, for CH, the range of the incompatibilities was considerably lower than for GA. With both CH-I and CH-II, the $\Delta\phi$ tended toward 0 at 70 °C, however, the patterns were different. A rapid change in $\Delta\phi$ was seen at 40 °C at CH-II level, which could indicate a molecular arrangement transition although at 70 °C the values were merging the X axis. At the highest concentration of chitosan (Fig. 7.2e), there is a permanent change in the storage properties of the high pressure treated samples (400 MPa and 600MPa). This is evident since the elastic modulus is higher than other samples even after cooling (+7 min).



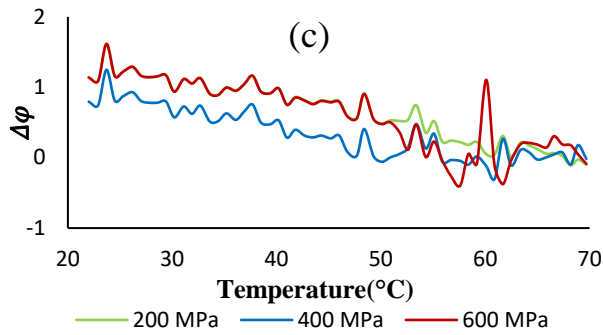


Fig. 7.3. The gradient of phase shift ($\Delta\phi$) vs. temperature semi-log graphs of Viscoelastic compatibility of samples after HP treatment at 200, 400, 600 MPa. Letters indicate as following: (a) GA-I, (b) GA-II, (c) GA-III, (d) CH-I, and (e) CH-II.

To describe, according to Fig. 7.3(d-e), there is a shift in the $\Delta\phi$ which is indicative of permanent changes in both loss and storage moduli at higher concentrations. Also, it can be concluded that despite a less change in the storage modulus at 200 MPa, the alterations in loss modulus are responsible for changes towards the liquid -likeness of the CH-II/200MPa. This fact also rationalizes that the changes at this level are more in terms of changing in the hydrogen bond network and hydration properties rather than structural changes.

Overall, such types of analysis could give a “thermo-viscoelasticity fingerprint” of dispersions. It is seen that the change in the viscoelastic behavior of the samples is due to the development of weak bonds. In this regard, for processing points of view and especially for elevated temperature treatments, such as thermal sterilization, pasteurization, for temperature assisted pressure (TAP) processing, and pressure assisted thermal (PAT) processing, using such dispersions would give unpredictable rheological changes at higher concentrations. However, from stability points of view, the rheological properties of the dispersions after elevated temperature treatment would not give considerable differences regarding the control samples.

7.4.5 HPI of Chitosan

The mass intake data of CH is shown in Figure 8. The mass intake CH ranged 0.18 to 0.23 kg/kg apple. Also, the average standard deviation ranged 0.03. As can be seen, the mass intake decreased at higher concentrations of CH. The least mass transfer was 18% which belonged to the 4% CH solution.

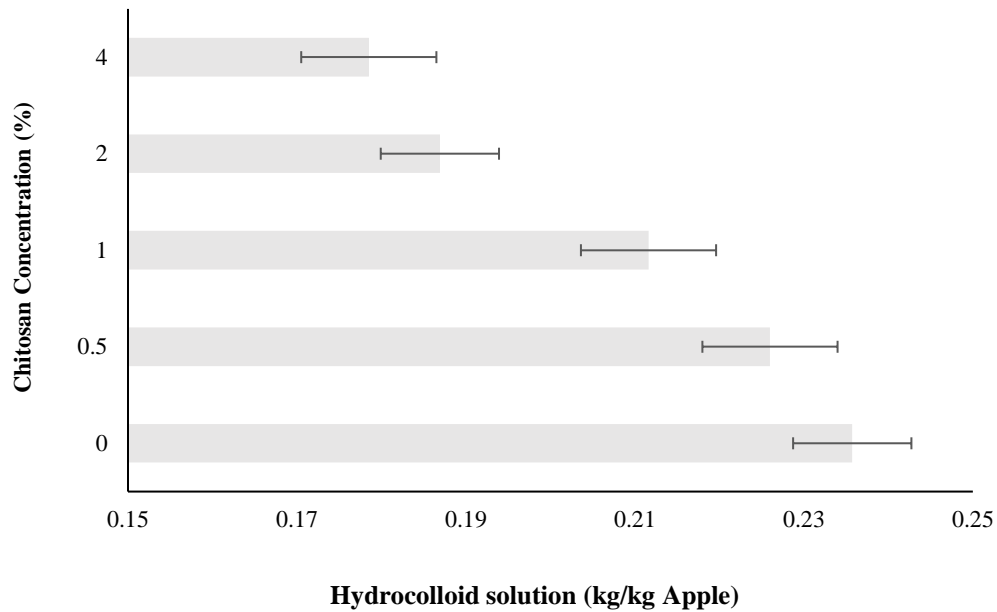


Fig. 7.4 The mass intake data (kg/kg) for impregnation of 0 % (water), 0.5%, 1%, 2%, 4% aqueous solution of chitosan into apple tissue after pressurization for 20 min at 100MPa.

7.4.6 Proposed model for HPI of non-Newtonian fluids

Representing a non-Newtonian flow model, CH was used in this study at different concentrations. A quadratic function (Eq. 7.10) was proposed for the mass transfer kinetics of the process which indicates that the results showed a second order decrease as a function of the concentration of the samples ($R^2 = 0.98$).

$$X = 0.0046C^2 - 0.0336C + 0.2385 \quad (7.10)$$

where C and X represented CH concentration (%) and solution intake (kg/kg), respectively.

It is important to mention that the results should not be fitted to the related viscosity values without further studies since during the process the molecular dynamics of the fluid phase is not necessarily at a constant state, and this aspect has not yet been explored and adopted. In other words, during the process, there may be different viscosity regimes in different regions of the porous medium and various time steps.

7.4.7 Texture analysis

Figure 7.5a shows the hardness of apple samples right after the impregnation as well as after the subsequent freezing and thawing stage. The hardness of the impregnated samples was higher than the fresh cut apples. The highest hardness was associated with samples impregnated with 1% CH and 2% CH. At this CH level, the data are significantly different from the other CH levels ($P < 0.05$). Regarding the fact that HPI results in filling the pores with compressible fluids, HPI acts as an enhancer to of increasing textural integrity. It was seen that the hardness texture analysis results showed no specific trend as a function of CH concentration. This lack of trend indicated that, in addition to CH concentration, different physical factor may also be involved in textural properties.

The effect of thawing on HPI samples, also showed a higher level of hardness in these samples as compared to the control samples. This value was almost 4 times higher than thawed unpressurized samples. It was also seen that even the pressurized samples without any impregnation were harder than the fresh samples. However, the main negative point was that pressure treatment of samples without CH would result in a tissue collapse. This happens because the gaseous phase present in the pores is removed from the sample under high pressure. Generally, the participation of porous network and tissue collapse is more observable as a constant gap relative to the volumetric collapse between the mass intake blanched and unblanched fruit tissue during HPI (Vatankhah & Ramaswamy, 2017).

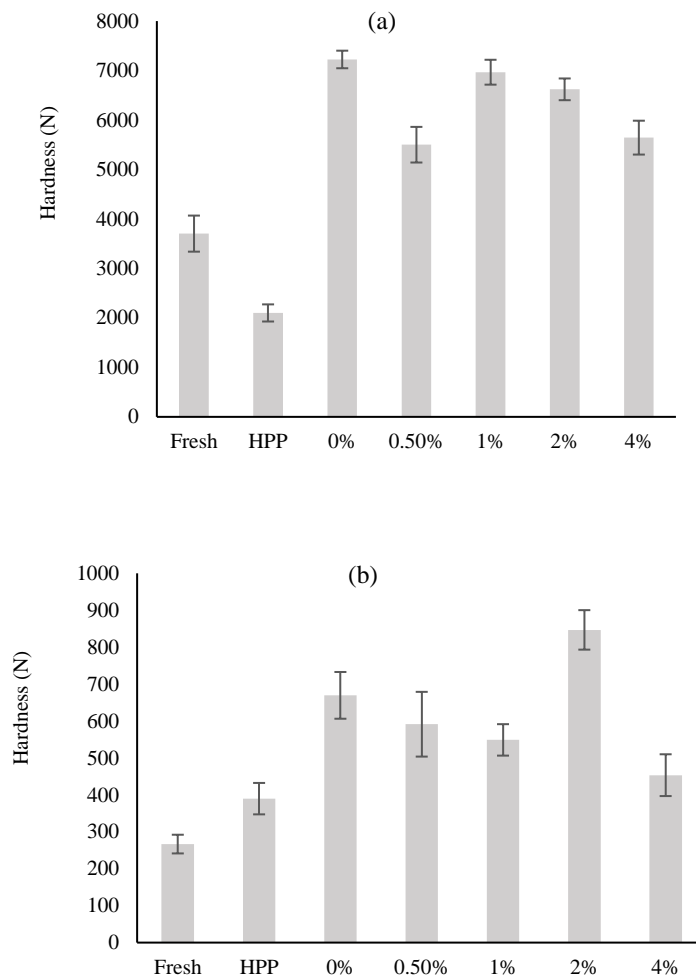


Fig. 7.5. The hardness of the apple cubes impregnated with 0%, 0.5%, 1%, 2%, and 4% CH compared to the fresh samples and simply pressurized (HPP) before air freezing (a) and after thawing (b). The high-pressure conditions for HPP and all HPI samples were 20min at 100MPa. Error bars represent standard deviation.

7.4.8 Drip loss

The freeze thaw drip loss results before and after HPI under different conditions are presented in Fig. 7.6. Drip loss ranged 9% to 18%. The drip loss was lower at the midrange concentrations of CH. As shown in Fig. 7.6, the drip loss increased at higher CH concentration. Such a behavior could be defined by the lower flowability of CH solutions at higher concentrations. It was also in agreement to the mass intake data in Figure 8 which demonstrated lower mass transfer rate of CH at higher concentration of CH.

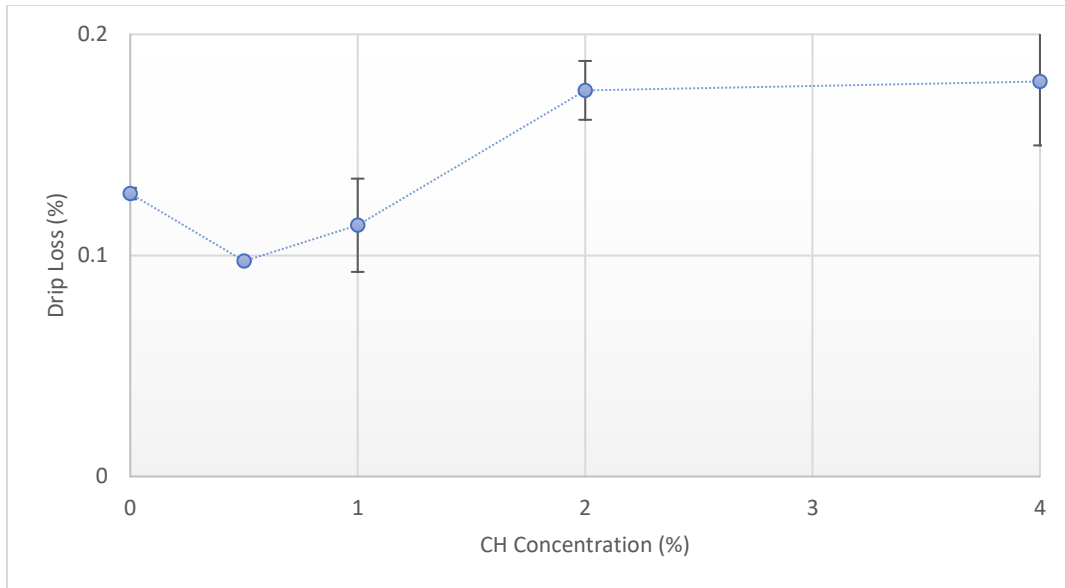


Fig. 7.6 The drip loss (%) after freezing (-18 °C, 10h) and thawing (23 °C, 2h) apple cubes impregnated (20min at 100MPa) with 0% to 4% CH. Error bars represent standard deviation.

Obviously, lower transfer rate leads to more intense squeeze and collapse of the inner cellular layers. As a result, this textural deterioration would lead to more drip loss in the tissue. The higher drip loss of the samples impregnated with water (0% CH) demonstrated that CH also acts as an enhancer of water holding capacity within the tissue. Overall, the drip loss and texture analysis data demonstrated existence of an optimal point in the midrange concentration of CH in which the Hardness is the highest after thawing and the drip loss is minimal.

7.5 Conclusion

It was observed that the combination of three main physical parameters, the shear rate, frequency of oscillation and temperature ramp, could provide a better means of evaluation of structural changes in hydrocolloid systems as a function of pressure treatment. Looking at the results, it is obvious that CH is a more reliable material for studying impregnation of viscose fluids. The food processors must take this point into account that in order to use high viscosity fluids in HPI as a career or for technical texture modifications, the pressure resistance of the fluid is important regarding the product homogeneity and accurate time-dependent pace

Preface to Chapter 8

Chapter 8 was a study on an innovative method of impregnation of plant tissues with emulsions. Such process is one of the first of its kind regarding the technology of enrichment of porous biomaterials- which are generally hydrophilic regarding their high-water content- with fat-containing fluids. The research could be defined in two parts. At first part, the stability of the emulsion as the fat carrier was examined under high pressure. Then, different qualitative and quantitative strategies were defined to illustrate the impregnation into the intercellular space and to study the kinetics of the impregnation at selected pressure levels and selected emulsion compositions.

Parts of this chapter have been adapted for presentations and publications as follows:

Vatankhah, H., Ramaswamy. H. S. (2017). High pressure Impregnation (HPI) of W/O emulsions into selected fruits: A novel method. (*Prepared for submission*).

CHAPTER 8

High Pressure Impregnation of Emulsions into Selected Fruit Tissues: Mass Transfer Dynamics and Emulsion Stability

8.1 Abstract

High pressure impregnation (HPI) process was evaluated as a means of enrichment of fruit tissue with model oil and water emulsions. Cubic samples of size 1.2 cm x 1.2 cm x 1.2 cm were cut from apple, strawberry, pear, Asian pear, and melon as fruit tissues. Coconut oil to polysorbate (Tween 80) emulsions were prepared at different weight to weight basis (oil to emulsifier): 50-50 (I), 75-25 (II), 87.5-12.5 (II), and 93.75-6.25 (IV), and mixed 20:80 with water. The emulsion stability after the high pressure treatment (100 MPa for 20 min) was studied by dynamic rheology, pH, and particle size distribution analysis. The high pressure treatment slightly decreased the pH and apparent viscosity of the emulsions, but particle size distribution was not affected. The mass transfer during 0-20 min at 100 MPa HPI treatment of emulsion-I followed a time-based quadratic model in all samples. The highest and the lowest final mass intake belonged to apple (18 %) and strawberry (6%), respectively. Effect of different combinations of emulsions was evaluated at 20 min of HPI at 100 MPa for all fruits. The results showed a reverse relationship between in the final mass intake and oil content. The light microscopy was used as an illustration of impregnation of the oil droplets within the water phase into the intercellular space.

8.2 Introduction

Impregnation techniques are used as efficient ways of quick introduction of an active solution into fruits and vegetables. High controllability, quickness, and simplicity are the main technically attractive characteristics of such techniques (Petersen 2014). The main reason for such impregnation techniques is the value imparting characteristics of impregnant solution and its capability of having a certain role in further processing stages. Thus, using diverse types of sugars, acids, colors, minerals, and vitamins, the food processor can improve the product quality, texture building, nutritional fortification, or an

aid to facilitate a process. These enrichments could be very functional as texturizers such as calcium salts (Shahidul et al., 2007), chelating agents such as phosphates (Pilizita & Sapers 2004), anti-browning agents and enzyme inhibitors such as 4-hexyl resorcinol and sodium chlorites (Dong et al 2000; Lu et al 2007), reducing agents such as cysteine (Lamikanra 2002), acidulants such as citric, malic, and phosphoric acids (Rojas-Garu 2007; Tola & Ramaswamy 2013), antioxidants such as ascorbic acid (Vatankhah & Ramaswamy 2017; Gorny et al 2002), and antimicrobial agents such as acidic and chlorine compounds (Parish 2003). Moreover, fruit and vegetables are not rich in certain micronutrients. For instance, the fat-soluble vitamins are low in plant tissues. This issue has caused high consumption of supplements in the world. It was reported that 35 million people in United States use Vitamin E supplements on a daily basis while it was observed that bioavailability of vitamin E in nutritionally fortified foods are higher nutritional supplements (Traber 2004).

In this regard, emulsions are deemed as proper carriers in order to implement desired fortifications of oil-based nutrients. Emulsions are deemed as carriers for lipophilic compounds. These are means to solubilize fat-soluble compounds such as several types of food colours, vitamins, and essential fatty acids (Binks 1998; Tadros & Vincent 1983; Han et al., 2000; Qian et al., 2012).

The high water content of fruits and vegetable tissues make it difficult for impregnation with hydrophobic compounds because of hydrophilic – hydrophobic conflicts. In this regard, there is a need for a strong driving force to overcome such conditions. One of the methods to impregnate fruits and vegetables is the well-recognized vacuum impregnation (VI) method. In this method, the principal driving force for the impregnation process is the pressure difference between the fluid phase and the soaked tissue. This pressure difference is achieved by a negative pressure provided by the vacuum environment. In this process, the trapped gas inside the tissue is sucked out and the intercellular space is expanded by the vacuum which is replaced by the surrounding solution during the vacuum release (Allali et al., 2010; Castagnini et al., 2015; Fito 1994; Fito et al., 2001). In other words, the gas phase will be removed from the tissue and substituted by the fluid. But, due to the low mass transfer kinetics associated with such phenomenon and osmotic pressure exerted by the

water phase, this method is not an efficient way to impregnate the emulsions. Hence, serious alternative considerations must be given for the impregnation of the oil phase. A more efficient way would be to impose a considerably higher pressure difference between the fluid and the solid phase by the application of a positive pressure (which has unlimited possibilities) as compared to vacuum (where the maximum pressure difference can only be one atmosphere) (Vatankhah & Ramaswamy, 2017). In this study, high pressure processing (HPP) is utilized in order to implement a rapid and considerable pressure difference.

HPP is a non-thermal technology developed and commercialized as an alternative to conventional thermal processing (Knorr et al., 2002). The process can be used to inactivate enzymes and kill microorganisms without any need for elevated temperatures. Consumers prefer the fresh-like, healthy and minimally processed food products. HPP aims to maintain food flavors and quality fresh by keeping food naturally preserved and additive-free. Furthermore, HPP is a technique that is independent of size, form, shape or mass of the food and can take packages in any flexible form; this is a great advantage giving many possibilities for novel process, product, package and equipment in the food industry (Bignon 1996; Knorr et al., 2006; Miao et al., 2011). Numerous studies have demonstrated a promising future for high pressurized foods in terms of capability of killing pathogenic bacteria while minimally affecting the flavor and textural characteristics (Hiremath & Ramaswamy 2012; Knorr 1995; Pinela & Ferreira 2017; Ramaswamy et al., 2010). Moreover, several modifications in functional and physical properties of proteins and carbohydrates have been achieved by HPP (De Maria et al., 2015; Vatankhah et al., 2018). These characteristics are usually deemed as positive side effects of such techniques.

A new aspect of utilizing HPP has been introduced as high pressure impregnation (HPI). This method is deemed as a rapid way of the introduction of certain enriched fluids to the fruit and vegetable tissues (Vatankhah & Ramaswamy 2017; Vatankhah et al., 2018). Generally, the fruits and vegetables have a porous structure. This structure is based on the noticeable void/air space between and within parenchyma cells. These gas-filled channels – known as pores- are the main spaces in which the fluid can be directed to.

This study is focused on taking advantage of high driving force of HPP to impregnate emulsion model systems (trapping oil soluble vitamins and other active component) into selected fruit and vegetable tissues. Using a coconut oil / Tween oil/emulsion system the mass transfer kinetics were evaluated under HPP conditions. In addition, the stability of the emulsion after HPP was also evaluated. Also, an inclusive evaluation of mass transfer kinetics modeling at different levels of oil/ water ratio and various types of fruits was presented in order to characterize the dynamics of the impregnation process.

8.3 Materials and methods

8.3.1 Emulsion Preparation

In this study, commercial coconut oil (Presidents choice, Canada) and polysorbate (Tween 80) (Sigma Aldrich) were chosen as the main oil and emulsifier compounds. Selected combinations of oil-emulsifier phase were prepared on a weight to weight (oil to emulsifier) basis including different combinations of oil and emulsifiers: 50-50, 75-25, 87.5-12.5, and 93.75-6.25. To prepare every 100 g of emulsions, 20 g of each combination were gradually added to 80 g of double distilled water (conductance: 18 V, Milli-Q, Millipore, Bedford, USA) and emulsified using a homogenizer (PowerGen 700, Fisher Scientific, Pittsburg, PA) at 14,000 rpm for 4 min. All sample preparations were done at room temperature (25°C), and the experiments were carried out using freshly prepared emulsions. As shown in Fig. 8.1, the final percentage of oil/emulsion in every 100 g of emulsion was: 10 % -10% (I), 15 % -5 % (II), 17.5%-2.5% (III), 18.75%-1.25 (IV).

8.3.2 Emulsion stability factors after HPP

First, a comprehensive study was carried out on the stability of all emulsions. In this regard, 50 g of each emulsion was packed and sealed in low-density 2 oz. polyethylene bags (Whirl Pak(R), Nasco, Fort Atkinson, WI, USA) and subjected to 100 MPa HP treatment for 20 min. The experiments were performed in triplicate and the physical properties of the emulsions were measured before and after each HPP treatment.

In this study, all high pressure treatments were given in a pilot scale high pressure equipment containing a cylindrical pressure chamber of 5 L volume (ACIP 6500/5/12VB-ACB Pressure Systems, Nantes, France). The pressure-time (P-t) program was designed using a computer connected to a data logger (SA-32, AOIP, Nantes, France). The medium used for pressure transmission in the system was water. The P-t program was designed including three stages: i) A 1 min pressure come-up to the desired pressure value ii) A holding time at the final pressure iii) a rapid decompression until the atmospheric pressure is reached.

8.3.3 Flow rheology tests

The flow rheology tests were carried out based on logarithmic measurements of the shear stress as a function of a shear rate ramp from 0.1 to 100 s⁻¹ in 180 s. The rheology measurements were made out using a cone/plate AR2000 Rheometer (TA Instruments, New Castle, DE, U.S.A.) equipped with 60 mm, 1.59° cone and attached computer and run by the software supplied by the company (Rheology Advantage Data Analysis Program, TA Instrument). A constant controlled temperature was maintained during the measurements. The flow behavior of each emulsion was measured before and after HPP.

8.3.4 Particle size distribution

The mean particle size and particle size distribution of the emulsions was measured using a Mastersizer (Hydro 2000MU Malvern Instruments Ltd., Malvern, UK). To prevent multiple scattering effects, each sample was diluted 1:1000 using double distilled water. The measurements were made for each emulsion, before and after a 20-min HP treatment at 100 MPa according to the processing conditions detailed in section 2.2. All measurements were carried at room temperature (22 °C).

8.3.5 pH measurement

Thirty grams of each emulsion was used for pH measurements. The pH measurements were made at room temperature (22 °C) using an ACCUMET pH-meter (Model 15, Guelph, ON, Canada).

8.3.6 *HPI of emulsions into fruit tissue*

8.3.6.1 *Sample preparation for HPI*

Fresh fruits from local market were obtained, washed and peeled. Melon, apple, Asian pear and pear were cut in $1.5 \times 1.5 \times 1.5$ (cm) cubes. The strawberry samples were used in whole form. Each time 30 g of fresh fruit samples were weighed (APX-200 Digital weighing Balance, Denver Instruments) and immersed into 50 g of various emulsion combinations. The samples were kept in low-density 2 oz. polyethylene bags (Whirl Pak(R), Nasco, Fort Atkinson, WI, USA). The bags were then heat sealed and immediately subjected to HP treatment.

8.3.7 *HPI operation*

The HPI tests were carried out at 6 different holding times including 0, 2, 5, 10, 15, and 20 (min) considering a final pressure level of 100 MPa. The samples were introduced into high pressure vessel at 18 °C. Basically, considering the applied approach of the literature, it was attempted to simulate industrial processing practices. Hence, sample preparation and measurements were made at room temperature, and the tests were performed in triplicate at each P-t combination.

8.3.8 *Emulsion intake calculation*

After each HPI the impregnated fruits were taken out of the polyethylene bags. The fruits were then drained and blotted for 15 s. The emulsion intake was measured based on relative mass intake using Eq. 8.1.

$$M_t = (m_2 - m_1)/(m_1) \quad (8.1)$$

where M_t , m_2 , and m_1 represent the relative mass intake after HPI for certain holding time (t) in min, the mass of impregnated and initial fruits, respectively.

8.3.9 *Light microscopy*

The impregnated samples were hand-sectioned from the mid-thickness layers using a razor blade immediately after HPI. Each slice was placed carefully on a microscope slide

and was observed using a transmitted-light system (EVOS-xl CORE, AMG, Bothell, WA) at 40X magnification.

8.3.10 Spectroscopic Verification of HPI of Emulsions

The oil phase impregnation was verified by using FTIR analysis of impregnated of fruits with emulsion IV (20 min at 100 MPa). A Bruker Alpha-spectrometer (Bruker Optic GmbH, Ettlingen, Germany), equipped with a temperature-controlled single-bounce diamond ATR crystal was used to obtain the spectrum within the range of 500 to 4000 cm^{-1} . To prepare the samples, first, each impregnated fruit was crushed and dried in benchtop oven (Fisher Scientific Isotemp 625G Gravity Oven) at 75 °C for 5h. Then, ethanol extract of each sample was prepared by adding 50 ml of pure ethanol. Finally, ethanol was removed by drying for 1h at 75 °C, and 0.1 ml of each extract was spread over the ATR surface for FTIR analysis. The OPUS (Bruker Optic) software was used to observe the spectrum. Further data analysis was done in OMNIC software environment.

8.4 Results and discussions

8.4.1 Emulsion stability

According to Fig. 8.1, there were slight differences in the viscosity of the emulsion. The apparent viscosity value was less than 0.15 Pa s for all the samples. As can be seen, the high pressure led to a slight decrease in apparent viscosity. The effect of high pressure was more observable for with II and III formulations.

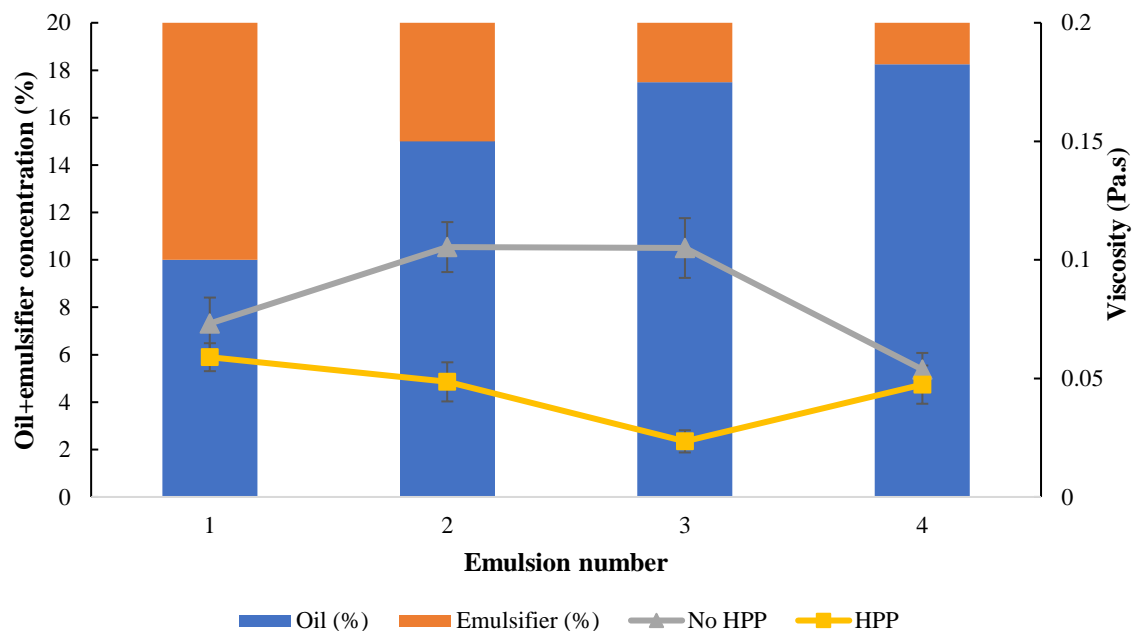


Fig. 8.1. Effect of HPP (100 MPa for 20 min) on apparent viscosity of different emulsions.

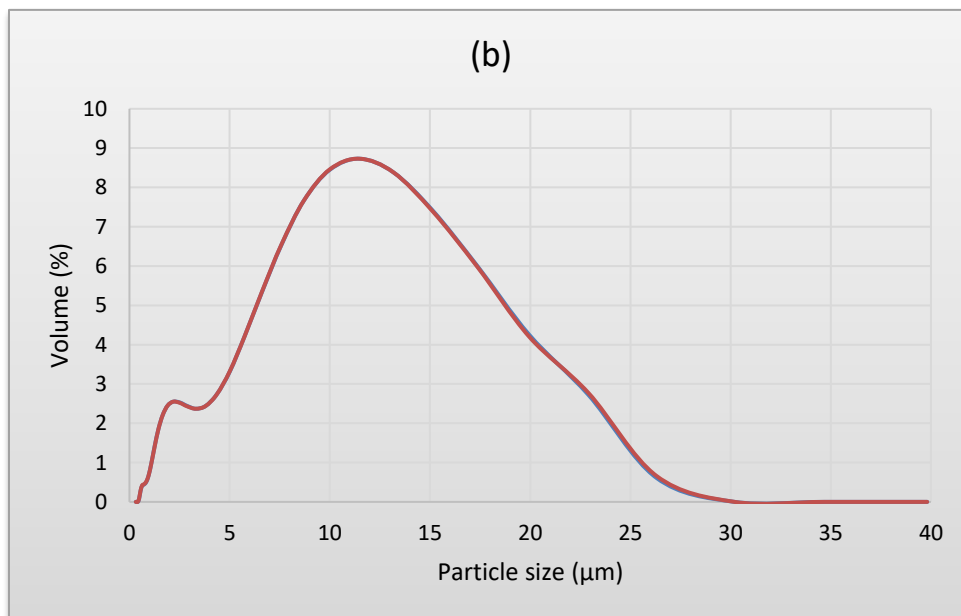
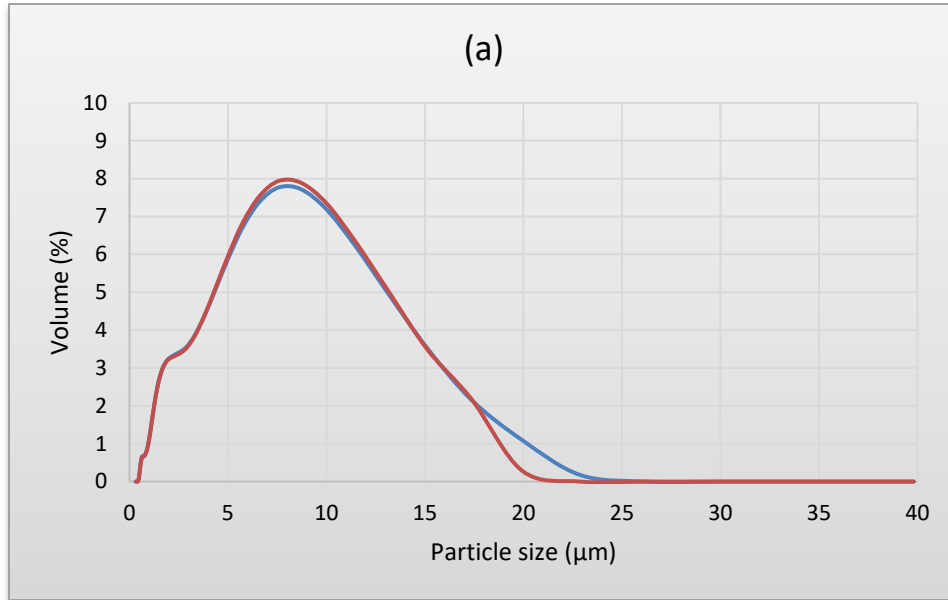
It was observed that after HPP, pH of all samples showed a slight decrease. According to Table 8.1, the initial pH of the samples ranged 5.31 to 5.21. The initial pH value decreased at higher proportions of oil. This was likely due to introduction of higher concentration of free fatty acids (Juan et al., 2007).

The $d_{0.9}$ value represents the size of particle below which 90% of the sample lies (Covis et al., 2014). Initially, the $d_{0.9}$ value ranged 12.04 μm to 19.24 μm . With a decrease in the emulsifier proportion, the size of the particles increased. The same order was observed in the HP treated samples. However, HPP slightly decreased the $d_{0.9}$ values for sample III and VI. The most noticeable change occurred after HP treatment of sample I in which the emulsion percentage was at the highest level. At this level, the HPI process led to increasing the particle size from 12.04 to 14.20 (μm).

Table 8.1 Effect of high pressure on pH and particle mean diameter (μm) of selected emulsions.

sample	pH no-HP	pH HPP	d_{0.9} (μm) no-HP	d_{0.9} (μm) HPP
Emulsion I	5.31 \pm 0.02	5.29 \pm 0.01	12.04 \pm 0.10	14.20 \pm 0.32
Emulsion II	5.27 \pm 0.02	5.15 \pm 0.03	16.36 \pm 0.14	16.37 \pm 0.19
Emulsion III	5.21 \pm 0.01	5.18 \pm 0.02	18.67 \pm 0.21	18.58 \pm 0.38
Emulsion IV	5.21 \pm 0.02	5.2 \pm 0.02	19.24 \pm 0.26	19.21 \pm 0.20

The particle size distribution of the samples is shown in Fig. 8.2. As the emulsion concentration level increased, the particle size decreased, although the distribution pattern remained the same at all levels. The HP treatment did not result in a major influence on the particle size or overall patterns. This was in agreement with Dumay et al. (1996) who reported no effect of HPP on particle size distribution of model O/W emulsions.



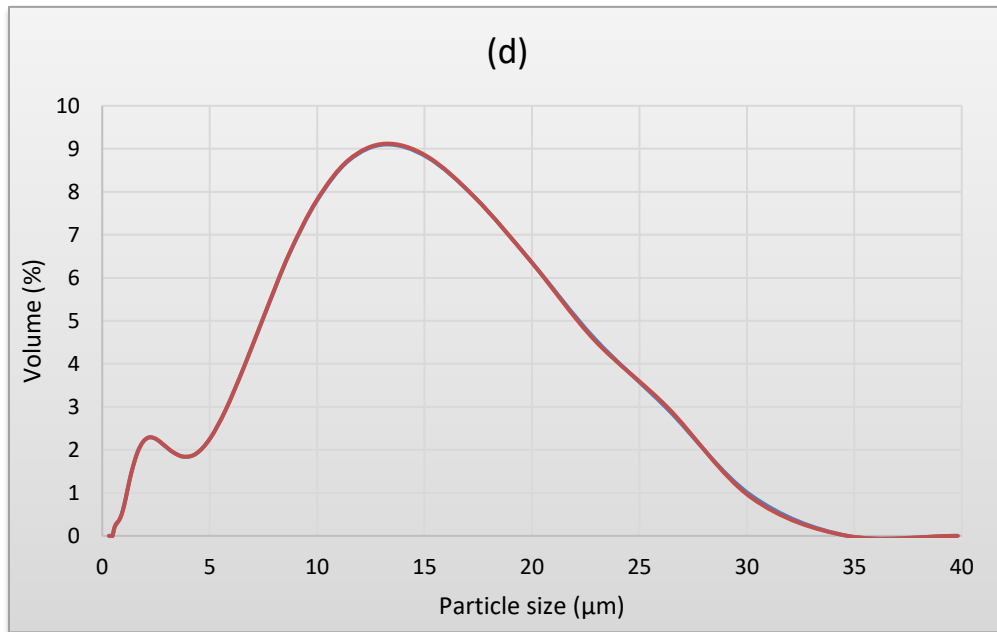
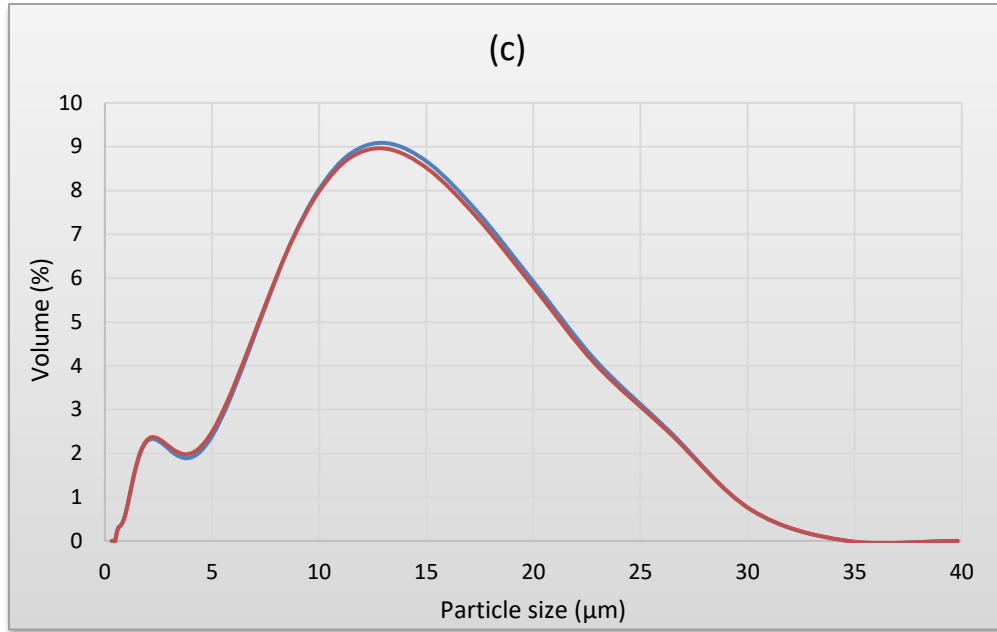
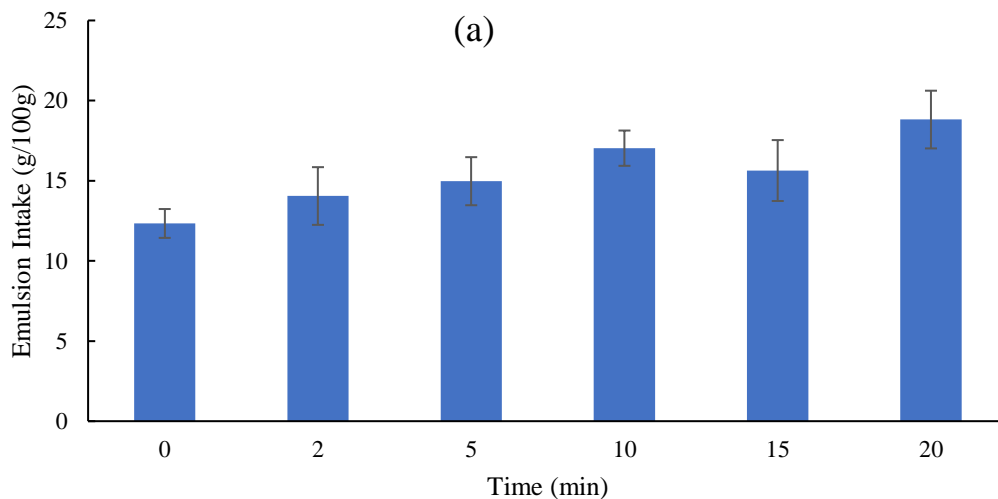
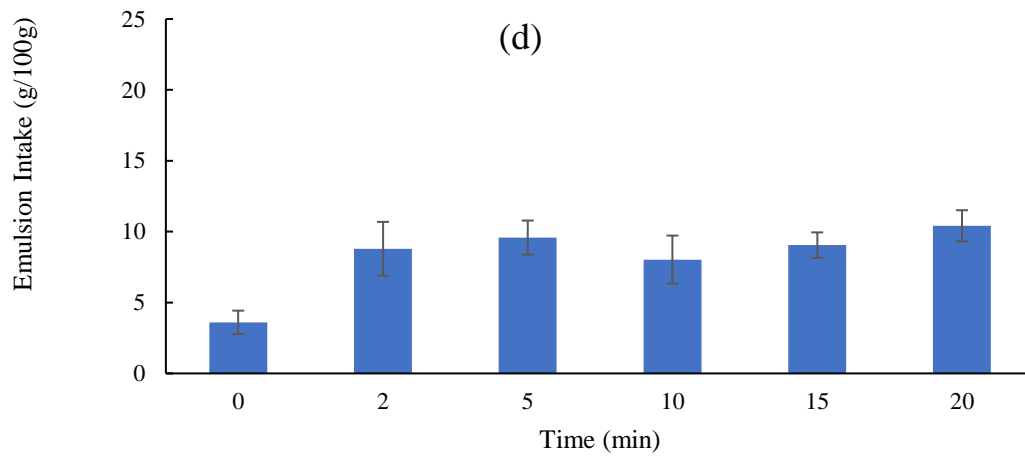
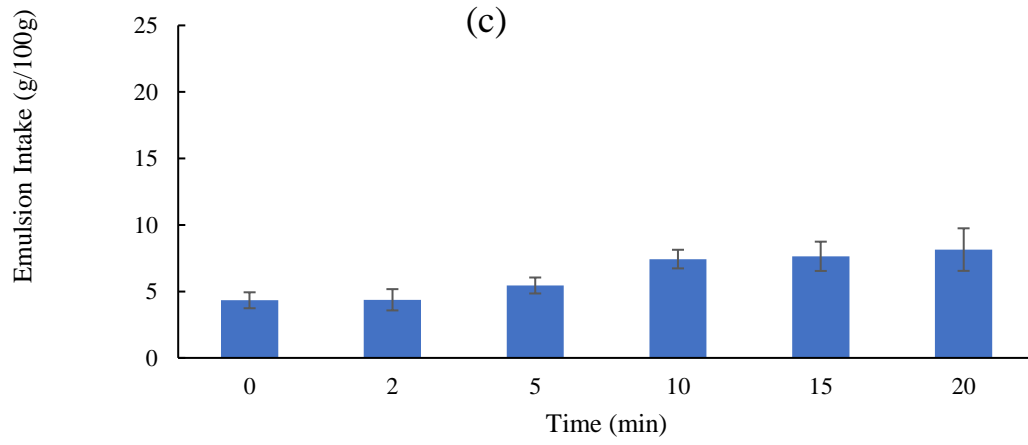
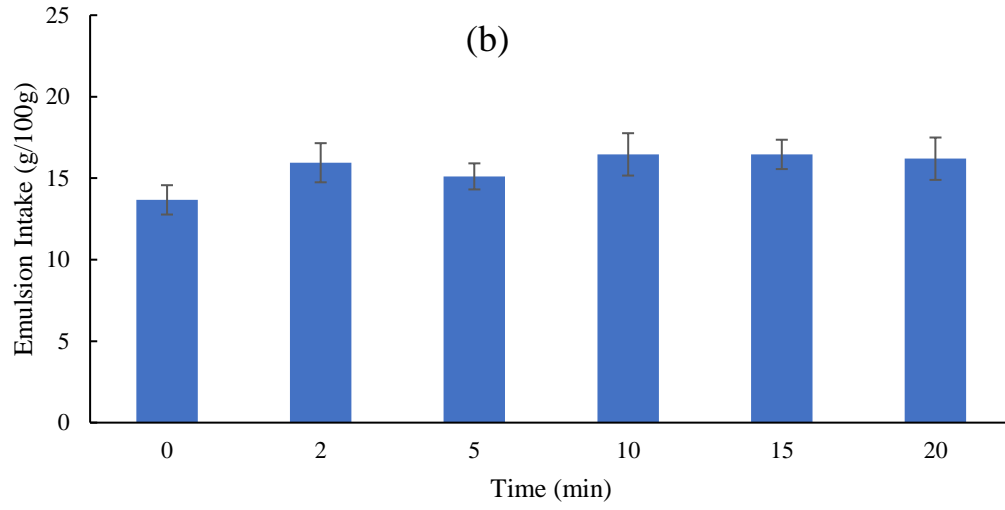


Fig. 8.2. Effect of high pressure (100 MPa, 20 min) on particle size distribution. The blue and red graphs are related to pressurized and unpressurized samples. The letters belong to (a) emulsion I, (b) emulsion II, (c) emulsion III, (d) emulsion IV.

8.4.2 Mass Intake data

Figure 8.3 shows the mass intake data for the tested fruits. In general, apple and pear showed higher mass intake than the other samples. Mass intake data for all samples showed an asymptotical trend towards a maximum limit. In theory, this limit is deemed as the total void space in the tissue. This total void space is also known as the total porosity. However, during impregnation, the fluid flow takes place only in certain open paths. As a result, there are some closed pores and unavailable void space. That is the reason the term “effective or apparent porosity” is used. In other words, the effective porosity is the maximum void space which is available for a certain phenomenon such as HPI. This case was though not verifiable regarding the strawberry samples. Because as mentioned before, the strawberries were not cut, thus, there was a structural barrier towards the flow. This factor did not let all the flow paths to be exposed to the samples. Nevertheless, in terms of industrial applications, the strawberries are commonly used in the whole form.





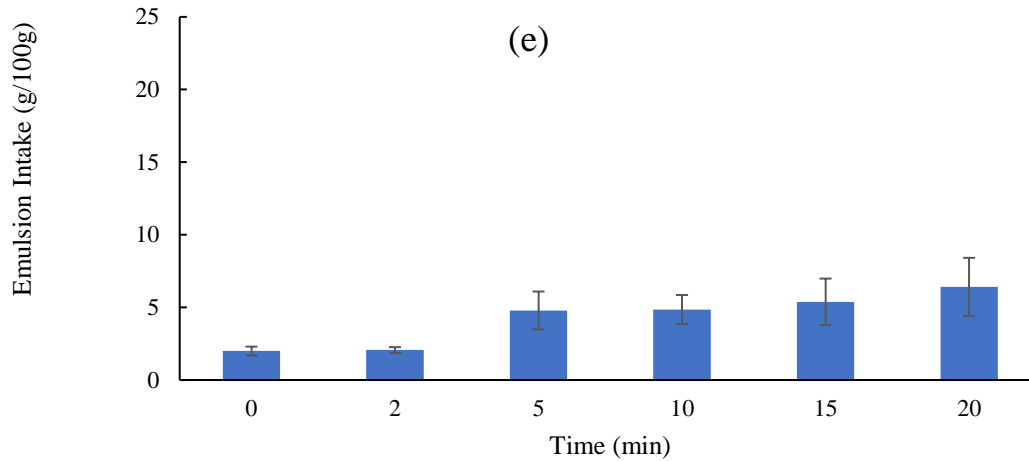


Fig. 8.3. Impregnation of emulsion I into apple (a), pear (b), Asian pear (c), melon (d), and strawberry (e). The HPI was done in different holding times including 0, 2, 5, 10, 15, and 20 min at 100 MPa.

8.4.3 Mass intake modeling

There are two main characteristic factors related to the fruit structure which affect the kinetics of migration of the fluids in to its matrix. The first one is the maximum void space that can be filled. This parameter is a representative of both structural changes under the pressure and the porosity characteristics such as pore connectivity and the tortuosity parameter. These can be deemed as the effective porosity. This parameter is based on the maximum level of intake during the asymptotical trend of impregnation. On the other hand, the second main factor is the pressure-time based kinetic parameter of filling the pores. This is a representative of the pace of impregnation of the fluid inside the tissue. In order to count both variables, a kinetics model should be presented with two main constraints which can describe such situations. The pseudo-second order kinetics models were used to estimate the M_e and the D parameters for each fruit (Eq. 8.2). This model is recognized as one of the important models in studying adsorption phenomena (Onyango et al., 2010).

$$\frac{t}{M_t} = \frac{1}{DM_e^2} + \frac{1}{M_e}t \quad (8.2)$$

where M_e (kg kg⁻¹), t (min), D (kg kg⁻¹ min⁻¹), and M_t (kg kg⁻¹) represent equilibrium moisture content, time, the pseudo-second order rate constant, and mass intake, respectively.

Table 8.2 Estimated HPI mass transfer parameters based on a pseudo-second order model (Eq. 8.2) of impregnation of Emulsion I into selected fruits during 0 to 20 min pressure holding at 100 MPa.

	M_e (kg kg ⁻¹)	D (kg kg ⁻¹ min ⁻¹)	R^2
Apple	0.18 ± 0.02	9.61 ± 0.47	0.98
Pear	0.17 ± 0.02	17.16 ± 0.83	0.99
Asian pear	0.08 ± 0.01	8.04 ± 0.22	0.99
Melon	0.10 ± 0.00	17.58 ± 0.75	0.98
Strawberry	0.07 ± 0.02	6.17 ± 0.10	0.95

Table 8.2 shows the estimated parameters for each fruit. The highest M_e was seen in apple which was 0.18. The highest rate constant was associated with pear and melon. Although, comparing these two fruits, due to the considerably lower M_e in melon, it provides less void space for impregnation targets.

8.4.4 Effect of emulsifier level

According to the mass intake data, the impregnation efficiency was higher at lower levels of the emulsifier (Fig. 8.4). The results indicated the dynamics of migration is in a direct relationship with the density of the fluids. In addition, the higher yield at higher percentage

of oil content was in direct relationship with the measured viscosity data in which the highest viscosity was seen with the highest level of emulsifier. In strawberry fruits, the mass intake showed less dependence on the combination of oil/emulsifier. This was logical regarding the fact that the structural resistance of whole fruit was the main barrier in the mass intake within the tissue.

From fluid dynamics point of view, such flows can be studied in two different aspects. Microscopically, the fluid flow represents a two-phase flow in the channels, known as pores. The effect of a dispersed phase in the flow is characterized based on an empirical value known as the mobility reduction or scale factor (f). This factor represents the ratio of the microfluid flow of the continuous phase and the emulsion. The f factor is a representative of the flow resistance based on the interactions between the droplet size and the channel radius. Obviously, when the radius of the droplets is bigger than the channel size, a pressure drop happens as a result of the pore blockage issue. However, when the droplet size is much lower, such resistance is negligible. As discussed in section 3.1, in all cases, the mean droplet size was less than 20 μm . This is less than the typical intercellular space of plant tissues such as apple, which is reported to be between $269.0 \pm 93.0 \mu\text{m}$ (width) and $487.8 \pm 154.0 \mu\text{m}$ (length) (Mohsenin 1986). Thus, in such cases the f parameter is equal to 1.

However, the effect of a dispersed phase in dynamic flow within a macroscopic porous domain is known as the macroscopic mobility reduction factor F . This parameter is derived from the Darcian flow definition. To elaborate, dividing the Darcy's equation (Eq. 8.3) only for the continuous phase flow by the one for the flow of the emulsion, one can get the F value (Eq. 8.4).

$$\Delta p = \frac{\mu Q L}{K A} \quad (8.3)$$

$$F = \frac{\Delta p_c}{\Delta p_e} = \frac{\mu_c Q_c}{\mu_e Q_e} = \frac{\mu_c M_c}{\mu_e M_e} \quad (8.4)$$

where K , p , Q , A , L and μ are permeability of the porous medium, pressure (Pa) and dynamic viscosity (Pa s), mass flow rate ($\text{m}^3 \text{s}^{-1}$), area (m^2), and length (m). As can be seen, the F is a dimensionless value which can reflect the efficiency of the impregnation. Within

the constant L, A, and K, as the structural characteristics of the porous media, the calculated F ranged 1 % to 4 % in all samples and emulsions. This issue indicated the high dominance of the imposed pressure on the viscose forces.

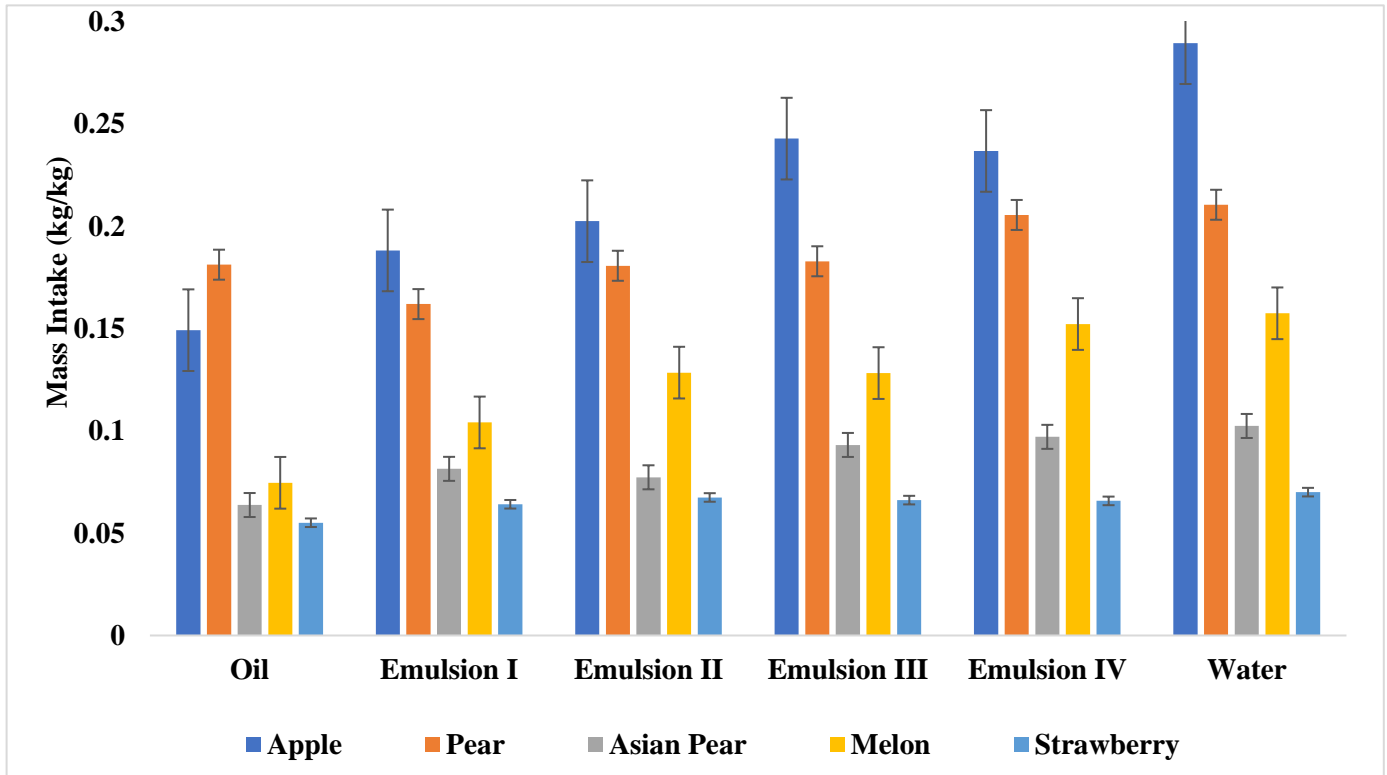


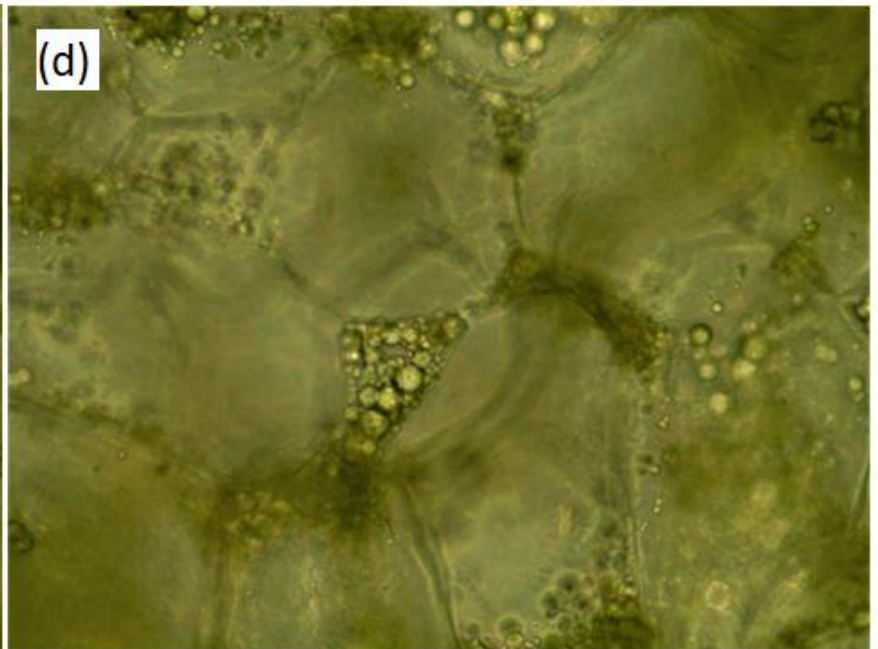
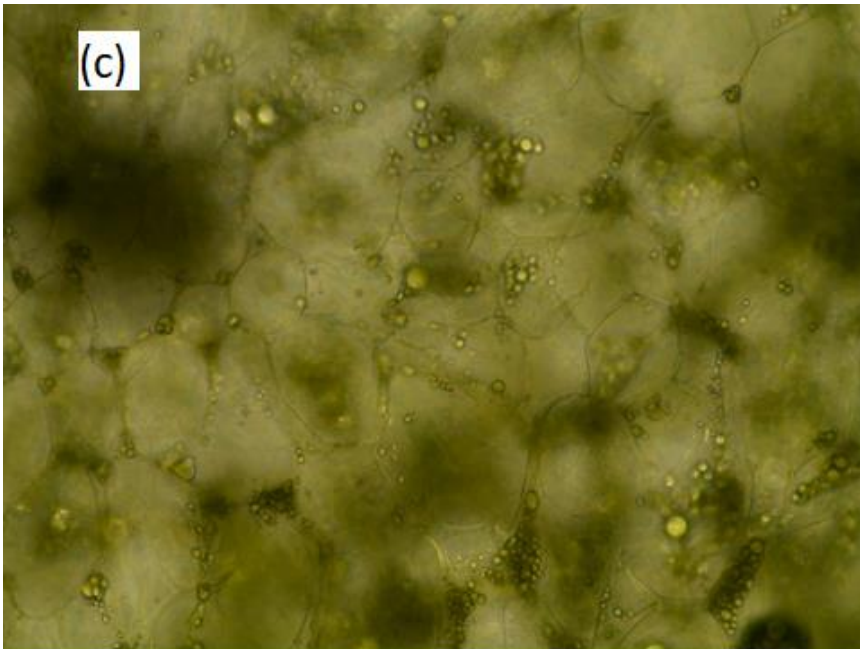
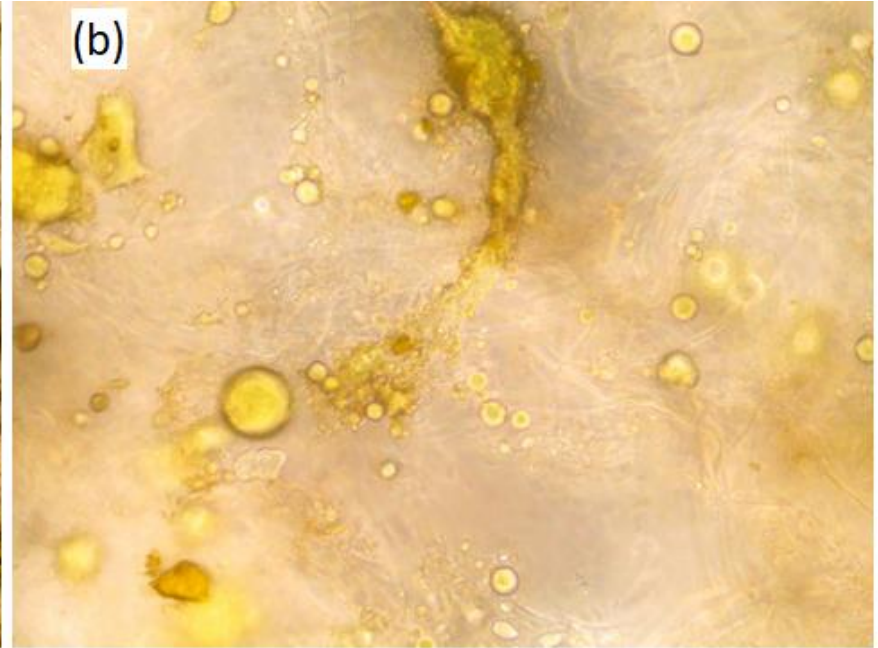
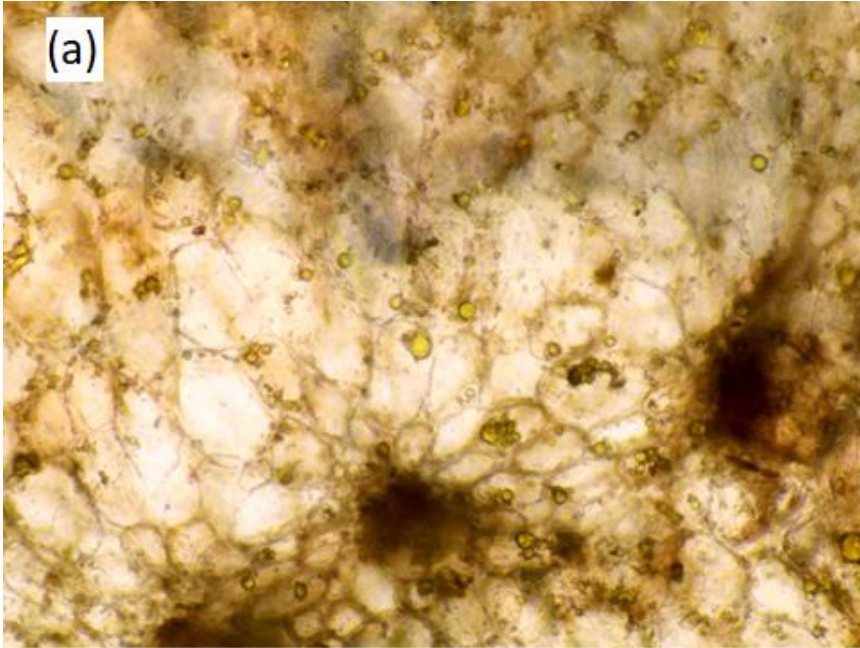
Fig. 8.4. Effect different of levels of oil/emulsifier(s), water, and pure oil after HPI (100MPa, 20min) on mass intake percentage into selected fruits.

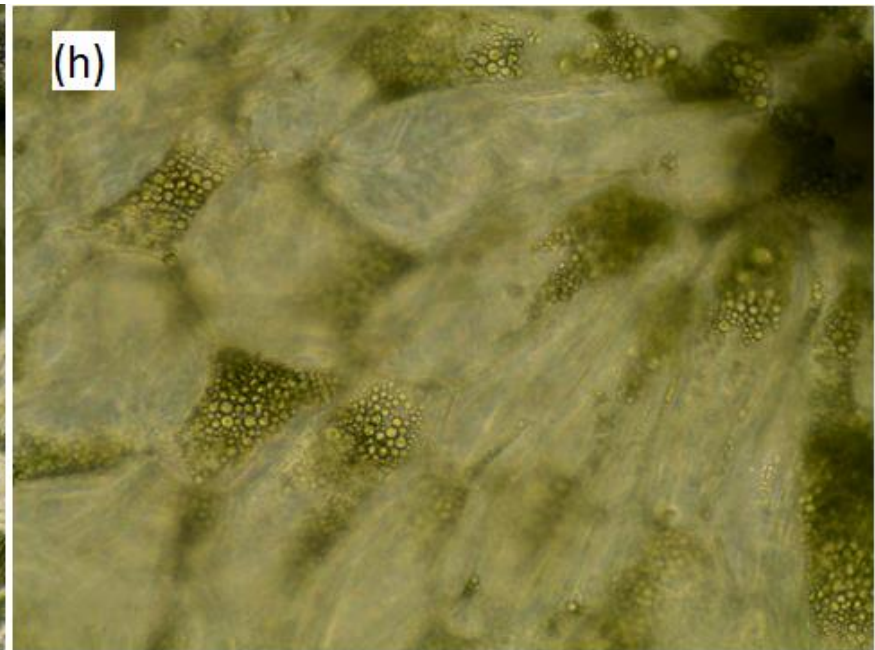
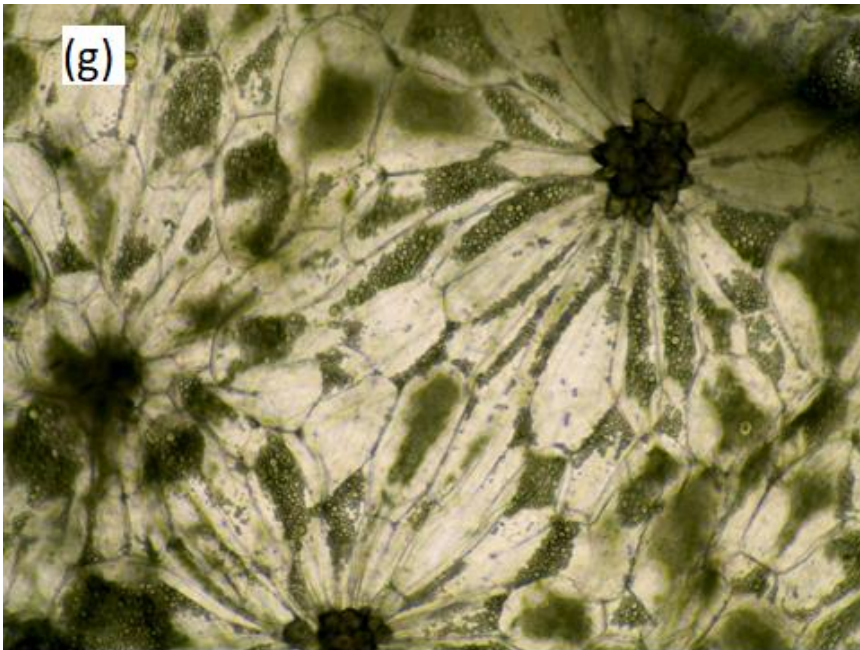
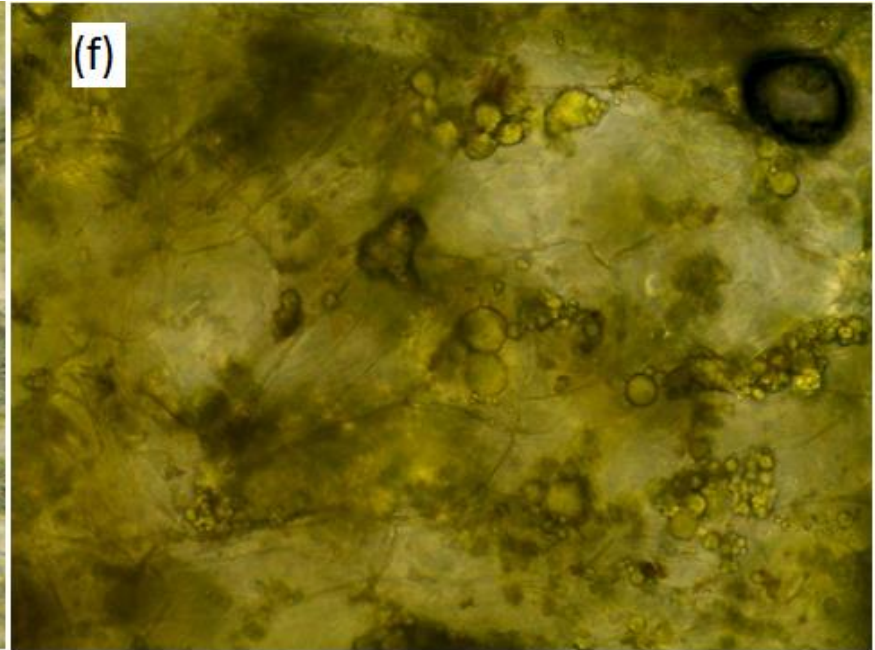
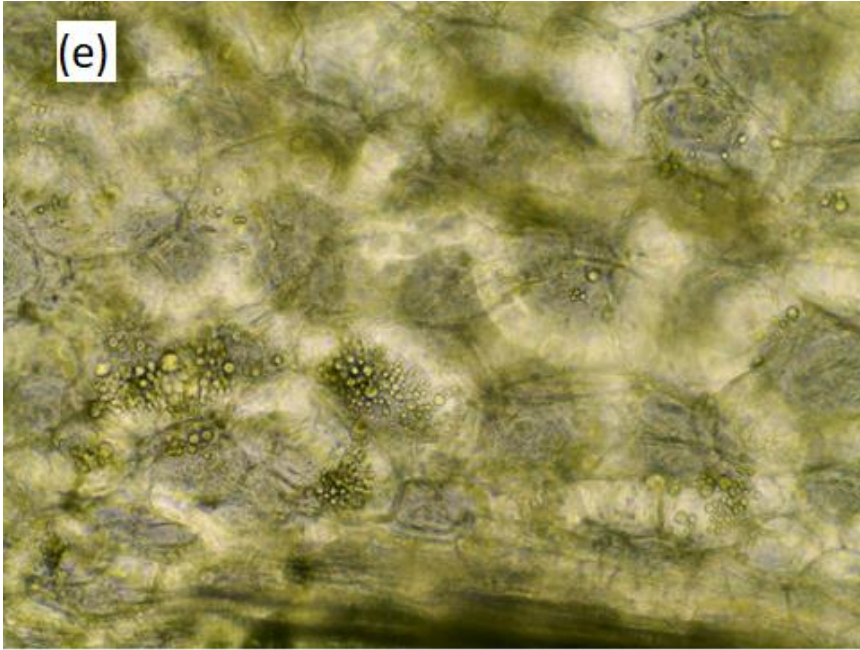
8.4.5 *Microstructure studies*

Figure 8.5 shows the cellular structure of the HP treated fruits. The endurance of cellular tissue is observable. In addition, the cellular integrity and the porosity as the intercellular space is visible. Vatankhah and Ramaswamy (2017) observed that the apple tissue had an acceptable level of cellular endurance after impregnation. This resistance was due to removing the gaseous phase and, subsequently, filling the void space with incompressible fluids.

As shown, the flow current within the interconnected paths facilitated the storage of the oil droplets in the larger pores. Due to the efficient migration of both water and oil phases, a continuous biphasic fluid flow is evident. In general, larger droplets were more visible in the larger pores, which could indicate a lower mass transfer ability as a matter of larger droplet diameter. Although, the main point was the coalescence of the small droplets in such spaces. The high number of droplets, as well as their tendency to accumulate in the pores, helped the coalescence phenomenon.

It has been reported that depending on the nature of the texture and pressure level, the permeability of the cell walls could be affected (Prestamo & Arroyo 1998). This issue would cause diffusion of the free water into the cells. In addition to this phenomenon, infusion of emulsions would have one more consequence. The high water content of the cell walls (>65%) would act as a barrier to impregnation of fat droplets (Cosgrove 2000; Thompson 2005). Thus, as can be seen in the micrographs, a more rapid coalescence of the fat droplets would happen within the intercellular space. It could also be hypothesized that, diffusion of water would lead to higher turgidity in cells and help in existence of more blind pores. These blind pores would obviously help the tissue to maintain a higher fat holding capacity during the storage.





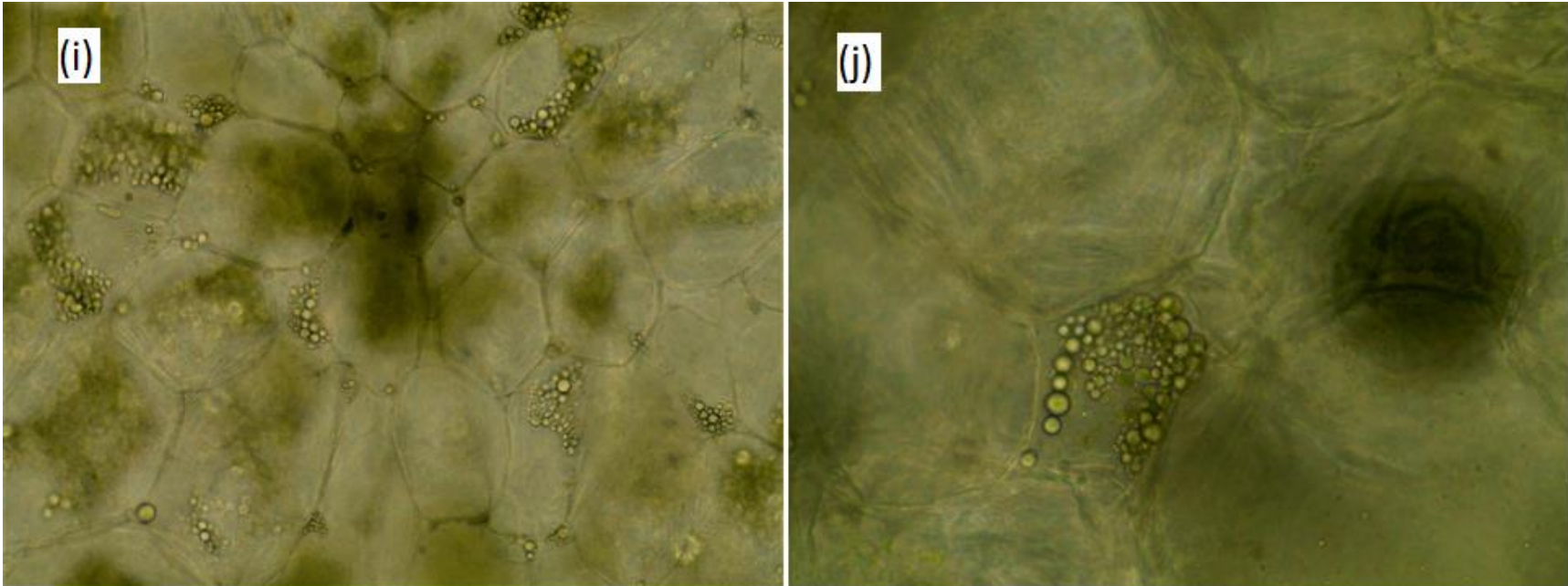
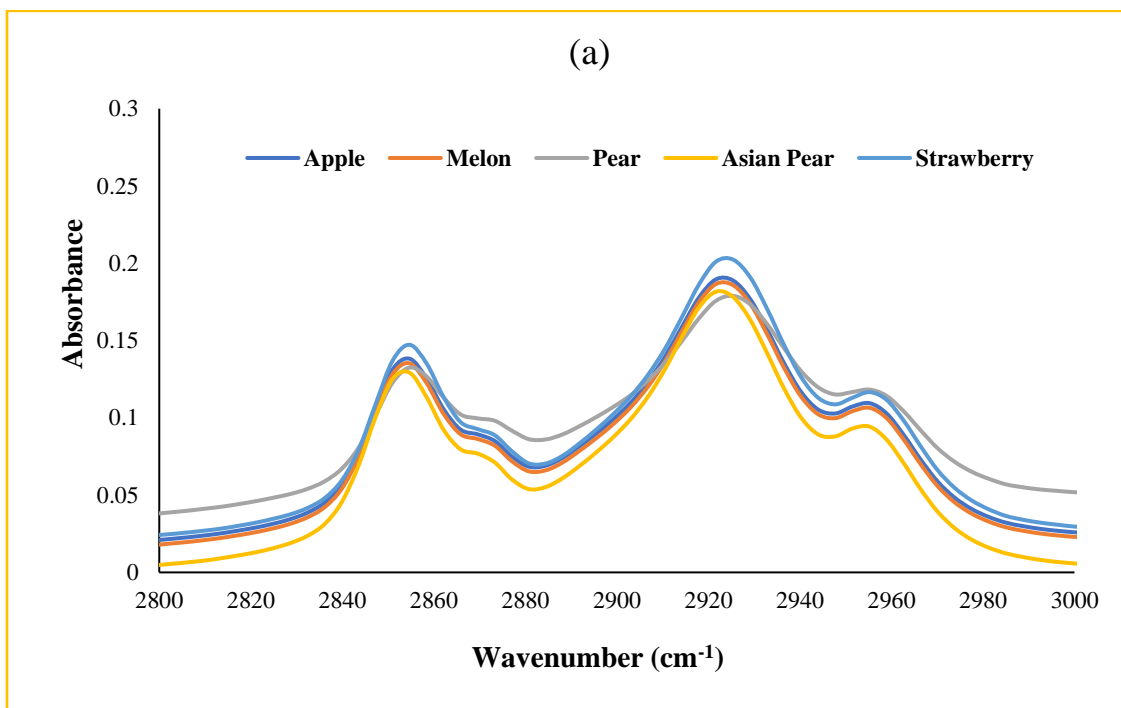


Fig. 8.5. The microstructural demonstration of cellular tissue of impregnation of emulsion i into selected fruits for 20 min at 100 mpa. The images belong to strawberry (a,b), pear (c,d), melon (e,f), asian pear (g,h), and apple (i,j). The right and left side images are taken at 80x and 40x magnification.

8.4.6 Spectrophotometric evaluation of HPI

The spectrum of the fruits with respect to same operation conditions is expected to show same combination of oil and emulsifier in the ethanol extract. According to Fig. 8.6a, two characteristic peaks were observed at 2921 and 2855 which represented the asymmetric and symmetric -CH₂- vibrations. This was in agreement with Tarhan et al. (2017).

As shown in Fig. 8.6b, to identify the emulsifier phase, a characteristic peak was observed at 1110 regarding the -CO-O-CH₂- groups (Liu et al., 2015). These spectra show equal heights at the mentioned peaks. This point was an indication of infusion of oil and emulsifier in a similar and homogenous combination regardless to the type and texture of the fruits.



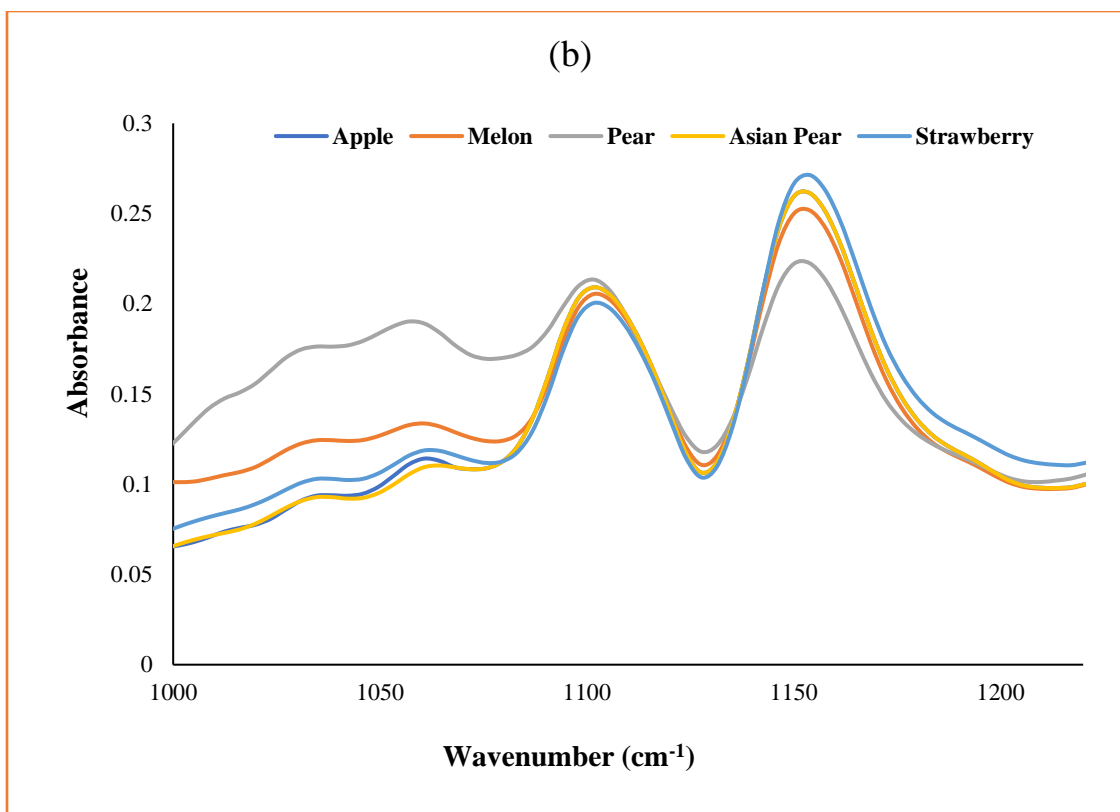


Fig. 8.6. FTIR spectra of selected fruits after impregnation of emulsion IV into for 20 min at 100 MPa.

8.5 Conclusion

HPP was effective in impregnation if considerable amounts of oil-based emulsions in to fruit tissue. Despite the high proportion of oil phase in some emulsion groups, the hydrophilic nature of resistance of the tissue could be neglected since ultra-high hydrostatic forces were involved during HPI.

Using the emulsions as carriers for oil soluble compounds would be a promising method for nutritional fortifications. Specifically, these days there is no easy way to enrich vegetable/fruit tissues with vitamin D, K, E and A. Thus, using HPI concept, a promising technique could be developed toward the enrichment of such porous tissues. Although, more research should be done regarding the analytical measurement of hydrophobic micronutrients, the study provides a proof of concept for the impregnation of oil-based fluid medium in to a porous solid food matrix.

CHAPTER 9

GENERAL CONCLUSIONS, CONTRIBUTION TO THE KNOWLEDGE AND RECOMMENDATIONS

9.1 General conclusions

The new generation of food processing techniques is known as non-thermal methods. In this regard, high pressure processing is going to play a key role. Considering this issue in our research objective, it was tried to participate in obtaining a deeper knowledge about the phenomena involved while pressurization such as characterizing the fluid migration into the fruits and vegetable tissues under pressure. The research introduced one of the new aspects of high pressure processing as well. To describe, the high pressure impregnation was discussed as an intentional enrichment technology in which any desirable compound -in a solute/solution form- can be impregnated into a porous biomaterial medium. A number of general conclusions from this research could be summerized as:

1- The term “High-pressure impregnation (HPI)” was introduced as a novel processing technique in which numerous functional properties on the porous tissue could be changed intentionally.

2- The mass transfer during HPI was investigated, and one of the handiest mass transfer models in food engineering studies was fully adopted to model the mentioned transport phenomenon. Both analytical and numerical solutions were conducted and validated by novel techniques such as dye infusion image processing.

3- A comprehensive study of fluid migration onto porous biomaterial was conducted. In this term, the asymptotical behavior of mass intake was characterized and two mass transfer models including Fick’s second law and pseudo-second order kinetics were developed for process control designs.

4-The mass intake yield was monitored and modeled as a result of a wide time-pressure combination including 100 to 600 MPa and 0 to 30 min of holding time. In addition to

merely focusing on the holding time as the main processing stages, the effect of pressurization rate was studied as a function of pressurization rate, pressure come-up time, and final pressure level.

5- In addition to theoretical modeling of the process, it was tried to present useful and simplified zero-order kinetics models for industrial uses. These models showed high capabilities in an approximation of mass intake as a function of pressure holding time.

6- The textural deterioration effects due to pressurization rate was modeled and studied. The model constants could give useful insight about the desired pressurization rate in order to yield a higher mass transfer.

7- The microstructural studies of the impregnated samples were done using different techniques of microscopy. The obtained images were used to demonstrate the flow progression trend within the tissue. In addition, the SEM and light microscopy images verified endurance of the porous network after the impregnation.

8- Impregnation of porous textures using dying agents were done for the first time to model the flow front progression. In this regard, a time-dependent flow front function was obtained, and the results helped in better understanding of permittivity function during the processing time.

9- As the most important physical properties of the impregnant phase, the effect of viscosity of the impregnant agent on the HPI mass intake was studied at different levels of hydrocolloid gum concentrations.

10- Regarding introductions of technical applications of HPI, in chapter 7, the physical properties of chitosan-impregnated apples were evaluated before and after freezing. The results revealed interesting data regarding the optimal concentration of chitosan in order to improve the quality of the frozen products after thawing.

11- The effect of emulsion/emulsifier combinations on the final mass intake of HPI of emulsions was investigated. The results showed that the mass intake was inversely proportional to the viscosity of the emulsions. In addition, the preliminary results about

emulsion stability under high pressure showed no considerable change in terms of their particle size distribution.

9.2 Contribution to knowledge

1- Using any model, especially a theoretical model, needs a deep knowledge and a high ability of parameter definition and certain computational modifications. In this regard, the needed parameters for an analytical solution to Fick's second law was identified. The methods of obtaining these model parameters were also introduced and presented in analogy to drying kinetics modeling. In this regard, certain approximations, and assumptions were discussed; and as the final stage, the diffusivity value estimation was conducted using two well-known inverse parameter approximation algorithms.

2- The proposed empirical models were not only able to approximate the processing yield but also, the obtained model constants could be deemed as a novel technique for estimation of the effective porosity value as a function of operating pressure level.

3- A novel computational procedure was proposed to couple the Fick's and Darcy's law which is known as the most important partial differential equations in studying mass transport phenomena in porous media. The mentioned coupling method was also summarized in the form of process diagram. It is strongly believed that this method would be useful in numerous engineering aspects dealing with "flow in confined porous media".

4- Novel rheological methodologies were introduced to study the effect of pressure on selected hydrocolloid systems as the impregnant phase. In this regard, a shift phase parameter was introduced as a means of evaluation of Thermoviscoelastic patterns of the pressurized solutions.

5- For the first time, a novel method of enrichment of high moisture porous biomaterials was introduced as one of the applications of HPI. The mentioned technique could be a promising method for the fortification of such product by fat-soluble compounds in the form of emulsions.

6- As one of the novel aspects of utilization of HPI, the impregnation of hydrocolloid solutions was introduced and fully evaluated as an efficient way to decrease the drip loss and textural damage in frozen fresh-cut products.

9.3 Recommendations for future research

- 1- HPI of salt solution into vegetable tissue in order to increase the heat transfer properties as a pre-treatment for ohmic heating.
- 2- HPI of sugar solutions for improvement of product yield and decrease in water activity content for drying purposes.
- 3- Studying the effect of temperature on the evaluation of mass transfer during HPI.
- 4- Analytical analysis of fortification of selected fruit using emulsions which contain fat-soluble vitamins such as E, K, D, and A.
- 5- Quality evaluations and shelf life measurements of HPI of antimicrobial agents into biomaterials. The study could also be done regarding estimation of the assistance of HPI on the microbial destruction aspects of HPP.
- 6- Food safety assessment of microbial load of impregnant agent. To describe, more actions could be done in order to evaluate the possible critical points of impregnation of non-sterile impregnant. The results could describe whether any microbial contamination takes place during such processing techniques.

References

- Adam, H., Jouannic, S., Escoute, J., Duval, Y., Verdeil, J. L., & Tregear, J. W. (2005). Reproductive developmental complexity in the African oil palm (*Elaeis guineensis*, Arecaceae). *American Journal of Botany*, 92(11), 1836-1852.
- Ahmed, J., & Ramaswamy, H. S. (2006). Viscoelastic properties of sweet potato puree infant food. *Journal of Food Engineering*, 74(3), 376-382.
- Ahmed, J., & Ramaswamy, H.S. (2003). Effect of high-hydrostatic pressure and temperature on rheological characteristics of glycomacropeptide. *Journal of Dairy Science*, 86(5), 1535-1540.
- Ahmed, J., & Ramaswamy, H.S. (2004). Effect of high-hydrostatic pressure and concentration on rheological characteristics of xanthan gum. *Food Hydrocolloids*, 18(3), 367-373.
- Ahmed, J., Ramaswamy, H. S., Alli, I., & Ngadi, M. (2003). Effect of high pressure on rheological characteristics of liquid egg. *LWT-Food Science and Technology*, 36(5), 517-524.
- Ahmed, J., Ramaswamy, H.S., Ayad, A., Alli, I., & Alvarez, P. (2007). Effect of high-pressure treatment on rheological, thermal and structural changes in Basmati rice flour slurry. *Journal of Cereal Science*, 46(2), 148-156.
- Ahmed, J., Singh, A., Ramaswamy, H.S., Pandey P.K., & Raghavan, G.S.V., (2014). Effect of high-pressure on calorimetric, rheological and dielectric properties of selected starch dispersions. *Carbohydrate Polymers*, 103, 12-21.
- Ahmed, J., Varshney, S.K., & Ramaswamy, H. S. (2009). Effect of high pressure treatment on thermal and rheological properties of lentil flour slurry. *LWT-Food Science and Technology*, 42(9), 1538-1544.
- Akbarzadeh, A. H., & Chen, Z. T. (2012). Transient heat conduction in a functionally graded cylindrical panel based on the dual phase lag theory. *International Journal of Thermophysics*, 33(6), 1100-1125.
- Akbarzadeh, A. H., & Chen, Z. T. (2013). Heat conduction in one-dimensional functionally graded media based on the dual-phase-lag theory. Proceedings of the

- Institution of Mechanical Engineers, *Part C: Journal of Mechanical Engineering Science*, 227(4), 744-759.
- Akbarzadeh, A. H., & Chen, Z. T. (2014). Dual phase lag heat conduction in functionally graded hollow spheres. *International Journal of Applied Mechanics*, 6(01), 1450002.
 - Akbarzadeh, A. H., & Pasini, D. (2014). Phase-Lag Heat Conduction in Multilayered Cellular Media with Imperfect Bonds. *International Journal of Heat and Mass Transfer*, 75, 656-667.
 - Albahrani, A. A., & Greaves, R. F. (2016). Fat-soluble vitamins: clinical Indications and current challenges for chromatographic measurement. *The Clinical Biochemist Reviews*, 37(1), 27.
 - Allali, H., Marchal, L., & Vorobiev, E. (2010). Effects of vacuum impregnation and ohmic heating with citric acid on the behaviour of osmotic dehydration and structural changes of apple fruit. *Biosystems Engineering*, 106(1), 6-13.
 - Alvarez, P.A., Ramaswamy, H.S., & Ismail, A.A. (2008). High pressure gelation of soy proteins: effect of concentration, pH and additives. *Journal of Food Engineering*, 88(3), 331-340.
 - Aymerich, T., Picouet, P. A., & Monfort, J. M. (2008). Decontamination technologies for meat products. *Meat Science*, 78(1), 114-129.
 - Balasubramaniam, V. M., Barbosa-Cánovas, G. V., & Lelieveld, H. L. (Eds.). (2016). *High Pressure Processing of Food: Principles, Technology and Applications*. New York (NY): Springer.
 - Balasubramaniam, V. M., Farkas, D., & Turek, E. J. (2008). Preserving foods through high-pressure processing. *Food technology*.
 - Barba, F.J., Terefe, N.S., Buckow, R., Knorr, D., & Orlien, V., 2015. New opportunities and perspectives of high pressure treatment to improve health and safety attributes of foods. A review. *Food Research International*, 77,725-742.
 - Barbosa-Cánovas, G. V., Ortega-Rivas, E., Juliano, P., & Yan, H. (2005). Mixing. In *Food Powders: Physical Properties, Processing, and Functionality*. (pp. 221-246). New York (NY): Springer.

- Barrett, D. M., Beaulieu, J. C., & Shewfelt, R. (2010). Color, flavor, texture, and nutritional quality of fresh-cut fruits and vegetables: desirable levels, instrumental and sensory measurement, and the effects of processing. *Critical reviews in food science and nutrition*, 50(5), 369-389.
- Basak, S., Ramaswamy H. S., & Piette, J., P., G. (2002). High pressure destruction kinetics of *Leuconostoc mesenteroides* and *Saccharomyces cerevisiae* in single strength and concentrated orange juice. *Innovative Food Science & Emerging Technologies*, 3(3): 223-231.
- Bear, J. (1979). *Hydraulics of Groundwater*. New York (NY): McGraw-Hill International Book.
- Berger, D., & Pei, D. C. T. (1973). Drying of hygroscopic capillary porous solids—a theoretical approach. *International Journal of Heat and Mass Transfer*, 16(2), 293-302.
- Betoret, E., Sentandreu, E., Betoret, N., Codoñer-Franch, P., Valls-Bellés, V., & Fito, P. (2012). Technological development and functional properties of an apple snack rich in flavonoid from mandarin juice. *Innovative Food Science & Emerging Technologies*, 16, 298-304.
- Bignon, J. (1996). Cold pasteurizers Hyperbar for the stabilization of fresh fruit juices. *Fruit processing*, 6, 46-49.
- Bilbao-Sáinz, C., Andrés, A., & Fito, P. (2005). Hydration kinetics of dried apple as affected by drying conditions. *Journal of Food Engineering*, 68(3), 369-376.
- Binks, B.P. (ed.), (1998). *Modern Aspects of Emulsion Science*, London (UK): The Royal Society of Chemistry Publication.
- Boukouvalas, C. J., Krokida, M. K., Maroulis, Z. B., & Marinou-Kouris, D. (2006). Density and porosity: Literature data compilation for foodstuffs. *International Journal of Food Properties*, 9(4), 715-746.
- Bréard, J., Henzel, Y., Trochu, F., & Gauvin, R. (2003). Analysis of dynamic flows through porous media. Part I: Comparison between saturated and unsaturated flows in fibrous reinforcements. *Polymer Composites*, 24(3), 391-408.
- Bruce, D. M. (1985). Exposed-layer barley drying: three models fitted to new data up to 150 C. *Journal of Agricultural Engineering Research*, 32(4), 337-348.

- Buckow, R., Weiss, U., & Knorr, D. (2009). Inactivation kinetics of apple polyphenol oxidase in different pressure–temperature domains. *Innovative Food Science & Emerging Technologies*, 10(4), 441-448.
- Bundy, F. P. (1961). Effect of pressure on emf of thermocouples. *Journal of Applied Physics*, 32(3), 483-488.
- Calbo, A., G., & Sommer, N., F. (1987). Intercellular volume and resistance to air flow of fruits and vegetables. *Journal of the American Society for Horticultural Science*, 112, 131–134.
- Cano, M. P., & De Ancos, B. (2005). *Advances in use of high pressure to processing and preservation of plant foods* (pp. 283-310). New York (NY): CRC Press.
- Carman, P. C. (1937). *Fluid flow through granular beds* (Vol. 15 pp. 150-166). London (UK): Transactions-Institution of Chemical Engineers.
- Castagnini, J.M., Betoret, N., Betoret, E., & Fito, P. (2015). Vacuum impregnation and air drying temperature effect on individual anthocyanins and antiradical capacity of blueberry juice included into an apple matrix. *LWT-Food Science and Technology*. 64(2), 1289-1296.
- Chen, L., Xie, Z. G., Zhuang, X. L., Chen, X. S., & Jing, X. B. (2008). Controlled release of urea encapsulated by starch-g-poly (L-lactide). *Carbohydrate Polymers*, 72, 342–348.
- Chhabra, R. P., Comiti, J., & Machač, I. (2001). Flow of non-Newtonian fluids in fixed and fluidised beds. *Chemical Engineering Science*, 56(1), 1-27.
- Choi, H. D., Lee, H. C., Kim, Y. S., Choi, I. W., Park, Y. K., & Seog, H. M. (2008). Effect of Osmotic Dehydration and Vacuum Impregnation on the Quality of Dried Apple. *Korean Journal of Food Science and Technology*, 40(2), 178-183.
- Cioni, P. (2006). Role of protein cavities on unfolding volume change and on internal dynamics under pressure. *Biophysical journal*, 91(9), 3390-3396.
- Civan, F. (2011). *Porous Media Transport Phenomena*. (p. 463). New Jersey (NY): John Wiley & Sons.
- Coleman, T. F., & Li, Y. (1996). An interior trust region approach for nonlinear minimization subject to bounds. *SIAM Journal on Optimization*, 6(2), 418-445.

- Colon, G., & Avilés, E. I. (1993). Transport mechanisms in the drying of granular solids. In *AICHE SYMPOSIUM SERIES* (pp. 46-46). American Institute of Chemical Engineers.
- Cosgrove, D. J. (2000). Loosening of plant cell walls by expansions. *Nature*, *407*(6802), 321-326.
- Covis, R., Desbrieres, J., Marie, E., & Durand, A. (2014). Dilational rheology of air/water interfaces covered by nonionic amphiphilic polysaccharides. Correlation with stability of oil-in-water emulsions. *Colloids and Surfaces A: Physicochemical and Engineering Aspects*, *441*, 312-318.
- Crank, J. (1975). *The Mathematics of Diffusion*. (2nd ed.). London (UK): Oxford University Press.
- Crank, J., & Nicolson, P. A. (1947). practical method for numerical evaluation of solutions of partial differential equations of the heat-conduction type. *Mathematical Proceedings of the Cambridge Philosophical Society*, *43*(1), 50-67.
- Da Silva, C. K. F., Da Silva, Z. E., & Mariani, V. C. (2009). Determination of the diffusion coefficient of dry mushrooms using the inverse method. *Journal of Food Engineering*, *95*(1), 1-10.
- Daryaei, H., Yousef, A. E., & Balasubramaniam, V. M. (2016). Microbiological Aspects of High-Pressure Processing of Food: Inactivation of Microbial Vegetative Cells and Spores. In *High Pressure Processing of Food*. (pp. 271-294). New York (NY): Springer.
- De Ancos, B., Gonzalez, E., & Cano, M. P. (2000). Effect of high-pressure treatment on the carotenoid composition and the radical scavenging activity of persimmon fruit purees. *Journal of Agricultural and Food Chemistry*, *48*(8), 3542-3548.
- De Ancos, B., Sgroppo, S., Plaza, L., & Cano, M. P. (2002). Possible nutritional and health-related value promotion in orange juice preserved by high-pressure treatment. *Journal of the Science of Food and Agriculture*, *82*(8), 790-796.
- De Maria, S., Ferrari, G., & Maresca, P. (2015). Rheological characterization and modelling of high pressure processed Bovine Serum Albumin. *Journal of Food Engineering*, *153*, 39-44.

- De Roeck, A., Duvetter, T., Fraeye, I., Van der Plancken, I., Sila, D. N., Van Loey, A., & Hendrickx, M. (2009). Effect of high-pressure/high-temperature processing on chemical pectin conversions in relation to fruit and vegetable texture. *Food Chemistry*, 115(1), 207-213.
- Ding, M., & Kantzas, A. (2004). Capillary number correlations for gas-liquid systems. In Canadian International Petroleum Conference. Petroleum Society of Canada.
- Dong, X., Wrolstad, R. E., & Sugar, D. (2000). Extending Shelf Life of Fresh-cut Pears. *Journal of Food Science*, 65(1), 181-186.
- Dumay, E., Lambert, C., Funtenberger, S., & Cheftel, J. C. (1996). Effects of high pressure on the physico-chemical characteristics of dairy creams and model oil/water emulsions. *LWT-Food Science and Technology*, 29(7), 606-625.
- Duvetter, T., Fraeye, I., Hoang, T. V., Buggenhout, S. V., Verlent, I., Smout, C., ... & Hendrickx, M. (2005). Effect of pectinmethylesterase infusion methods and processing techniques on strawberry firmness. *Journal of food science*, 70(6).
- Duvetter, T., Sila, D. N., Van Buggenhout, S., Jolie, R., Van Loey, A., & Hendrickx, M. (2009). Pectins in processed fruit and vegetables: Part I—Stability and catalytic activity of pectinases. *Comprehensive Reviews in Food Science and Food Safety*, 8(2), 75-85.
- Farkas, D. F., & Hoover, D. G. (2000). High pressure processing. *Journal of Food Science*, 65(s8): 47-64.
- Feng, H. (2000). Microwave drying of particulate foods in a spouted bed. PhD Thesis, Washington State University.
- Feng, H., Tang, J., Cavalieri, R. P., & Plumb, O. A. (2001). Heat and mass transport in microwave drying of porous materials in a spouted bed. *AIChE Journal*, 47(7), 1499-1512.
- Feng, H., Tang, J., Plumb, O. A., & Cavalieri, R. P. (2004). Intrinsic and relative permeability for flow of humid air in unsaturated apple tissues. *Journal of Food Engineering*, 62(2), 185-192.
- Fito, P. (1994). Modelling of vacuum osmotic dehydration of food. *Journal of Food Engineering*, 22(1): 313-328.

- Fito, P., Andrés, A., Chiralt, A., & Pardo, P. (1996). Coupling of hydrodynamic mechanism and deformation-relaxation phenomena during vacuum treatments in solid porous food-liquid systems. *Journal of Food Engineering*, 27(3), 229-240.
- Fito, P., Chiralt, A., Barat, J. M., Andrés, A., Martínez-Monzó, J., & Martínez-Navarrete, N. (2001). Vacuum impregnation for development of new dehydrated products. *Journal of Food Engineering*, 49(4), 297-302.
- Folch, A. (2016). *Introduction to bioMEMS*. Boca Raton (FL): CRC Press.
- Galazka, V. B., & Ledward, D. A. (1995). Developments in high pressure food processing. *Food Technology International Europe*, 12, 123-125.
- Garcia, E., & Barrett, D. M. (2002). Preservative treatments for fresh-cut fruits and vegetables. *Fresh-cut fruits and vegetables*, 267-304.
- Gekas, V. (1992) *Transport phenomena of foods and biological materials*, 1st edn. London, UK: CRC Press, 237 pp.
- George, J. M., Selvan, T. S., & Rastogi, N. K. (2016). High-pressure-assisted infusion of bioactive compounds in apple slices. *Innovative Food Science and Emerging Technologies*, 33, 100-107.
- Gill, A. O., & Ramaswamy, H. S. (2008). Application of high pressure processing to kill *Escherichia coli* O157 in ready-to-eat meats. *Journal of Food Protection*, 71 (11), 2182–2189.
- Gobran, B. D., Brigham, W. E., & Ramey Jr, H. J. (1987). Absolute permeability as a function of confining pressure, pore pressure, and temperature. *SPE Formation Evaluation*, 2(01), 77-84.
- Gorny, J. R., Hess-Pierce, B., Cifuentes, R. A., & Kader, A. A. (2002). Quality changes in fresh-cut pear slices as affected by controlled atmospheres and chemical preservatives. *Postharvest Biology and Technology*, 24(3), 271-278.
- Gras, M., Vidal-Brotóns, N., Betoret, A., & Fito, P. (2002). The response of some vegetables to vacuum impregnation. *Innovative Food Science and Emerging Technologies*, 3(3), 263-269.
- Gross, M., & Jaenicke, R. (1994). Proteins under pressure. *European Journal of Biochemistry*, 221(2), 617-630.

- Guamis, B., Trujillo, A. J., Ferragut, V., Chiralt, A., Andres, A., & Fito, P. (1997). Ripening control of Manchego type cheese salted by brine vacuum impregnation. *International Dairy Journal*, 7(2), 185-192.
- Guillard, V., Bourlieu, C., Gontard, N. (2013). Food Structure and Moisture Transfer: A Modeling Approach. New York (NY): Springer.
- Guillard, V., Broyart, B., Bonazzi, C., Guilbert, S., & Gontard, N. (2003). Moisture diffusivity in sponge cake as related to porous structure evaluation and moisture content. *Journal of Food Science*, 68(2), 555-562.
- Han, K., Geurden, I., & Sorgeloos, P. (2000). Enrichment strategies for Artemia using emulsions providing different levels of n-3 highly unsaturated fatty acids. *Aquaculture*, 183(3), 335-347.
- Henderson, S. M. (1961). Grain drying theory temperature effect of drying coefficient. *J. Agri. Eng. Res.*, 6, 169-174.
- Hendrickx, M., Ludikhuyze, L., Van den Broeck, I., & Weemaes, C. (1998). Effects of high pressure on enzymes related to food quality. *Trends in Food Science and Technology*, 9(5), 197-203.
- Heremans, K. (1995). High pressure effects on biomolecules. In D. A. Ledward, D.E. Johnston, R.G. Earnshaw, & A.P.M. Hasting (Eds), *High Pressure Processing of Foods*. Leicestershire, UK.
- Hiremath, D.N., & Ramaswamy, H.S., (2012). High-pressure destruction kinetics of spoilage and pathogenic microorganisms in mango juice. *Journal of Food Processing and Preservation*, 36, 113–125.
- Honest, K. N., Zhang, H. W., & Zhang, L. (2011). Lycopene: Isomerization effects on bioavailability and bioactivity properties. *Food Reviews International*, 27(3), 248-258.
- Hussain, R., Singh, A., Vatankhah, H., & Ramaswamy, H. S. (2017). Effects of locust bean gum on the structural and rheological properties of resistant corn starch. *Journal of Food Science and Technology*, 54(3), 650-658.
- Hussain, R., Vatankhah, H., Singh, A., & Ramaswamy, H. S. (2016). Effect of high-pressure treatment on the structural and rheological properties of resistant corn starch/locust bean gum mixtures. *Carbohydrate Polymers*, 150, 299-307.

- Hygreeva, D., & Pandey, M. C. (2016). Novel approaches in improving the quality and safety aspects of processed meat products through high pressure processing technology-A review. *Trends in Food Science & Technology*, 54, 175-185.
- Jemai, A. B., Vorobiev, E. (2002). Effect of moderate electric field pulses on the diffusion coefficient of soluble substances from apple slices. *International Journal of Food Science and Technology*, 37(1): 73-86.
- Juan, B., Ferragut, V., Buffa, M., Guamis, B., & Trujillo, A. J. (2007). Effects of high-pressure treatment on free fatty acids release during ripening of ewes' milk cheese. *Journal of Dairy Research*, 74(4), 438-445.
- Kaushik, N., Kaur, B. P., & Rao, P. S. (2014). Application of high pressure processing for shelf life extension of litchi fruits (*Litchi chinensis* cv. Bombai) during refrigerated storage. *Revista de Agroquímica y Tecnología de Alimentos*, 20(7), 527-541.
- Kerkhof, P. J. (1994). The role of theoretical and mathematical modelling en scale-up. *Drying Technology*, 12(1-2), 1-46.
- Khurana, M., Karwe, M. V. (2009). Numerical prediction of temperature distribution and measurement of temperature in a high hydrostatic pressure food processor. *Food and Bioprocess Technology*, 2(3), 279-290.
- Knorr, D., Ade-Omowaye, B. I. O., & Heinz, V. (2002). Nutritional improvement of plant foods by non-thermal processing. *Proceedings of the Nutrition Society*, 61(2), 311-318.
- Knorr, D., Heinz, V., & Buckow, R. (2006). High pressure application for food biopolymers. *Biochimica et Biophysica Acta (BBA)-Proteins and Proteomics*, 1764(3), 619-631.
- Knorr, D (1995) 'High pressure effects on plant derived foods', in High Pressure Processing of Foods, eds Ledward D A, Johnston D E, Earnshaw R G and Hasting A P M, Nottingham University Press, Loughborough, 123–35
- Kowalski, S. J. (2015). Ultrasound in wet materials subjected to drying: A modeling study. *International Journal of Heat and Mass Transfer*, 84, 998-1007.
- Kozeny, J. (1927). *Über kapillare Leitung des Wassers im Boden* [Capillary flow of water in soils]. (Vol. 136 pp. 271–306). Austria: Akademie der Wissenschaften.

- Krebbers, B., Matser, A. M., Koets, M., & Van den Berg, R. W. (2002). Quality and storage-stability of high-pressure preserved green beans. *Journal of Food Engineering*, 54(1), 27-33.
- Kumar, M. N. R. (2000). A review of chitin and chitosan applications. *Reactive and Functional Polymers*, 46(1), 1-27.
- Lamikanra, O. (Ed.). (2002). *Fresh-cut fruits and vegetables: science, technology, and market*. Boca Raton (FL): CRC press.
- Li, X., Fang, Y., Al-Assaf, S., Phillips, G. O., Nishinari, K., & Zhang, H. (2009). Rheological study of gum Arabic solutions: Interpretation based on molecular self-association. *Food Hydrocolloids*, 23(8), 2394-2402.
- Li, X., Fang, Y., Zhang, H., Nishinari, K., Al-Assaf, S., & Phillips, G. O. (2011). Rheological properties of gum Arabic solution: from Newtonianism to thixotropy. *Food Hydrocolloids*, 25(3), 293-298.
- Lin, L., Lv, S. & Li, B. (2012). Angiotension-I-converting enzyme (ACE)-inhibitory and antihypertensive properties of squid skin gelatin hydrolysates. *Food Chemistry*, 131, 225–230
- Liu, Y., Gu, J., Zhang, J., Yu, F., Wang, J., Nie, N., & Li, W. (2015). LiFePO₄ nanoparticles growth with preferential (010) face modulated by Tween-80. *RSC Advances*, 5(13), 9745-9751.
- Lopez-Torrez, L., Nigen, M., Williams, P., Doco, T., & Sanchez, C. (2015). Acacia senegal vs. Acacia seyal gums—Part 1: Composition and structure of hyperbranched plant exudates. *Food Hydrocolloids*, 51, 41-53.
- Luikov, A. V. (1966). Application of irreversible thermodynamics methods to investigation of heat and mass transfer. *International Journal of Heat and Mass Transfer*, 9(2), 139-152.
- Luikov, A. V. (1975). Systems of differential equations of heat and mass transfer in capillary-porous bodies. *International Journal of Heat and mass transfer*, 18(1), 1-14.
- Luscher, C., Schlüter, O., & Knorr, D. (2005). High pressure–low temperature processing of foods: impact on cell membranes, texture, color and visual

- appearance of potato tissue. *Innovative Food Science & Emerging Technologies*, 6(1), 59-71.
- MacMinn, C. W., Dufresne, E. R., & Wettlaufer, J. S. (2016). Large deformations of a soft porous material. *Physical Review Applied*, 5(4), 044020.
 - Mahadevan, S., & Karwe, M. V. (2016). Effect of High-Pressure Processing on Bioactive Compounds. In *High Pressure Processing of Food* (pp. 479-507). New York (NY): Springer.
 - Medina-Meza, I. G., Barnaba, C., & Barbosa-Cánovas, G. V. (2014). Effects of high pressure processing on lipid oxidation: A review. *Innovative Food Science & Emerging Technologies*, 22, 1-10.
 - Mendoza, F., Verboven, P., Ho, Q. T., Kerckhofs, G., Wevers, M., & Nicolai, B. (2010). Multifractal properties of pore-size distribution in apple tissue using X-ray imaging. *Journal of Food Engineering*, 99(2), 206-215.
 - Mertens, B. (1995). Hydrostatic pressure treatment of food: equipment and processing. In *New methods of food preservation*. (p. 135). New York (NY): Blackie Academic and Professional.
 - Miao, M., Wang, Q., Zhang, T., & Jiang, B. (2011). Effect of high hydrostatic pressure (HHP) treatment on texture changes of water bamboo shoots cultivated in China. *Postharvest Biology and Technology*, 59(3), 327-329.
 - Mohsenin, N. H. (1986). *Physical properties of plant and animal materials* (2nd ed.). Netherlands: Gordon and Breach Publishers.
 - Moreno, H. M., Herranz, B., Borderías, A. J., & Tovar, C. A. (2016). Effect of high pressure treatment on the structural, mechanical and rheological properties of glucomannan gels. *Food Hydrocolloids*, 60, 437-444.
 - Mothe, C. G., & Rao, M. A. (1999). Rheological behavior of aqueous dispersions of cashew gum and gum Arabic: effect of concentration and blending. *Food Hydrocolloids*, 13(6), 501-506.
 - Mozhaev, V.V., Heremans, K., Johannes, F., Patrick, M., & Claude, B. (1996). High pressure effects on protein structure and function. *Proteins: Structure: Function and Genetics*, 24, 81-91

- Muskat, M., Wyckoff, R. D., Botset, H. G., & Meres, M. W. (1937). Flow of gas-liquid mixtures through sands. *Transactions of the AIME*, 123(01), 69-96.
- Muzzarelli, R. A., Morganti, P., Morganti, G., Palombo, P., Palombo, M., Biagini, G., Belmonte, M. M., Giantomassi, F., Orlandi, F., & Muzzarelli, C. (2007). Chitin nanofibrils/chitosan glycolate composites as wound medicaments. *Carbohydrate Polymers*, 70(3), 274-284.
- Nasehi, B., & Javaheri, S. (2012). Application of high hydrostatic pressure in modifying functional properties of starches: a review. *Middle East Journal of Scientific Research*, 11, 856-861.
- Nguyen, L., Rastogi, N. K., & Balasubramaniam, V. M. (2007). Evaluation of the Instrumental Quality of Pressure-Assisted Thermally Processed Carrots. *Journal of Food Science*, 5, 72.
- Norton, T. & Sun, D.W. (2008). Recent advances in the use of high pressure as an effective processing technique in the food industry. *Food and Bioprocess Technology*, 1(1), 2-34.
- Oey, I., Lille, M., Van Loey, A., & Hendrickx, M. (2008). Effect of high-pressure processing on colour, texture and flavour of fruit-and vegetable-based food products: a review. *Trends in Food Science & Technology*, 19(6), 320-328.
- Okuzono, T., & Doi, M. (2008). Effects of elasticity on drying processes of polymer solutions. *Physical Review E*, 77(3), 030501.
- Onyango, M. S., Masukume, M., Ochieng, A., & Otieno, F. (2010). Functionalised natural zeolite and its potential for treating drinking water containing excess amount of nitrate. *Water SA*, 36(5), 655-662.
- Palou, E., Hernández-Salgado, C., López-Malo, A., Barbosa-Cánovas, G. V., Swanson, B. G., & Welti-Chanes, J. (2000). High pressure-processed guacamole. *Innovative Food Science & Emerging Technologies*, 1(1), 69-75.
- Panteloglou, A. G., Bell, A. E., & Ma, F. (2010). Effect of high-hydrostatic pressure and pH on the rheological properties of gum Arabic. *Food Chemistry*, 122(4), 972-979.
- Parish, M. E., Beuchat, L. R., Suslow, T. V., Harris, L. J., Garrett, E. H., Farber, J. N., & Busta, F. F. (2003). Methods to reduce/eliminate pathogens from fresh and

- fresh-cut produce. *Comprehensive Reviews in Food Science and Food Safety*, 2(s1), 161-173.
- Patel, S., & Goyal, A. (2015). Applications of Natural Polymer Gum Arabic: A Review. *International Journal of Food Properties*, 18(5), 986-998.
 - Patras, A., Brunton, N. P., Da Pieve, S., & Butler, F. (2009). Impact of high pressure processing on total antioxidant activity, phenolic, ascorbic acid, anthocyanin content and colour of strawberry and blackberry purées. *Innovative Food Science & Emerging Technologies*, 10(3), 308-313.
 - Peleg, M. (1988). An empirical model for the description of moisture sorption curves. *Journal of Food Science*, 53, 1216–1217.
 - Petersen, B. (2014) Fortification and Impregnation Practices in Food Processing. In S. Bhattacharya (Ed), *Conventional and Advanced Food Processing Technologies*. UK: John Wiley & Sons.
 - Petrich, C., Langhorne, P. J., & Sun, Z. F. (2006). Modelling the interrelationships between permeability, effective porosity and total porosity in sea ice. *Cold Regions Science and Technology*, 44(2), 131-144.
 - Pham-Huy, L. A., He, H., & Pham-Huy, C. (2008). Free radicals, antioxidants in disease and health. *International Journal of Biomedical Science: IJBS*, 4(2), 89.
 - Philip, J. R., & De Vries, D. A. (1957). Moisture movement in porous materials under temperature gradients. *Eos, Transactions American Geophysical Union*, 38(2), 222-232.
 - Pilizota, V., & Sapers, G. M. (2004). Novel browning inhibitor formulation for fresh-cut apples. *Journal of Food Science*, 69(4).
 - Pinela, J., & Ferreira, I. C. (2017). Nonthermal physical technologies to decontaminate and extend the shelf-life of fruits and vegetables: Trends aiming at quality and safety. *Critical Reviews in Food Science and Nutrition*, 57(10), 2095-2111.
 - Prestamo, G., & Arroyo, G. (1998). High hydrostatic pressure effects on vegetable structure. *Journal of Food Science*, 63(5), 878-881.

- Qian, C., Decker, E. A., Xiao, H., & McClements, D. J. (2012). Physical and chemical stability of β -carotene-enriched nanoemulsions: Influence of pH, ionic strength, temperature, and emulsifier type. *Food Chemistry*, 132(3), 1221-1229.
- Ramaswamy, H. S., Chen, C. R., & Rattan, N. S. (2015). Comparison of viscoelastic properties of set and stirred yogurts made from high pressure and thermally treated milks. *International Journal of Food Properties*, 18(7), 1513-1523.
- Ramaswamy, H. S., Lo, K. V., & Tung, M. A. (1982). Simplified equations for transient temperatures in conductive foods with convective heat transfer at the surface. *Journal of Food Science*, 47(6), 2042-2047.
- Ramaswamy, H. S., Shao, Y., & Zhu, S. (2010). High-pressure destruction kinetics of *Clostridium sporogenes* ATCC 11437 spores in milk at elevated quasi-isothermal conditions. *Journal of Food Engineering*, 96(2), 249-257.
- Ramaswamy, H. S., Singh, A., & Sharma, M. (2015). Back extrusion rheology for evaluating the transitional effects of high pressure processing of egg components. *Journal of Texture Studies*, 46(1), 34-45.
- Ramaswamy, H.S., & Shao. Y. (2010). High pressure destruction kinetics of *Clostridium sporogenes* spores in salmon slurry at elevated temperatures. *International Journal of Food Properties*, 13 (5), 1074–1091
- Ramaswamy, H. S., Zaman, S. U., & Smith, J. P. (2008). High pressure destruction kinetics of *Escherichia coli* (O157:H7) and *Listeria monocytogenes* (Scott A) in a fish slurry. *Journal of Food Engineering*, 87 (1), 99–106.
- Randall, R. C., Phillips, G. O., & Williams, P. A. (1988). The role of the proteinaceous component on the emulsifying properties of gum Arabic. *Food Hydrocolloids*, 2(2), 131-140.
- Rastogi, N. K., Nguyen, L. T., & Balasubramaniam, V. M. (2008). Effect of pretreatments on carrot texture after thermal and pressure-assisted thermal processing. *Journal of Food Engineering*, 88(4): 541-547.
- Rastogi, N. K., Nguyen, L. T., Jiang, B., & Balasubramaniam, V. M. (2010). Improvement in texture of pressure-assisted thermally processed carrots by

- combined pretreatment using response surface methodology. *Food and Bioprocess Technology*, 3(5): 762-771.
- Rastogi, N. K., Raghavarao, K. S. M. S., Balasubramaniam, V. M., Niranjana, K., & Knorr, D. (2007). Opportunities and challenges in high pressure processing of foods. *Critical Reviews in Food Science and Nutrition*, 47(1), 69-112.
 - Rayner, M., Östbring, K., & Purhagen, J. (2016). Application of Natural Polymers in Food. In *Natural Polymers*. Switzerland: Springer International Publishing.
 - Reeve, R. M. (1953). Histological Investigations of Texture in Apples. *Journal of Food Science*, 18(1-6): 604-617.
 - Rezvani, E., Schleining, G., & Taherian, A. R. (2012). Assessment of physical and mechanical properties of orange oil-in-water beverage emulsions using response surface methodology. *LWT-Food Science and Technology*, 48(1), 82-88.
 - Rodriguez, E., Arques, J. L., Nunez, M., Gaya, P., & Medina, M. (2005). Combined effect of high-pressure treatments and bacteriocin-producing lactic acid bacteria on inactivation of Escherichia coli O157: H7 in raw-milk cheese. *Applied and Environmental Microbiology*, 71(7), 3399-3404.
 - Rojas-Graü, M. A., Tapia, M. S., Rodríguez, F. J., Carmona, A. J., & Martín-Belloso, O. (2007). Alginate and gellan-based edible coatings as carriers of antibrowning agents applied on fresh-cut Fuji apples. *Food Hydrocolloids*, 21(1), 118-127.
 - Romero, M. I., Carvalho, M. S., & Alvarado, V. (2011). Experiments and network model of flow of oil-water emulsion in porous media. *Physical Review E*, 84(4), 046305.
 - Sahimi, M. (2011). *Flow and transport in porous media and fractured rock: from classical methods to modern approaches*. New Jersey (NY): John Wiley & Sons.
 - Salvatori, D., Andres, A., Chiralt, A., & Fito, P. (1998). The response of some properties of fruits to vacuum impregnation. *Journal of Food Engineering*, 21(1), 59-73.
 - Sanchez, C., Renard, D., Robert, P., Schmitt, C., & Lefebvre, J. (2002). Structure and rheological properties of acacia gum dispersions. *Food Hydrocolloids*, 16(3), 257-267.

- Schulze, B., Peth, S., Hubbermann, E. M., & Schwarz, K. (2012). The influence of vacuum impregnation on the fortification of apple parenchyma with quercetin derivatives in combination with pore structures X-ray analysis. *Journal of Food Engineering*, 109(3), 380-387.
- Serment-Moreno, V., Fuentes, C., Barbosa-Cánovas, G., Torres, J. A., & Welti-Chanes, J. (2015). Evaluation of high pressure processing kinetic models for microbial inactivation using standard statistical tools and information theory criteria, and the development of generic time-pressure functions for process design. *Food and Bioprocess Technology*, 8(6), 1244-1257.
- Shahidul, I. M., Igura, N., Shimoda, M., & Hayakawa, I. (2007). The synergistic effect of moderate heat and pressure on the physical properties and pectic substances of potato tissue. *International Journal of Food Science and Technology*, 42, 434–440.
- Sila, D. N., Duvetter, T., De Roeck, A., Verlent, I., Smout, C., Moates, G. K., ... & Van Loey, A. (2008). Texture changes of processed fruits and vegetables: potential use of high-pressure processing. *Trends in Food Science & Technology*, 19(6), 309-319.
- Sila, D. N., Smout, C., Vu, T. S. & Hendrickx, M. E. (2004). Effects of high-pressure pretreatment and calcium soaking on the texture degradation kinetics of carrots during thermal processing. *Journal of Food Science*, 69(5), 205-211.
- Silva, L. F. M. S. (2010). Merging meshes using dynamic regular triangulation. Masters Thesis, Federal University of Rio Grande do Sul, Brazil.
- Simpson, R., Ramírez, C., Birchmeier, V., Almonacid, A., Moreno, J., Nuñez, H., & Jaques, A. (2015). Diffusion mechanisms during the osmotic dehydration of granny smith apples subjected to a moderate electric field. *Journal of Food Engineering*, 166, 204–211.
- Singh, A., & Ramaswamy, H. S. (2015). High pressure modification of egg components: Exploration of calorimetric, structural and functional characteristics. *Innovative Food Science and Emerging Technologies*, 32, 45-55.

- Singh, A., & Ramaswamy, H. S. (2014). Effect of high-pressure treatment on trypsin hydrolysis and antioxidant activity of egg white proteins. *International Journal of Food Science & Technology*, 49(1), 269-279.
- Su, G., Yu, Y., Ramaswamy, H. S., Hu, F., Xu, M., & Zhu, S. (2014). Kinetics of Escherichia coli inactivation in frozen aqueous suspensions by high pressure and its application to frozen chicken meat. *Journal of Food Engineering*, 142, 23-30.
- Sulaiman, A., & Silva, F. V. (2013). High pressure processing, thermal processing and freezing of 'Camarosa' strawberry for the inactivation of polyphenoloxidase and control of browning. *Food Control*, 33(2), 424-428.
- Tadros, Th. F. & Vincent, B. (1983). Becher, P (Ed.) in: *Encyclopedia of Emulsion Technology* New York (NY): Marcel Dekker.
- Tarhan, İ., Ismail, A. A., & Kara, H. (2017). Quantitative Determination of Free Fatty Acids in Extra Virgin Olive Oils by Multivariate Methods and Fourier Transform Infrared Spectroscopy Considering Different Absorption Modes. *International Journal of Food Properties*. 1-8.
- Terefe, N.S., Buckow, R., & Versteeg, C. (2014). Quality-related enzymes in fruit and vegetable products: effects of novel food processing technologies, part 1: high-pressure processing. *Critical Reviews in Food Science and Nutrition*, 54(1), 24-63.
- Thomas, K., Susanne, R. & Maya, T. (2005). Trimethylated chitosans as non-viral gene delivery vectors: cytotoxicity and transfection efficiency. *Journal of Controlled Release*, 103(3), 643–653.
- Thompson, D. S. (2005). How do cell walls regulate plant growth?. *Journal of experimental botany*, 56(419), 2275-2285.
- Thompson, T. L., Peart, R. M., & Foster, G. H. (1968). Mathematical Simulation of Corn Drying: A New Model. *Transactions of the ASAE*, 11(4): 582-586.
- Thorvaldsson, K., & Janestad, H. (1999). A model for simultaneous heat, water and vapour diffusion. *Journal of Food Engineering*, 40(3), 167-172.
- Ting, V. J., Silcock, P., Bremer, P. J., & Biasioli, F. (2013). X-Ray Micro-Computer Tomographic Method to Visualize the Microstructure of Different Apple Cultivars. *Journal of Food Science*, 78(11), 1735-1742.

- Tola, Y. B., & Ramaswamy, H. S. (2013). Evaluation of high pressure (HP) treatment for rapid and uniform pH reduction in carrots. *Journal of Food Engineering*, 116(4), 900-909.
- Tola, Y. B., & Ramaswamy, H. S. (2014). Combined effects of high pressure, moderate heat and pH on the inactivation kinetics of *Bacillus licheniformis* spores in carrot juice. *Food Research International*, 62, 50-58.
- Torres, J. A., Velazquez, G. (2005). Commercial opportunities and research challenges in the high pressure processing of foods. *Journal of Food Engineering*, 67(1), 95-112.
- Traber, M. G. (2004). Vitamin E, nuclear receptors and xenobiotic metabolism. *Archives of Biochemistry and Biophysics*, 423(1), 6-11.
- Tsuruta, T., Tanigawa, H., & Sashi, H. (2015). Study on Shrinkage Deformation of Food in Microwave–Vacuum Drying. *Drying Technology*, 33(15-16), 1830-1836.
- Tylewicz, U., Lundin, P., Cocola, L., Dymek, K., Rocculi, P., Svanberg, S., ... & Galindo, F. G. (2012). Gas in scattering media absorption spectroscopy (GASMAS) detected persistent vacuum in apple tissue after vacuum impregnation. *Food Biophysics*, 7(1), 28-34.
- Urrutia, G., Arabas, J., Autio, K., Brul, S., Hendrickx, M., Kąkolewski, A., ... & Ousegui, A. (2007). SAFE ICE: Low-temperature pressure processing of foods: Safety and quality aspects, process parameters and consumer acceptance. *Journal of Food Engineering*, 83(2), 293-315.
- Vafai, K. (2015). *Handbook of porous media*. Boca Raton (FL): CRC Press.
- Vatankhah, H., Akbarzadeh, A., & Ramaswamy, H. S. (2018a). Hybrid Fickian–Darcian flow model for high pressure impregnation of fluids into porous biomaterials. *Biosystems Engineering*, 166, 200-209.
- Vatankhah, H., & Ramaswamy, H. S. (2017). Dynamics of Fluid Migration into Porous Solid Matrix during High Pressure Treatment. *Food and Bioprocess Processing*, 103, 122–130.
- Vatankhah, H., Taherian, A. R., & Ramaswamy, H. S. (2018b). High-pressure induced thermo-viscoelasticity and dynamic rheology of gum Arabic and chitosan aqueous dispersions. *LWT-Food Science and Technology*, 89, 291-298.

- Vatankhah, H., Zamindar, N., & Baghekhanda, M. S. (2015). Heat transfer simulation and retort program adjustment for thermal processing of wheat based Haleem in semi-rigid aluminum containers. *Journal of Food Science and Technology*, 52(10), 6798-6803.
- Wang, C. Y., & Singh, R. P. (1978). Use of variable equilibrium moisture content in modeling rice drying. *Transactions of the ASAE*, 11(6): 668-672.
- Wang, C., Lin, Y., Ramaswamy, H. S., Ge, L., Hu, F., Zhu, S., & Yu, Y. (2015). Storage Stability of Chinese Bayberry Juice after High Pressure or Thermal Treatment. *Journal of Food Processing and Preservation*, 39(6), 2259-2266.
- Wang, Y. (2015). *Exploring Biopolymer-Clay Nanocomposite Materials by Molecular Modelling*. PhD Thesis, KTH Royal Institute of Technology, Sweden.
- Whitaker, S. (1980) Heat and mass transfer in granular porous media. In: Mujumdar AS (ed). *Advances in drying*, (Vol. 1). Hemisphere publishing, New York
- Whitaker, S. (1986). Flow in porous media II: The governing equations for immiscible, two-phase flow. *Transport in porous media*, 1(2), 105-125.
- Williams, P. A., & Phillips, G. O. (2009). *Handbook of Hydrocolloids*, (2nd ed.). Cambridge, UK: Woodhead Publishing.
- Wu, J. F., Zhang, R. M., Chen, Y., & Yin, C. Y. (2009). Rheological Behavior of the Urea Denatured Soybean Protein. *Journal of Fiber Bioengineering and Informatics*, 2(3), 158-161.
- Xie, J., & Zhao, Y. (2003). Nutritional enrichment of fresh apple (*Royal Gala*) by vacuum impregnation. *International Journal of Food Science and Nutrition*, 54(5), 387-398
- Yang, H., Khan, M. A., Yu, X., Zheng, H., Han, M., Xu, X., & Zhou, G. (2016). Changes in protein structures to improve the rheology and texture of reduced-fat sausages using high pressure processing. *Meat Science*, 121, 79-87.
- Zhang, H. Q., Balasubramaniam, V. B., Dunne, C. P., Farkas, D. F., & Yuan, J. T. (Eds.). (2011). *Nonthermal Processing Technologies for Food* (Vol. 45). New Jersey (NY): John Wiley & Sons.

- Zhu, S., Bail, A.L., and Ramaswamy, H. S. (2003). Ice crystal formation in pressure shift freezing of Atlantic salmon (*Salmo salar*) as compared to classical freezing methods. *Journal of Food Processing and Preservation*, 27(6), 427-444.
- Zhu, S., Bail, A.L, and Ramaswamy, H.S. (2006). High-pressure differential scanning calorimetry: Comparison of pressure-dependent phase transition in food materials. *Journal of Food Engineering*, 75(2), 215-222.
- Zhu, S., Ramaswamy, H. S., & Simpson, B. K. (2004). Effect of high-pressure versus conventional thawing on color, drip loss and texture of Atlantic salmon frozen by different methods. *LWT-Food Science and Technology*, 37(3), 291-299.
- Zhu, S., Ramaswamy, H. S., Marcotte, M., Chen, C., Shao, Y., & Le Bail, A. (2007). Evaluation of Thermal Properties of Food Materials at High Pressures Using a Dual-Needle Line-Heat-Source Method. *Journal of Food Science*, 72(2), 49-56.